

UNCLASSIFIED

AD NUMBER
AD911493
NEW LIMITATION CHANGE
TO Approved for public release, distribution unlimited
FROM Distribution authorized to U.S. Gov't. agencies only; Test and Evaluation; FEB 1972. Other requests shall be referred to Air Force Flight Dynamics Laboratory, Attn: AXM, Wright-Patterson AFB, OH 45433.
AUTHORITY
AFSC/DOOS[WPAFB, OH] Ltr, 28 Jun 1991

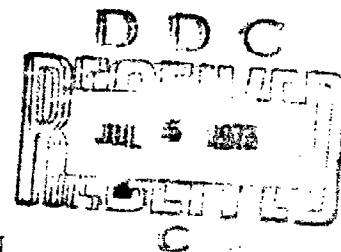
THIS PAGE IS UNCLASSIFIED

AD 911 493

AFFDL-TR-72-11
Volume II

INVESTIGATION OF THE EFFECTS OF
AIRFRAME DESIGN ON INLET FLOW FIELDS

CONSTANT PROKOP
FAIRCHILD REPUBLIC DIVISION



TECHNICAL REPORT AFFDL-TR-72-11 Volume II
May 1973

Distribution limited to U.S. Government agencies only; test and evaluation statement applied "April 1973." Other requests for this document must be referred to AF Flight Dynamics Laboratory (FXM), Wright-Patterson AFB, Ohio 45433.

AIR FORCE FLIGHT DYNAMICS LABORATORY
AIR FORCE SYSTEMS COMMAND
WRIGHT-PATTERSON AIR FORCE BASE, OHIO 45433

NOTICE

When Government drawings, specifications, or other data are used for any purpose other than in connection with a definitely related Government procurement operation, the United States Government thereby incurs no responsibility nor any obligation whatsoever; and the fact that the Government may have formulated, furnished, or in any way supplied the said drawings, specifications, or other data, is not to be regarded by implication or otherwise as in any manner licensing the holder or any other person or corporation, or conveying any rights or permission to manufacture, use, or sell any patented invention that may in any way be related thereto.

Copies of this report should not be returned unless return is required by security considerations, contractual obligations, or notice on a specific document.

AFFDL-TR-72-11
Volume II

INVESTIGATION OF THE EFFECTS OF
AIRFRAME DESIGN ON INLET FLOW FIELDS

Constant Prokop

Distribution limited to U.S. Government agencies only; test and evaluation statement applied "April 1973". Other requests for this document must be referred to AF Flight Dynamics Laboratory (FXM), Wright-Patterson AFB, Ohio 45433.

FOREWORD

This report was prepared by the Fairchild Republic Division of Fairchild Industries, Inc., Farmingdale, New York, for the Air Force Flight Dynamics Laboratory, Air Force Systems Command, United States Air Force, on Contract Number F33615-71-C-1451.

The program was a cooperative Air Force - NASA effort with funding provided by the Air Force and test facilities by NASA.

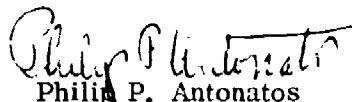
All the work reported herein was conducted under the technical cognizance of Capt. Edralin J. Maduli of the Air Force Flight Dynamics Laboratory, Internal Aerodynamics Group. The program was conducted as part of Project 1476, "Air-frame Propulsion Compatibility", Task 147603. The program began in March 1971. The first volume of this report was submitted by the author in January 1972, and the second volume in December 1972.

The contract effort was conducted at the Fairchild Republic Division of Fairchild Industries under the direction of Mr. Constant Prokop. Grateful acknowledgment is given to the staff of the NASA - Ames test facility and ARO Inc. for their cooperation throughout the experimental phase of the program.

Further acknowledgements are extended to Messrs. J. DeCarlo, M. Romano, and D. Torrillo for their assistance during the various phases of the program.

This report contains no classified information extracted from other classified documents.

This technical report has been reviewed and is approved.



Philip P. Antonatos
Chief, Flight Mechanics Division
Air Force Flight Dynamics Laboratory

ABSTRACT

The modern tactical class of aircraft weapon systems is required to perform effectively over a wide range of flight Mach number and altitude, providing large thrust margin and high maneuvering capability throughout the normal operating envelope. To achieve this combination of performance and maneuverability, a sophisticated propulsion system closely integrated with the airframe is required. Operational experience indicates that the vehicle induced flow environment can influence the performance of these closely integrated propulsion systems with the effects ranging from minor performance degradation to engine flame-out.

Recent exploratory and developmental research programs have served to improve the basic understanding of the effects of airframe-inlet interaction. These programs accomplished their major goals in that a large bank of relevant experimental data was generated and a basic understanding of the flow phenomena was obtained. The objective of the program reported herein was to expand this data bank by (1) providing a more extensive spatial documentation of the vehicle flow fields, (2) an increase in the Mach number regime included, and (3) investigations of additional geometric variables potentially impacting upon the propulsion system design process. All major program goals were attained.

PREFACE

The subject matter of this report, which represents the second of the two volumes comprising the document AFFDL-TR-72-11, deals mainly with the results of the wind tunnel investigation at Mach numbers of 2.5 and 3.5. Such topics as the model design philosophy, model description, instrumentation, data acquisition, and reduction have already been presented in Volume I of this document and, consequently, are not presented here. A table of the contents of Volume I has been included in the front matter of this report which, together with the table of contents of the present volume, should provide a clear outline of the program scope as well as a convenient referral guide.

TABLE OF CONTENTS

VOLUME I

<u>Section</u>		<u>Page</u>
I	INTRODUCTION	1
II	SUMMARY	2
III	MODEL DESIGN	4
	3.0 General	4
	3.1 Protuberances	4
	3.1.1 Canard Surfaces	4
	3.1.1.1 General Considerations	4
	3.1.1.2 Design Description	5
	3.1.2 Strakes	5
	3.1.2.1 General Considerations	5
	3.1.2.2 Design Description	9
	3.1.3 Missiles	9
	3.1.3.1 General Considerations	9
	3.1.3.2 Design Description	12
	3.2 Fuselage Nose Geometry	12
	3.2.1 General Considerations	12
	3.2.2 Design Description	15
	3.3 Cambered Fuselage Configuration	15
	3.3.1 General Considerations	15
	3.3.2 Design Description	20
	3.4 High Mach Number Nose and Canopy Design	20
	3.4.1 Sizing Criteria	20
	3.4.2 Fuselage Nose Geometry	20
	3.4.3 Canopy Geometry	26
	3.5 Structural Modifications	26
	3.5.1 General	26
	3.5.2 Sting Support	26
	3.5.3 Flow Field Survey Mechanism	29

TABLE OF CONTENTS (Cont'd)

<u>Section</u>	<u>VOLUME I</u>	<u>Page</u>
3.6	Instrumentation	29
3.6.1	General	29
3.6.2	Boundary Layer	29
3.6.3	Fuselage Static Pressure	31
3.6.4	Flow Field	31
IV	EXPERIMENTAL PROGRAM	37
4.0	General	37
V	DATA ANALYSIS	41
5.0	General	41
5.1	Mach Number 0.8	41
5.1.1	Low Angle of Attack	41
5.1.1.1	Local Mach Number	41
5.1.1.1.1	Effect of Vehicle Geometry	41
5.1.1.1.2	Effect of Protuberances	48
5.1.1.1.3	Effect of Yaw	48
5.1.1.2	Total Pressure Recovery	56
5.1.1.2.1	Effect of Vehicle Geometry	56
5.1.1.2.2	Effect of Protuberances	56
5.1.1.2.3	Effect of Yaw	62
5.1.1.3	Local Alpha	62
5.1.1.3.1	Effect of Vehicle Geometry	62
5.1.1.3.2	Effect of Protuberances	70
5.1.1.3.3	Effect of Yaw	70
5.1.1.4	Local Sigma	75
5.1.1.4.1	Effect of Vehicle Geometry	75
5.1.1.4.2	Effect of Protuberances	75
5.1.1.4.3	Effect of Yaw	75
5.1.2	Intermediate Angle of Attack	79
5.1.2.1	Local Mach Number	79
5.1.2.1.1	Effect of Vehicle Geometry	79
5.1.2.1.2	Effect of Protuberances	83
5.1.2.1.3	Effect of Yaw	83
5.1.2.2	Total Pressure Recovery	87
5.1.2.2.1	Effect of Vehicle Geometry	87
5.1.2.2.2	Effect of Protuberances	87
5.1.2.2.3	Effect of Yaw	90

TABLE OF CONTENTS (Cont'd)

<u>Section</u>	<u>VOLUME I</u>	<u>Page</u>
5.1.2.3	Local Alpha	90
5.1.2.3.1	Effect of Vehicle Geometry	90
5.1.2.3.2	Effect of Protuberances	100
5.1.2.3.3	Effect of Yaw	100
5.1.2.4	Local Sigma	102
5.1.2.4.1	Effect of Vehicle Geometry	102
5.1.2.4.2	Effect of Protuberances	102
5.1.2.4.3	Effect of Yaw	105
5.1.3	High Angle of Attack	105
5.1.3.1	Local Mach Number	105
5.1.3.1.1	Effect of Vehicle Geometry	105
5.1.3.1.2	Effect of Protuberances	105
5.1.3.1.3	Effect of Yaw	109
5.1.3.2	Total Pressure Recovery	109
5.1.3.2.1	Effect of Vehicle Geometry	109
5.1.3.2.2	Effect of Protuberances	109
5.1.3.2.3	Effect of Yaw	112
5.1.3.3	Local Alpha	112
5.1.3.3.1	Effect of Vehicle Geometry	112
5.1.3.3.2	Effect of Protuberances	112
5.1.3.3.3	Effect of Yaw	114
5.1.3.4	Local Sigma	114
5.1.3.4.1	Effect of Vehicle Geometry	114
5.1.3.4.2	Effect of Protuberances	117
5.1.3.4.3	Effect of Yaw	117
5.2	Mach Number 1.8	117
5.2.1	Low Angle of Attack	117
5.2.1.1	Local Mach Number	117
5.2.1.1.1	Effect of Vehicle Geometry	117
5.2.1.1.2	Effect of Protuberances	117
5.2.1.1.3	Effect of Yaw	121
5.2.1.2	Total Pressure Recovery	121
5.2.1.2.1	Effect of Vehicle Geometry	121
5.2.1.2.2	Effect of Protuberances	121
5.2.1.2.3	Effect of Yaw	125

TABLE OF CONTENTS (Cont'd)

<u>Section</u>	<u>VOLUME I</u>	<u>Page</u>
5.2.1.3	Local Alpha	125
5.2.1.3.1	Effect of Vehicle Geometry	125
5.2.1.3.2	Effect of Protuberances	129
5.2.1.3.3	Effect of Yaw	135
5.2.1.4	Local Sigma	135
5.2.1.4.1	Effect of Vehicle Geometry	135
5.2.1.4.2	Effect of Protuberances	138
5.2.1.4.3	Effect of Yaw	138
5.2.2	Intermediate Angle of Attack	144
5.2.2.1	Local Mach Number	144
5.2.2.1.1	Effect of Vehicle Geometry	144
5.2.2.1.2	Effect of Protuberances	144
5.2.2.1.3	Effect of Yaw	148
5.2.2.2	Total Pressure Recovery	148
5.2.2.2.1	Effect of Vehicle Geometry	148
5.2.2.2.2	Effect of Protuberances	148
5.2.2.3	Local Alpha	152
5.2.2.3.1	Effect of Vehicle Geometry	152
5.2.2.3.2	Effect of Protuberances	153
5.2.2.3.3	Effect of Yaw	153
5.2.2.4	Local Sigma	158
5.2.2.4.1	Effect of Vehicle Geometry	158
5.2.2.4.2	Effect of Protuberances	163
5.2.2.4.3	Effect of Yaw	163
5.2.3	High Angle of Attack	168
5.2.3.1	Local Mach Number	168
5.2.3.1.1	Effect of Vehicle Geometry	168
5.2.3.1.2	Effect of Protuberances	168
5.2.3.1.3	Effect of Yaw	168
5.2.3.2	Total Pressure Recovery	168
5.2.3.2.1	Effect of Vehicle Geometry	168
5.2.3.2.2	Effect of Protuberances	171
5.2.3.3	Local Alpha	171
5.2.3.3.1	Effect of Vehicle Geometry	171
5.2.3.3.2	Effect of Protuberances	173

TABLE OF CONTENTS (Cont'd)

<u>Section</u>	<u>VOLUME I</u>	<u>Page</u>
	5.2.3.4 Local Sigma	173
	5.2.3.4.1 Effect of Vehicle Geometry	173
5.3	Mach Number 2.2	173
5.3.1	Low Angle of Attack	173
5.3.1.1	Local Mach Number	173
	5.3.1.1.1 Effect of Vehicle Geometry	173
	5.3.1.1.2 Effect of Protuberances	176
	5.3.1.1.3 Effect of Yaw	176
5.3.1.2	Total Pressure Recovery	176
	5.3.1.2.1 Effect of Vehicle Geometry	176
	5.3.1.2.2 Effect of Protuberances	185
	5.3.1.2.3 Effect of Yaw	185
5.3.1.3	Local Alpha	190
	5.3.1.3.1 Effect of Vehicle Geometry	190
	5.3.1.3.2 Effect of Protuberances	190
	5.3.1.3.3 Effect of Yaw	193
5.3.1.4	Local Sigma	193
	5.3.1.4.1 Effect of Vehicle Geometry	193
	5.3.1.4.2 Effect of Protuberances	193
	5.3.1.4.3 Effect of Yaw	200
5.3.2	Intermediate Angle of Attack	200
5.3.2.1	Local Mach Number	200
	5.3.2.1.1 Effect of Vehicle Geometry	200
	5.3.2.1.2 Effect of Protuberances	206
5.3.2.2	Total Pressure Recovery	206
	5.3.2.2.1 Effect of Vehicle Geometry	206
	5.3.2.2.2 Effect of Protuberances	212
	5.3.2.2.3 Effect of Yaw	212
5.3.2.3	Local Alpha	214
	5.3.2.3.1 Effect of Vehicle Geometry	214
	5.3.2.3.2 Effect of Protuberances	214
	5.3.2.3.3 Effect of Yaw	214
5.3.2.4	Local Sigma	214
	5.3.2.4.1 Effect of Vehicle Geometry	214
	5.3.2.4.2 Effect of Protuberances	226
	5.3.2.4.3 Effect of Yaw	226

TABLE OF CONTENTS (Cont'd)

<u>Section</u>	VOLUME I	<u>Page</u>
	5.3.3 High Angle of Attack	231
	5.3.3.1 Local Mach Number	231
	5.3.3.1.1 Effect of Vehicle Geometry	231
VI	CONCLUSIONS	235
VII	REFERENCES	274

TABLE OF CONTENTS

VOLUME II

<u>Section</u>	<u>Page</u>
I INTRODUCTION	1
II SUMMARY	2
III DATA ANALYSIS	4
3.0 General	4
3.1 Mach Number 2.5	4
3.1.1 Low Angle of Attack	4
3.1.1.1 Local Mach Number	4
3.1.1.1.1 Effect of Vehicle Geometry	4
3.1.1.1.2 Effect of Yaw	9
3.1.1.2 Total Pressure Recovery	9
3.1.1.2.1 Effect of Vehicle Geometry	9
3.1.1.2.2 Effect of Yaw	10
3.1.1.3 Local Alpha	10
3.1.1.3.1 Effect of Vehicle Geometry	10
3.1.1.3.2 Effect of Yaw	28
3.1.1.4 Local Sigma	28
3.1.1.4.1 Effect of Vehicle Geometry	28
3.1.1.4.2 Effect of Yaw	36
3.1.2 Intermediate Angle of Attack	43
3.1.2.1 Local Mach Number	43
3.1.2.1.1 Effect of Vehicle Geometry	43
3.1.2.1.2 Effect of Yaw	43
3.1.2.2 Total Pressure Recovery	50
3.1.2.2.1 Effect of Vehicle Geometry	50
3.1.2.2.2 Effect of Yaw	50
3.1.2.3 Local Alpha	50
3.1.2.3.1 Effect of Vehicle Geometry	50
3.1.2.3.2 Effect of Yaw	54
3.1.2.4 Local Sigma	54
3.1.2.4.1 Effect of Vehicle Geometry	54
3.1.2.4.2 Effect of Yaw	54

TABLE OF CONTENTS (Cont'd)

VOLUME II

<u>Section</u>	<u>Page</u>
3.1.3 High Angle of Attack	63
3.1.3.1 Local Mach Number	63
3.1.3.1.1 Effect of Vehicle Geometry	63
3.1.3.1.2 Effect of Yaw	63
3.1.3.2 Total Pressure Recovery	63
3.1.3.2.1 Effect of Vehicle Geometry	63
3.1.3.2.2 Effect of Yaw	72
3.1.3.3 Local Alpha	72
3.1.3.3.1 Effect of Vehicle Geometry	72
3.1.3.3.2 Effect of Yaw	72
3.1.3.4 Local Sigma	82
3.1.3.4.1 Effect of Vehicle Geometry	82
3.1.3.4.2 Effect of Yaw	82
3.2 Mach Number 3.5	82
3.2.1 Low Angle of Attack	82
3.2.1.1 Local Mach Number	82
3.2.1.1.1 Effect of Vehicle Geometry	82
3.2.1.1.2 Effect of Yaw	92
3.2.1.2 Total Pressure Recovery	92
3.2.1.2.1 Effect of Vehicle Geometry	92
3.2.1.2.2 Effect of Yaw	97
3.2.1.3 Local Alpha	97
3.2.1.3.1 Effect of Vehicle Geometry	97
3.2.1.3.2 Effect of Yaw	97
3.2.1.4 Local Sigma	97
3.2.1.4.1 Effect of Vehicle Geometry	97
3.2.1.4.2 Effect of Yaw	110
3.2.2 Intermediate Angle of Attack	110
3.2.2.1 Local Mach Number	110
3.2.2.1.1 Effect of Vehicle Geometry	110
3.2.2.1.2 Effect of Yaw	122
3.2.2.2 Total Pressure Recovery	122

TABLE OF CONTENTS (Cont'd)

<u>Section</u>	VOLUME II	<u>Page</u>
	3.2.2.2.1 Effect of Vehicle Geometry	122
	3.2.2.2.2 Effect of Yaw	122
	3.2.2.3 Local Alpha	122
	3.2.2.3.1 Effect of Vehicle Geometry	122
	3.2.2.3.2 Effect of Yaw	130
	3.2.2.4 Local Sigma	130
	3.2.2.4.1 Effect of Vehicle Geometry	130
	3.2.2.4.2 Effect of Yaw	130
3.2.3	High Angle of Attack	130
	3.2.3.1 Local Mach Number	130
	3.2.3.1.1 Effect of Vehicle Geometry	130
	3.2.3.1.2 Effect of Yaw	141
	3.2.3.2 Total Pressure Recovery	141
	3.2.3.2.1 Effect of Vehicle Geometry	141
	3.2.3.2.2 Effect of Yaw	141
	3.2.3.3 Local Alpha	141
	3.2.3.3.1 Effect of Vehicle Geometry	141
	3.2.3.3.2 Effect of Yaw	151
	3.2.3.4 Local Sigma	151
	3.2.3.4.1 Effect of Vehicle Geometry	151
	3.2.3.4.2 Effect of Yaw	151
VI	CONCLUSIONS	162

LIST OF ILLUSTRATIONS

VOLUME II

<u>Figure</u>	<u>Description</u>	<u>Page</u>
1.	Pressure Measuring Port Schematic	3
2	Local Mach Number at 30% ACL, Fuselage 1, $M_\infty = 2.5$, $\alpha = 0^\circ$	5
3	Local Mach Number at 30% ACL, Fuselage 2, $M_\infty = 2.5$, $\alpha = 0^\circ$	6
4	Local Mach Number at 50% ACL, Fuselage 1, $M_\infty = 2.5$, $\alpha = 0^\circ$	7
5	Local Mach Number at 50% ACL, Fuselage 2, $M_\infty = 2.5$, $\alpha = 0^\circ$	8
6	Local Mach Number at 30% ACL, Fuselage 1, $M_\infty = 2.5$, $\alpha = 0^\circ$, $\beta = -4^\circ$	11
7	Local Mach Number at 30% ACL, Fuselage 1, $M_\infty = 2.5$, $\alpha = 0^\circ$, $\beta = 4^\circ$	12
8	Local Mach Number at 50% ACL, Fuselage 1, $M_\infty = 2.5$, $\alpha = 0^\circ$, $\beta = -4^\circ$	13
9	Local Mach Number at 50% ACL, Fuselage 1, $M_\infty = 2.5$, $\alpha = 0^\circ$, $\beta = 4^\circ$	14
10	Local Mach Number at 30% ACL, Fuselage 2, $M_\infty = 2.5$, $\alpha = 0^\circ$, $\beta = -4^\circ$	15
11	Local Mach Number at 30% ACL, Fuselage 2, $M_\infty = 2.5$, $\alpha = 0^\circ$, $\beta = 4^\circ$	16
12	Local Mach Number at 50% ACL, Fuselage 2, $M_\infty = 2.5$, $\alpha = 0^\circ$, $\beta = -4^\circ$	17
13	Local Mach Number at 50% ACL, Fuselage 2, $M_\infty = 2.5$, $\alpha = 0^\circ$, $\beta = 4^\circ$	18
14	Local P_T/P_{T_∞} at 30% ACL, Fuselage 1, $M_\infty = 2.5$, $\alpha = 0^\circ$	19
15	Local P_T/P_{T_∞} at 30% ACL, Fuselage 2, $M_\infty = 2.5$, $\alpha = 0^\circ$	20
16	Local P_T/P_{T_∞} at 50% ACL, Fuselage 1, $M_\infty = 2.5$, $\alpha = 0^\circ$	21
17	Local P_T/P_{T_∞} at 50% ACL, Fuselage 2, $M_\infty = 2.5$, $\alpha = 0^\circ$	22
8	Local P_T/P_{T_∞} at 50% ACL, Fuselage 1, $M_\infty = 2.5$, $\alpha = 0^\circ$, $\beta = 4^\circ$	23
19	Local Alpha at 30% ACL, Fuselage 1, $M_\infty = 2.5$, $\alpha = 0^\circ$	24
20	Local Alpha at 50% ACL, Fuselage 1, $M_\infty = 2.5$, $\alpha = 0^\circ$	25
21	Local Alpha at 30% ACL, Fuselage 2, $M_\infty = 2.5$, $\alpha = 0^\circ$	26
22	Local Alpha at 50% ACL, Fuselage 2, $M_\infty = 2.5$, $\alpha = 0^\circ$	27
23	High Mach Number Nose and Canopy Model: Schematic at Survey Regions and Main Shock Wave Locations	29

LIST OF ILLUSTRATIONS (Cont'd)

VOLUME II

<u>Figure</u>	<u>Description</u>	<u>Page</u>
24	Local Alpha at 30% ACL, Fuselage 1, $M_\infty = 2.5$, $\alpha = 0^\circ$, $\beta = 4^\circ$	30
25	Local Alpha at 30% ACL, Fuselage 1, $M_\infty = 2.5$, $\alpha = 0^\circ$, $\beta = -4^\circ$	31
26	Local Alpha at 50% ACL, Fuselage 1, $M_\infty = 2.5$, $\alpha = 0^\circ$, $\beta = 4^\circ$	32
27	Local Alpha at 50% ACL, Fuselage 1, $M_\infty = 2.5$, $\alpha = 0^\circ$, $\beta = -4^\circ$	33
28	Local Sigma at 30% ACL, Fuselage 1, $M_\infty = 2.5$, $\alpha = 0^\circ$	34
29	Local Sigma at 30% ACL, Fuselage 2, $M_\infty = 2.5$, $\alpha = 0^\circ$	35
30	Local Sigma at 50% ACL, Fuselage 1, $M_\infty = 2.5$, $\alpha = 0^\circ$	37
31	Local Sigma at 50% ACL, Fuselage 2, $M_\infty = 2.5$, $\alpha = 0^\circ$	38
32	Local Sigma at 30% ACL, Fuselage 1, $M_\infty = 2.5$, $\alpha = 0^\circ$, $\beta = 4^\circ$	39
33	Local Sigma at 30% ACL, Fuselage 2, $M_\infty = 2.5$, $\alpha = 0^\circ$, $\beta = 4^\circ$	40
34	Local Sigma at 50% ACL, Fuselage 1, $M_\infty = 2.5$, $\alpha = 0^\circ$, $\beta = 4^\circ$	41
35	Local Sigma at 50% ACL, Fuselage 2, $M_\infty = 2.5$, $\alpha = 0^\circ$, $\beta = 4^\circ$	42
36	Local Sigma at 50% ACL, Fuselage 1, $M_\infty = 2.5$, $\alpha = 0^\circ$, $\beta = -4^\circ$	44
37	Local Mach Number at 30% ACL, Fuselage 1, $M_\infty = 2.5$, $\alpha = 10^\circ$	45
38	Local Mach Number at 50% ACL, Fuselage 1, $M_\infty = 2.5$, $\alpha = 10^\circ$	46
39	Local Mach Number at 50% ACL, Fuselage 2, $M_\infty = 2.5$, $\alpha = 10^\circ$	47
40	Local Mach Number at 30% ACL, Fuselage 1, $M_\infty = 2.5$, $\alpha = 10^\circ$, $\beta = 4^\circ$	48
41	Local Mach Number at 30% ACL, Fuselage 1, $M_\infty = 2.5$, $\alpha = 10^\circ$, $\beta = -4^\circ$	49
42	Local P_T/P_{T_∞} at 50% ACL Fuselage 1, $M_\infty = 2.5$, $\alpha = 10^\circ$	51
43	Local Alpha at 30% ACL, Fuselage 1, $M_\infty = 2.5$, $\alpha = 10^\circ$	52
44	Local Alpha at 30% ACL, Fuselage 2, $M_\infty = 2.5$, $\alpha = 10^\circ$	53
45	Local Alpha at 50% ACL, Fuselage 1, $M_\infty = 2.5$, $\alpha = 10^\circ$	55
46	Local Alpha at 50% ACL, Fuselage 2, $M_\infty = 2.5$, $\alpha = 10^\circ$	56
47	Local Alpha at 30% ACL, Fuselage 1, $M_\infty = 2.5$, $\alpha = 10^\circ$, $\beta = -4^\circ$	57
48	Local Alpha at 30% ACL, Fuselage 1, $M_\infty = 2.5$, $\alpha = 10^\circ$, $\beta = 4^\circ$	58
49	Local Alpha at 50% ACL, Fuselage 1, $M_\infty = 2.5$, $\alpha = 10^\circ$, $\beta = -4^\circ$	59
50	Local Alpha at 50% ACL, Fuselage 1, $M_\infty = 2.5$, $\alpha = 10^\circ$, $\beta = 4^\circ$	60
51	Local Sigma at 30% ACL, Fuselage 1, $M_\infty = 2.5$, $\alpha = 10^\circ$	61
52	Local Sigma at 50% ACL, Fuselage 1, $M_\infty = 2.5$, $\alpha = 10^\circ$	62

LIST OF ILLUSTRATIONS (Cont'd)

VOLUME II

<u>Figure</u>	<u>Description</u>	<u>Page</u>
53	Local Sigma at 30% ACL, Fuselage 1, $M_\infty = 2.5$, $\alpha = 10^\circ$, $\beta = -4^\circ$	64
54	Local Sigma at 30% ACL, Fuselage 1, $M_\infty = 2.5$, $\alpha = 10^\circ$, $\beta = 4^\circ$	65
55	Local Sigma at 50% ACL, Fuselage 1, $M_\infty = 2.5$, $\alpha = 10^\circ$, $\beta = -4^\circ$	66
56	Local Sigma at 50% ACL, Fuselage 1, $M_\infty = 2.5$, $\alpha = 10^\circ$, $\beta = 4^\circ$	67
57	Local Mach Number at 30% ACL, Fuselage 1, $M_\infty = 2.5$, $\alpha = 20^\circ$	68
58	Local Mach Number at 30% ACL, Fuselage 2, $M_\infty = 2.5$, $\alpha = 20^\circ$	69
59	Local Mach Number at 50% ACL, Fuselage 2, $M_\infty = 2.5$, $\alpha = 20^\circ$	70
60	Local P_T/P_{T_∞} at 50% ACL, Fuselage 1, $M_\infty = 2.5$, $\alpha = 20^\circ$	71
61	Local P_T/P_{T_∞} at 50% ACL, Fuselage 2, $M_\infty = 2.5$, $\alpha = 20^\circ$	73
62	Local Alpha at 30% ACL, Fuselage 1, $M_\infty = 2.5$, $\alpha = 20^\circ$	74
63	Local Alpha at 30% ACL, Fuselage 2, $M_\infty = 2.5$, $\alpha = 20^\circ$	75
64	Local Alpha at 50% ACL, Fuselage 1, $M_\infty = 2.5$, $\alpha = 20^\circ$	76
65	Local Alpha at 50% ACL, Fuselage 2, $M_\infty = 2.5$, $\alpha = 20^\circ$	77
66	Local Alpha at 30% ACL, Fuselage 1, $M_\infty = 2.5$, $\alpha = 20^\circ$, $\beta = -4^\circ$	78
67	Local Alpha at 30% ACL, Fuselage 1, $M_\infty = 2.5$, $\alpha = 20^\circ$, $\beta = 4^\circ$	79
68	Local Alpha at 50% ACL, Fuselage 2, $M_\infty = 2.5$, $\alpha = 20^\circ$, $\beta = -4^\circ$	80
69	Local Alpha at 50% ACL, Fuselage 1, $M_\infty = 2.5$, $\alpha = 20^\circ$, $\beta = 4^\circ$	81
70	Local Sigma at 30% ACL, Fuselage 1, $M_\infty = 2.5$, $\alpha = 20^\circ$	83
71	Local Sigma at 50% ACL, Fuselage 1, $M_\infty = 2.5$, $\alpha = 20^\circ$	84
72	Local Sigma at 50% ACL, Fuselage 2, $M_\infty = 2.5$, $\alpha = 20^\circ$, $\beta = 4^\circ$	85
73	Local Sigma at 50% ACL, Fuselage 2, $M_\infty = 2.5$, $\alpha = 20^\circ$, $\beta = 0^\circ$	86
74	Local Sigma at 50% ACL, Fuselage 2, $M_\infty = 2.5$, $\alpha = 20^\circ$, $\beta = -4^\circ$	87
75	Local Mach Number at 30% ACL, Fuselage 1, $M_\infty = 3.5$, $\alpha = 0^\circ$	88
76	Local Mach Number at 50% ACL, Fuselage 1, $M_\infty = 3.5$, $\alpha = 0^\circ$	89
77	Local Mach Number at 30% ACL, Fuselage 2, $M_\infty = 3.5$, $\alpha = 0^\circ$	90
78	Local Mach Number at 50% ACL, Fuselage 2, $M_\infty = 3.5$, $\alpha = 0^\circ$	91
79	Fuselage Static Pressure Distribution, $\theta = 0^\circ$, $M_\infty = 3.5$, $\alpha = 0^\circ$, $\beta = 0^\circ$	91
80	Local Mach Number at 50% ACL, Fuselage 1, $M_\infty = 3.5$, $\alpha = 0^\circ$, $\beta = -4^\circ$	93
81	Local Mach Number at 50% ACL, Fuselage 1, $M_\infty = 3.5$, $\alpha = 0^\circ$, $\beta = 4^\circ$	94

LIST OF ILLUSTRATIONS (Cont'd)

VOLUME II

<u>Figure</u>	<u>Description</u>	<u>Page</u>
82	Local P_T/P_{T_∞} at 30% ACL, Fuselage 1, $M_\infty = 3.5$, $\alpha = 0^\circ$	95
83	Local P_T/P_{T_∞} at 30% ACL, Fuselage 2, $M_\infty = 3.5$, $\alpha = 0^\circ$	96
84	Local P_T/P_{T_∞} at 50% ACL, Fuselage 1, $M_\infty = 3.5$, $\alpha = 0^\circ$	98
85	Local P_T/P_{T_∞} at 50% ACL, Fuselage 2, $M_\infty = 3.5$, $\alpha = 0^\circ$	99
86	Local P_T/P_{T_∞} at 50% ACL, Fuselage 1, $M_\infty = 3.5$, $\alpha = 0^\circ$, $\beta = -4^\circ$	100
87	Local P_T/P_{T_∞} at 50% ACL, Fuselage 1, $M_\infty = 3.5$, $\alpha = 0^\circ$, $\beta = 4^\circ$	101
88	Local Alpha at 30% ACL, Fuselage 1, $M_\infty = 3.5$, $\alpha = 0^\circ$	102
89	Local Alpha at 30% ACL, Fuselage 2, $M_\infty = 3.5$, $\alpha = 0^\circ$	103
90	Local Alpha at 50% ACL, Fuselage 1, $M_\infty = 3.5$, $\alpha = 0^\circ$	104
91	Local Alpha at 50% ACL, Fuselage 2, $M_\infty = 3.5$, $\alpha = 0^\circ$	105
92	Local Alpha at 30% ACL, Fuselage 1, $M_\infty = 3.5$, $\alpha = 0^\circ$, $\beta = -4^\circ$	106
93	Local Alpha at 30% ACL, Fuselage 1, $M_\infty = 3.5$, $\alpha = 0^\circ$, $\beta = 4^\circ$	107
94	Local Alpha at 50% ACL, Fuselage 1, $M_\infty = 3.5$, $\alpha = 0^\circ$, $\beta = -4^\circ$	108
95	Local Alpha at 50% ACL, Fuselage 1, $M_\infty = 3.5$, $\alpha = 0^\circ$, $\beta = 4^\circ$	109
96	Local Sigma at 30% ACL, Fuselage 1, $M_\infty = 3.5$, $\alpha = 0^\circ$	111
97	Local Sigma at 30% ACL, Fuselage 2, $M_\infty = 3.5$, $\alpha = 0^\circ$	112
98	Local Sigma at 50% ACL, Fuselage 1, $M_\infty = 3.5$, $\alpha = 0^\circ$	113
99	Local Sigma at 50% ACL, Fuselage 2, $M_\infty = 3.5$, $\alpha = 0^\circ$	114
100	Local Sigma at 30% ACL, Fuselage 1, $M_\infty = 3.5$, $\alpha = 0^\circ$, $\beta = -4^\circ$	115
101	Local Sigma at 30% ACL, Fuselage 2, $M_\infty = 3.5$, $\alpha = 0^\circ$, $\beta = 4^\circ$	116
102	Local Sigma at 50% ACL, Fuselage 1, $M_\infty = 3.5$, $\alpha = 0^\circ$, $\beta = -4^\circ$	117
103	Local Sigma at 50% ACL, Fuselage 2, $M_\infty = 3.5$, $\alpha = 0^\circ$, $\beta = 4^\circ$	118
104	Local Sigma at 50% ACL, Fuselage 1, $M_\infty = 3.5$, $\alpha = 0^\circ$, $\beta = -4^\circ$	119
105	Local Mach Number at 30% ACL, Fuselage 1, $M_\infty = 3.5$, $\alpha = 10^\circ$	120
106	Local Mach Number at 50% ACL, Fuselage 1, $M_\infty = 3.5$, $\alpha = 10^\circ$	121
107	Local Mach Number at 50% ACL, Fuselage 2, $M_\infty = 3.5$, $\alpha = 10^\circ$	123
108	Local Mach Number at 50% ACL, Fuselage 1, $M_\infty = 3.5$, $\alpha = 10^\circ$, $\beta = -4^\circ$	124
109	Local Mach Number at 50% ACL, Fuselage 1, $M_\infty = 3.5$, $\alpha = 10^\circ$, $\beta = 4^\circ$	125

LIST OF ILLUSTRATIONS (Cont'd)

VOLUME II

<u>Figure</u>	<u>Description</u>	<u>Page</u>
110	Local P_T/P_{T_∞} at 30% ACL, Fuselage 2, $M_\infty = 3.5$, $\alpha = 10^\circ$	126
111	Local P_T/P_{T_∞} at 50% ACL, Fuselage 2, $M_\infty = 3.5$, $\alpha = 10^\circ$	127
112	Local Alpha at 30% ACL, Fuselage 1, $M_\infty = 3.5$, $\alpha = 10^\circ$	128
113	Local Alpha at 30% ACL, Fuselage 2, $M_\infty = 3.5$, $\alpha = 10^\circ$	129
114	Local Alpha at 50% ACL, Fuselage 1, $M_\infty = 3.5$, $\alpha = 10^\circ$	131
115	Local Alpha at 50% ACL, Fuselage 2, $M_\infty = 3.5$, $\alpha = 10^\circ$	132
116	Local Alpha at 50% ACL, Fuselage 1, $M_\infty = 3.5$, $\alpha = 10^\circ$, $\beta = 4^\circ$	133
117	Local Alpha at 50% ACL, Fuselage 1, $M_\infty = 3.5$, $\alpha = 10^\circ$, $\beta = -4^\circ$	134
118	Local Sigma at 30% ACL, Fuselage 1, $M_\infty = 3.5$, $\alpha = 10^\circ$	135
119	Local Sigma at 50% ACL, Fuselage 1, $M_\infty = 3.5$, $\alpha = 10^\circ$	136
120	Local Sigma at 50% ACL, Fuselage 1, $M_\infty = 3.5$, $\alpha = 10^\circ$, $\beta = -4^\circ$	137
121	Local Sigma at 50% ACL, Fuselage 1, $M_\infty = 3.5$, $\alpha = 10^\circ$, $\beta = 4^\circ$	138
122	Local Sigma at 50% ACL, Fuselage 2, $M_\infty = 3.5$, $\alpha = 10^\circ$, $\beta = -4^\circ$	139
123	Local Sigma at 50% ACL, Fuselage 2, $M_\infty = 3.5$, $\alpha = 10^\circ$, $\beta = 4^\circ$	140
124	Local Mach Number at 30% ACL, Fuselage 1, $M_\infty = 3.5$, $\alpha = 20^\circ$	142
125	Local Mach Number at 50% ACL, Fuselage 1, $M_\infty = 3.5$, $\alpha = 20^\circ$	143
126	Local Mach Number at 50% ACL, Fuselage 2, $M_\infty = 3.5$, $\alpha = 20^\circ$	144
127	Local Mach Number at 50% ACL, Fuselage 1, $M_\infty = 3.5$, $\alpha = 20^\circ$, $\beta = -4^\circ$	145
128	Local Mach Number at 50% ACL, Fuselage 1, $M_\infty = 3.5$, $\alpha = 20^\circ$, $\beta = 4^\circ$	146
129	Local P_T/P_{T_∞} at 50% ACL, Fuselage 1, $M_\infty = 3.5$, $\alpha = 20^\circ$	147
130	Local P_T/P_{T_∞} at 50% ACL, Fuselage 2, $M_\infty = 3.5$, $\alpha = 20^\circ$	148
131	Local Alpha at 30% ACL, Fuselage 1, $M_\infty = 3.5$, $\alpha = 20^\circ$	149

LIST OF ILLUSTRATIONS (Cont'd)

VOLUME II

<u>Figure</u>	<u>Description</u>	<u>Page</u>
132	Local Alpha at 30% ACL, Fuselage 2, $M_\infty = 3.5$, $\alpha = 20^\circ$	150
133	Local Alpha at 50% ACL, Fuselage 1, $M_\infty = 3.5$, $\alpha = 20^\circ$	152
134	Local Alpha at 50% ACL, Fuselage 2, $M_\infty = 3.5$, $\alpha = 20^\circ$	153
135	Local Alpha at 30% ACL, Fuselage 1, $M_\infty = 3.5$, $\alpha = 20^\circ$, $\beta = -4^\circ$	154
136	Local Alpha at 30% ACL, Fuselage 1, $M_\infty = 3.5$, $\alpha = 20^\circ$, $\beta = 4^\circ$	155
137	Local Alpha at 50% ACL, Fuselage 1, $M_\infty = 3.5$, $\alpha = 20^\circ$, $\beta = -4^\circ$	156
138	Local Alpha at 50% ACL, Fuselage 1, $M_\infty = 3.5$, $\alpha = 20^\circ$, $\beta = 4^\circ$	157
139	Local Sigma at 30% ACL, Fuselage 1, $M_\infty = 3.5$, $\alpha = 20^\circ$	158
140	Local Sigma at 50% ACL, Fuselage 1, $M_\infty = 3.5$, $\alpha = 20^\circ$	159
141	Local Sigma at 50% ACL, Fuselage 1, $M_\infty = 3.5$, $\alpha = 20^\circ$, $\beta = -4^\circ$	160
142	Local Sigma at 50% ACL, Fuselage 1, $M_\infty = 3.5$, $\alpha = 20^\circ$, $\beta = 4^\circ$	161
143	Average Total Pressure Recovery, $M_\infty = 2.5$	165
144	Average Total Pressure Recovery, $M_\infty = 3.5$	166
145	Average Steady State Distortion, $M_\infty = 2.5$	167
146	Average Steady State Distortion, $M_\infty = 3.5$	168
147	Average Local Angle of Attack, $M_\infty = 2.5$	169
148	Average Local Angle of Attack, $M_\infty = 3.5$	170
149	Average Local Sidewash, $M_\infty = 2.5$	171
150	Average Local Sidewash, $M_\infty = 3.5$	172

SECTION I

INTRODUCTION

This report is the second of two volumes presenting the results of an investigation closely related to a recently completed USAF contract, F33615-68-C-1658, "Investigation of Airframe - Inlet Interactions." Both programs are part of a large effort within the USAF and NASA to develop propulsion system design criteria for supersonic air superiority fighter aircraft. In contract 1658, airframe and inlet models were designed and tested in the NASA Ames Research Center 6' x 6' and 8' x 7' supersonic wind tunnels in order to define the effect of airframe design features on inlet flow fields and inlet performance for a wide range of supersonic air superiority aircraft designs.

In the investigation outlined in the first volume of this document, much of the same hardware employed in contract 1658 was used in the wind tunnel tests in order to supplement and expand the information generated in this program. The models and tests were designed to produce an extremely wide range of parametric airframe flow field data within a reasonable tunnel occupancy time. In particular, the versatile building block model design concept employed in that contract made it possible for both programs to provide a relatively large bank of parametric, systems-oriented, experimental data.

The present program had four major objectives. One objective was to gain a better understanding of the effect of geometry variations on inlet flow fields. The geometry variations included fuselage nose droop, body camber, canopy shape, aerodynamic control surfaces, and weapon installations. The second objective was to establish the effects of yawed flight on inlet flow fields. The third major objective was to establish the important effects of fuselage design on inlet flow fields of higher design Mach number aircraft such as the advanced manned interceptor. Boundary layer growth characteristics were to be defined for various fuselage shapes as was the axial progression of flow field properties around the entire periphery of these shapes for various Mach numbers and vehicle attitudes.

The subject of this volume deals with the third major objective mentioned above, namely, the effects of fuselage design at various angles of attack and yaw, on inlet flow fields of higher design Mach number aircraft such as the advanced manned interceptor type.

SECTION II

SUMMARY

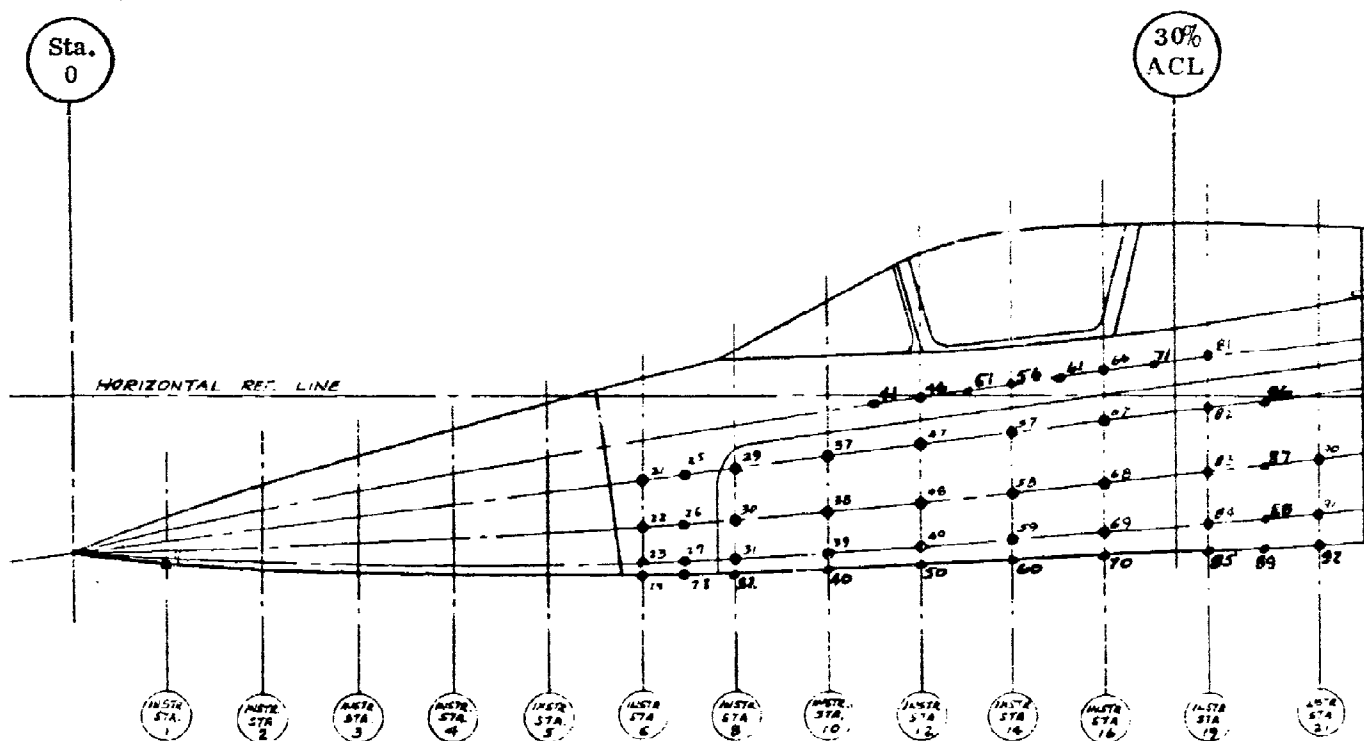
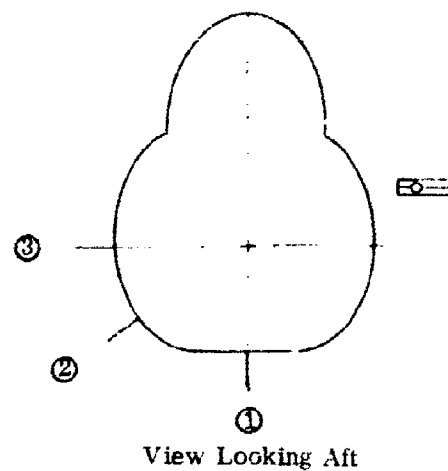
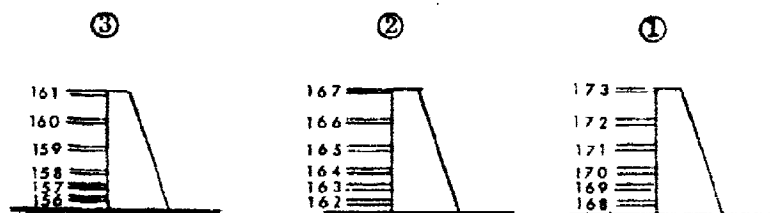
The results reported here were obtained from tests made at Mach numbers of 2.5 and 3.5, conducted in the 8' x 7' wind tunnel of the NASA Ames Research Center. The basic model configuration used for these tests is representative of a typical high design Mach number aircraft. The model itself was built up from a basic Contract 1658 model, modified by the incorporation of a high fineness ratio nose and canopy.

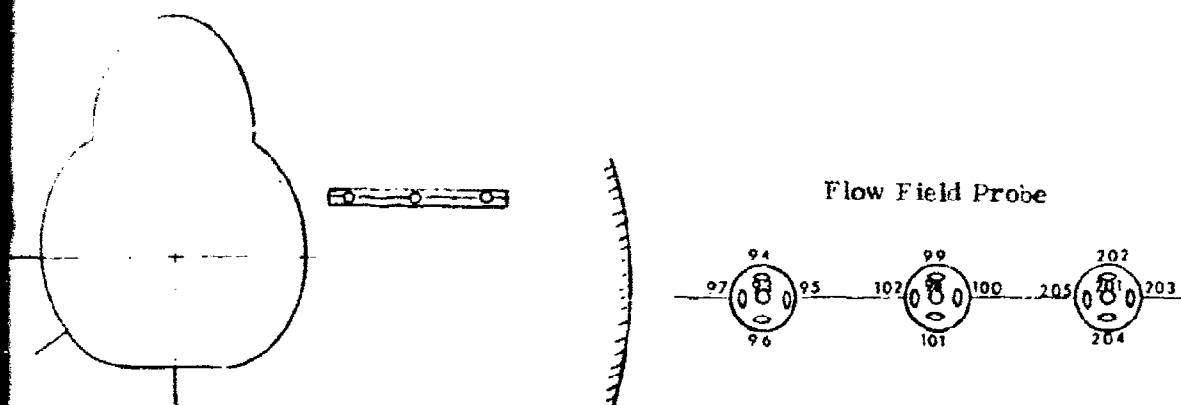
The design of this high design Mach number fuselage model also permitted studying two basic fuselage cross section shapes having two different lower shoulder radii - one small, the other large. Complete design details, including schematics of the model, are given in Volume I of this document.

Data production focused primarily on acquiring flow field data in the region adjacent to the side of the fuselage at the 30% and 50% ACL longitudinal locations. Surface static pressure distributions were also obtained in the various meridional plane intersections shown in Figure 1. This data was reduced and flow field maps of local Mach number, total pressure recovery, angles of attack and yaw, and fuselage static pressure distributions generated.

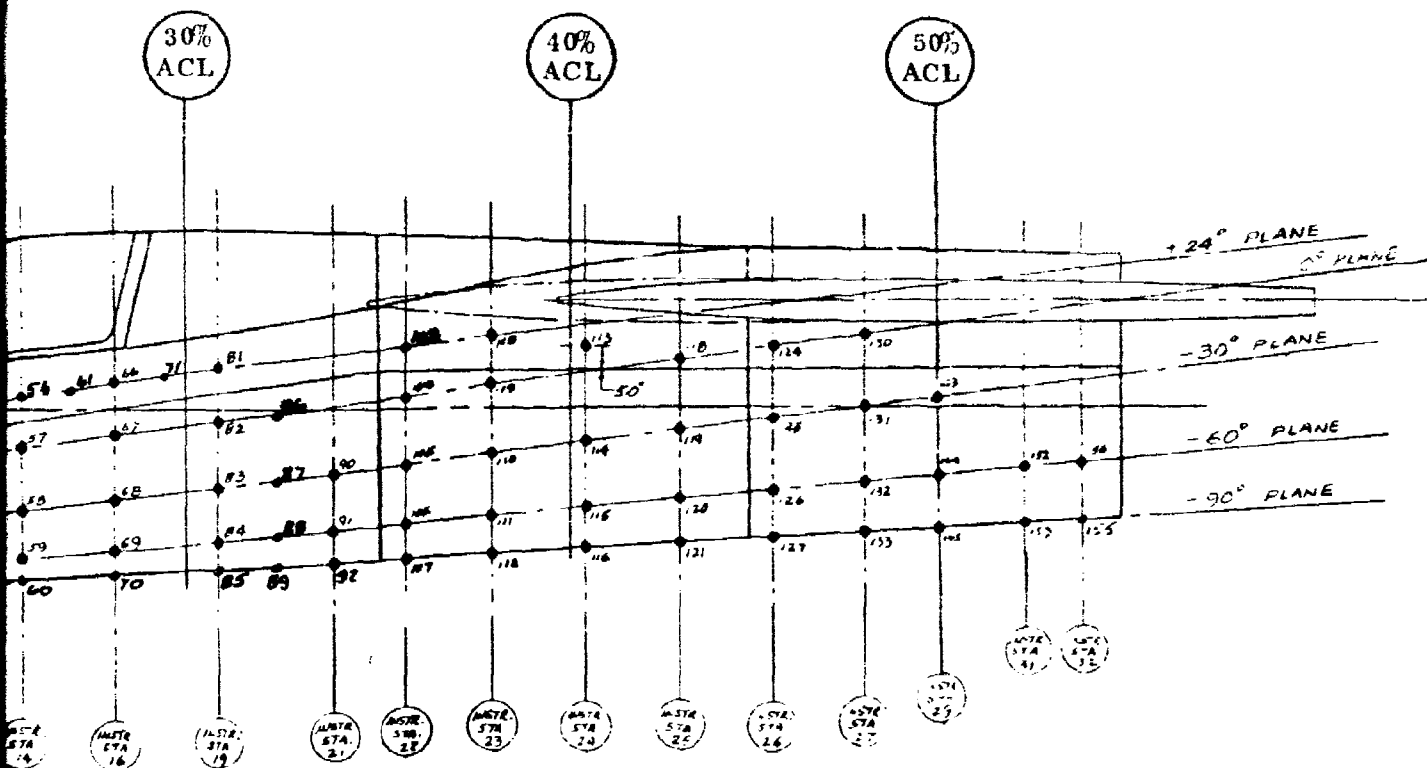
1

Boundary Layer Rakes





①
View Looking Aft



SECTION V

DATA ANALYSIS

3.0 GENERAL

This section presents an analysis of the flow field data obtained in the 8' x 7' wind tunnel of the NASA Ames Research Center. The influence of fuselage geometry and vehicle attitude, relative to free-stream direction, upon the local flow field properties of Mach number, total pressure recovery, angle of attack, and angle of yaw are discussed. The results are grouped according to test Mach number, with the Mach 2.5 data discussed first, followed by the Mach 3.5 results.

3.1 Mach Number 2.5

3.1.1 Low Angle of Attack

3.1.1.1 Local Mach Number

3.1.1.1.1 Effect of Vehicle Geometry

At zero angle of attack the local Mach numbers in the regions of the flow field surveyed do not vary appreciably from the free stream value. This can be seen by an examination of Figures 2 to 5 where the local Mach numbers are presented for fuselages 1 and 2 at two axial locations, namely, the 30% and 50% ACL stations, respectively. Inspection of the inboard and outboard regions (the first and last columns) of Figures 2 and 3 shows a decrease in local Mach number in the outboard direction. This is to be expected since the outboard region is not affected as much as the inboard region by the flow expansion which takes place along the side of the fuselage downstream of the conical-like nose tip. This effect was seen previously at the lower Mach number test conditions.

A direct effect of the differences in the geometry of fuselages 1 and 2 can be seen in the lower Mach numbers measured in the lower inboard region of Figure 2 as compared to Figure 3. This difference in flow field diffusion is attributed to the differences in the body cross-section geometry in this region; i. e., fuselage 1, by virtue of its greater width in this region, produces relatively more sideward displacement (compression) than does fuselage 2 with its slimmer bottom.

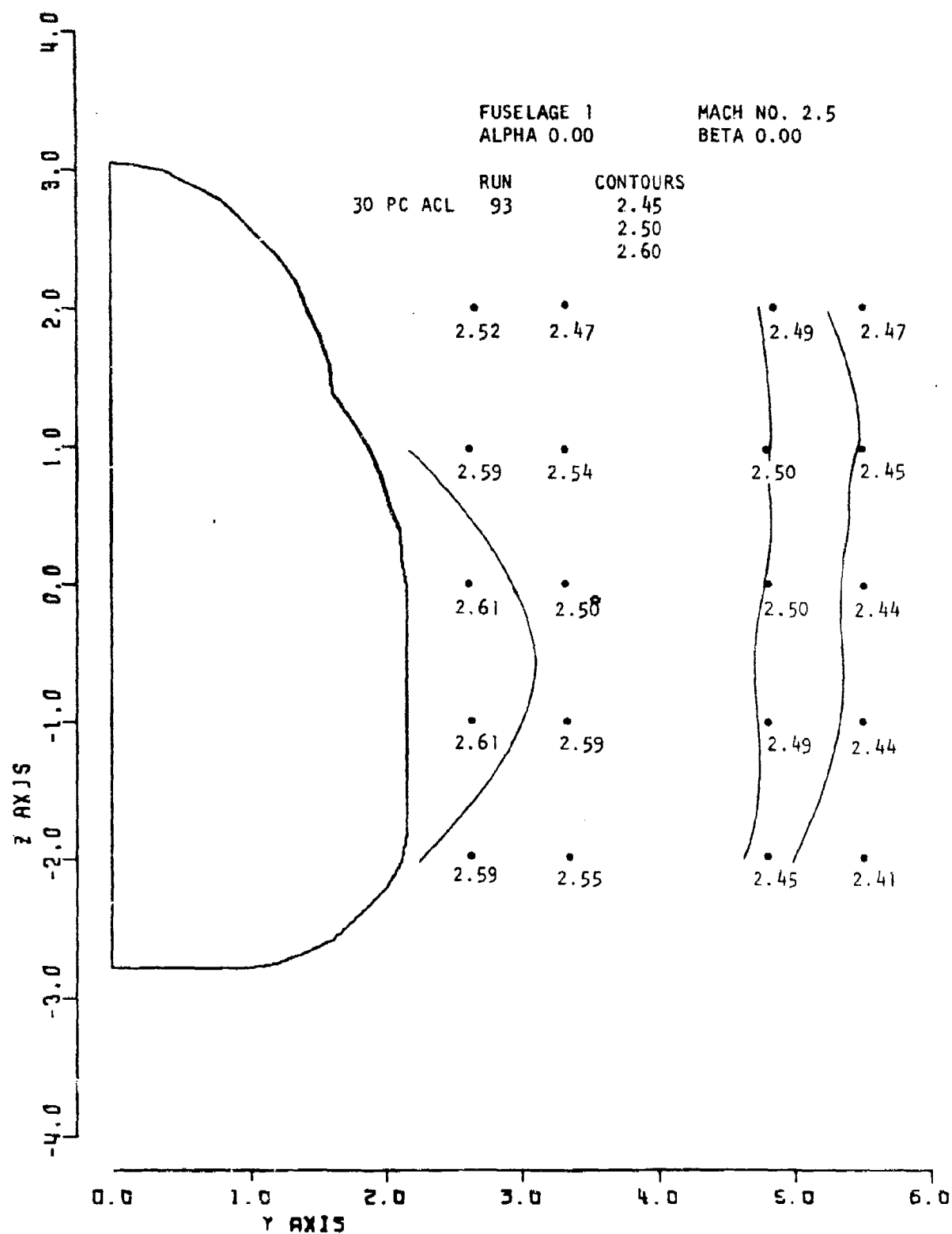


Figure 2. Local Mach No.

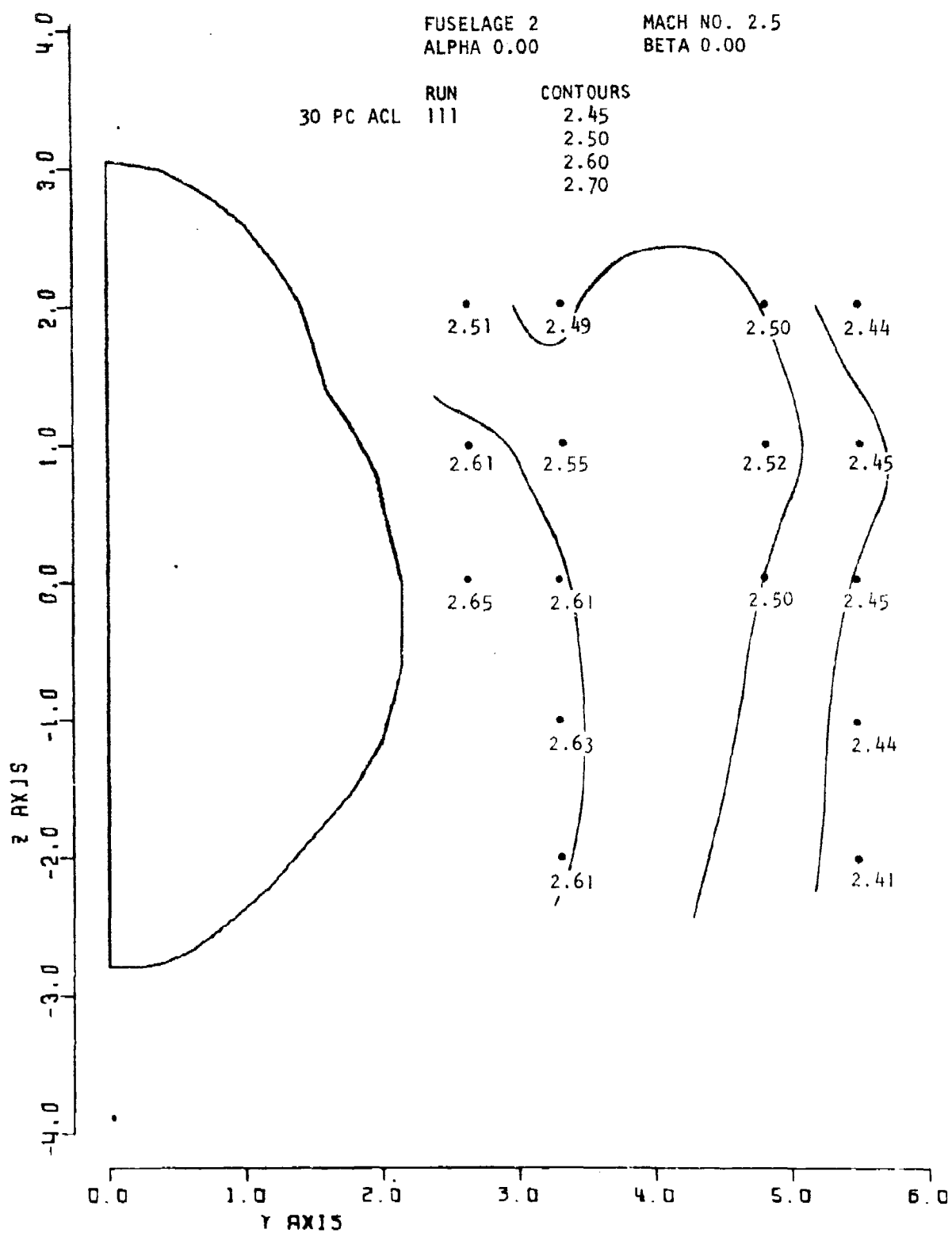


Figure 3. Local Mach No.

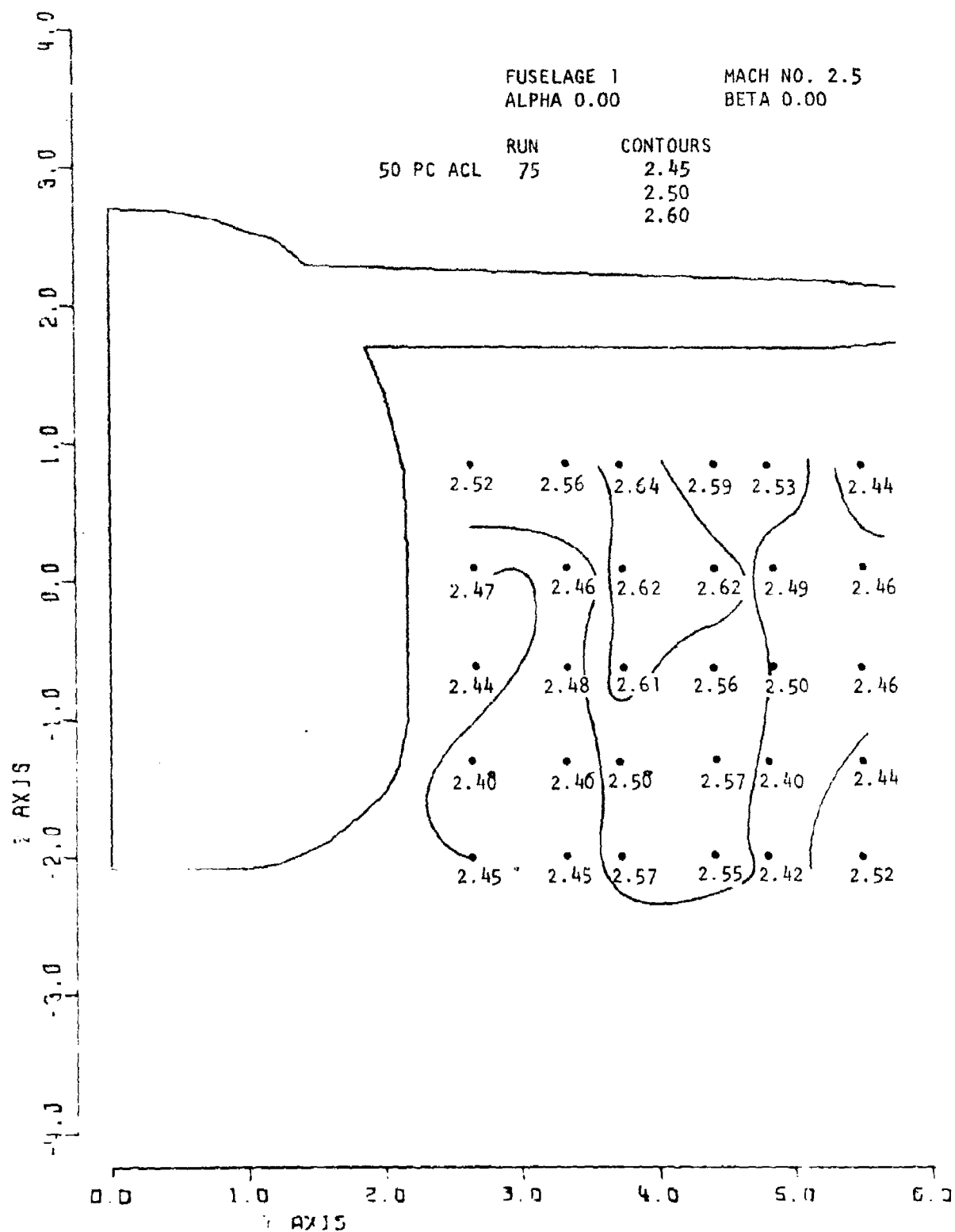


Figure 4. Local Mach No.

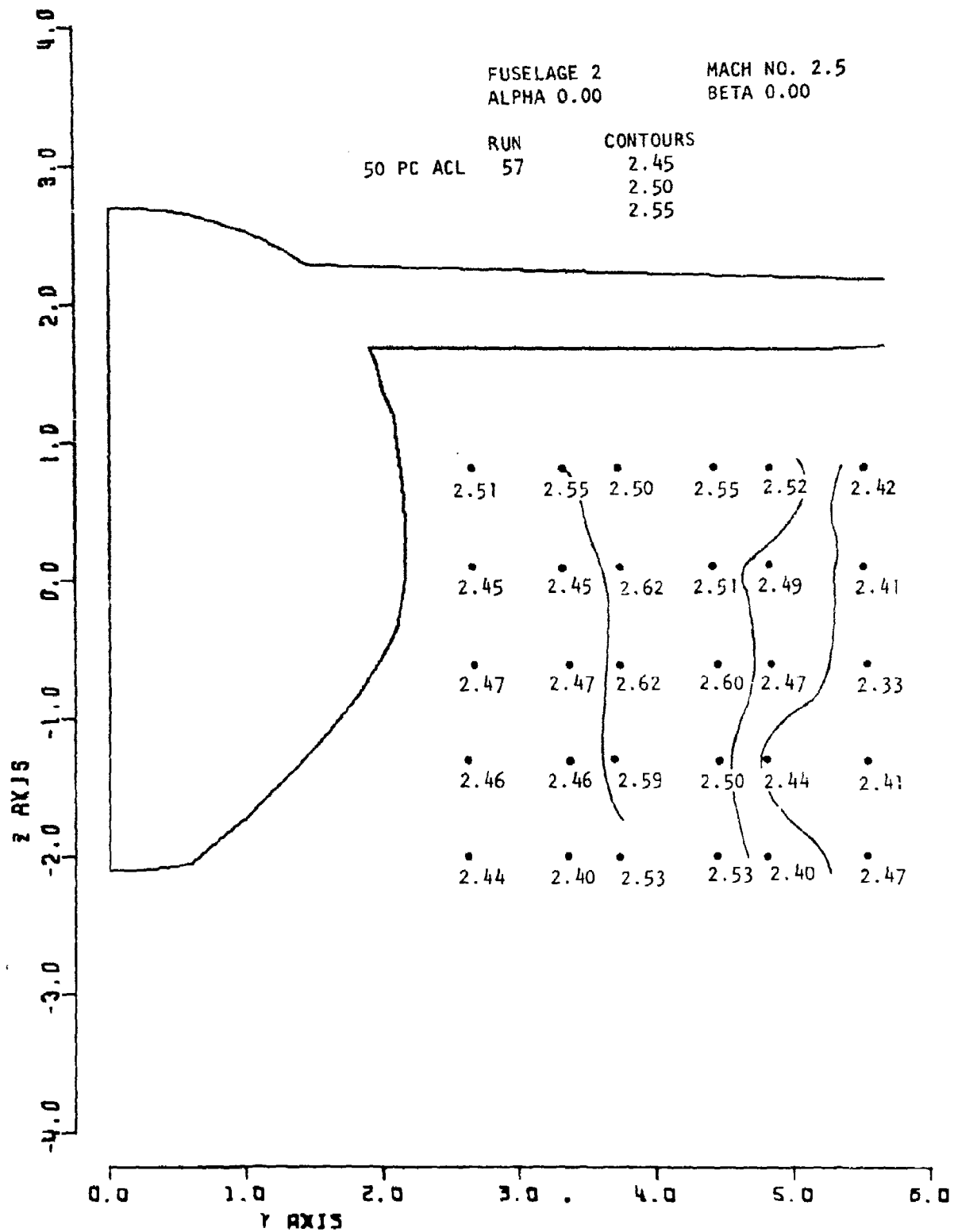


Figure 5. Local Mach No.

Figures 2 and 3 also show local Mach numbers in the upper region (first and second rows of data points) which are less than those in the lower regions. This is probably due to the canopy-induced compression together with the more pronounced compression along the top contour of the fuselage, due to the nose droop, as compared to the bottom contour. Further downstream, however, at the 50% ACL station, the Mach numbers in the upper region as shown in Figures 4 and 5 are somewhat higher than those below. This region is evidently affected by both the flow-expansion along the top and sides of the canopy as well as the local expansion of the flow along the wing undersurface downstream of its leading edge. It should be noted that, with the exception of the uppermost row, the local Mach numbers at the 50% ACL station are in general lower for both fuselages, than at the 30% ACL station, due primarily to the wing induced compression and a recovery from the over-expansion along the side of the fuselage. Figures 4 and 5 also show very little effect of the differences in the shapes of the lower portions of fuselages 1 and 2 on the local Mach numbers in that region, as compared to the values measured at the 30% ACL station shown in Figures 3 and 4.

3.1.1.1.2 Effect of Yaw

The effect of yaw (sideslip) at zero angle of attack at Mach 2.5 is illustrated in Figures 6 to 9 for fuselage 1 and Figures 10 to 13 for fuselage 2. In general, the primary effect of yaw, relative to the unyawed case, is to increase slightly the local Mach numbers on the leeward side and lower those on the windward side, as may be seen by comparing Figures 6 and 7 with Figure 2. Examination of the local Mach numbers at the 30% and 50% ACL stations for either fuselage indicates more or less the same fuselage geometry, canopy, and wing induced influences at work as the unyawed case at this low angle of attack.

3.1.1.2 Total Pressure Recovery

3.1.1.2.1 Effect of Vehicle Geometry

Figures 14 to 17 show relatively low canopy, fuselage and wing induced losses as evidenced by the relatively high pressure recoveries measured for both fuselages at this low angle of attack condition at the two survey stations. Moreover, little, if any, effect of fuselage geometry differences on the pressure recovery is discernible in the lower inboard regions of the flow field, as shown in Figures 14 and 15 for the forward flow survey station. The same is true for the aft station, as may be seen

from Figures 16 and 17, where the pressure recoveries for both fuselages 1 and 2 are generally the same, but lower than the values obtained at the upstream station shown in Figures 14 and 15. These lower recoveries appear due to canopy and wing generated shock wave losses which manifest themselves at the aft survey station.

3.1.1.2.2 Effect of Yaw

The effect of yaw on the low angle of attack pressure recovery in the flow survey regions adjacent to the windward and leeward sides of the fuselage for both fuselages was found to be small. In general the total pressure recoveries for the leeward side were only slightly higher than for the unyawed case, as may be seen by comparing Figure 18 with Figure 16, whereas those on the windward side showed very little decrease from the unyawed case. Apparently, for this combination of low-drag nose and canopy shape, the modulation in shock wave strength is negligibly small at low angle of attack for the angles of yaw tested ($\pm 4^\circ$).

3.1.1.3 Local Alpha

3.1.1.3.1 Effect of Vehicle Geometry

The local angles of attack measured at the fore and aft survey stations are shown in Figures 19 and 20 for fuselage 1, and in Figures 21 and 22 for fuselage 2. For this zero angle of attack condition negative local angles of attack are indicative of a canopy produced downwash at the 30% ACL station, and a wing induced downwash at the 50% ACL station. Due to the nose droop the canopy pressure field at this angle of attack is stronger than that of the lower fuselage, with the result that a downward pressure gradient is established which gives rise to the downwash pattern observed at the forward station.

A comparison of Figure 19 and 21 indicates that the canopy pressure field is able to drive somewhat further down into the flow field for fuselage 2 than for fuselage 1 as evidenced by the slightly larger downwash values for fuselage 2. This is undoubtedly due to the greater ability of the smaller corner of fuselage 1 to segregate, or isolate, the bottom and side pressure fields as compared to fuselage 2, a characteristic feature which had been pointed out earlier in Volume I of this report.

At the aft station the wing pressure field comes into play, increasing slightly the downwash in the upper portions of the survey region. The estimated region of

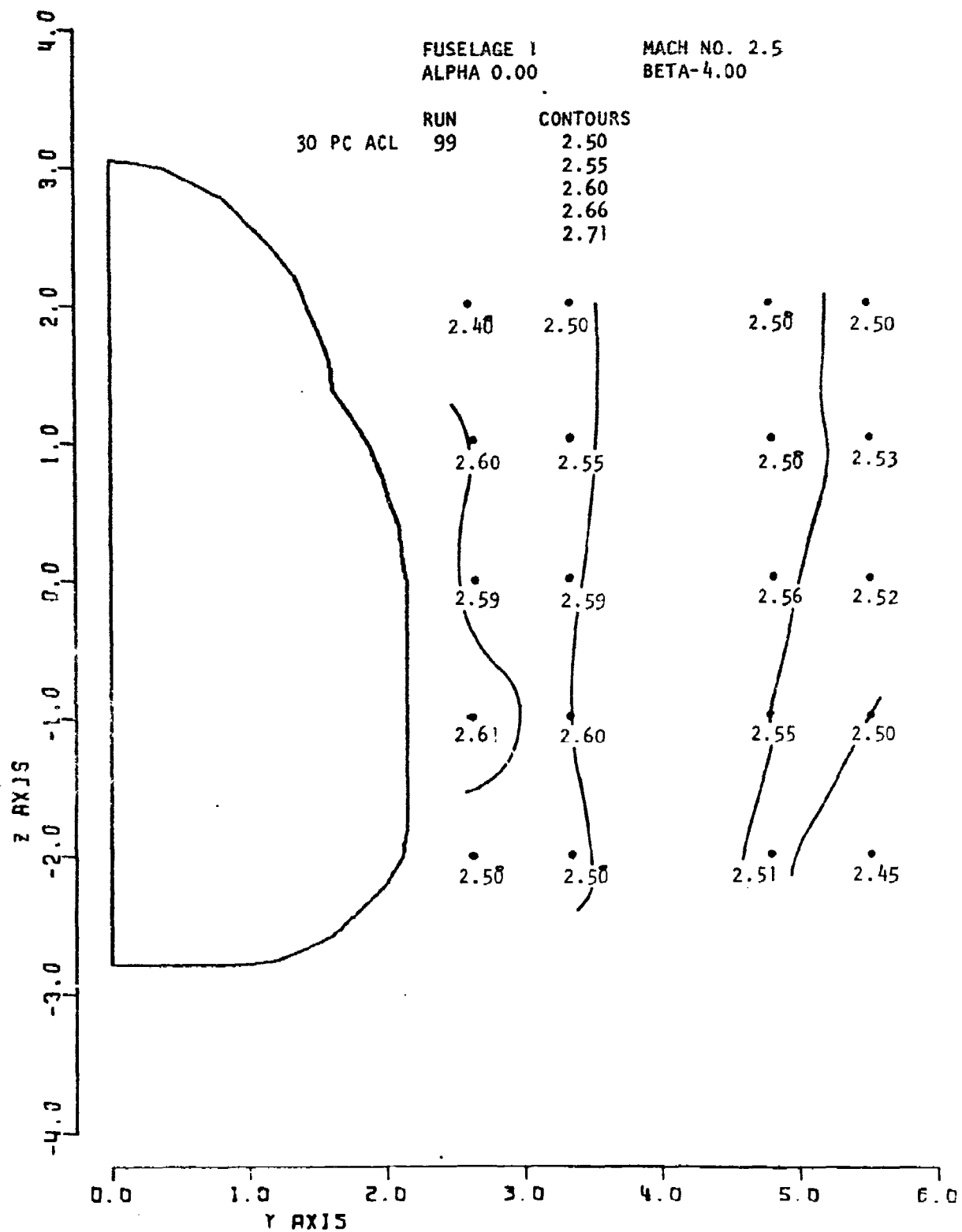


Figure 6. Local Mach No.

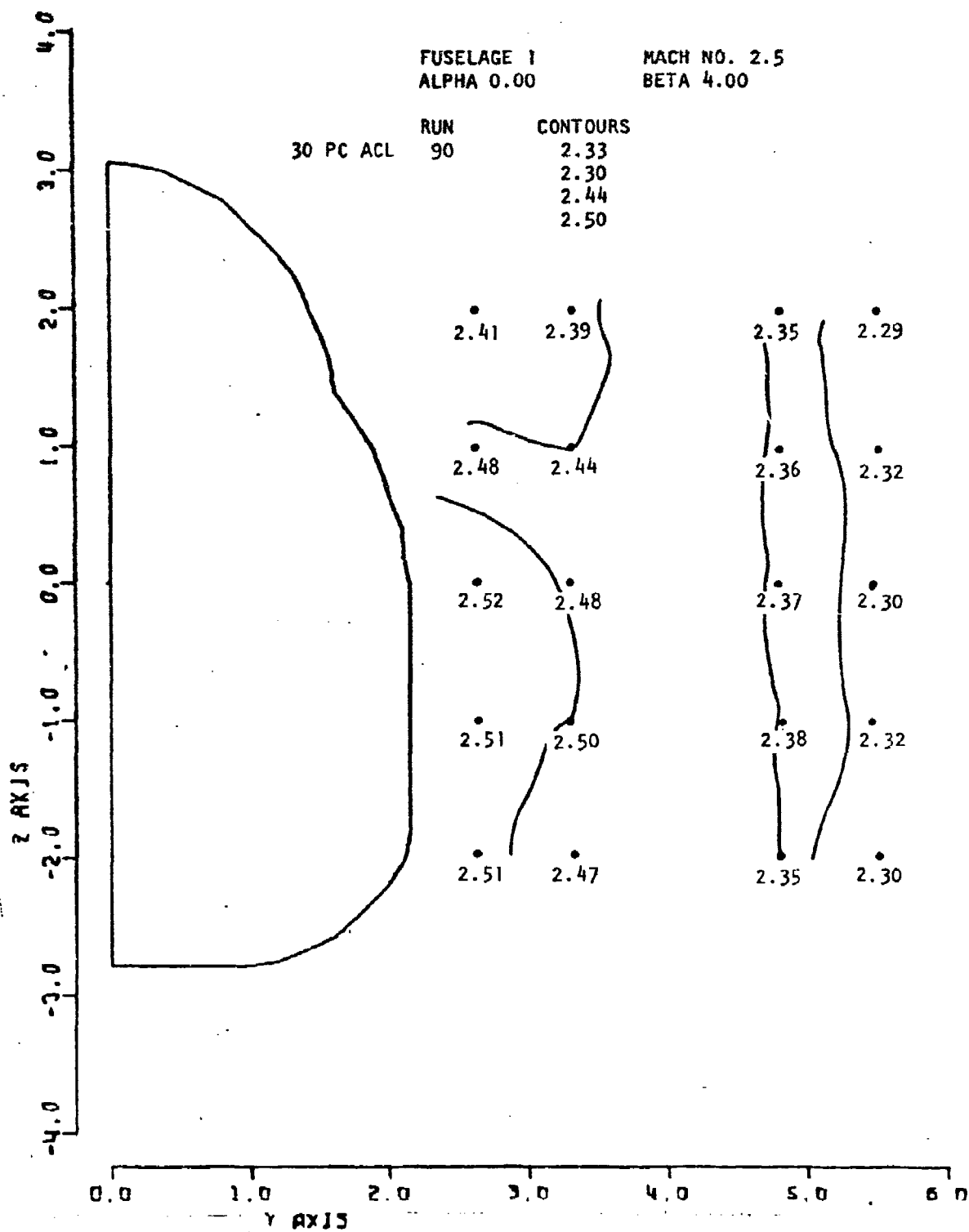


Figure 7. Local Mach No.

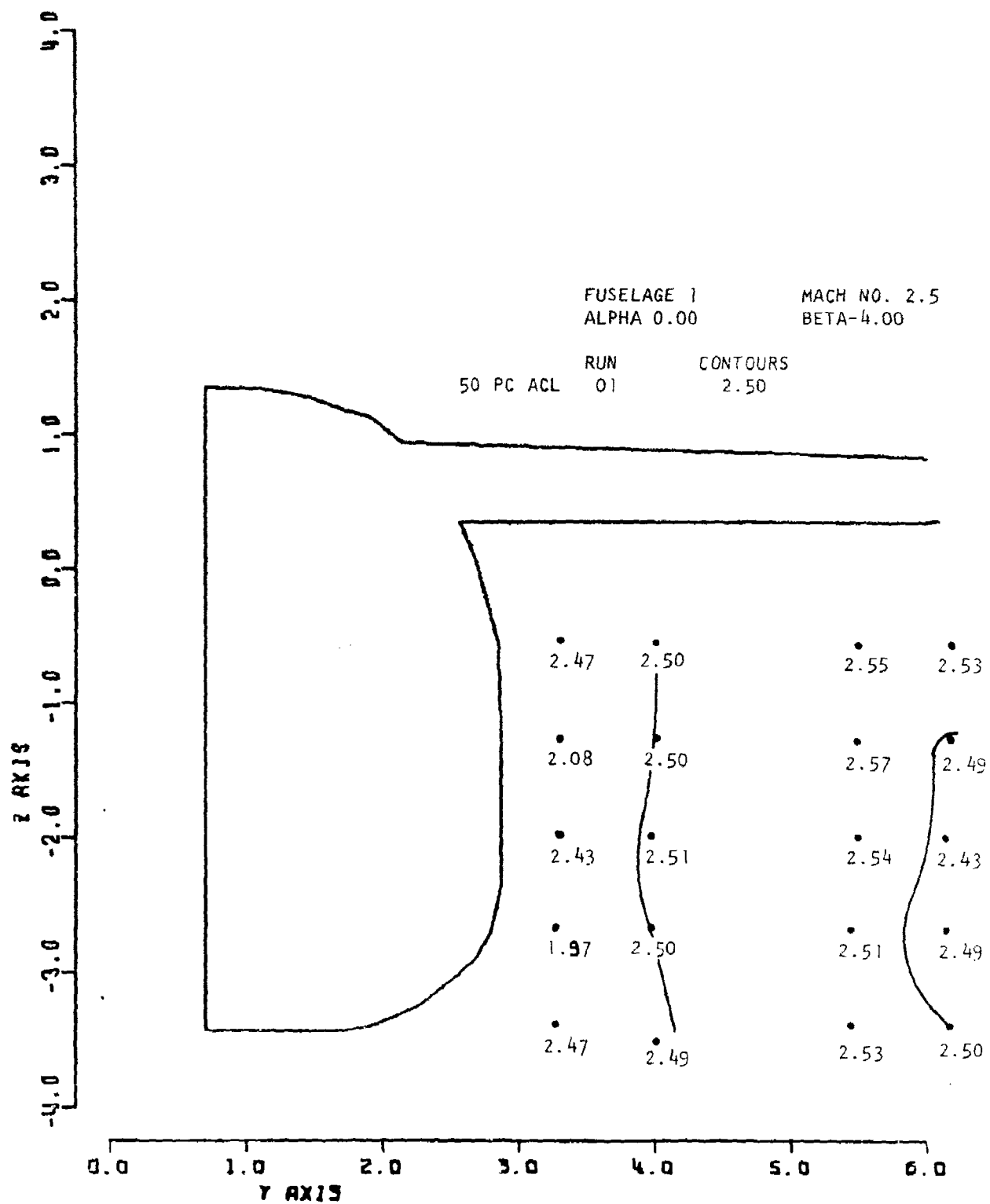


Figure 8. Local Mach No.

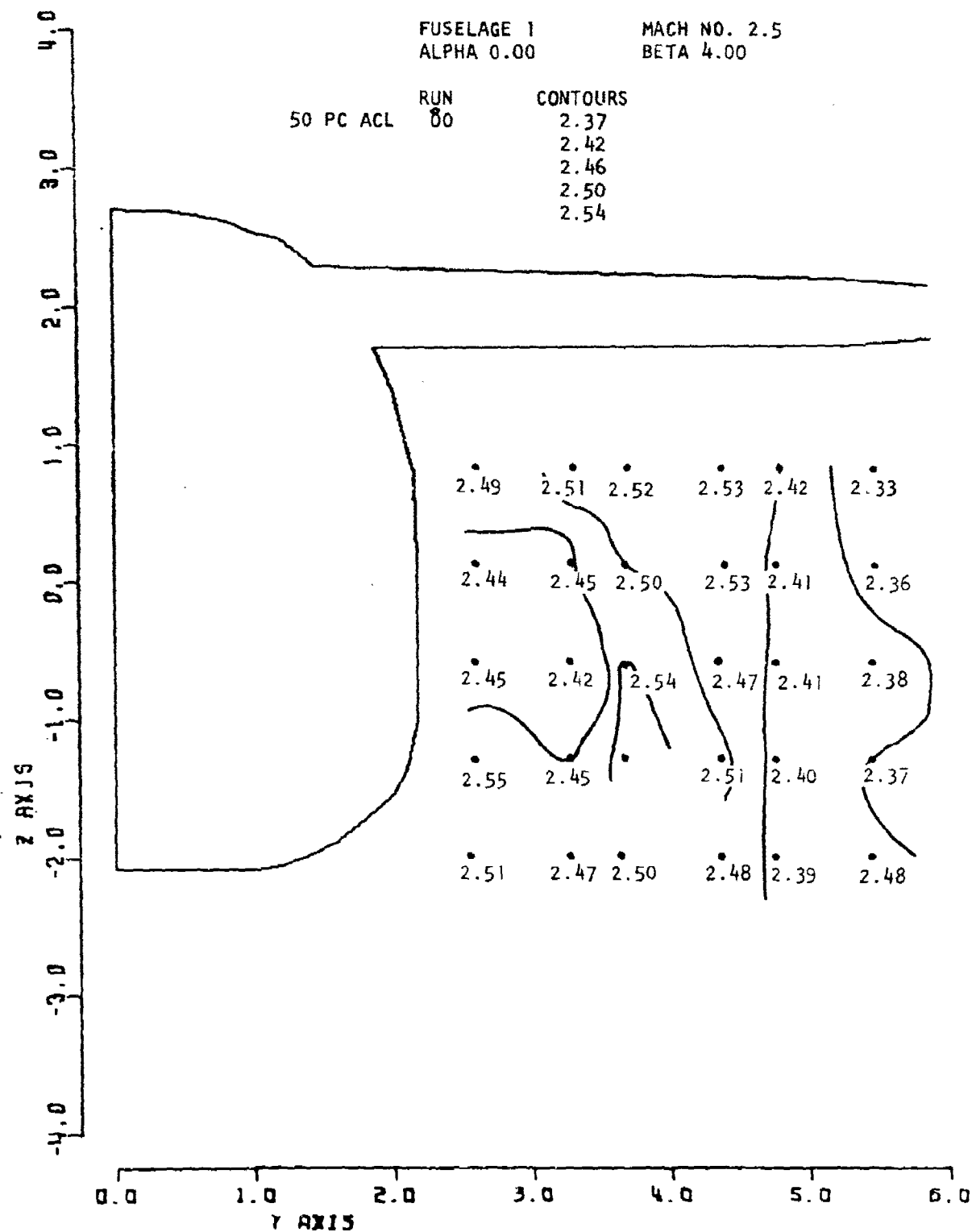


Figure 9. Local Mach No.

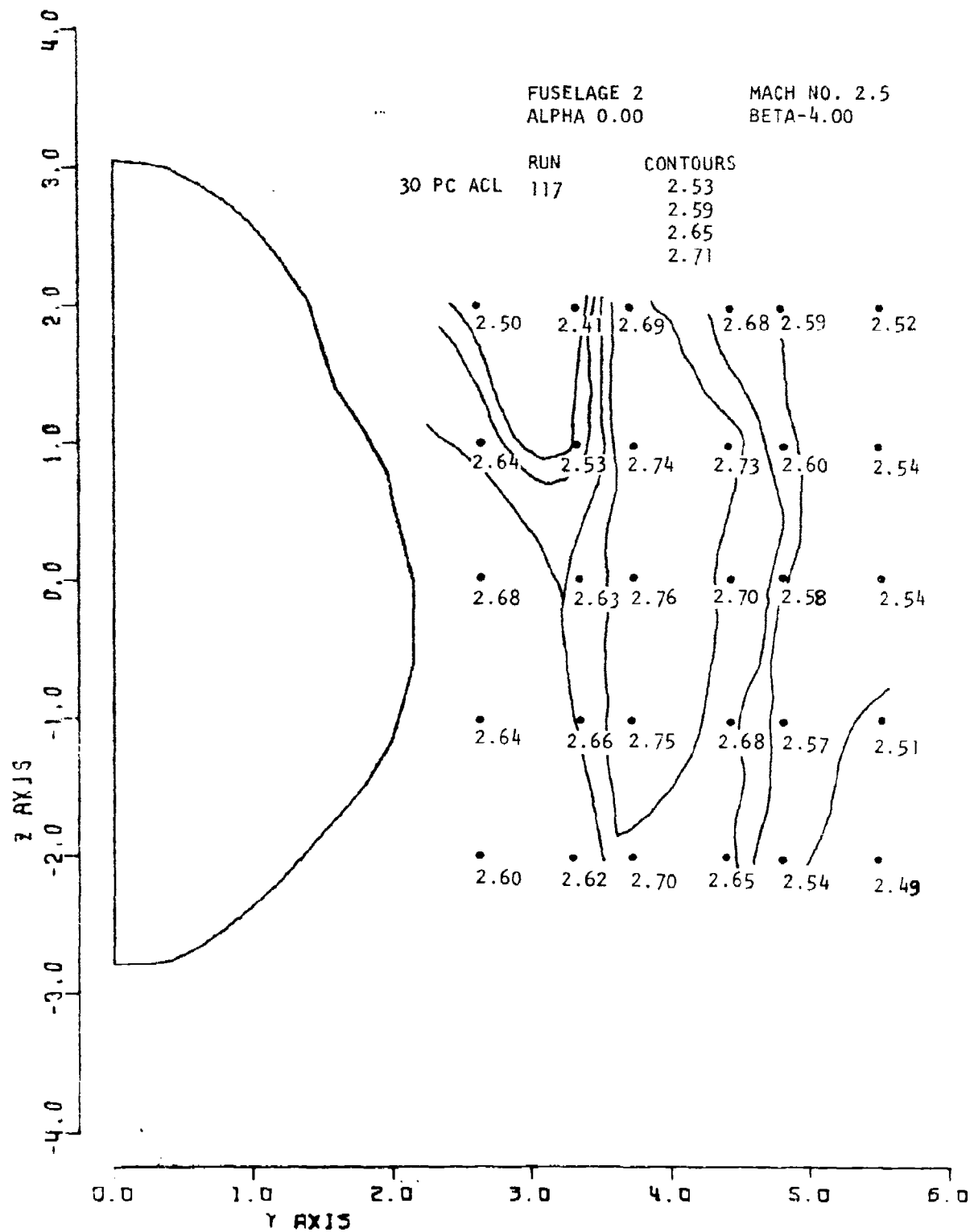


Figure 10. Local Mach No.

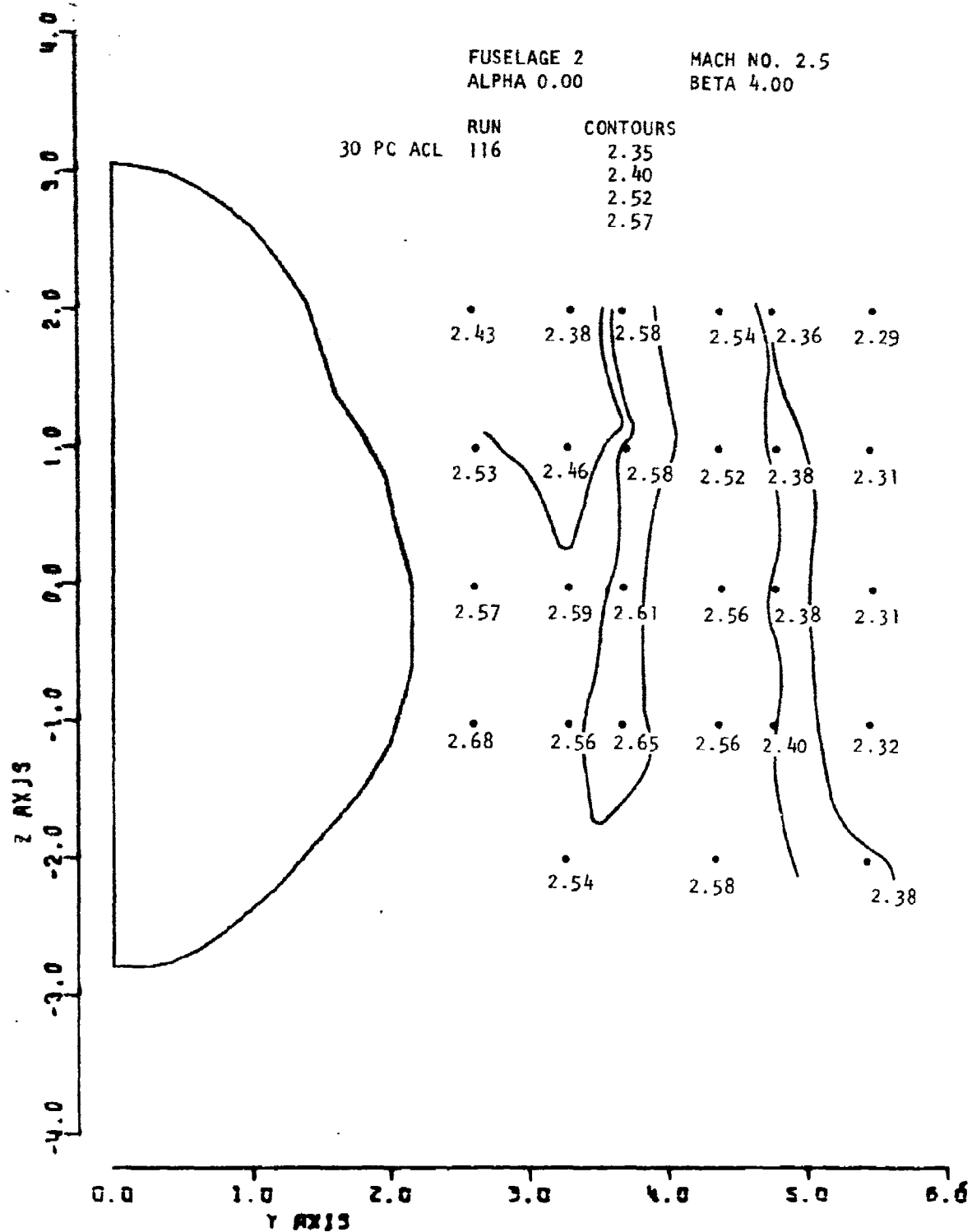


Figure 11. Local Mach No.

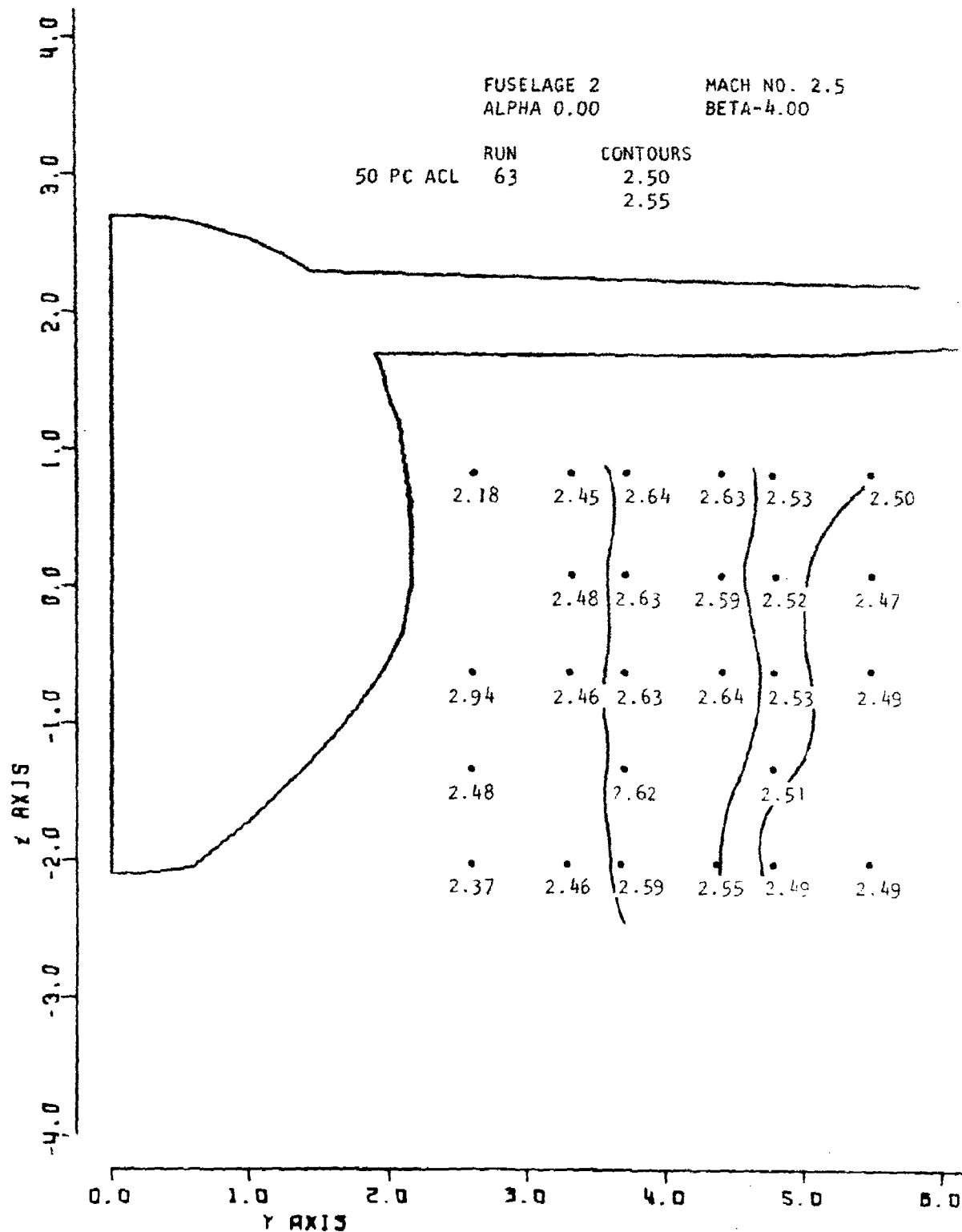


Figure 12. Local Mach No.

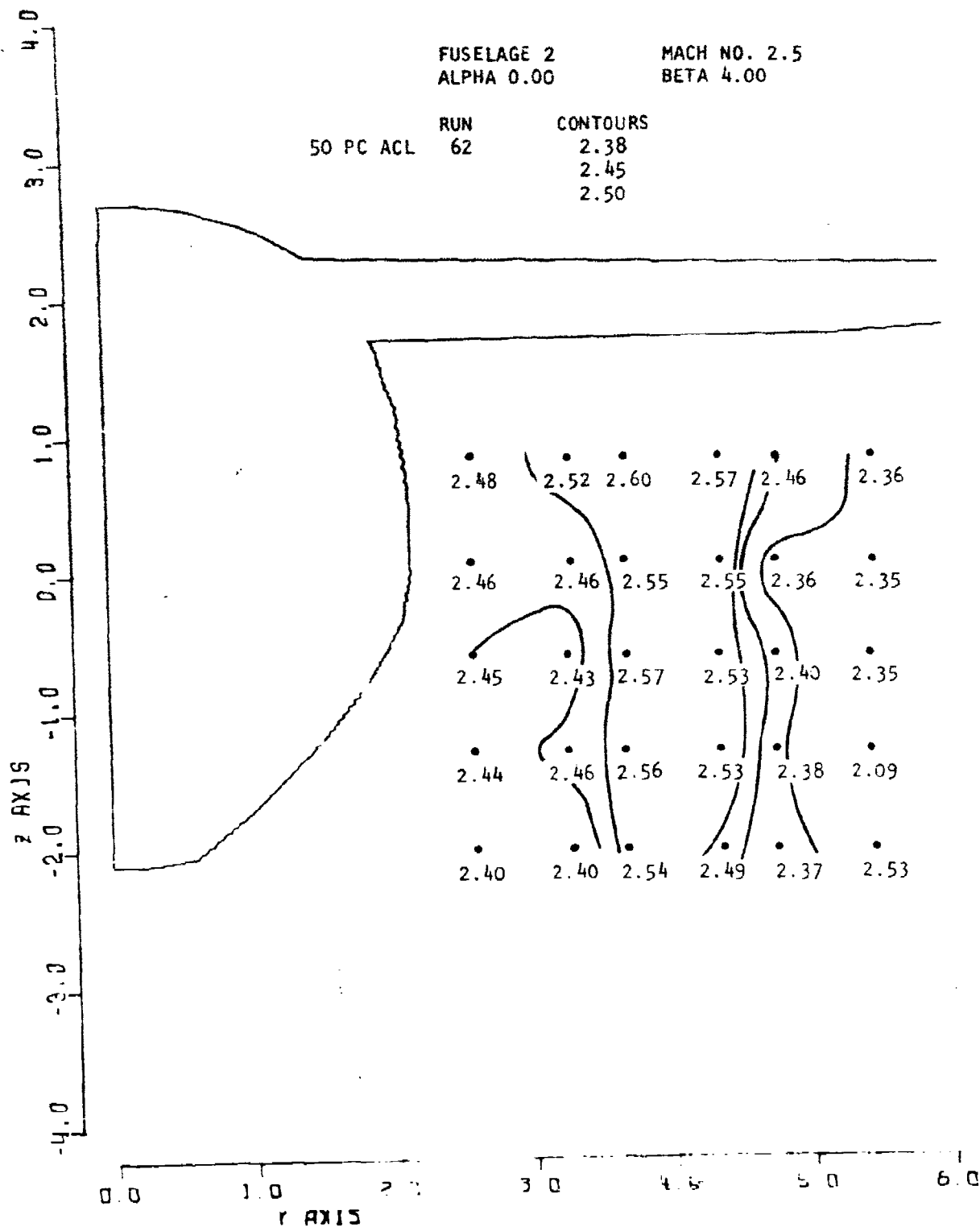


Figure 13. Local Mach No.

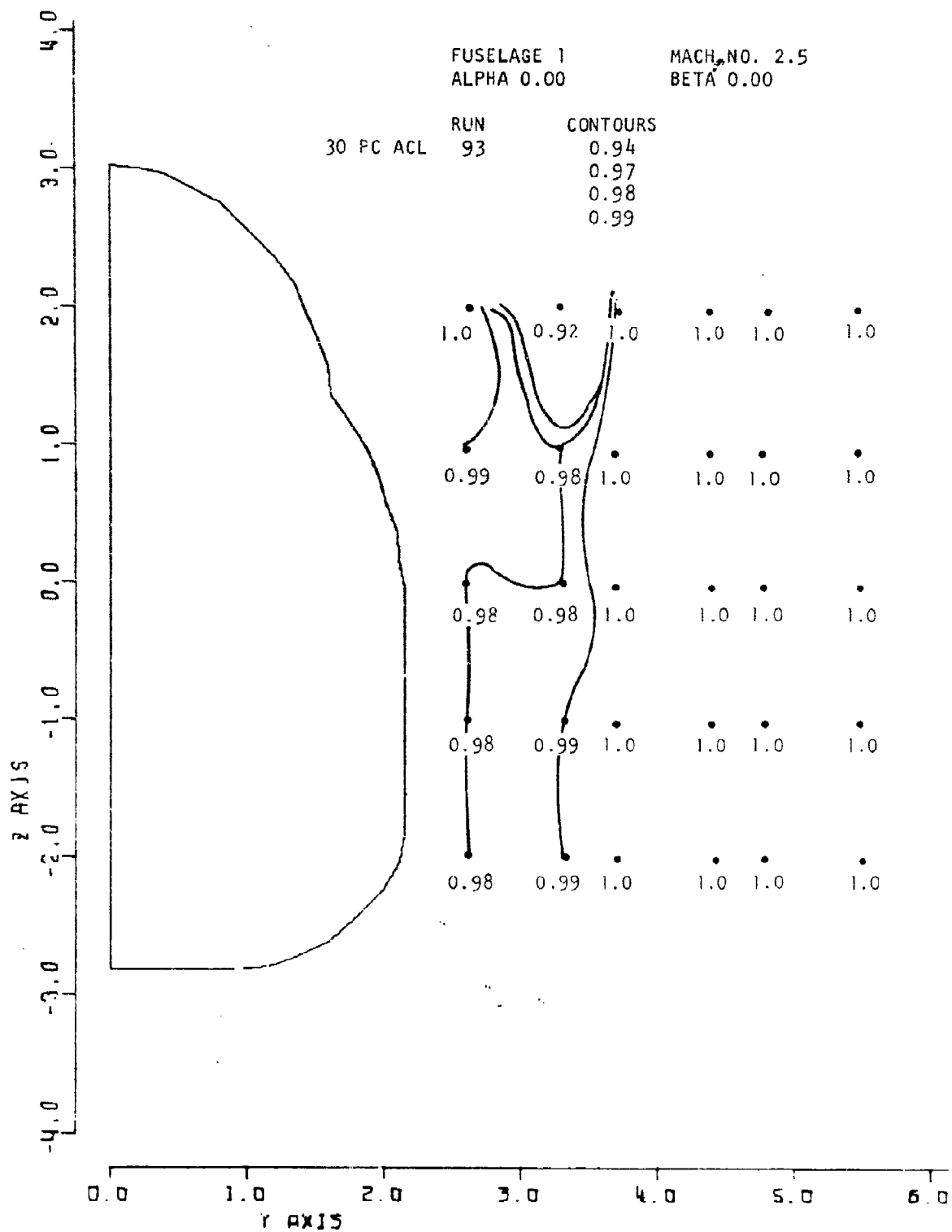


Figure 14. Local PT/PT

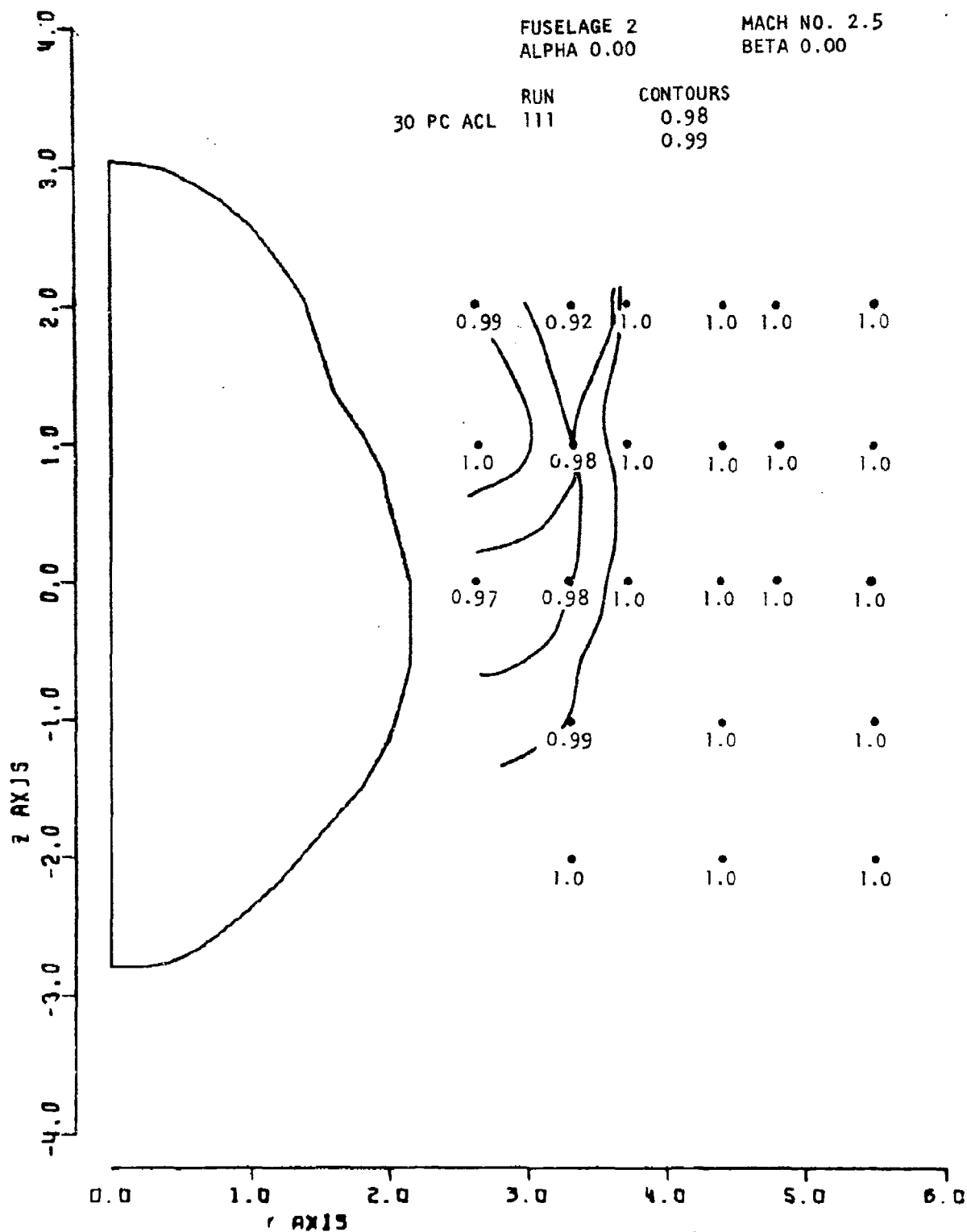


Figure 15. Local PT/PT

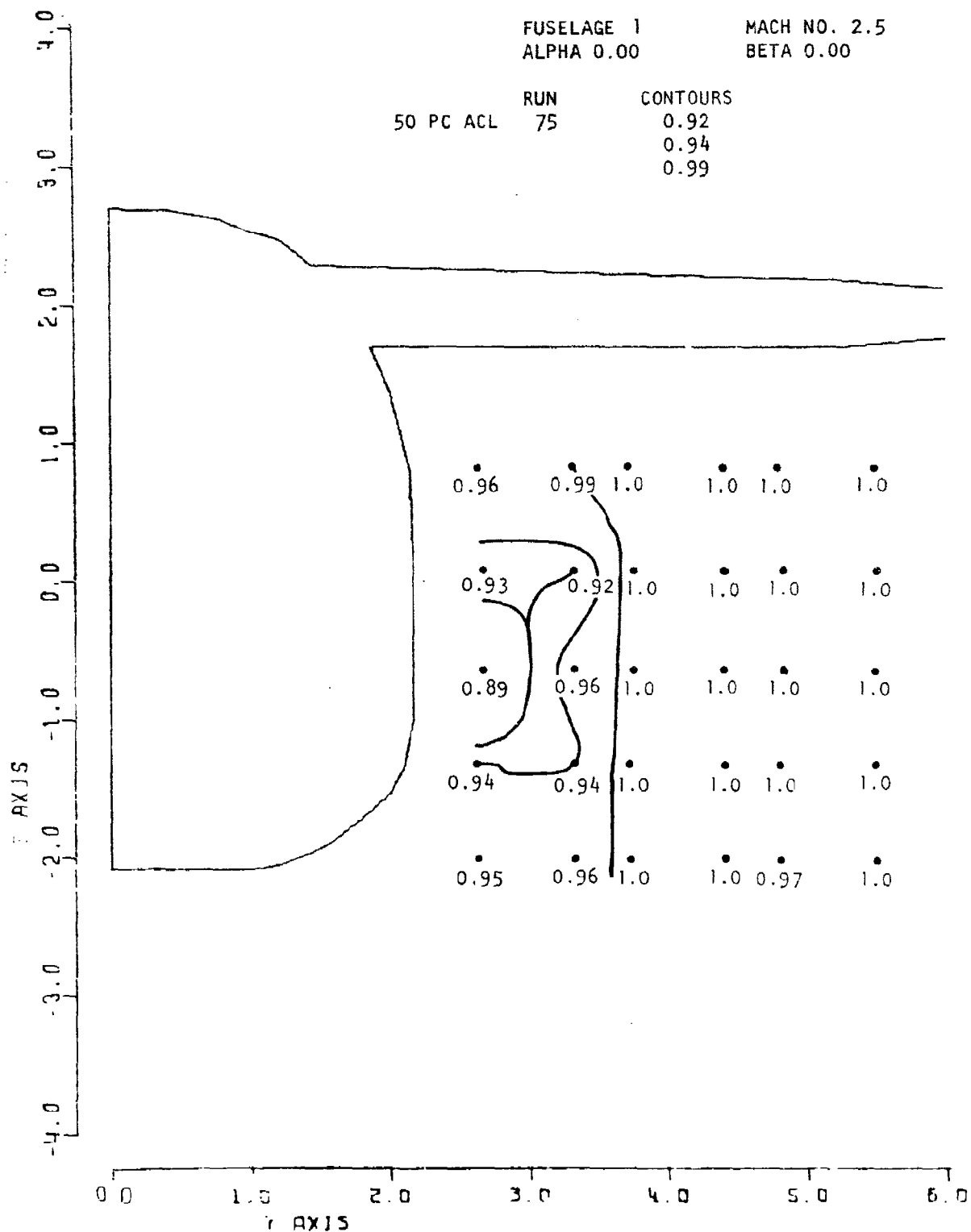


Figure 16. Local PT/PT

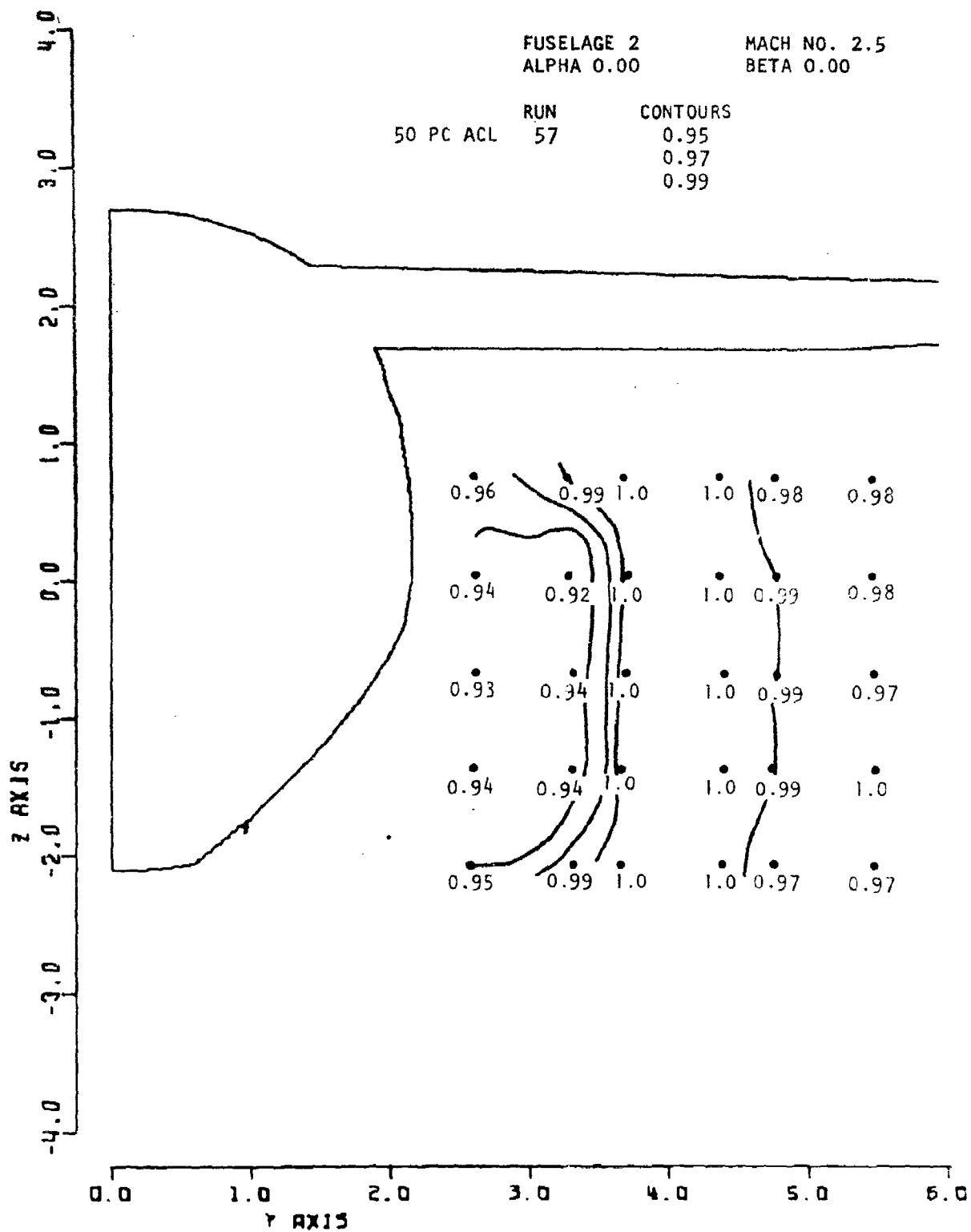


Figure 17. Local PT/PT

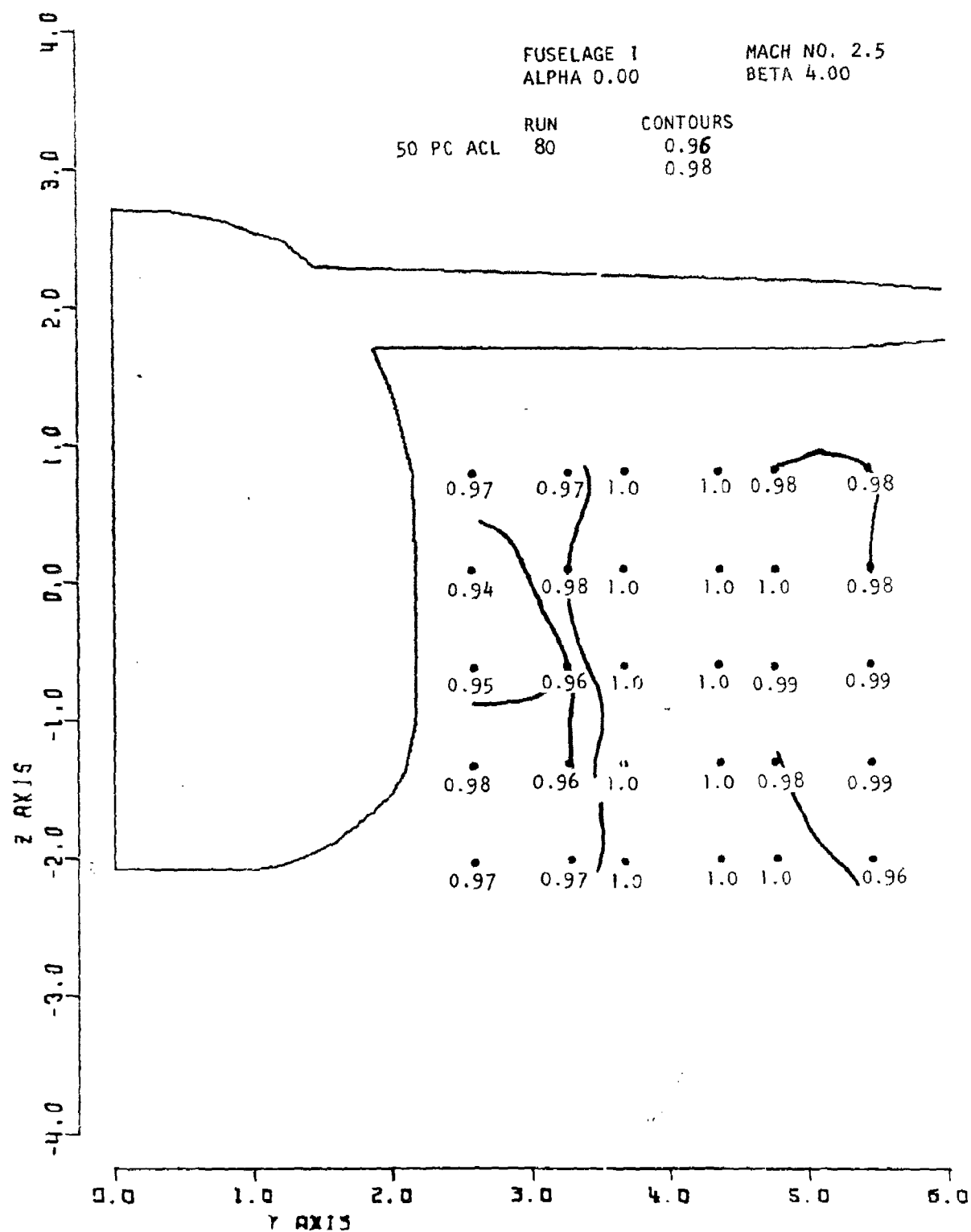


Figure 18. Local PT/PT

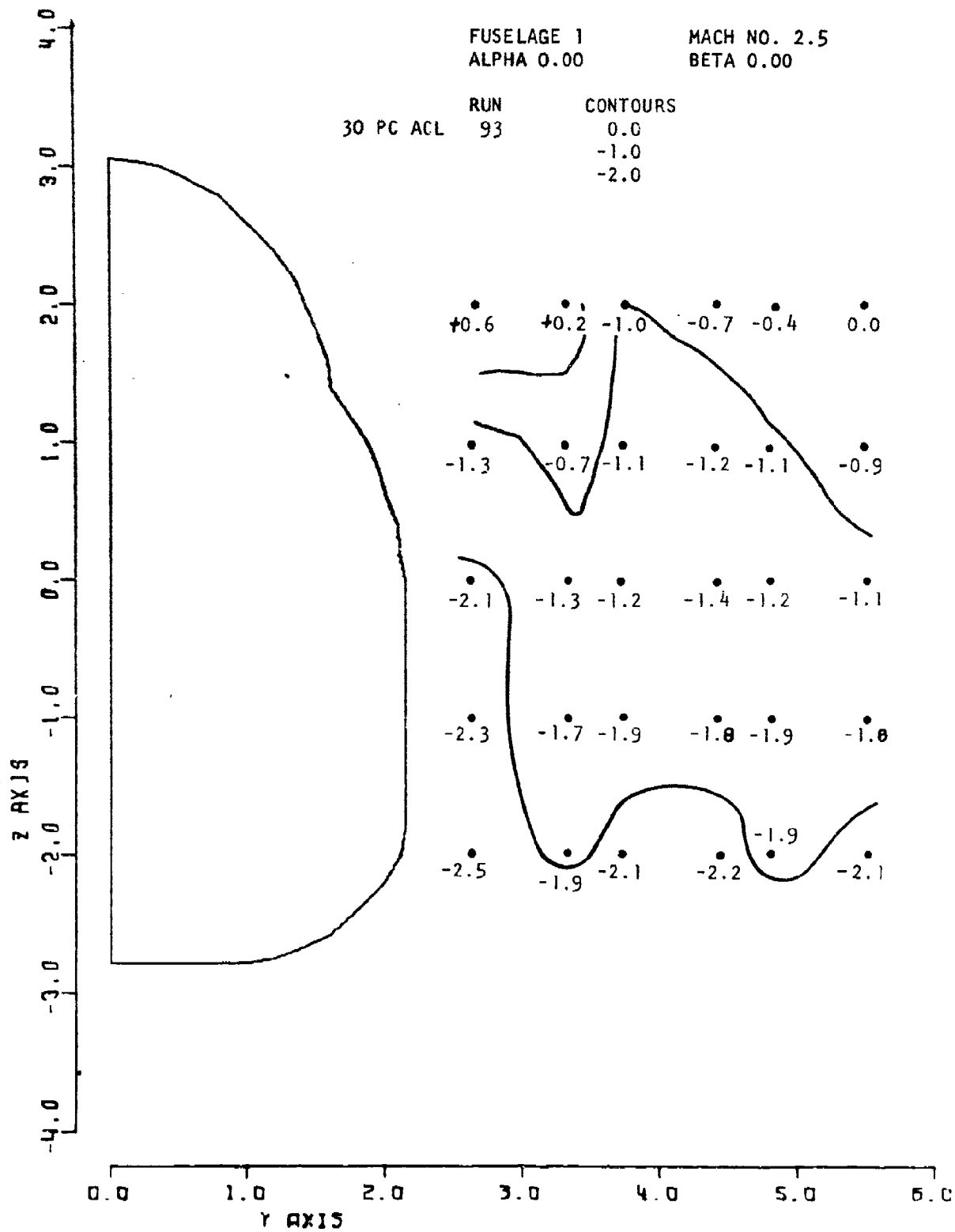


Figure 19. Local Alpha

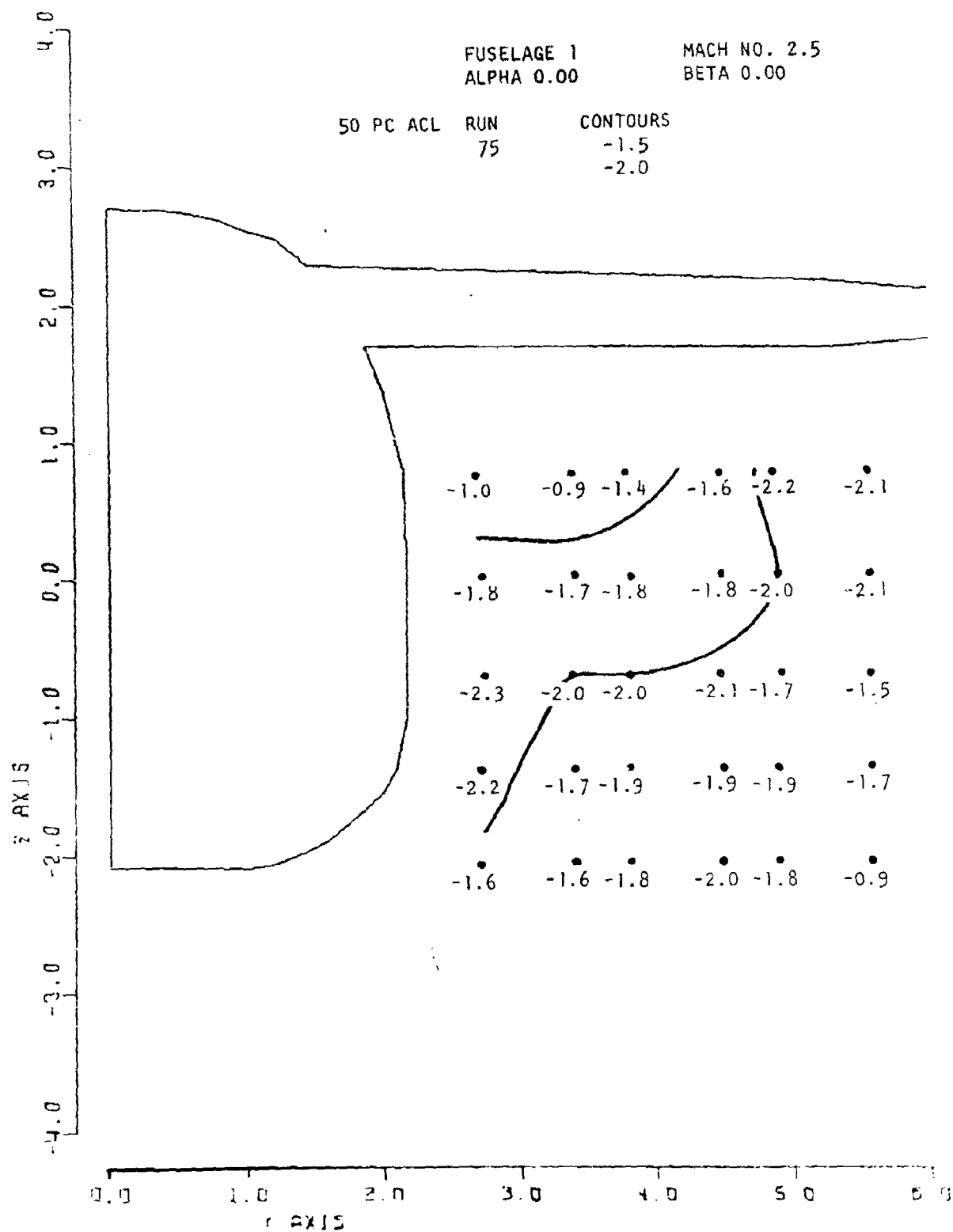


Figure 20. Local Alpha

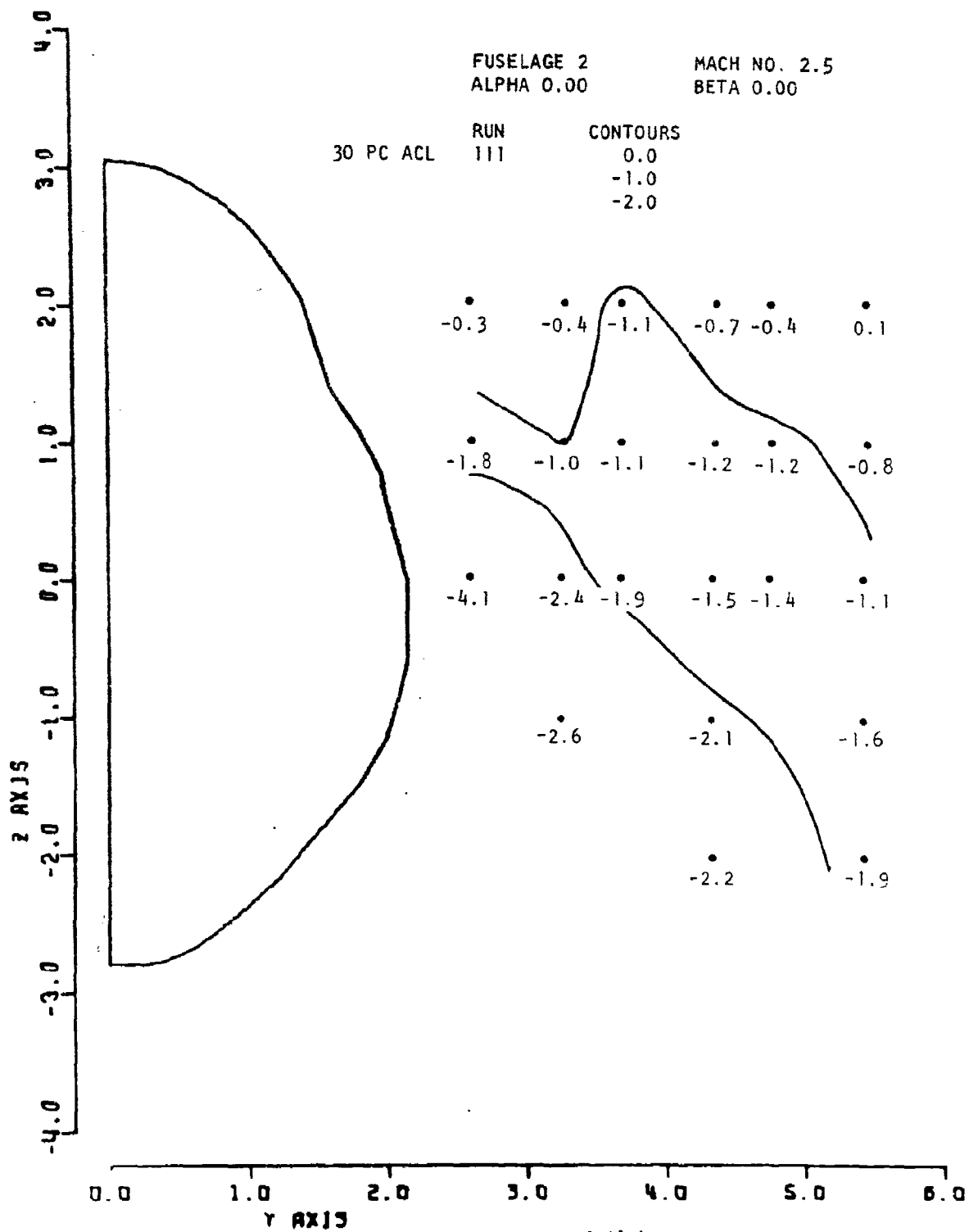


Figure 21. Local Alpha

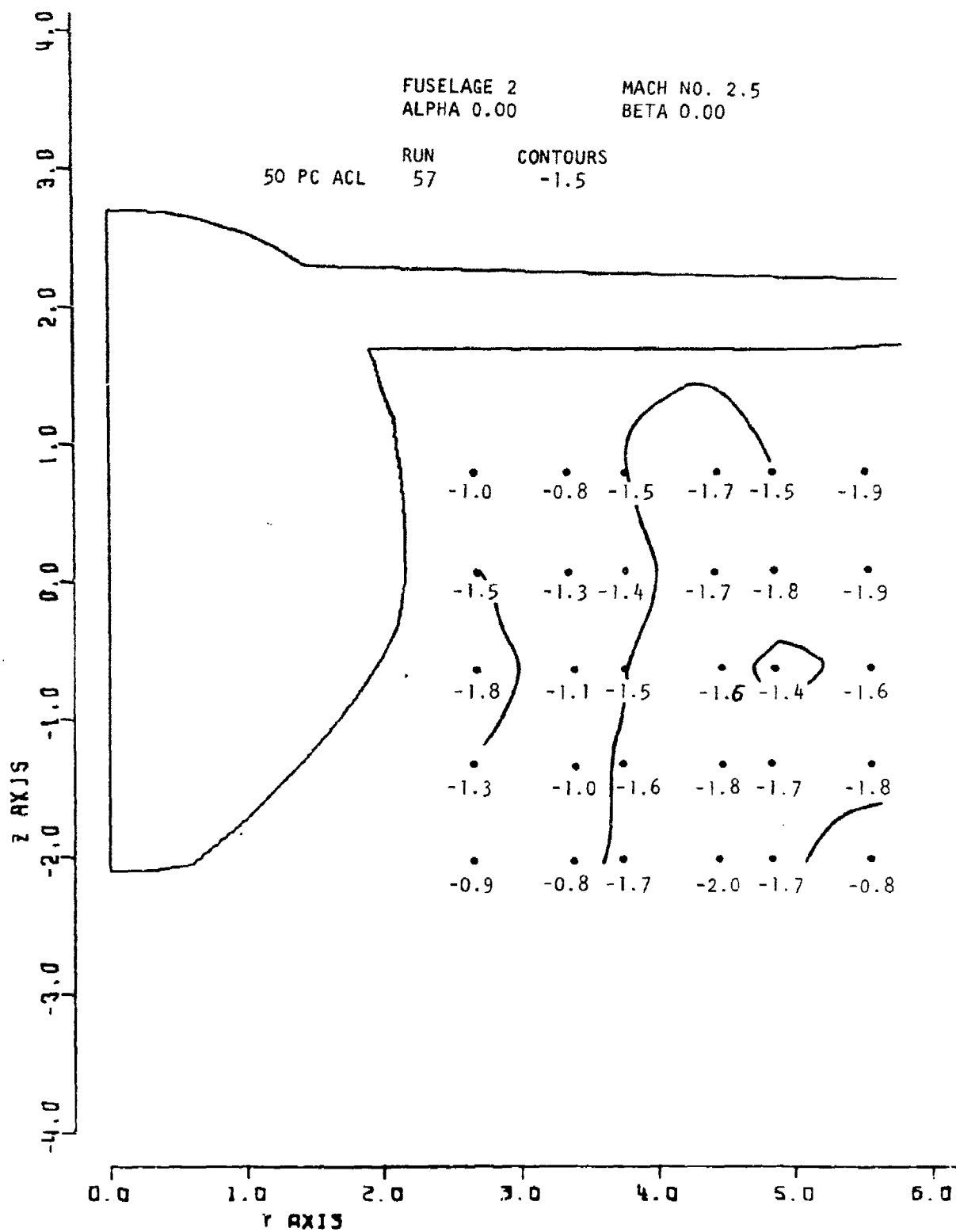


Figure 22. Local Alpha

influence of the wing pressure field are shown in Figure 23 for each of the several angles of attack at Mach numbers of 2.5 and 3.5.

3.1.1.3.2 Effect of Yaw

For the leeward side at the forward station, the downwash, as shown in Figure 25, increased in the upper region and decreased in the lower region relative to the unyawed case. This indicates a strengthening of the canopy and bottom fuselage pressure field due to the cross flow. On the windward side of the effect of yaw was to increase the pressure field of the fuselage side relative to both the top and bottom contours, as evidenced by the existence of local downwash in the lower region of the survey plane and upwash in the upper portion, as shown in Figure 24. This effect of yaw was common to both fuselage shapes.

At the downstream survey station Figure 26 shows that on the windward side the effect of yaw, and of the wing presence, is to produce a downwash pattern which increases in the downward direction. On the leeward side the cross flow around the bottom of the fuselage due to its yawed attitude serves to produce a mild upwash in the lower inboard corner of the survey region. The wing presence is manifested here too by the mild level of downwash in the upper portion of the region. The effects of yaw at this low angle of attack were also found to be generally the same for fuselage 2. The larger corner radius of fuselage 2 served to introduce the bottom pressure field earlier to the fuselage side flow field with a resulting increase in local angles of attack in the inboard regions at both 30% and 50% ACL.

An aid to understanding the chief effects of yaw on flow angularity is provided by recognizing that, to a good approximation, the flow field about a yawed body can generally be assumed to be the result of superposing a simple cross flow on the basic unyawed flow field. This fact will be noted again in subsequent sections dealing with the intermediate and high angle of attack results.

3.1.1.4 Local Sigma

3.1.1.4.1 Effect of Vehicle Geometry

At the forward survey station the effects of differences in fuselage geometry on local sidewash angle (denoted by sigma) were restricted to the inboard region adjacent to the corners and sides of fuselages 1 and 2, as shown in Figures 28 and 29, respectively.

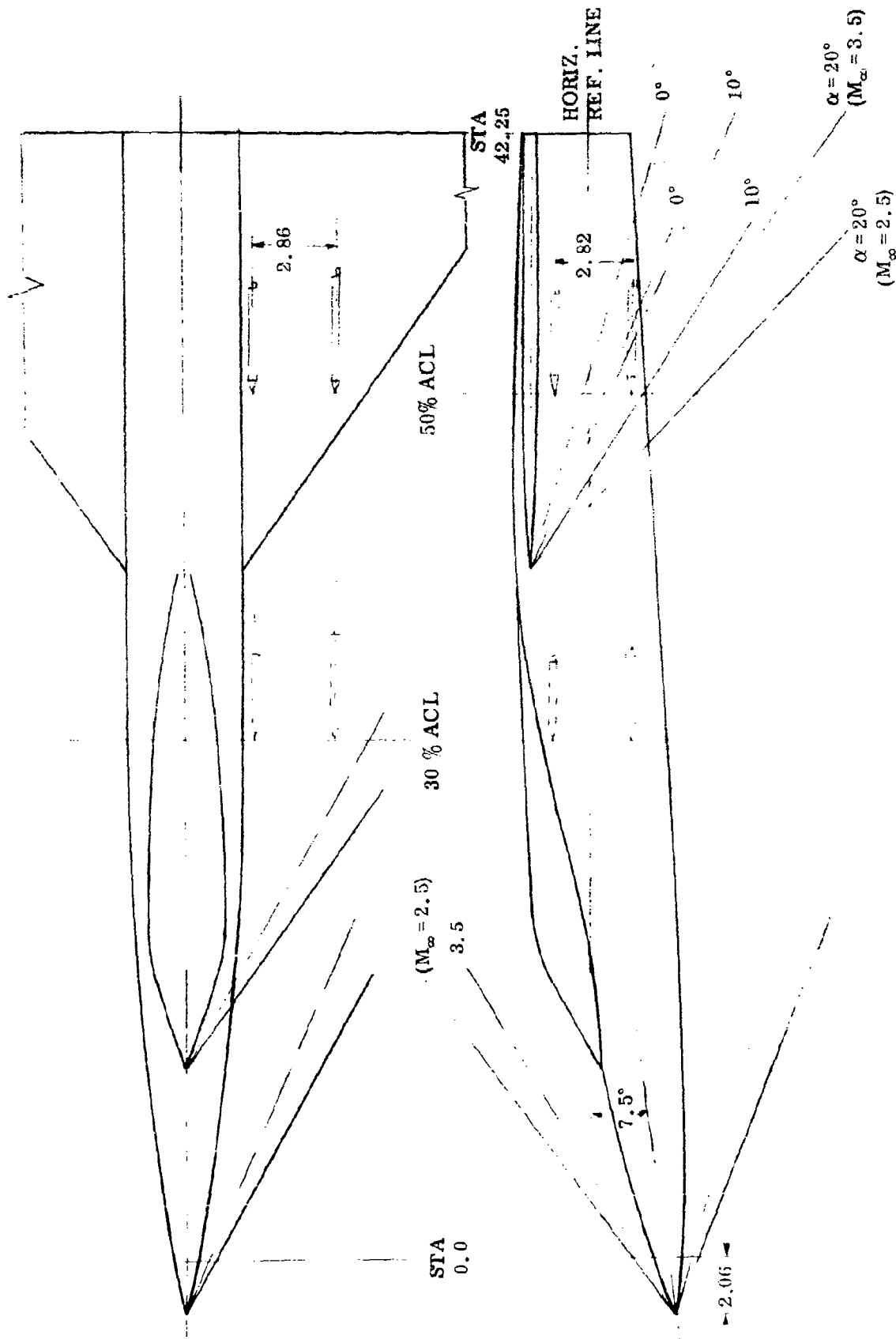


Figure 23. High Mach Number Nose and Canopy Model: Schematic of Survey Regions and Main Shock Wave Locations

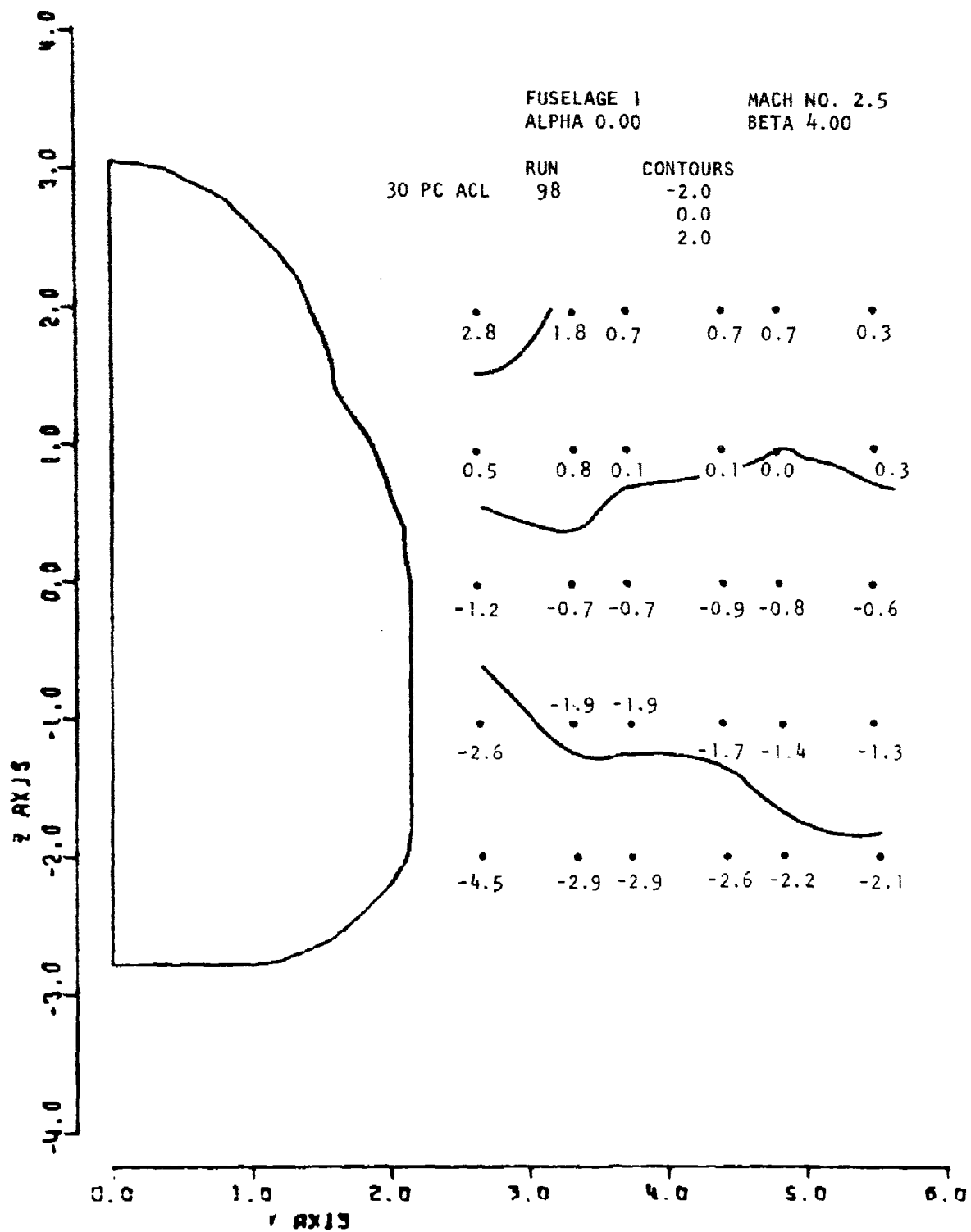
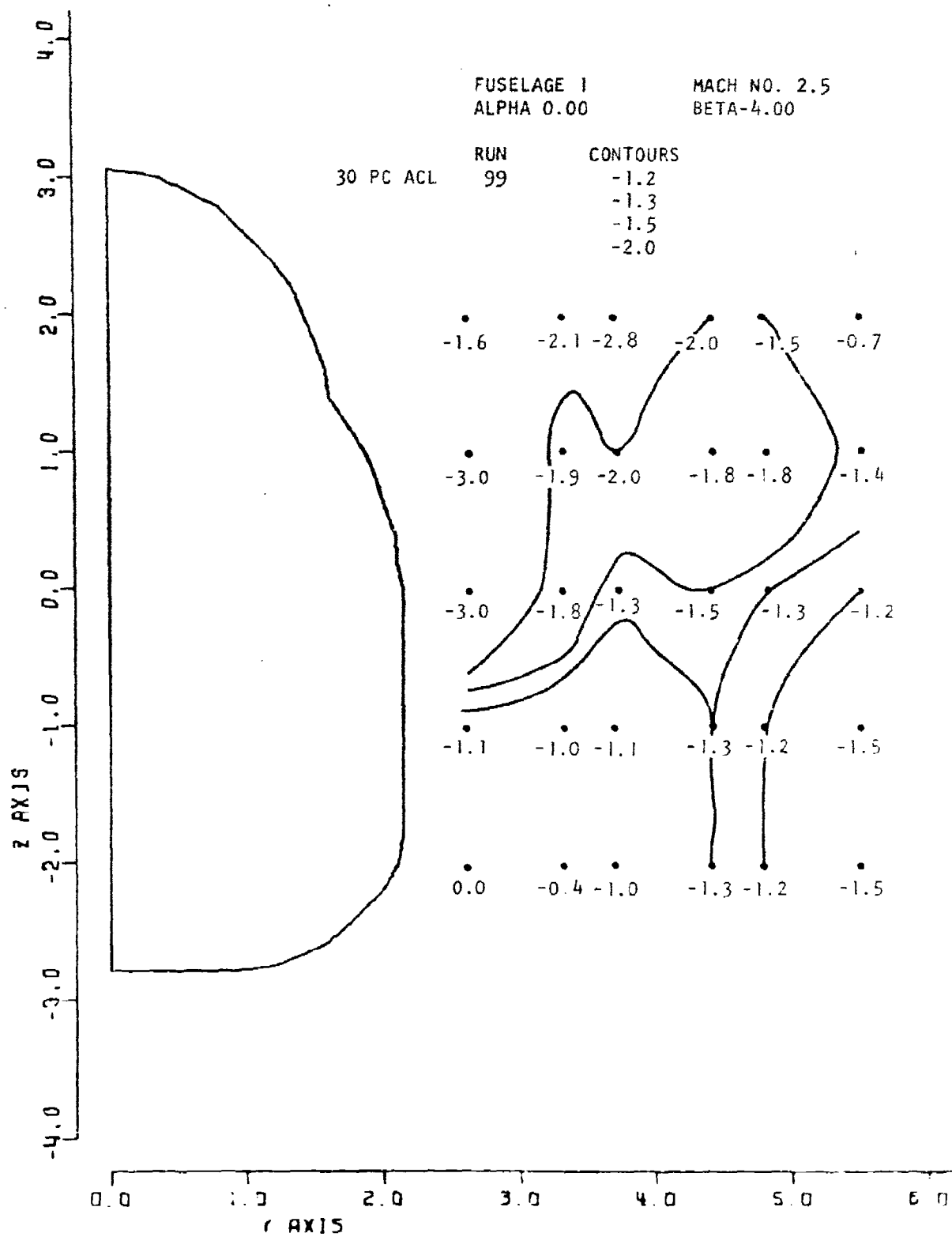


Figure 24. Local Alpha



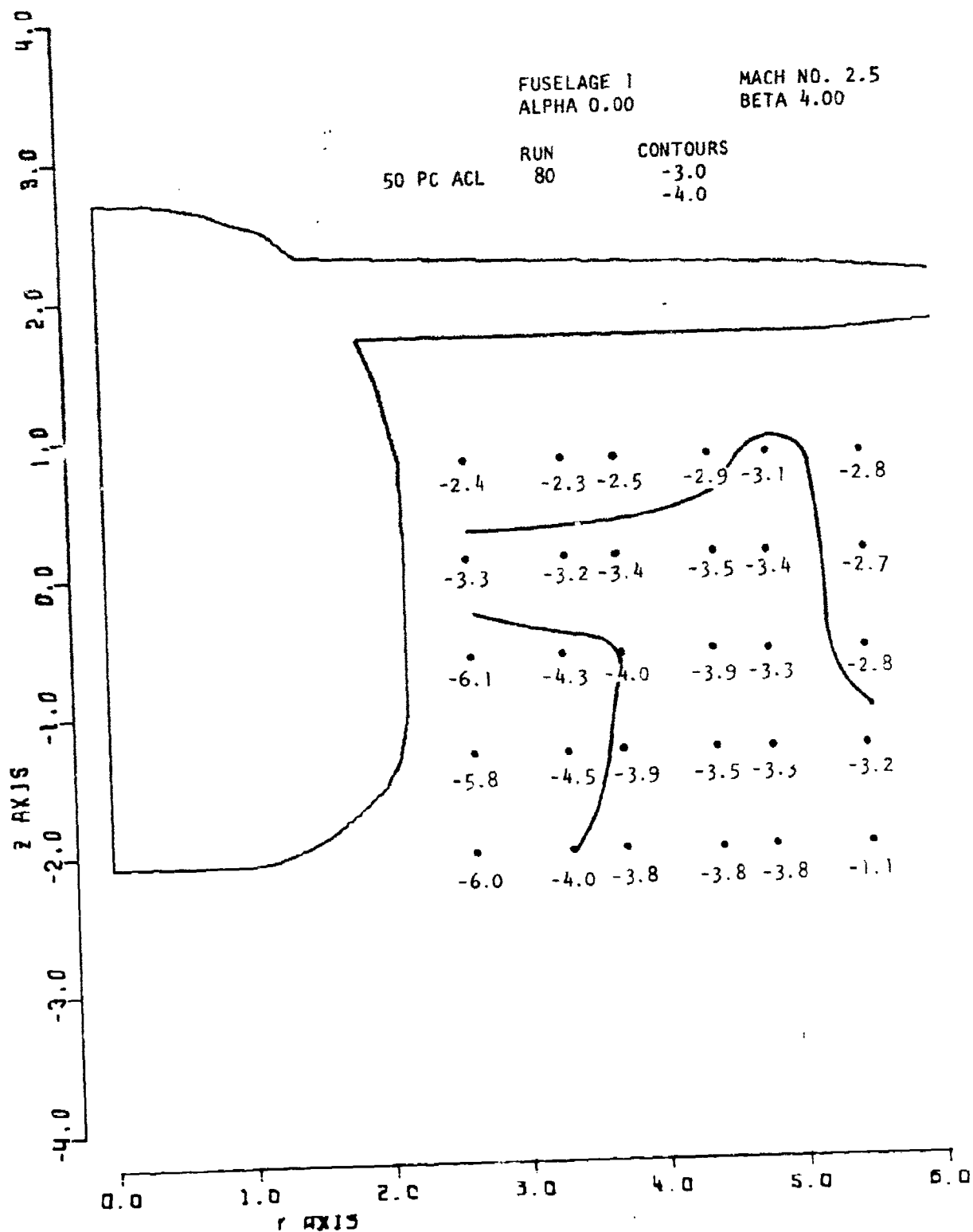


Figure 26. Local Alpha

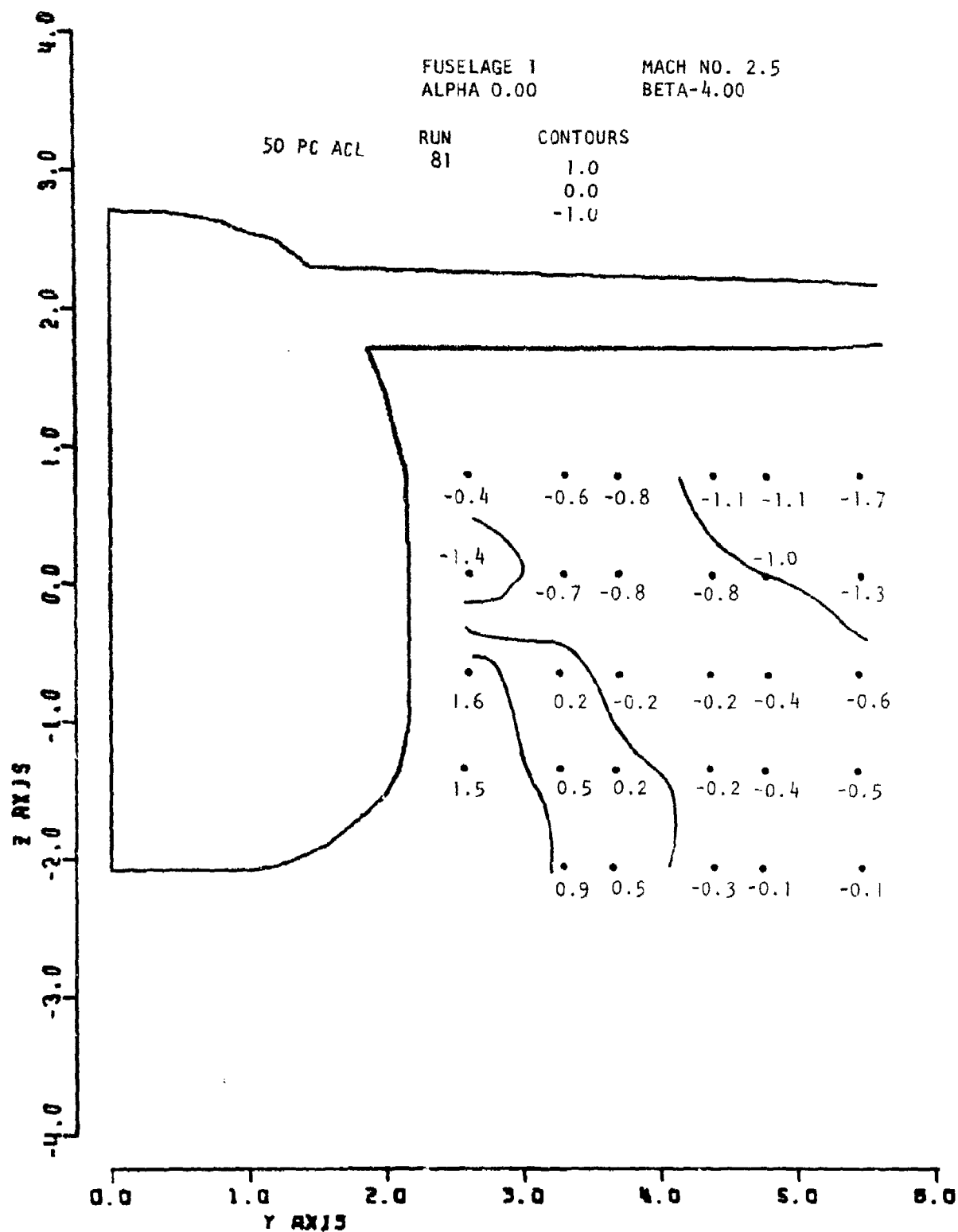


Figure 27. Local Alpha

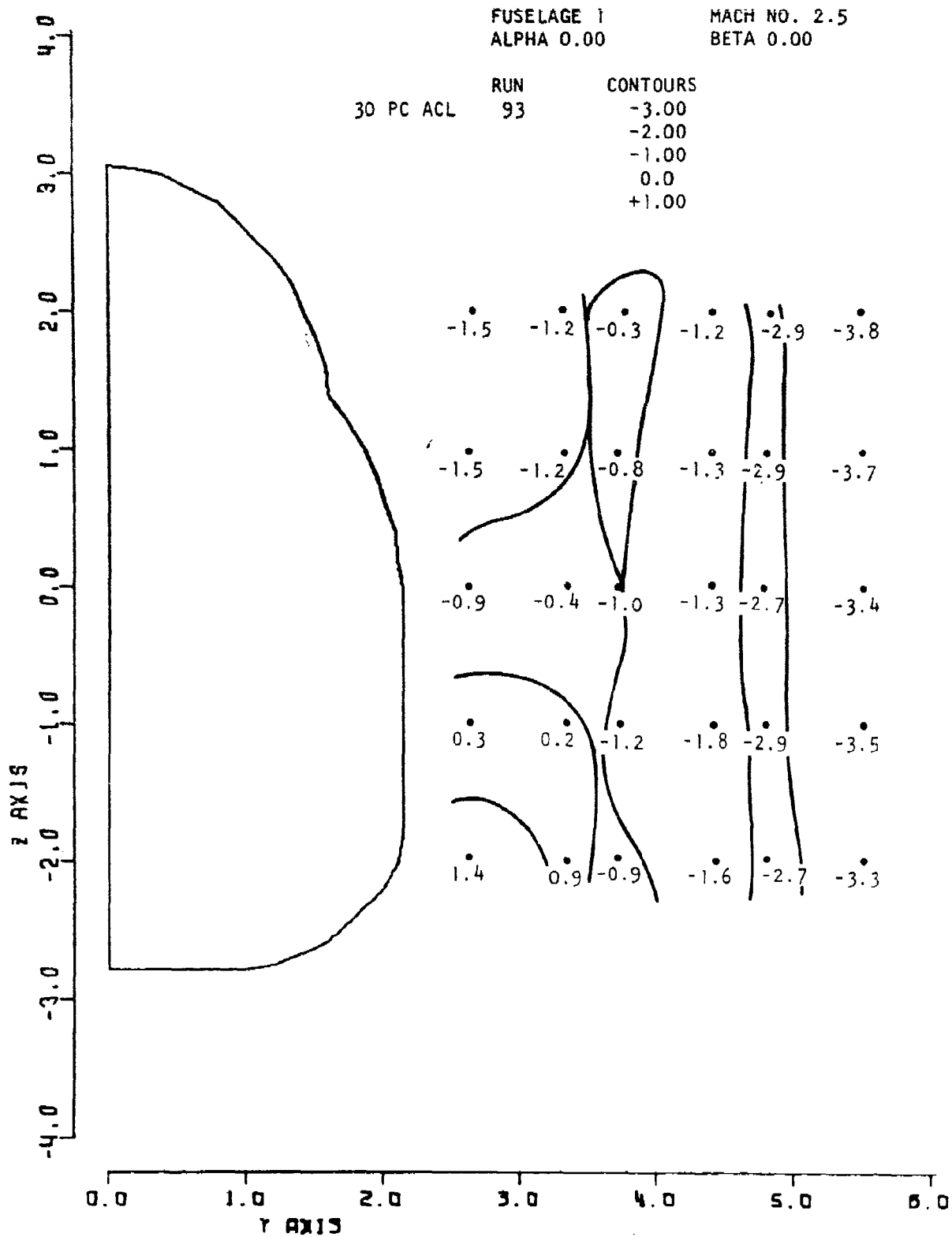


Figure 28. Local Sigma

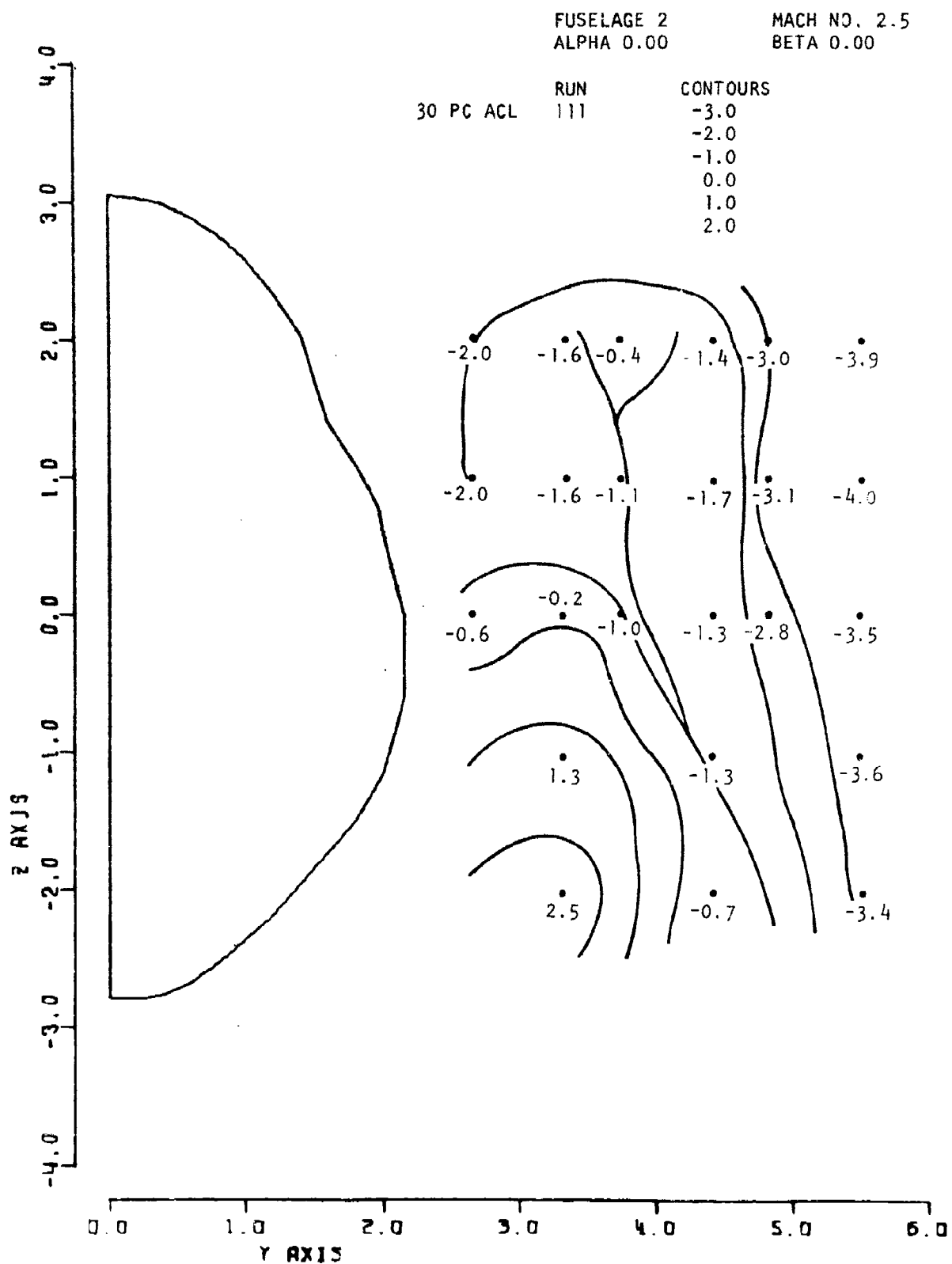


Figure 29. Local Sigma

It can be seen that only positive sidewash angles were confined to this region, and that all the other values were negative. It should be noted that negative and positive values of sigma denote components of velocity directed out from, and into the body, respectively.

Composition of the survey region is dictated by the axisymmetric shock layer generated by the fuselage nose and canopy. The flow re-expansion effects emanating from the convex surface curvature downstream of the slender nose and canopy windshield penetrate the flow field slowly, thereby delaying complete decay of this compression field to a point downstream of the forward survey station. Consequently, at the forward station the influence of re-expansion diminishes with distance from the fuselage and the local sidewash angularity tends to be more negative outboard. This radial gradient is stronger in the upper position of the flow field due to the proximity of the canopy. The local angles of sidewash shown in Figures 28 and 29, together with the local angles of attack shown in Figures 19 and 21 are indicative of a helical streamline pattern spiraling downward and to the right (looking aft) on the right side of the fuselage.

At the downstream station flow re-expansion is more complete and the values of local sidewash become more positive, tending to align with the fuselage surface inboard and the free stream outboard. The changes are greatest in the upper part of the survey region, as may be seen by comparing Figures 28 and 29 to 30 and 31. This change can be attributed to the influence of the large reduction in cross-sectional area of the canopy and the change in local slope of the upper fuselage which takes place between the 30% and 50% ACL stations, and to the absence of wing compression in inhibiting the inward directed flow tendency at this low angle of attack.

In summary, the flow field sidewash characteristics at zero angle of attack in the region surveyed, are dependent upon local cross section shape as well as body slope changes in the vicinity of the region in question.

3.1.1.4.2 Effect of Yaw

The windward field local angles of sidewash were generally the same for both fuselages in the region above the horizontal reference line at both the 30% and 50% ACL stations. Below the horizontal reference line the fuselage corner shape did affect the sidewash in the inboard region at both stations. Thus, fuselage 2, with its larger corner radius introduced in effect the cross flow associated with this yawed condition into the inboard region, as may be seen by comparing Figures 32 and 33, and 34 to 35.

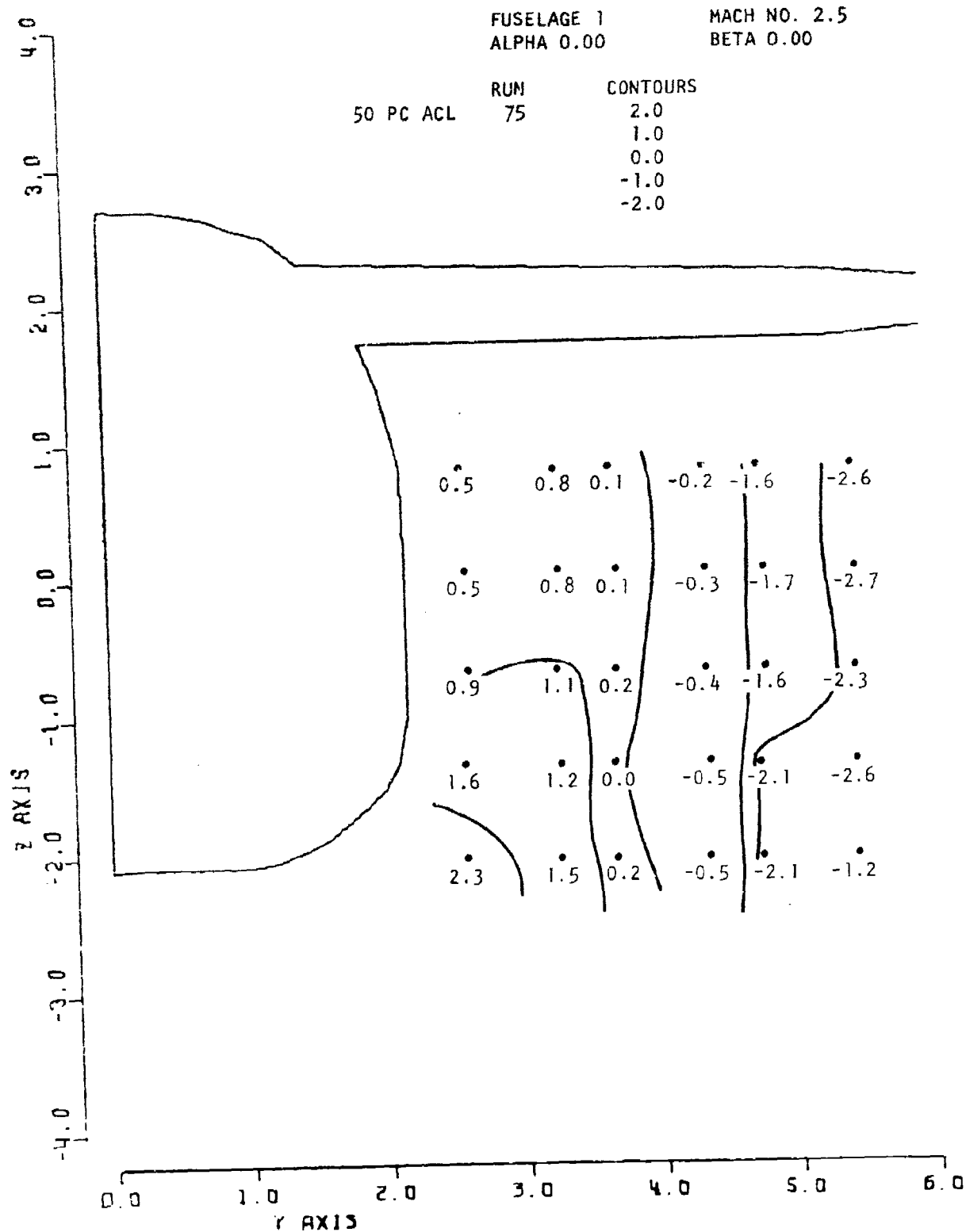


Figure 30. Local Sigma

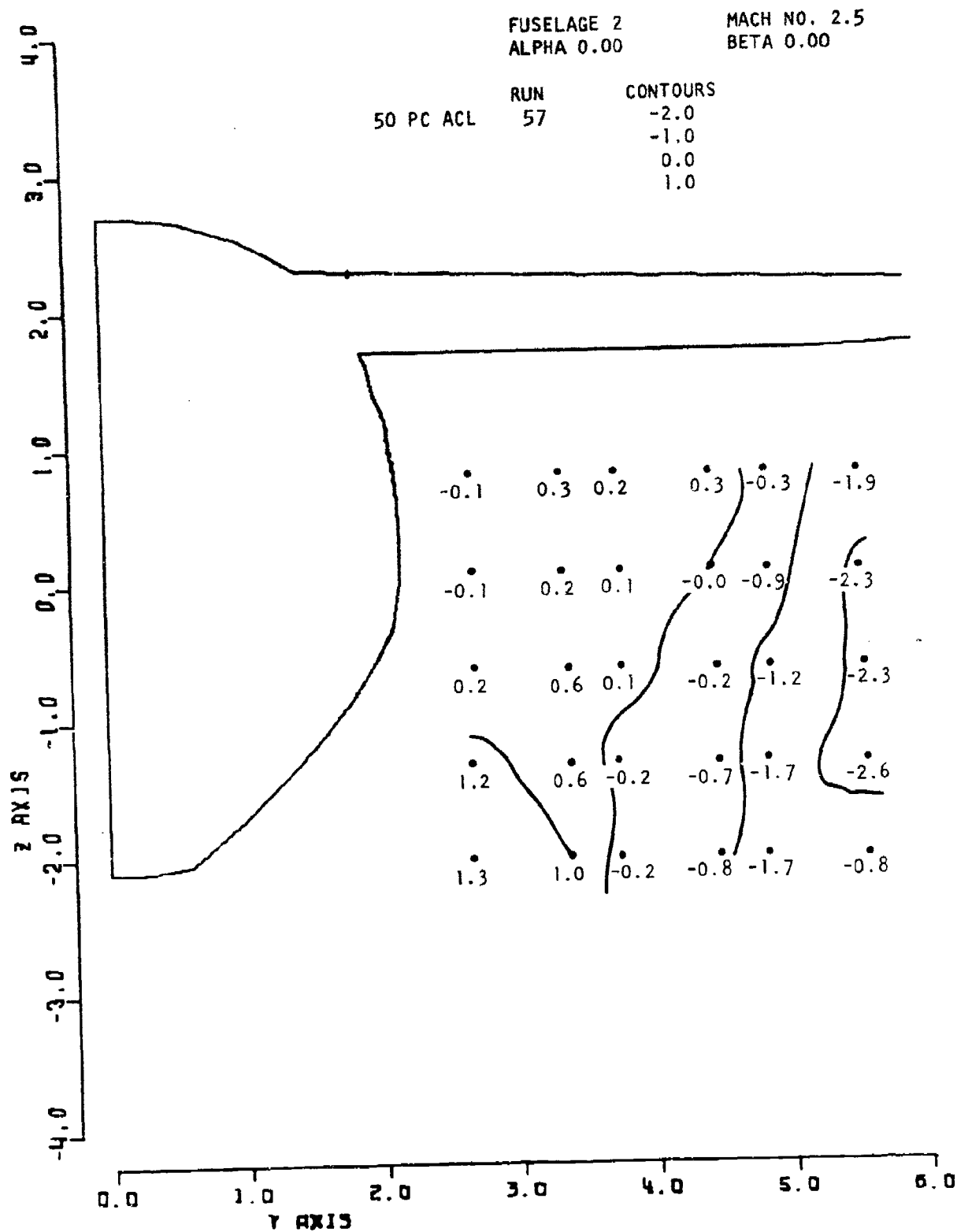


Figure 31. Local Sigma

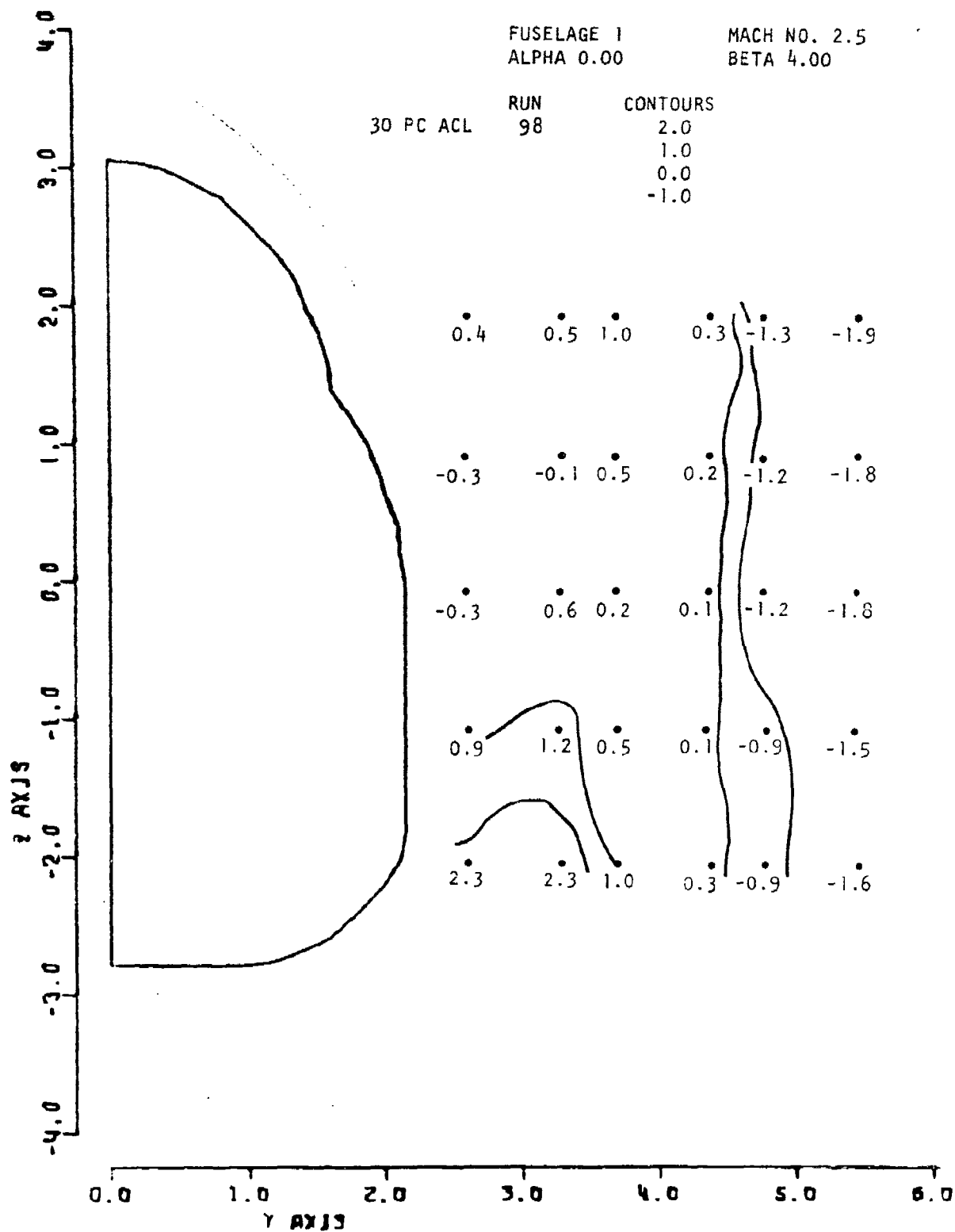


Figure 32. Local Sigma

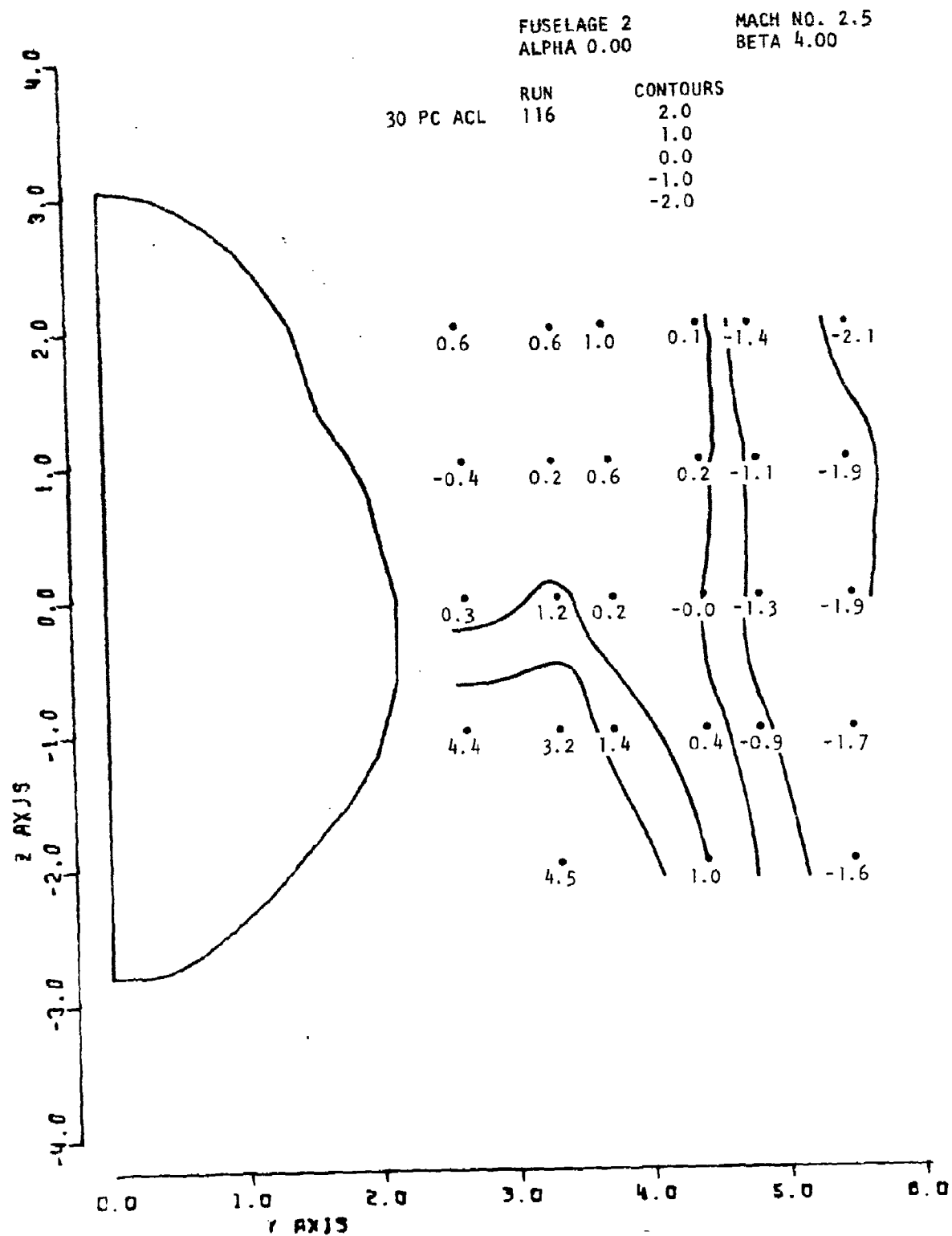


Figure 33. Local Sigma
40

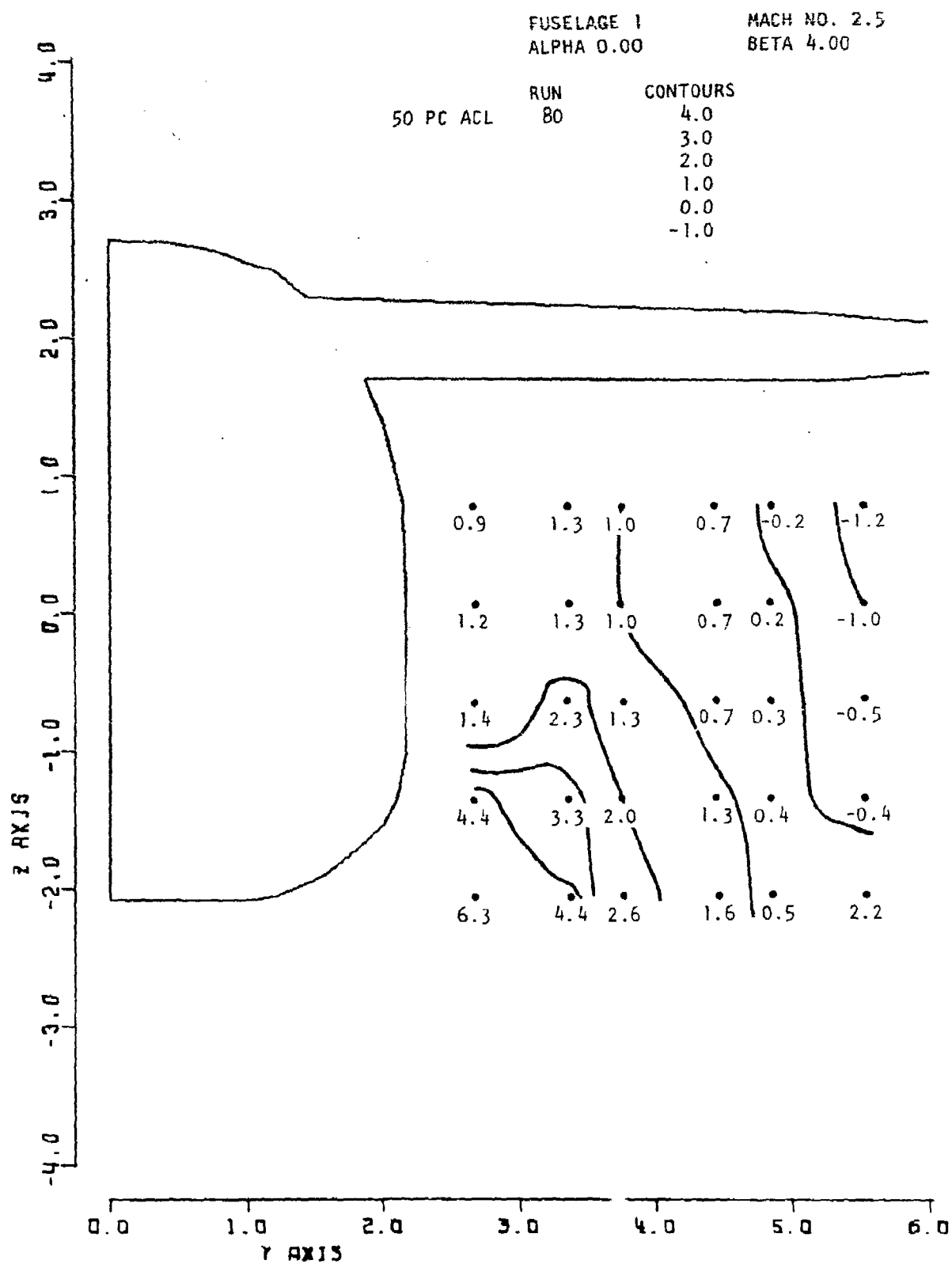


Figure 34. Local Sigma

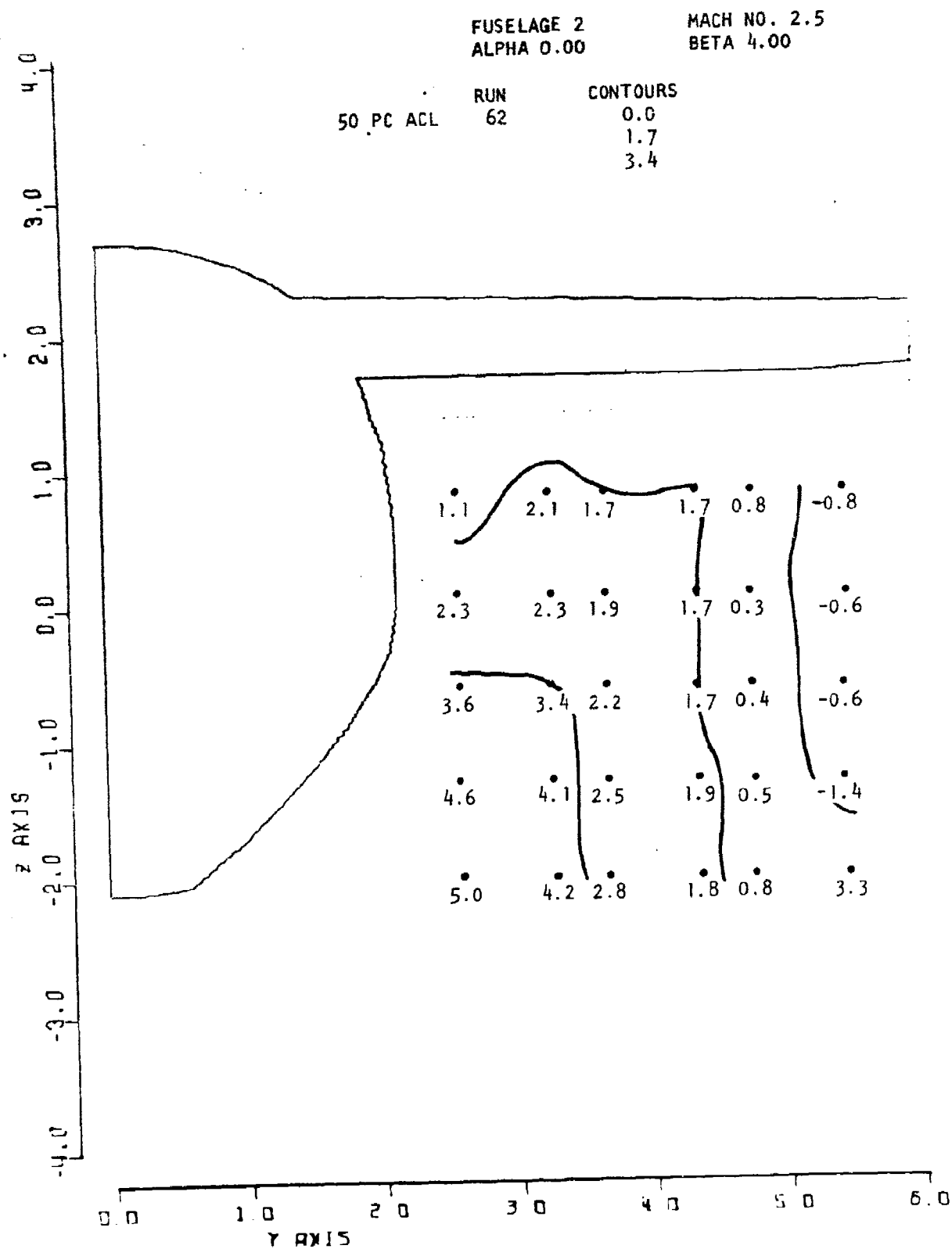


Figure 35. Local Sigma

On the leeward side the effect of fuselage geometry differences was negligible. The local sidewash was similar for both fuselages at the fore and aft stations. As shown in Figure 36 the sidewash decreased from levels equal to almost the free stream yaw value in the outboard region, to only a fraction of that in the inner region adjacent to the fuselage.

3.1.2 Intermediate Angle of Attack

3.1.2.1 Local Mach Number

3.1.2.1.1 Effect of Vehicle Geometry

For both fuselages 1 and 2 the effect of increasing the angle of attack from 0° to 10° was to increase the strength of the compression of the lower fuselage contour relative to the upper; thus, at the forward survey station the local Mach numbers were lowest in the lower part of the surveyed region and generally highest in the upper part. This variation of local Mach number was reversed at the aft station by the lower wing surface flow field which raised the pressure levels, and decreased the local Mach numbers in all but the lower outboard part of the survey region. These effects can be seen in Figures 37 and 38 in the case of fuselage 1.

The effects on the flow field of the difference in fuselage geometry were confined to the lower inboard region adjacent to the fuselage corner and consisted of lower local Mach numbers in the case of fuselage 2 as compared to fuselage 1. As mentioned earlier, this is apparently due to the larger corner radius of fuselage 2 which introduces more of the lower fuselage produced compression into the side flow field than does fuselage 1 with its smaller corner radius and flatter bottom. This effect can be seen by comparing Figures 38 and 39.

3.1.2.1.2 Effect of Yaw

At the intermediate angle of attack of 10° there was virtually no discernible effect of yaw angle ($\pm 4^\circ$) on the local Mach number distributions on the windward and leeward side, for both fuselages 1 and 2 at the forward flow survey station. The composition was rather uniform and averaged about .08 lower than free stream Mach number on the windward side and .05 higher on the leeward at the forward station as exemplified in Figures 40 and 41. At the aft station, however, the average local Mach number on each side was lower than free stream, namely, .34 lower on the windward and .18 on the leeward, indicating the presence of the wing compression field at this station.

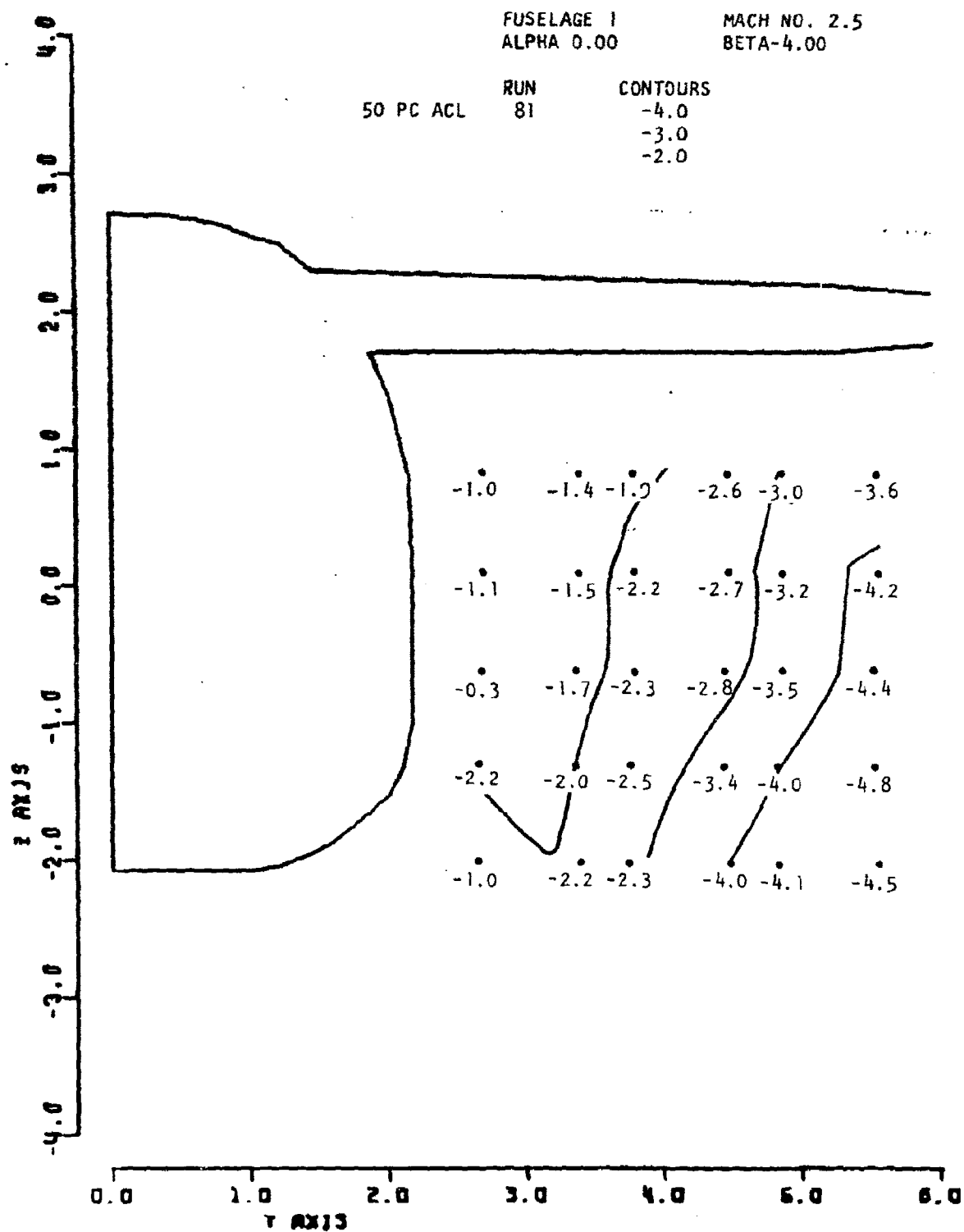


Figure 36. Local Sigma

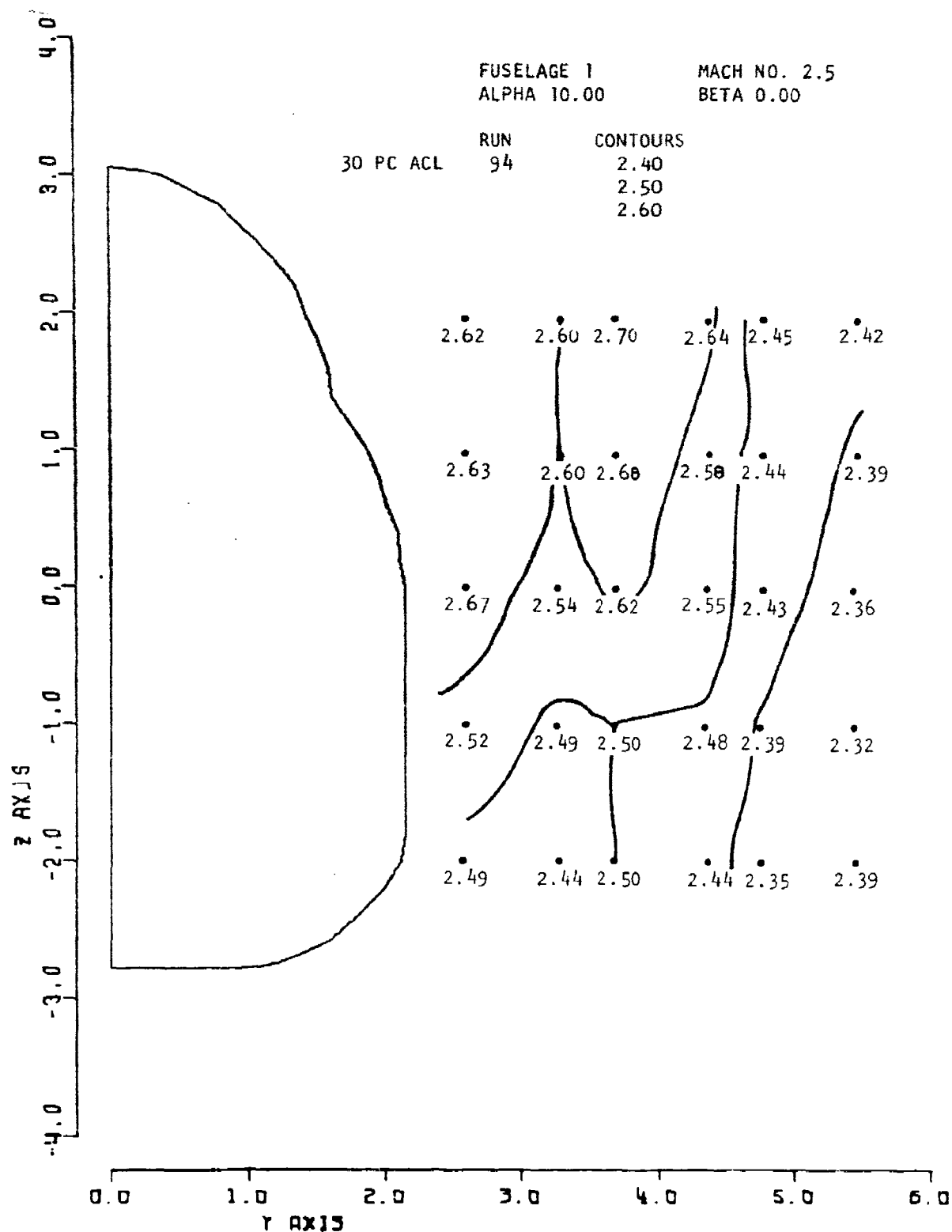


Figure 37. Local Mach No.

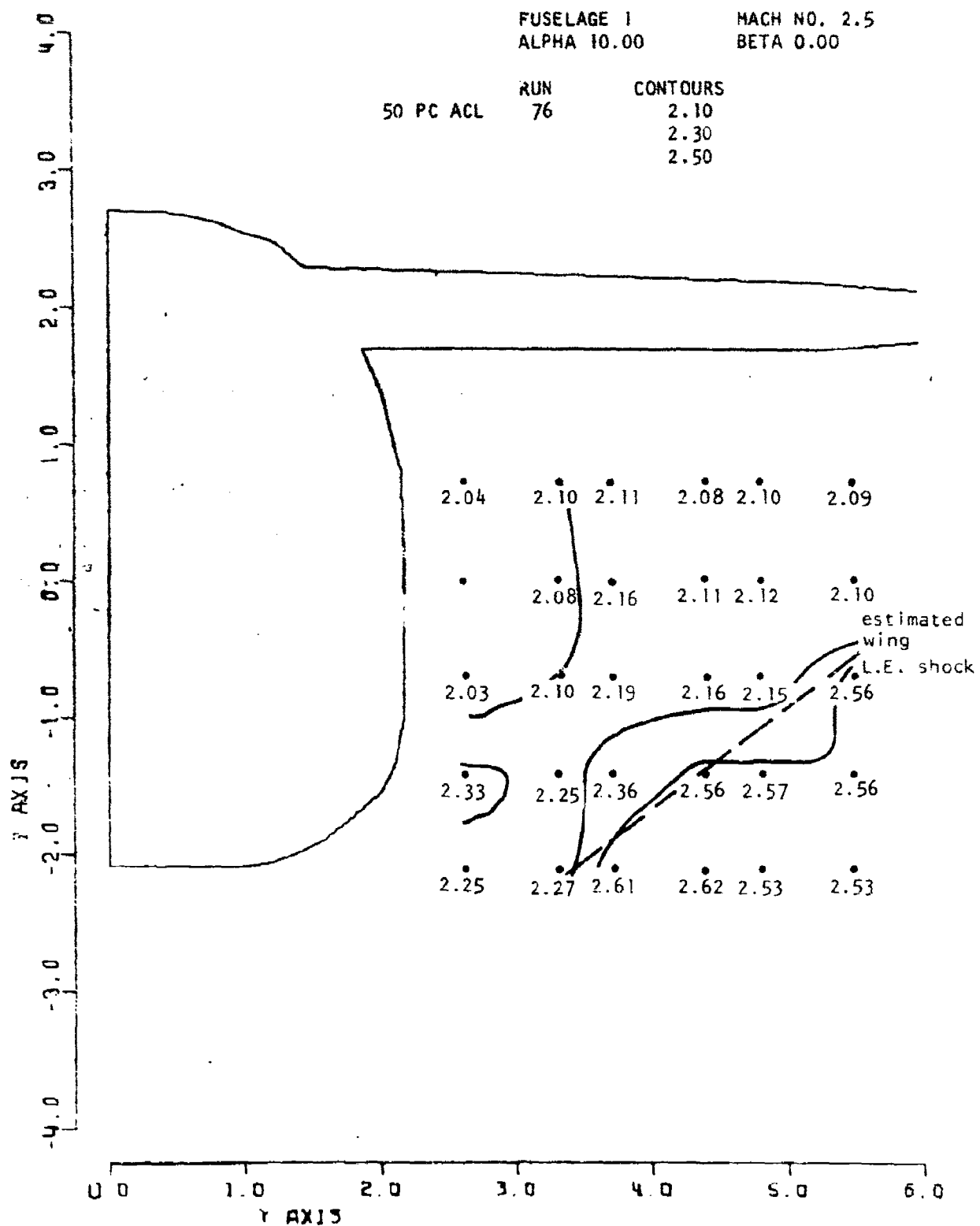


Figure 38. Local Mach No.

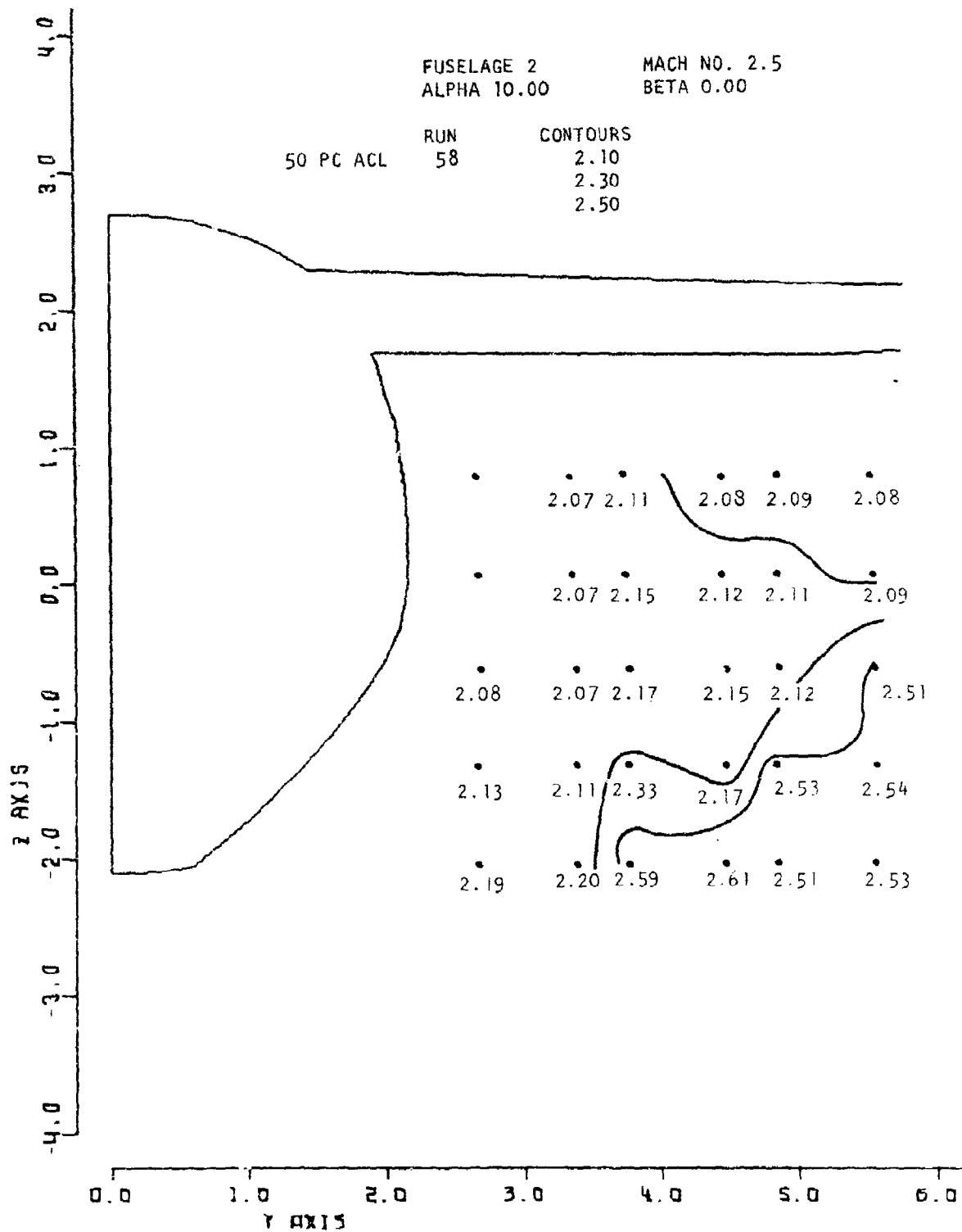


Figure 39. Local Mach No.

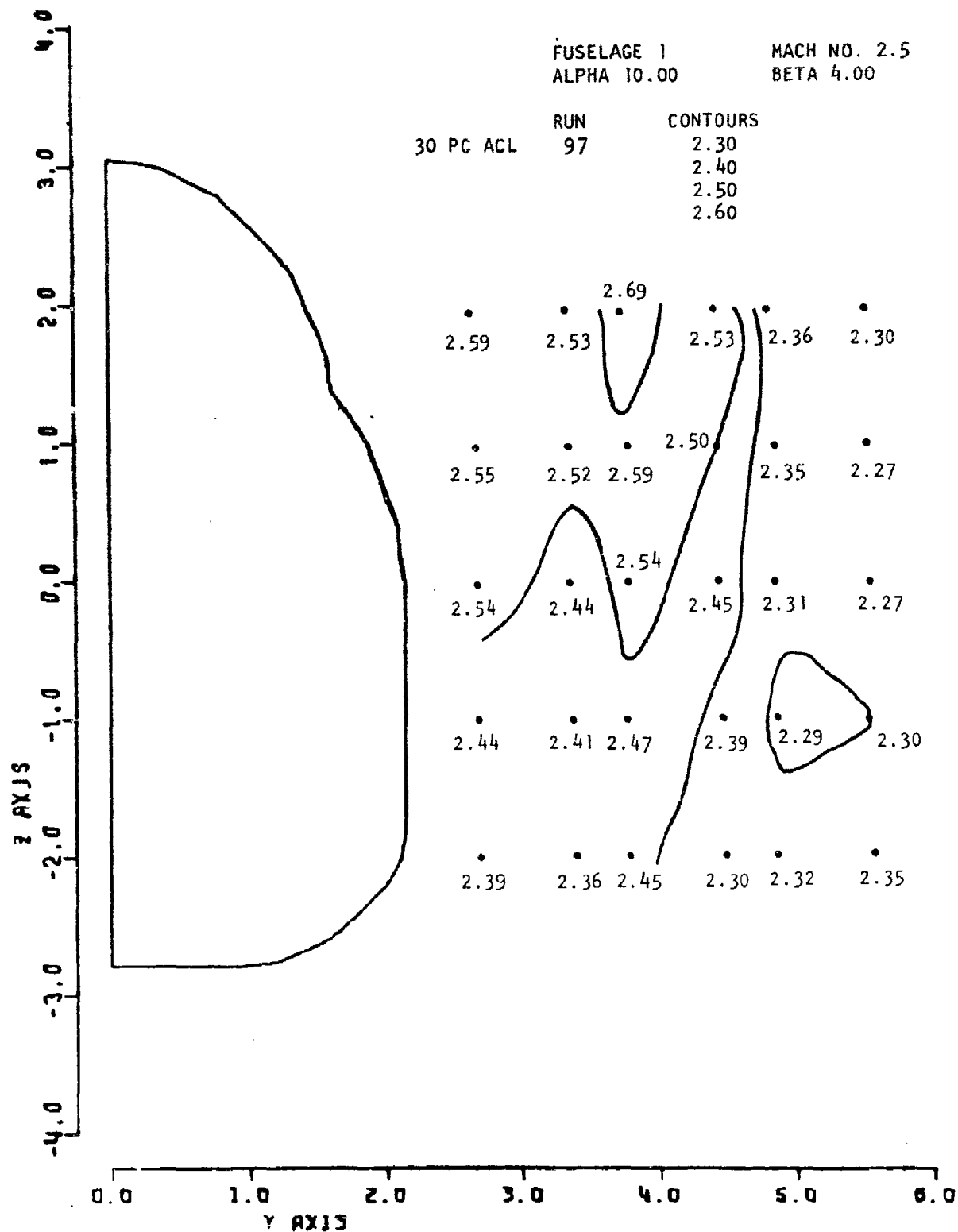


Figure 40. Local Mach No.

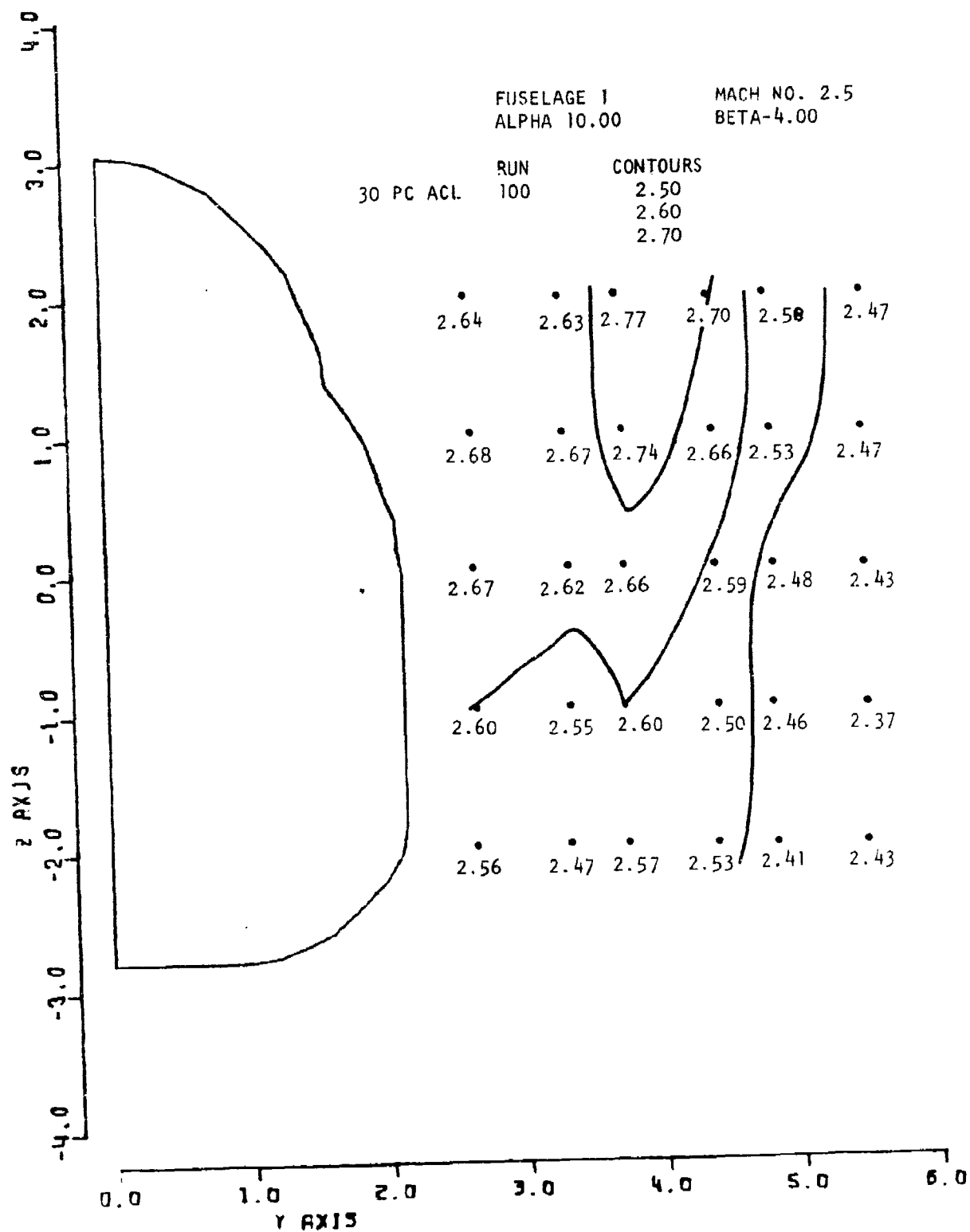


Figure 41. Local Mach No.

3.1.2.2 Total Pressure Recovery

3.1.2.2.1 Effect of Vehicle Geometry

The increase in angle of attack from zero to the intermediate value of 10° produced little difference in total pressure recovery at the forward station for both fuselages, with fuselage 2 displaying slightly higher recoveries in the vicinity of the fuselage corner at both survey stations.

The pressure recoveries at the aft station were generally lower than those of the low angle of attack case for both fuselages, indicative of the greater wing shock wave losses attendant upon this higher angle of attack. Moreover, as shown in Figure 42 the pressure recovery was lowest in the upper inboard region closest to the wing body intersection. This is probably due to the combined effects of canopy and wing generated shock waves whose strengths, and associated losses, are greatest in this region.

3.1.2.2.2 Effect of Yaw

Relative to the unyawed case the effect of yaw ($\pm 4^\circ$) on local total pressure recovery at this intermediate angle of attack was observed to be small at both survey stations for both fuselage shapes 1 and 2, as it was for the zero angle of attack case. Total pressures for both leeward and windward sides were practically the same as for zero yaw, testifying to the virtual lack of modulation in shock wave strength over the angle of yaw range tested for this essentially low-drag nose and canopy configuration. This was also observed in the zero angle of attack results.

3.1.2.3 Local Alpha

3.1.2.3.1 Effect of Vehicle Geometry

The effect of increasing the angle of attack from 0° to 10° was to strengthen the fuselage bottom pressure field relative to that of the upper. Consequently, all the local angles of attack at the forward survey station were positive for both fuselages as shown in Figures 43 and 44, unlike the zero angle of attack case where negative local angles of attack were observed over the whole of the side flow field. The effect of fuselage geometry was confined to the inboard region, where somewhat lower local values of upwash were observed for fuselage 2 as compared to fuselage 1. This indicates, again, how the rounder corner of fuselage 2 serves to introduce the pressure field into the side flow field gradually, thereby reducing the peripheral pressure

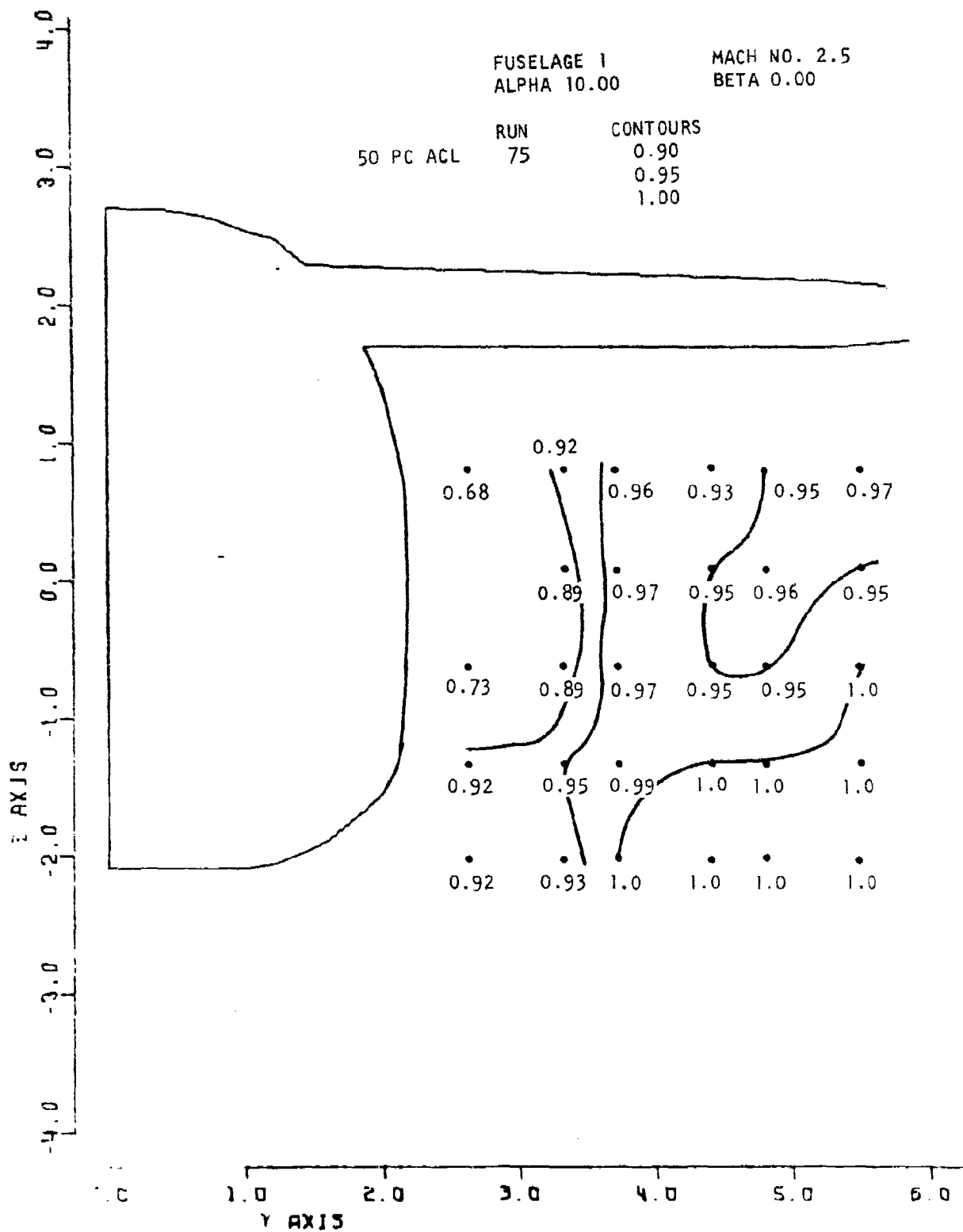


Figure 42. Local PT/PT

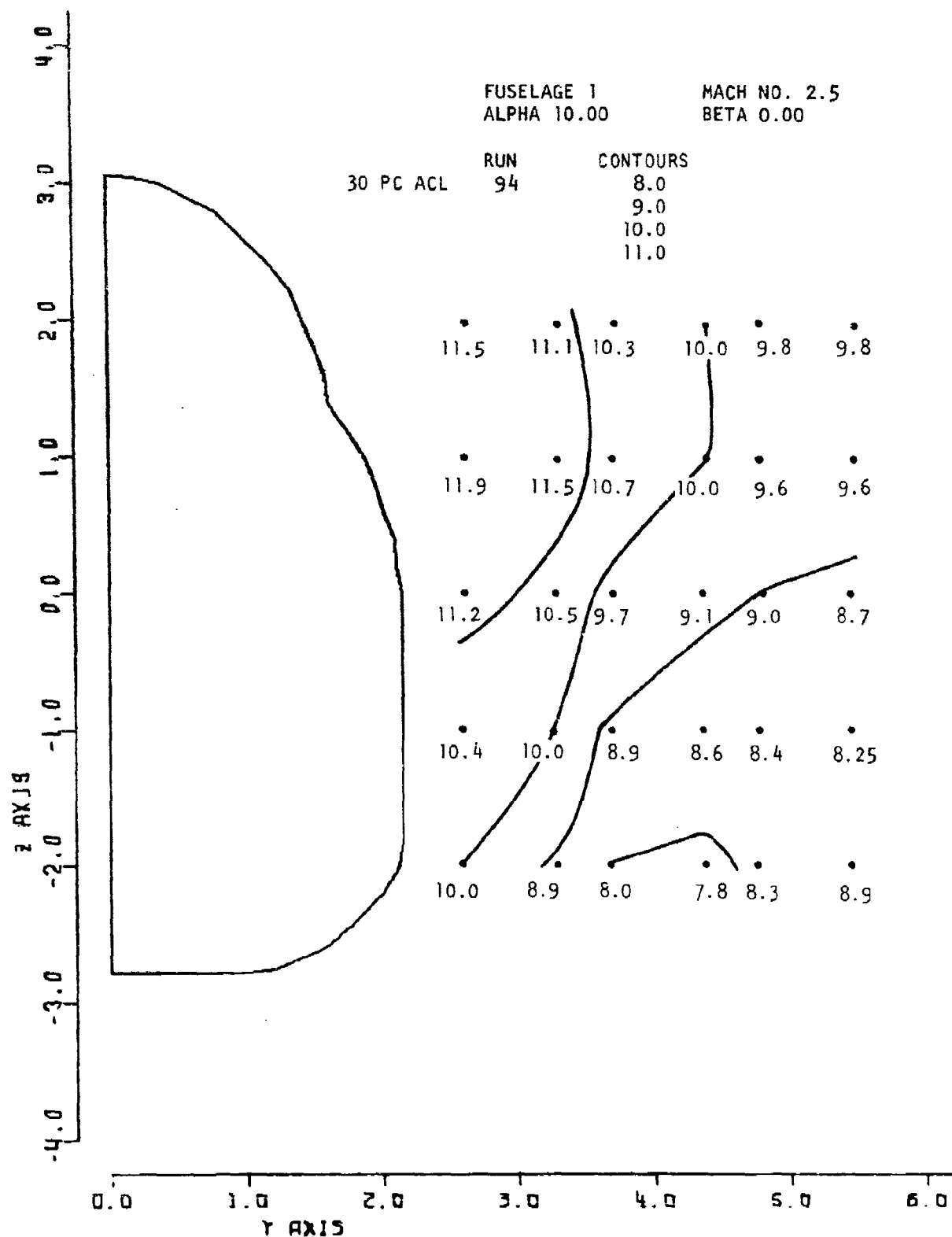


Figure 43. Local Alpha

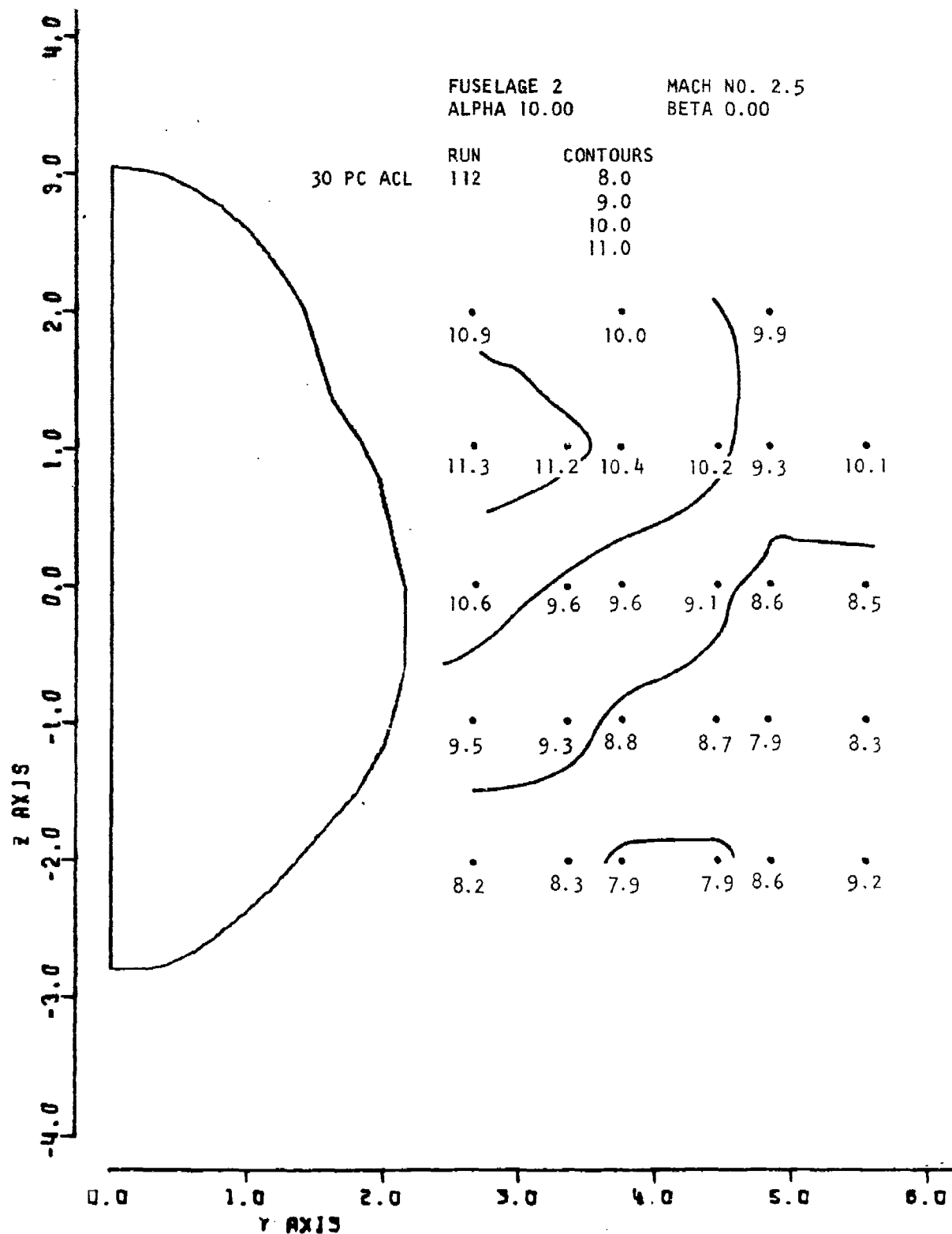


Figure 44. Local Alpha

gradient and consequently the upwash in the corner region. At the downstream station the shielding effect of the wing on reducing the level of downwash, especially in the upper part of the survey region, is clearly discernible in Figures 45 and 46. Again, in the region of the lower fuselage corner, the local upwash is slightly higher for fuselage 1 than for fuselage 2.

3.1.2.3.2 Effect of Yaw

At the forward survey station the effect of yaw was, on the leeward side, to increase the level of upwash in the lower inboard region and to decrease it in the upper inboard part. On the windward side the opposite occurred, namely a decrease in the lower, and an increase in the upper part of the side survey region. This behavior can perhaps be best explained as resulting from the superposition of a simple cross flow field, generated by the yaw, on the basic unyawed flow field. Thus on the windward side the cross flow streamlines divide at the fuselage side, going around the top and bottom of the fuselage and joining up again at the leeward side of the fuselage. At the aft station the constraint posed by the presence of the wing modifies this simple picture. Thus in the vicinity of the wing under surface the upwash is about the same on both leeward and windward sides. But in the lower region it is seen that the upwash on the windward side is greatly reduced while on the leeward side it is increased, in keeping with the cross-flow explanation. The effects are seen in Figures 47 through 50.

3.1.2.4 Local Sigma

3.1.2.4.1 Effect of Vehicle Geometry

At this angle of attack fuselage cross-flow affected local sidewash angles. Compared to the low angle of attack case, sidewash at the forward survey plane was more negative except for the upper inboard corner of the survey region where a small pocket of positive sigma resided. At the downstream station, the wing compression induced a higher and more negative, level of sidewash, as can be seen from Figures 51 and 52, with a pocket of positive sidewash still evident in the upper inboard corner which, at this station, could be induced by the wing-body juncture interference flow.

3.1.2.4.2 Effect of Yaw

At the forward survey station the effect of yaw was virtually the same for both fuselage cross section shapes. On the leeward side the local sidewash angles were all negative, diminishing in the direction approaching the side of the fuselage, as may

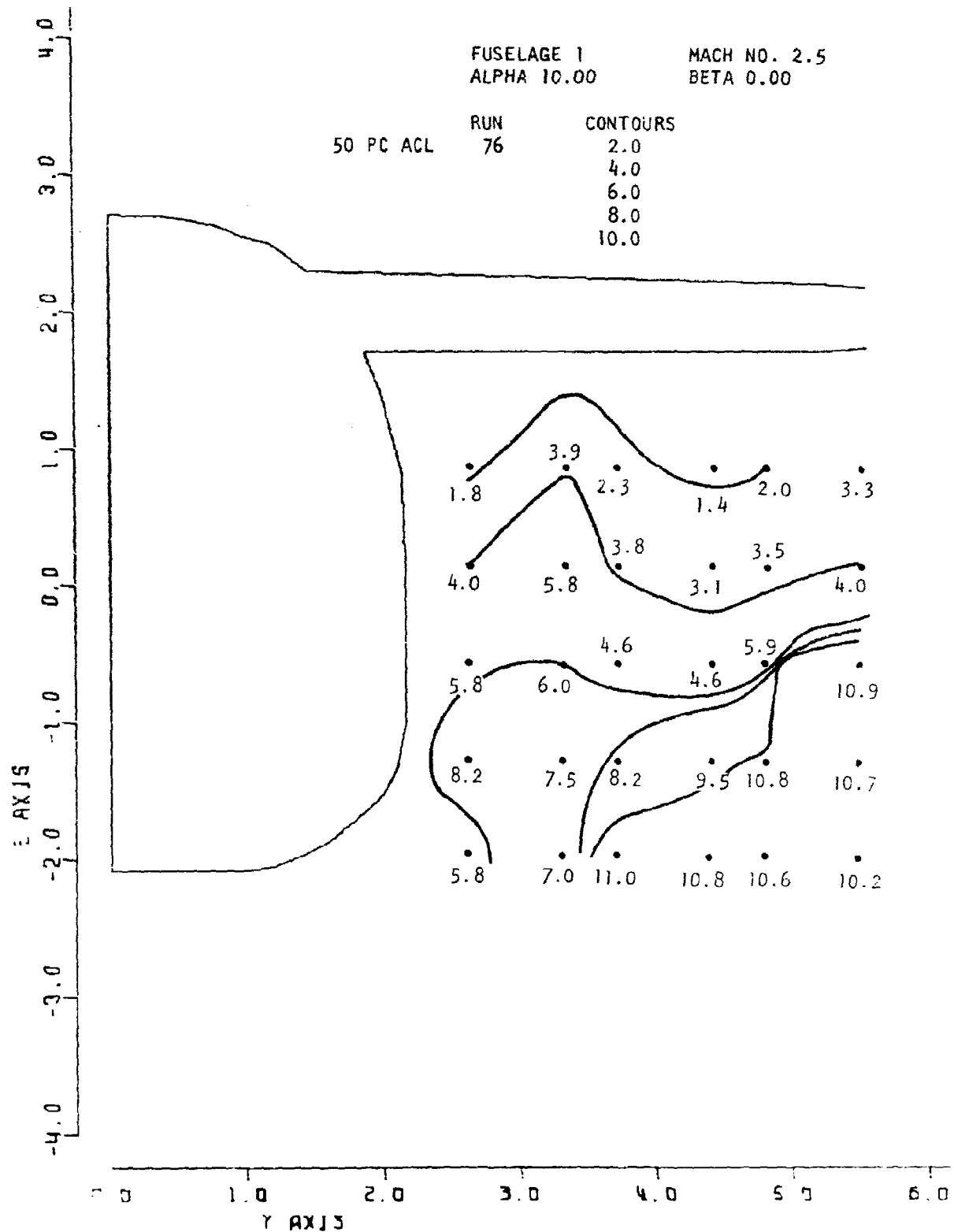


Figure 45. Local Alpha

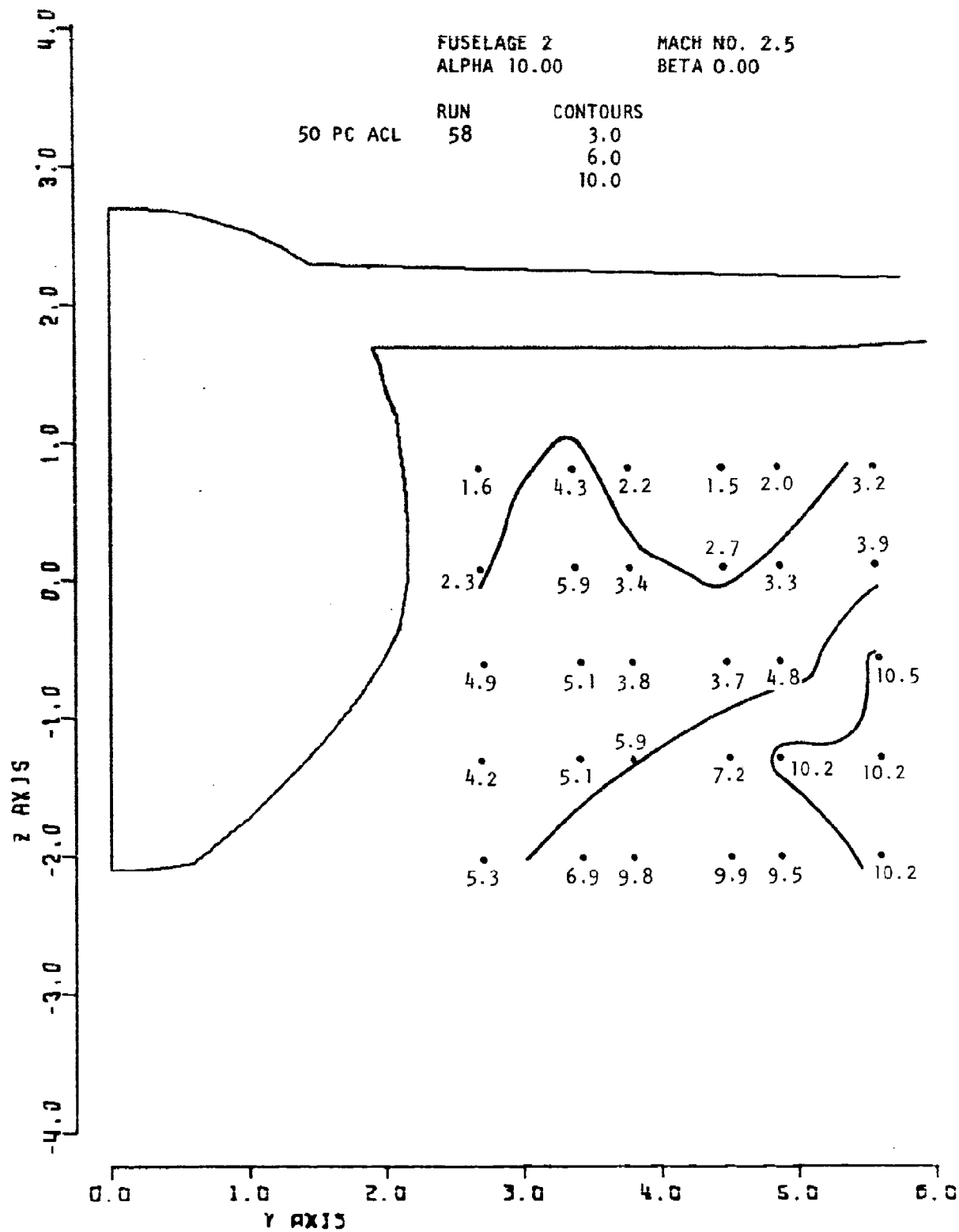
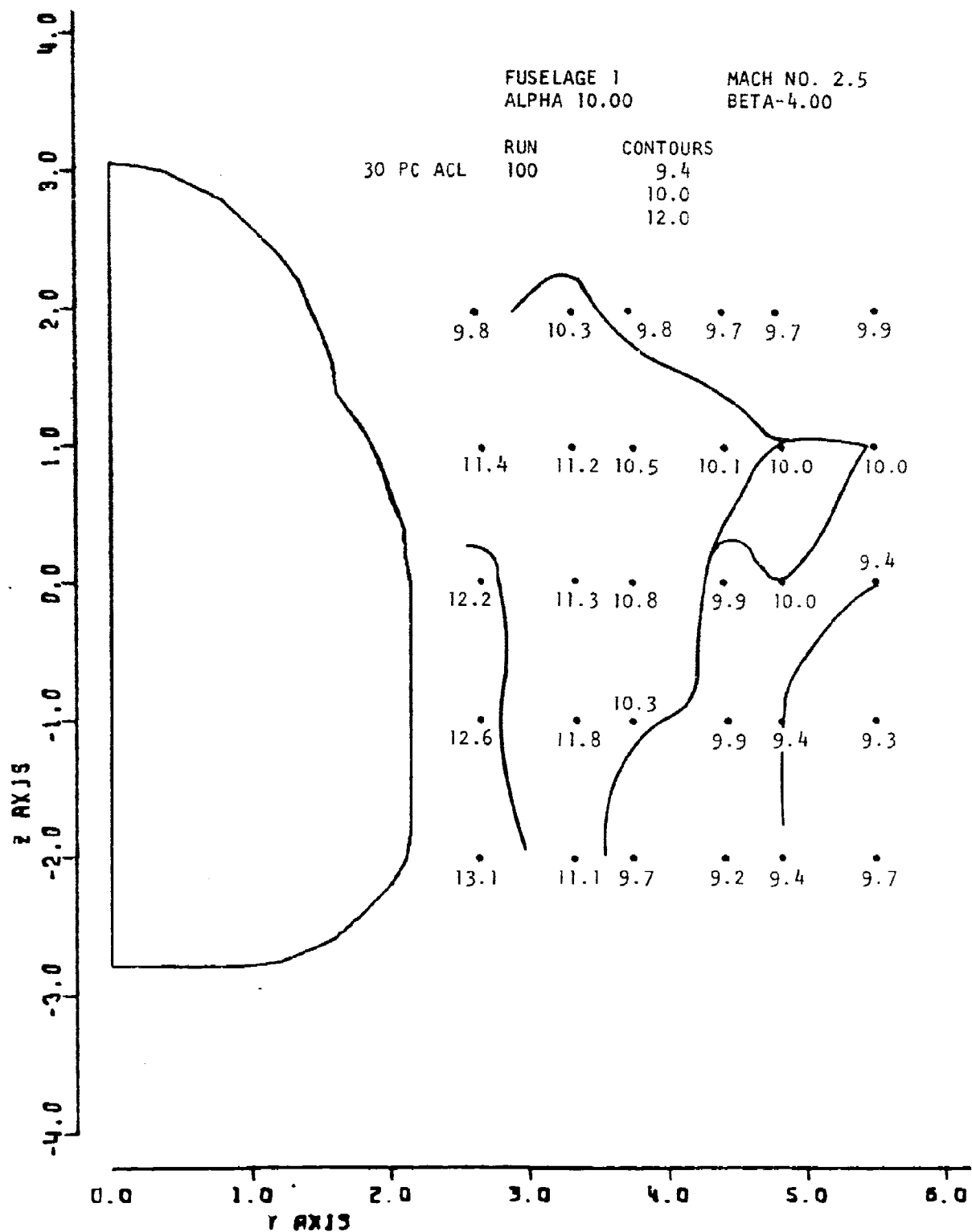


Figure 46. Local Alpha



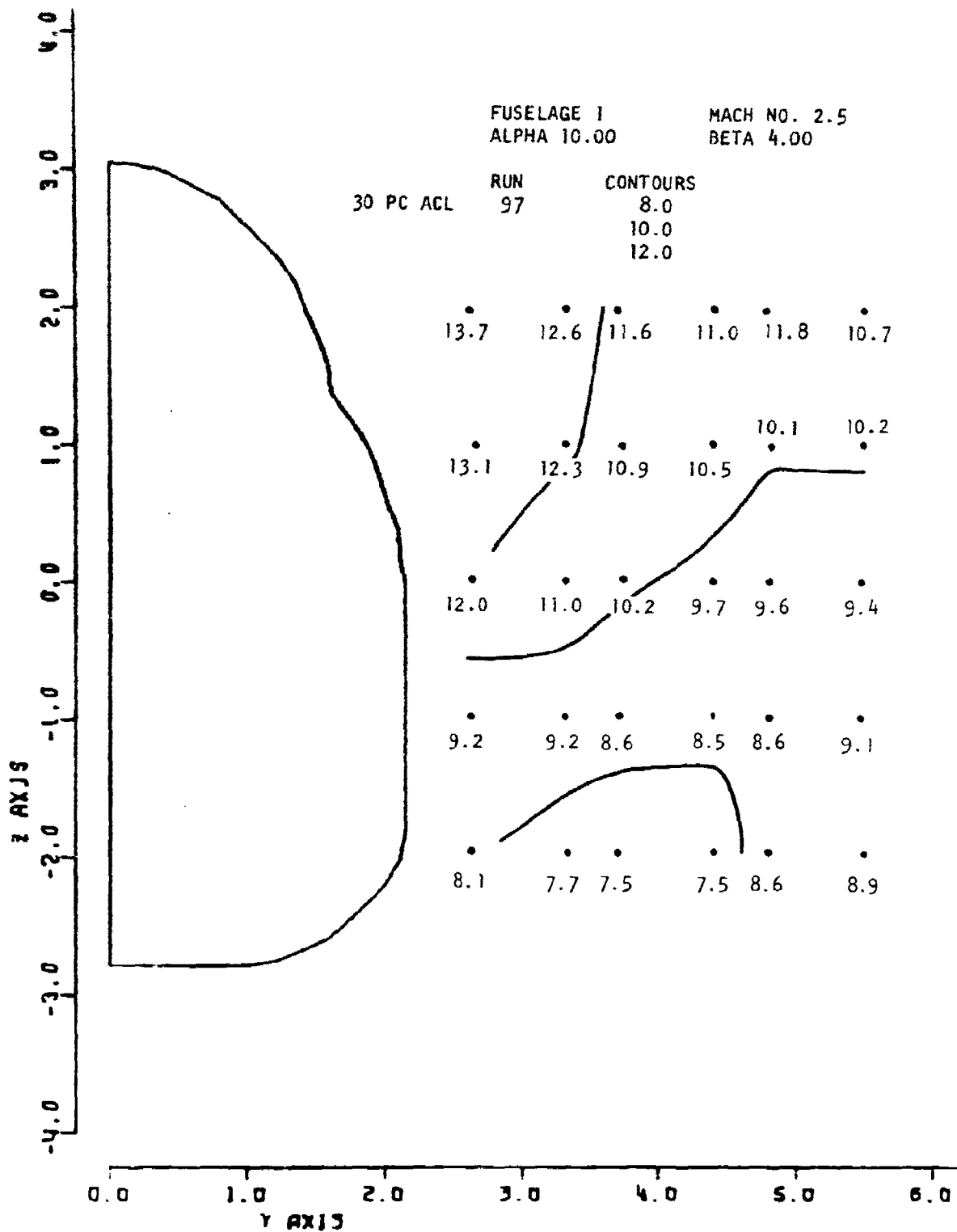


Figure 48. Local Alpha

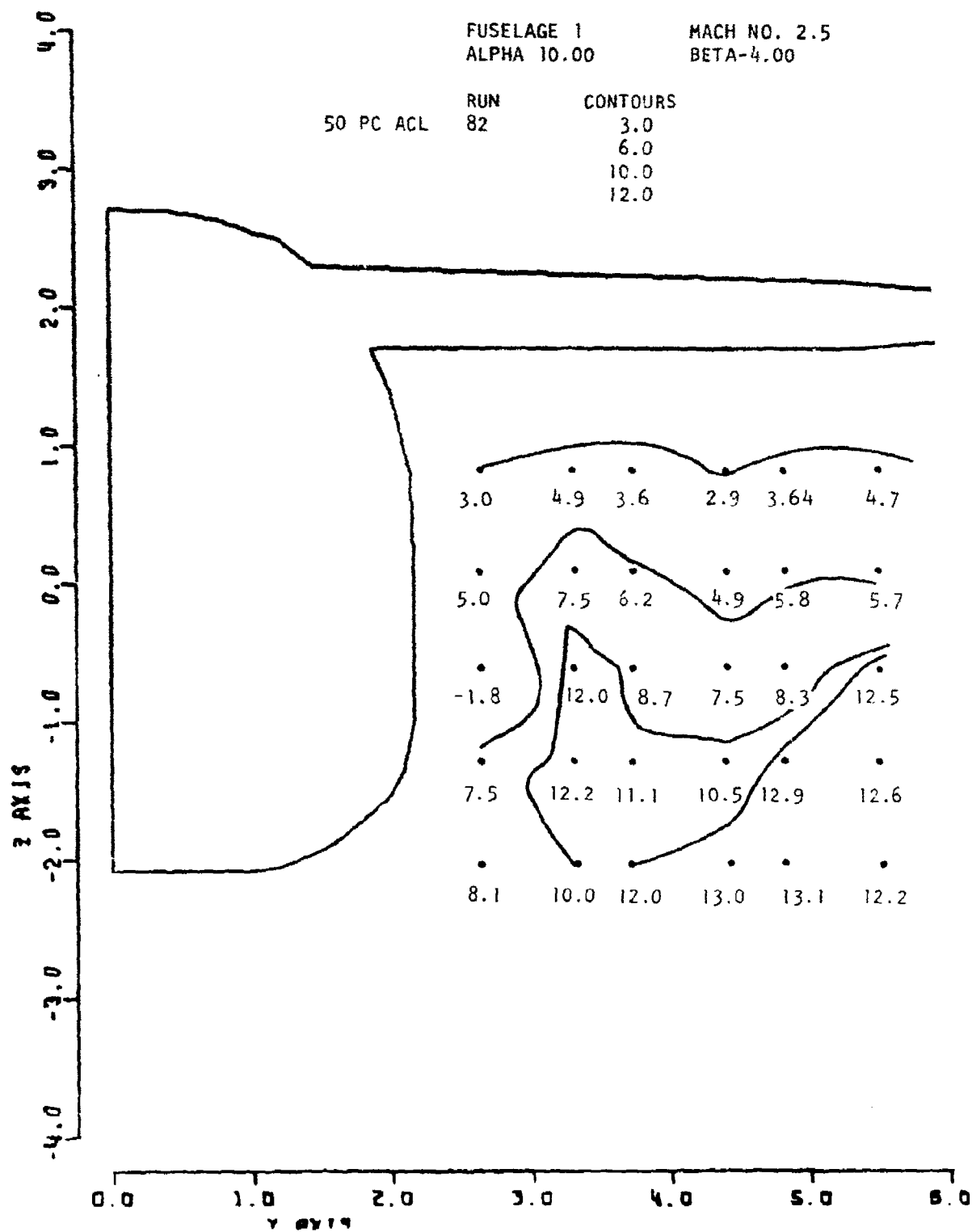


Figure 49. Local Alpha

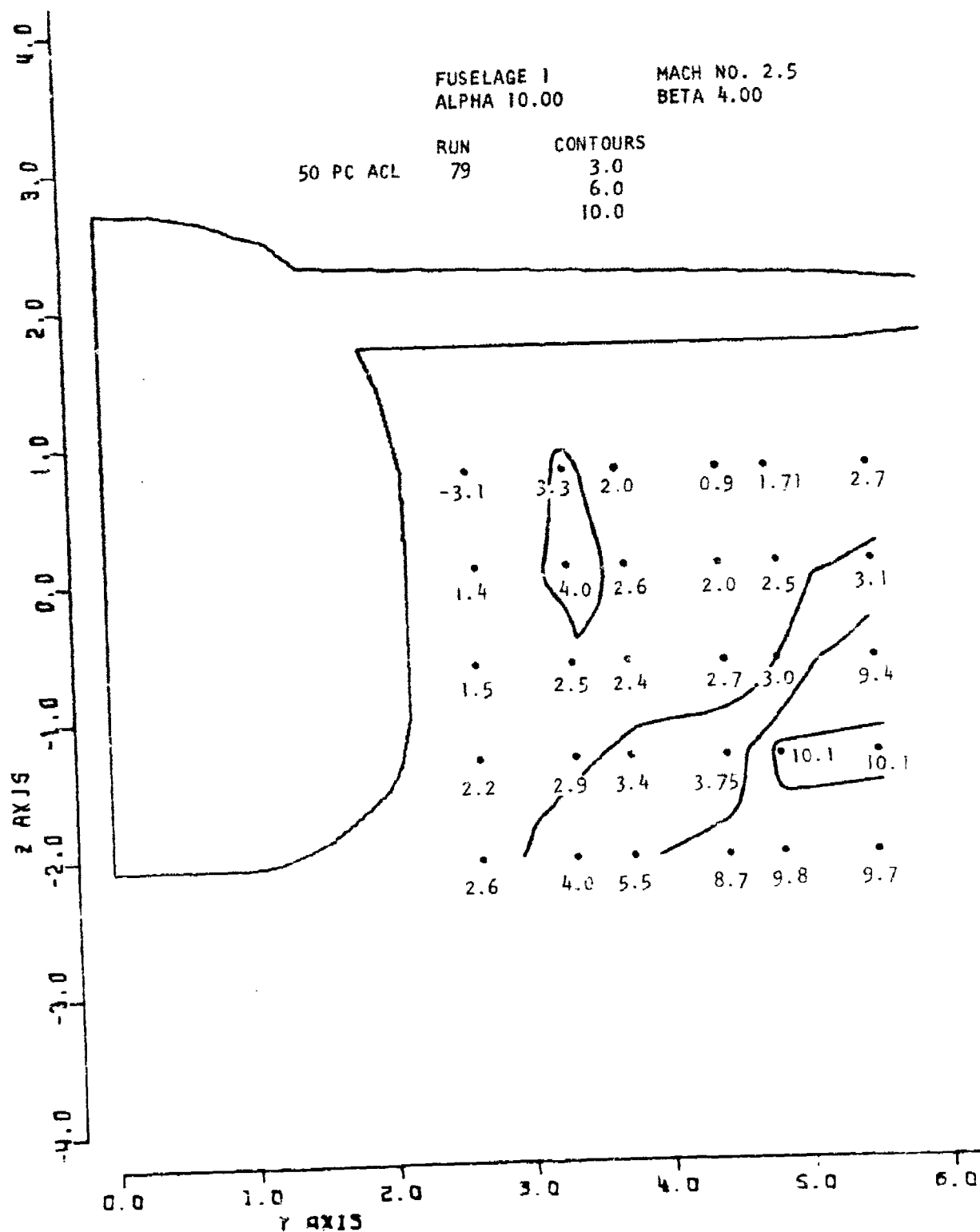
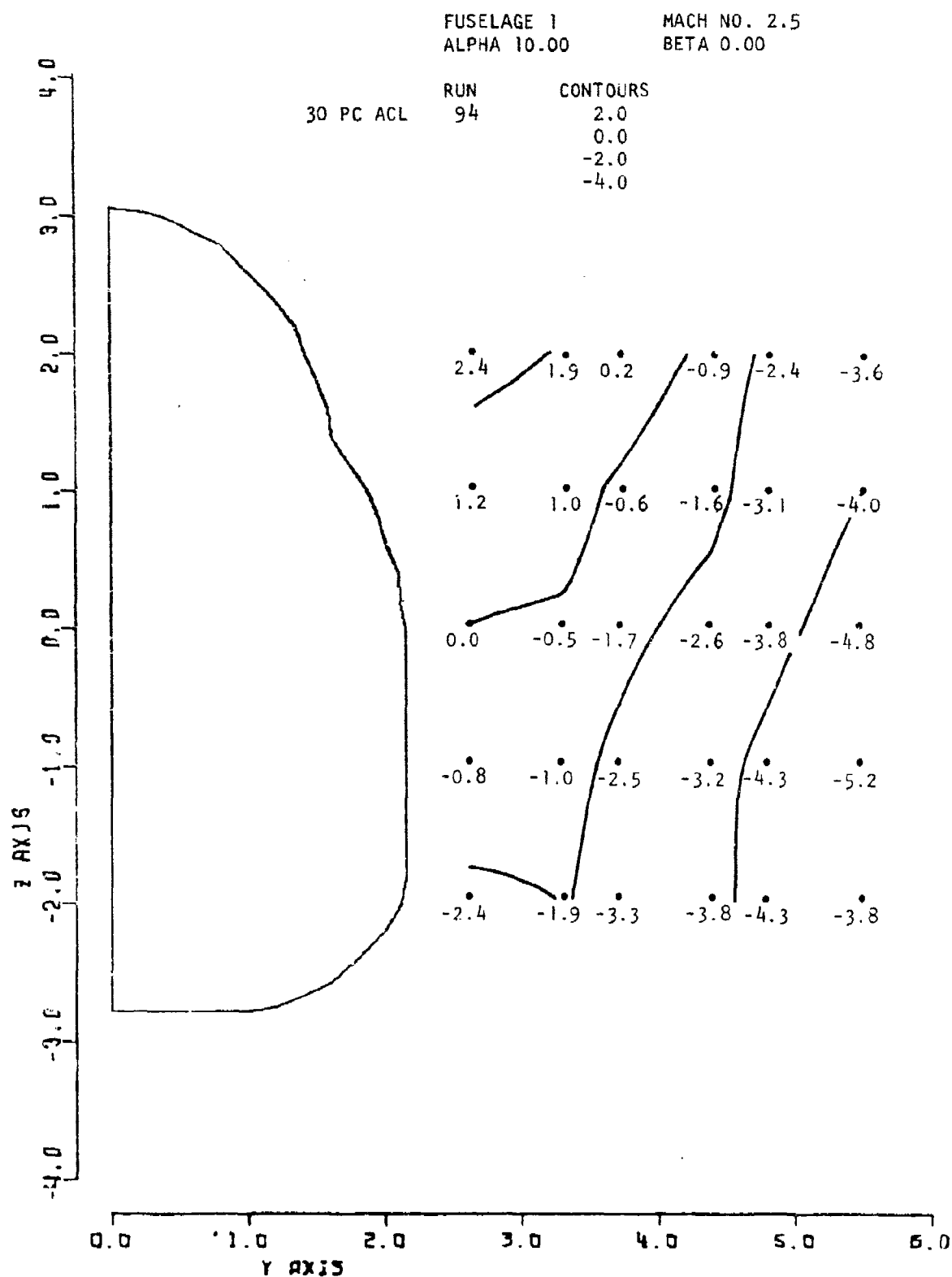


Figure 50. Local Alpha



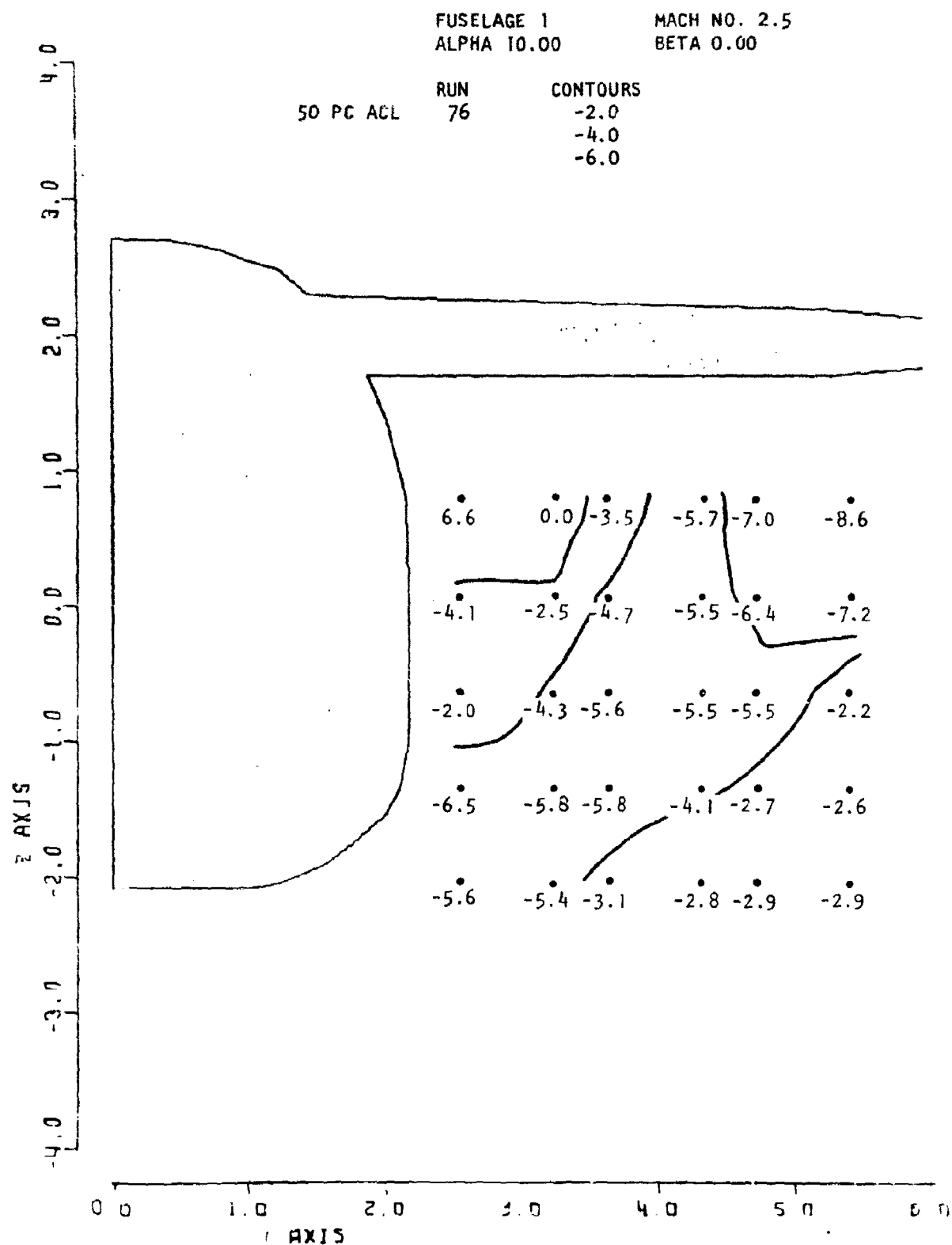


Figure 52, Local Sigma

be seen from the data shown in Figure 53 for fuselage 1. On the windward side the pattern of local sidewash was similar to that for the zero yaw case, but increased by an almost uniform positive increment in sidewash of about 1° , as can be seen by comparing Figures 51 and 54.

At the downstream survey plane for both fuselage shapes the sidewash angles on the leeward side became more negative, and on the windward side more positive due to the yaw which is to be expected. These effects are shown in Figures 55 and 56.

3.1.3 High Angle of Attack

3.1.3.1 Local Mach Number

3.1.3.1.1 Effect of Vehicle Geometry

At the forward station the same fuselage effects observed at the intermediate angle of attack were present at this higher angle of attack of 20° . Thus, the local Mach numbers in the vicinity of the lower corner of fuselage 1 were somewhat higher than for fuselage 2 which, with its larger radius, introduced the pressure field induced by the lower fuselage contour into the inner region of the survey area. The increased expansion over the upper fuselage contour was evidenced by local Mach numbers in the upper portion of the surveyed region which were higher than those of the preceding intermediate angle of attack case. These effects may be discerned in Figures 57 and 58. At the aft survey station differences in geometry produced no appreciable effect. The effect of the wing pressure field was evident in the lower Mach numbers measured over the major part of the survey region as shown in Figure 59.

3.1.3.1.2 Effect of Yaw

The excursion to 4° yaw at this high angle of attack produced virtually no change from the local Mach number distributions of the zero yaw case for both fuselage 1 and 2.

3.1.3.2 Total Pressure Recovery

3.1.3.2.1 Effect of Vehicle Geometry

At this high angle of attack the recovery levels still remained quite high even in the aft flow field, where it averaged about .91 for both fuselages. Fuselage effects were confined to the innermost region of the survey plane where, for fuselage 1, as

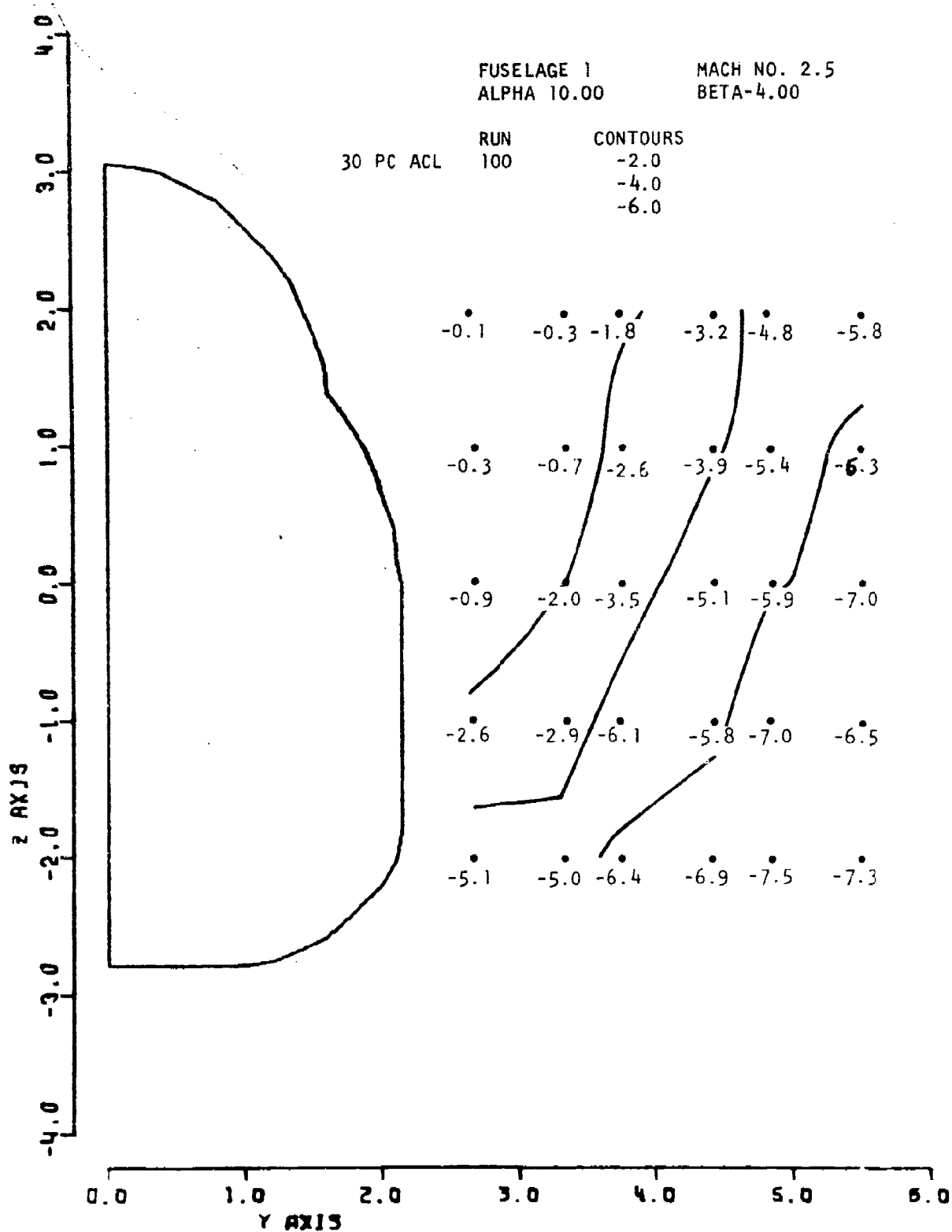


Figure 53. Local Sigma

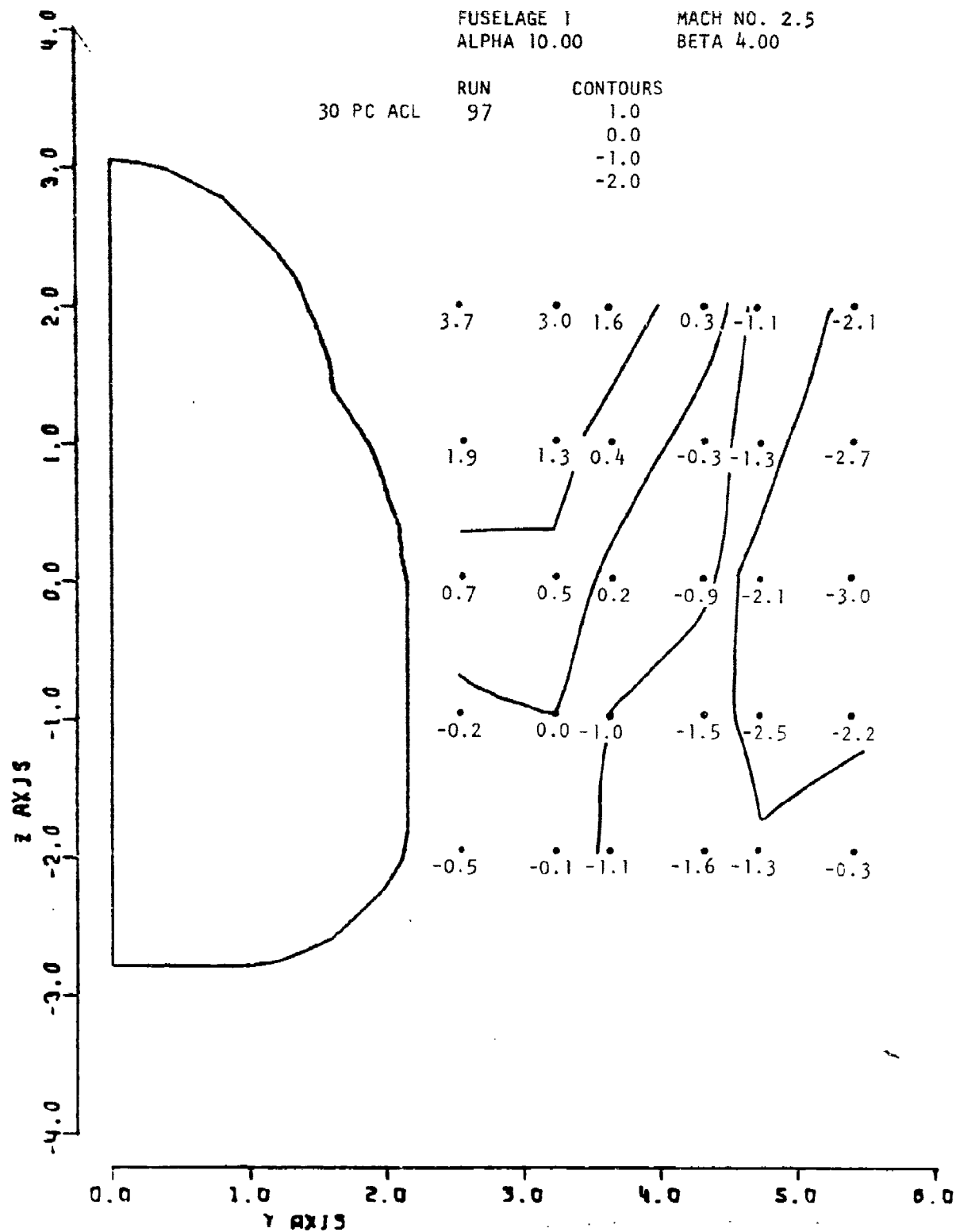


Figure 54. Local Sigma

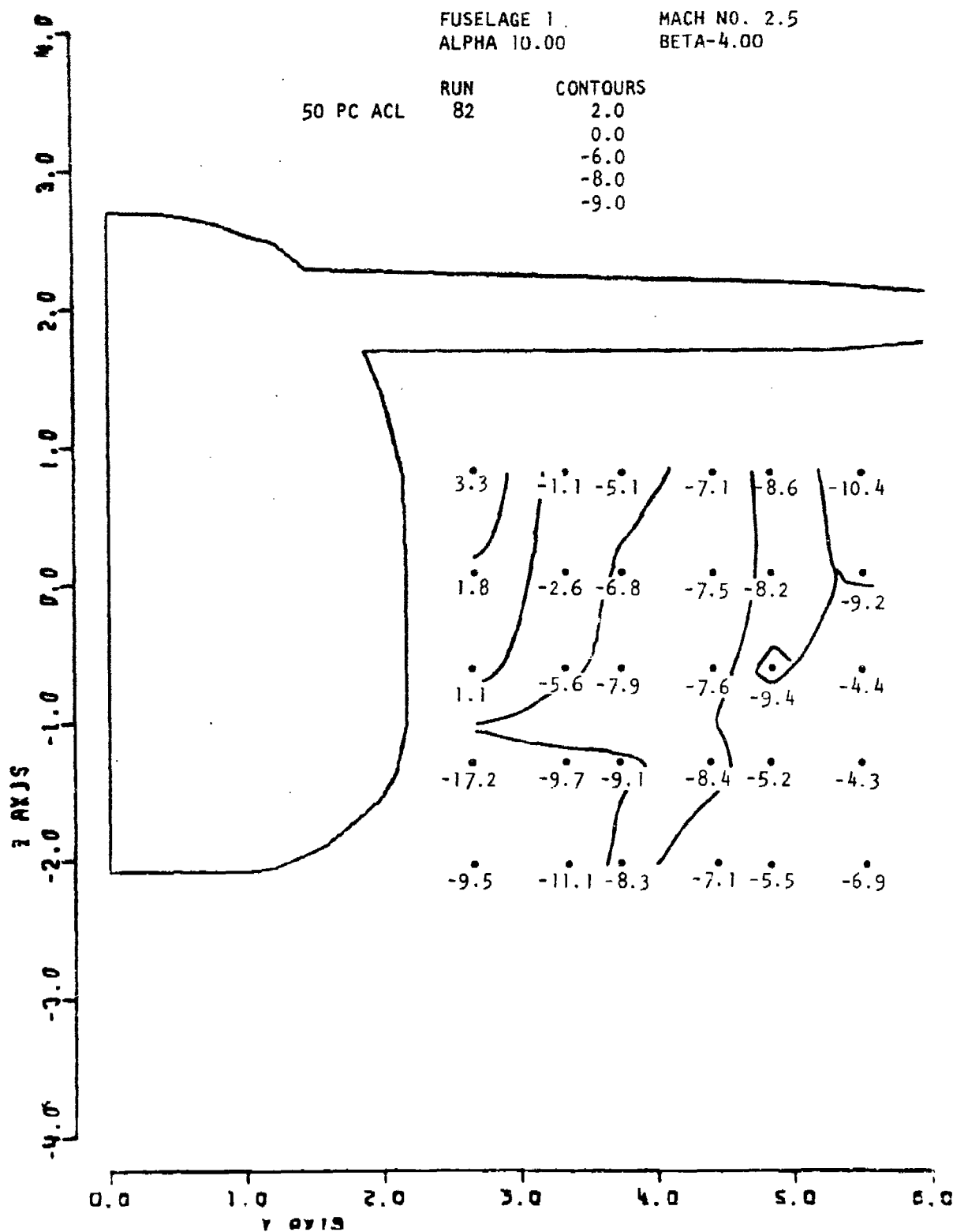


Figure 55. Local Sigma

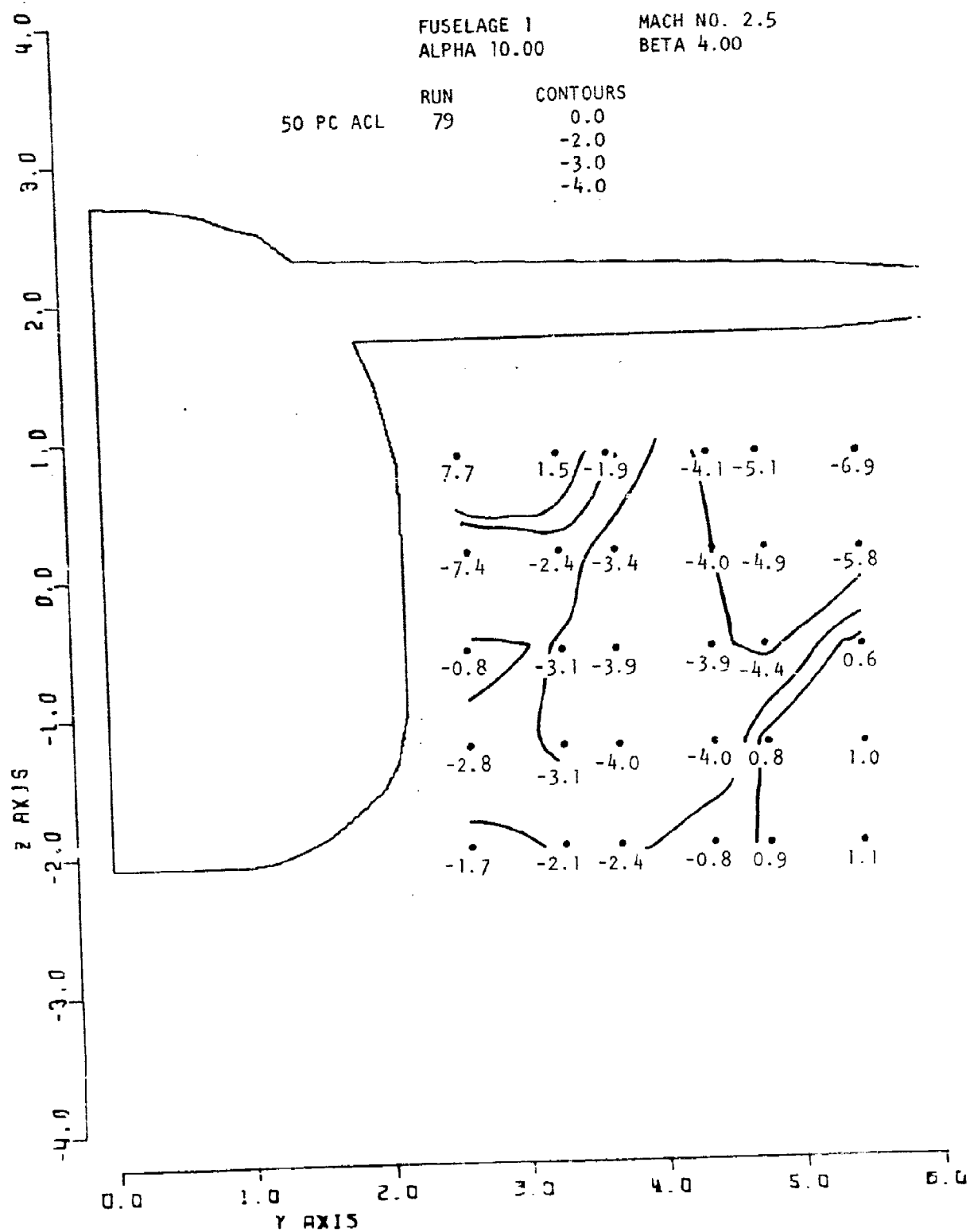
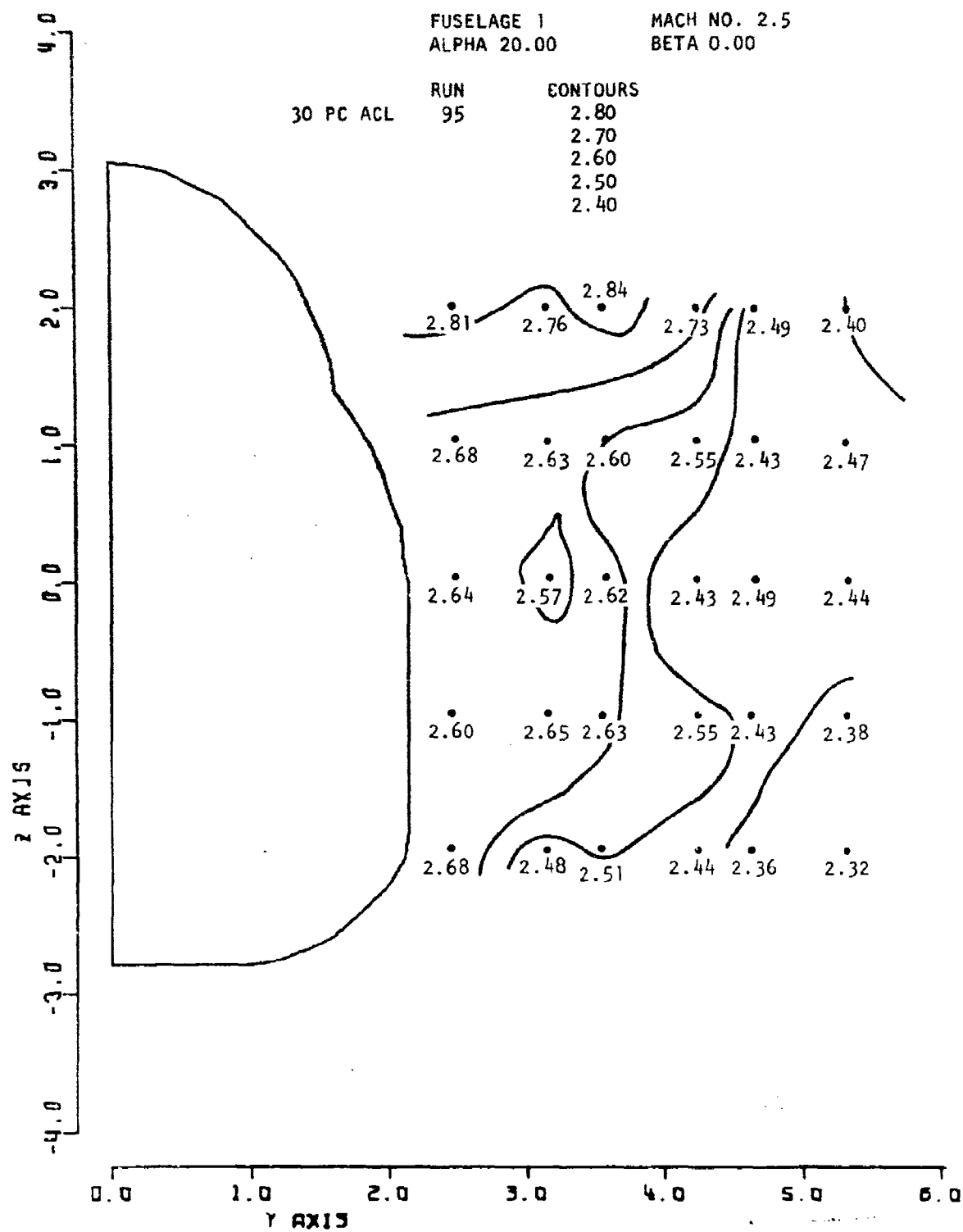


Figure 56. Local Sigma



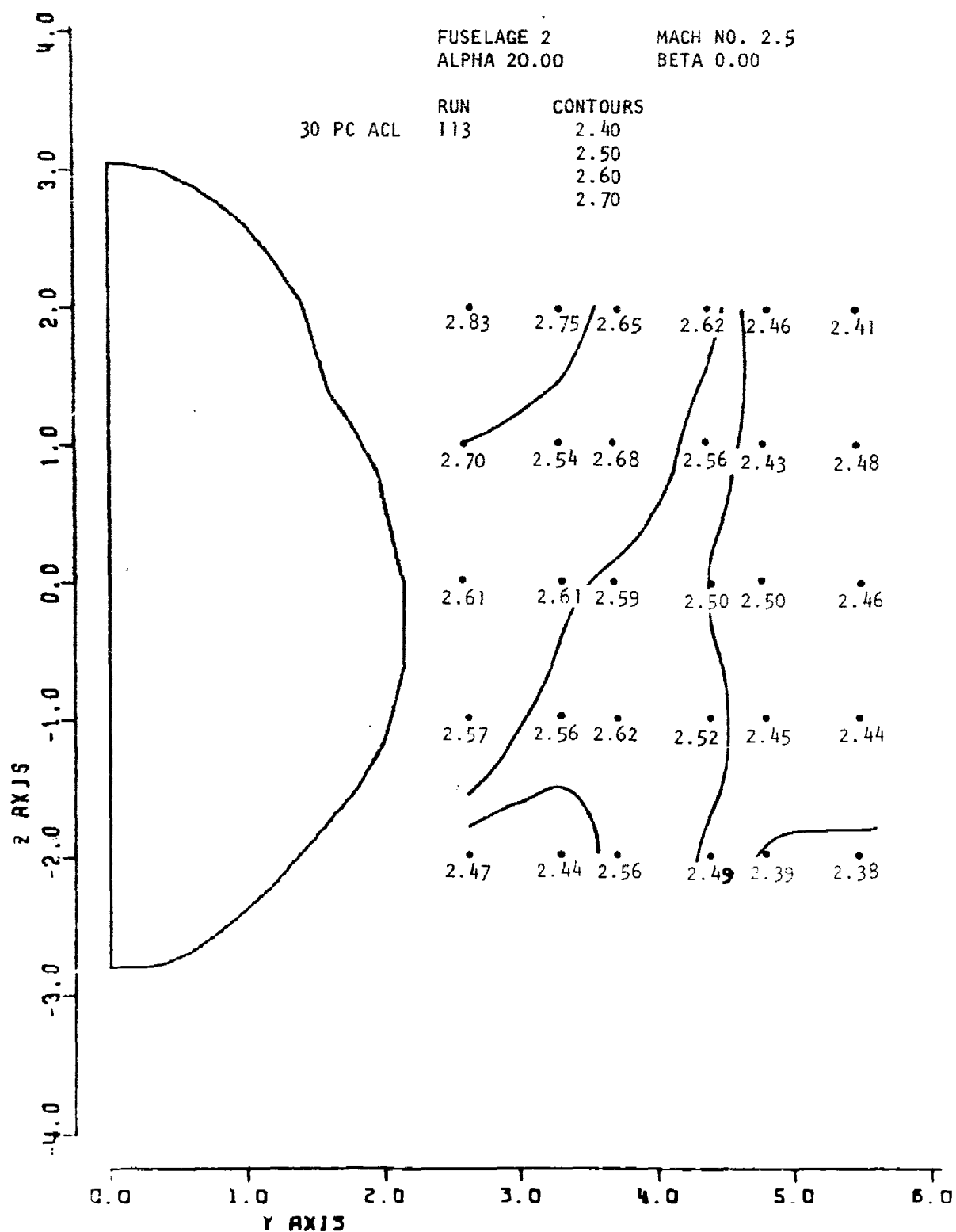


Figure 58. Local Mach No.

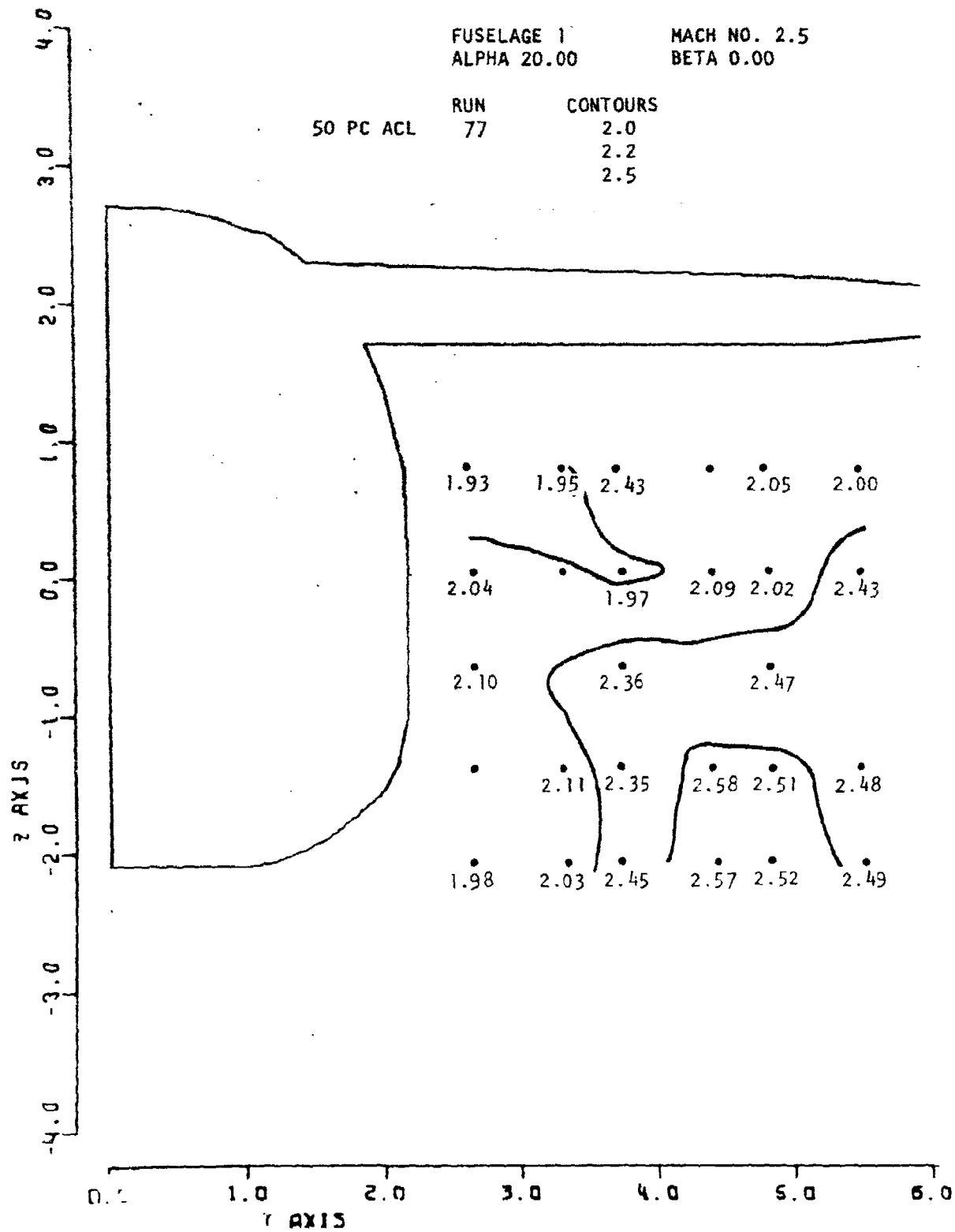


Figure 59. Local Mach No.

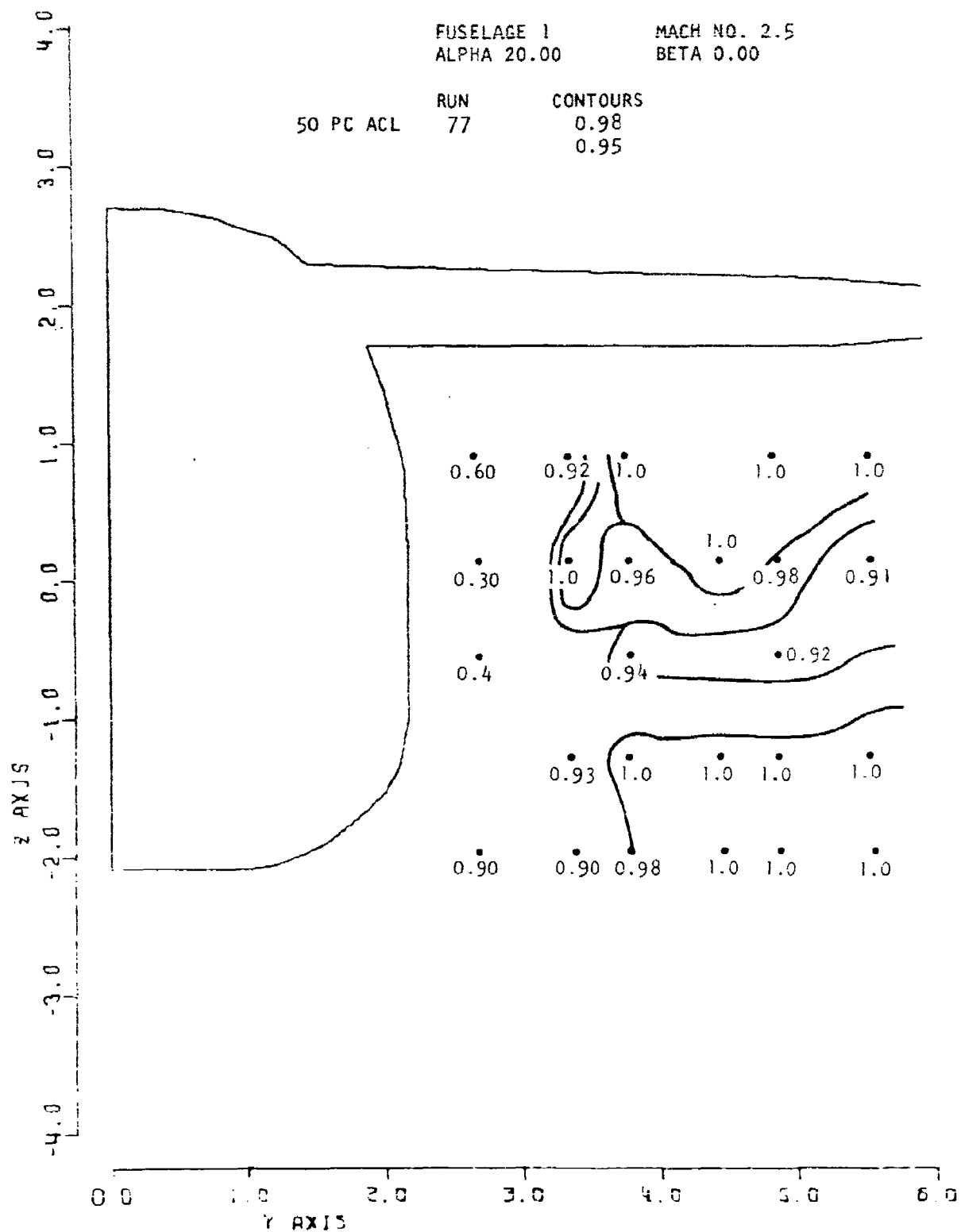


Figure 60. Local P_T/P_T

seen in Figure 60, the local total pressure recoveries were as low as 0.30, indicative of a local separation due probably to the stronger cross flow around the relatively sharper corner of fuselage 1. The fuselage 2 flow field did not display such losses as may be seen from Figure 61.

3.1.3.2.2 Effect of Yaw

The effect of $\pm 4^\circ$ yaw at this high angle of attack condition on local pressure recovery was very small, for both fuselage shapes at both survey stations, as it was for the intermediate angle of attack condition.

3.1.3.3 Local Alpha

3.1.3.3.1 Effect of Vehicle Geometry

At the 30% ACL survey station the same effect of vehicle geometry observed for the intermediate angle of attack case was evident, namely, higher flow angularity in the region of the lower fuselage corner for fuselage 1 as compared to fuselage 2. This can be seen from the data presented in Figures 62 and 63. At the downstream station the average level of upwash was significantly reduced due to the shielding effect of the wing, for both fuselages, as shown in Figures 64 and 65. This behavior was already noted in the intermediate angle of attack results. The negative values of downwash in the inboard region adjacent to the fuselage are indicative of a local vortex type flow condition caused by flow separation due to the interaction of the wing leading shock wave and the fuselage side boundary layer. This condition also manifested itself in the high angle of attack test results at Mach 3.5 described in a following section, as well as the lower Mach number tests reported on in the first volume of this report.

3.1.3.3.2 Effect of Yaw

At the forward survey plane the effect of yaw at this high angle of attack, relative to the unyawed case, was to increase the upwash slightly in the lower leeward region and decrease it on the windward side, which was observed in the intermediate angle of attack case. The same behavior was noted at the aft station although over a larger region. This effect of yaw on local angle of attack is exemplified in Figure 66 to 69 for fuselage 1. This effect of yaw was found to be practically independent of fuselage geometry.

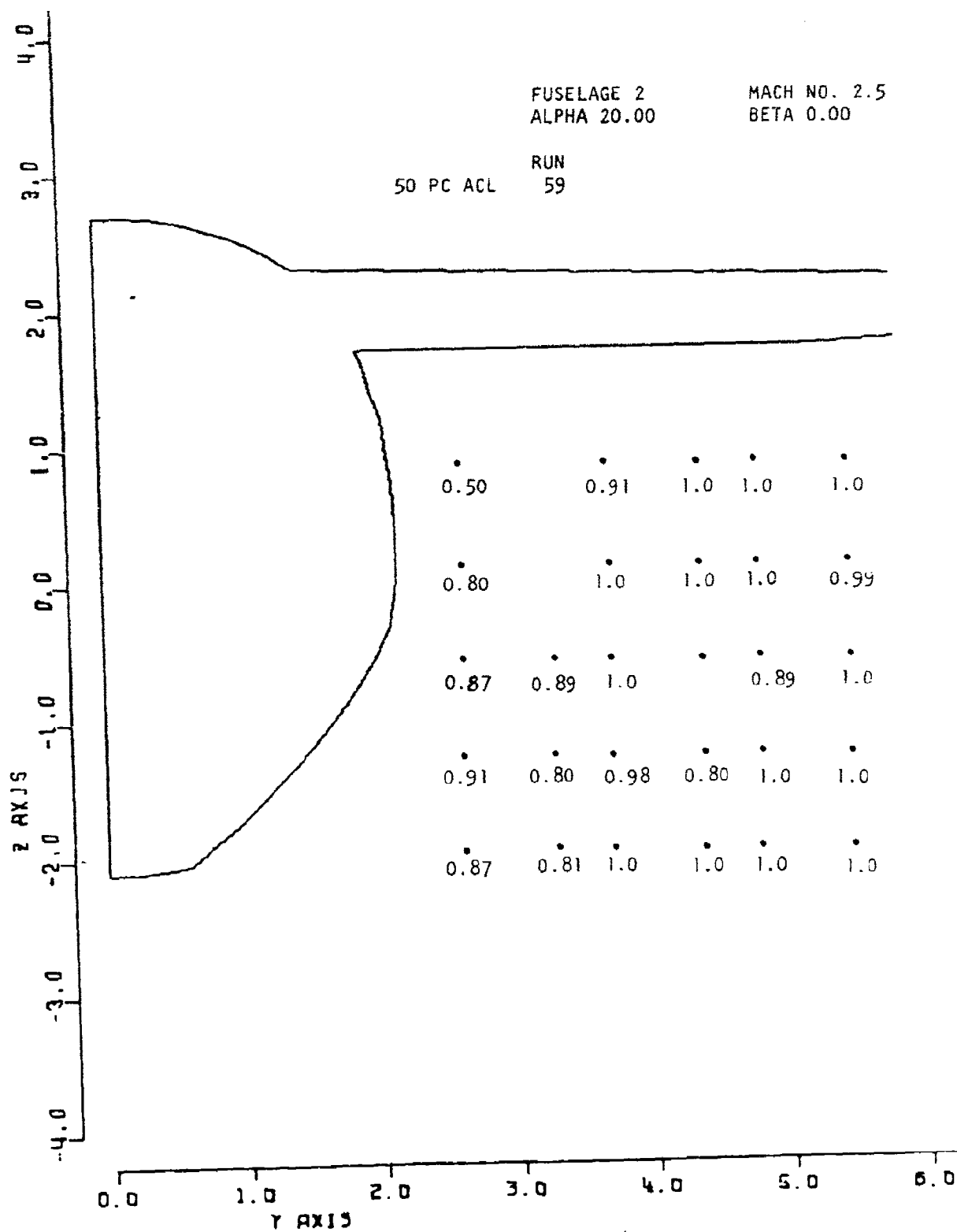


Figure 61 Local PT/PT

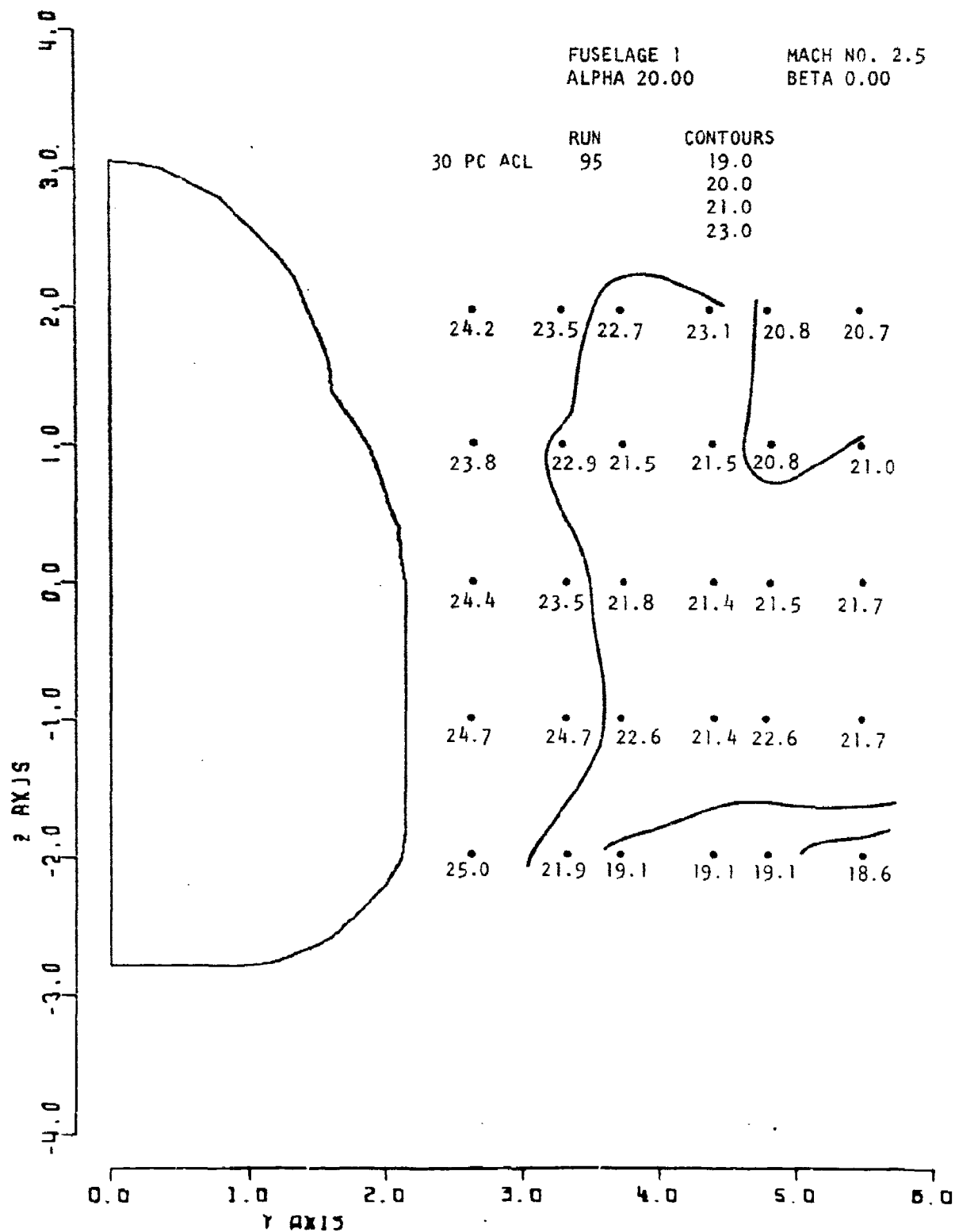


Figure 62. Local Alpha

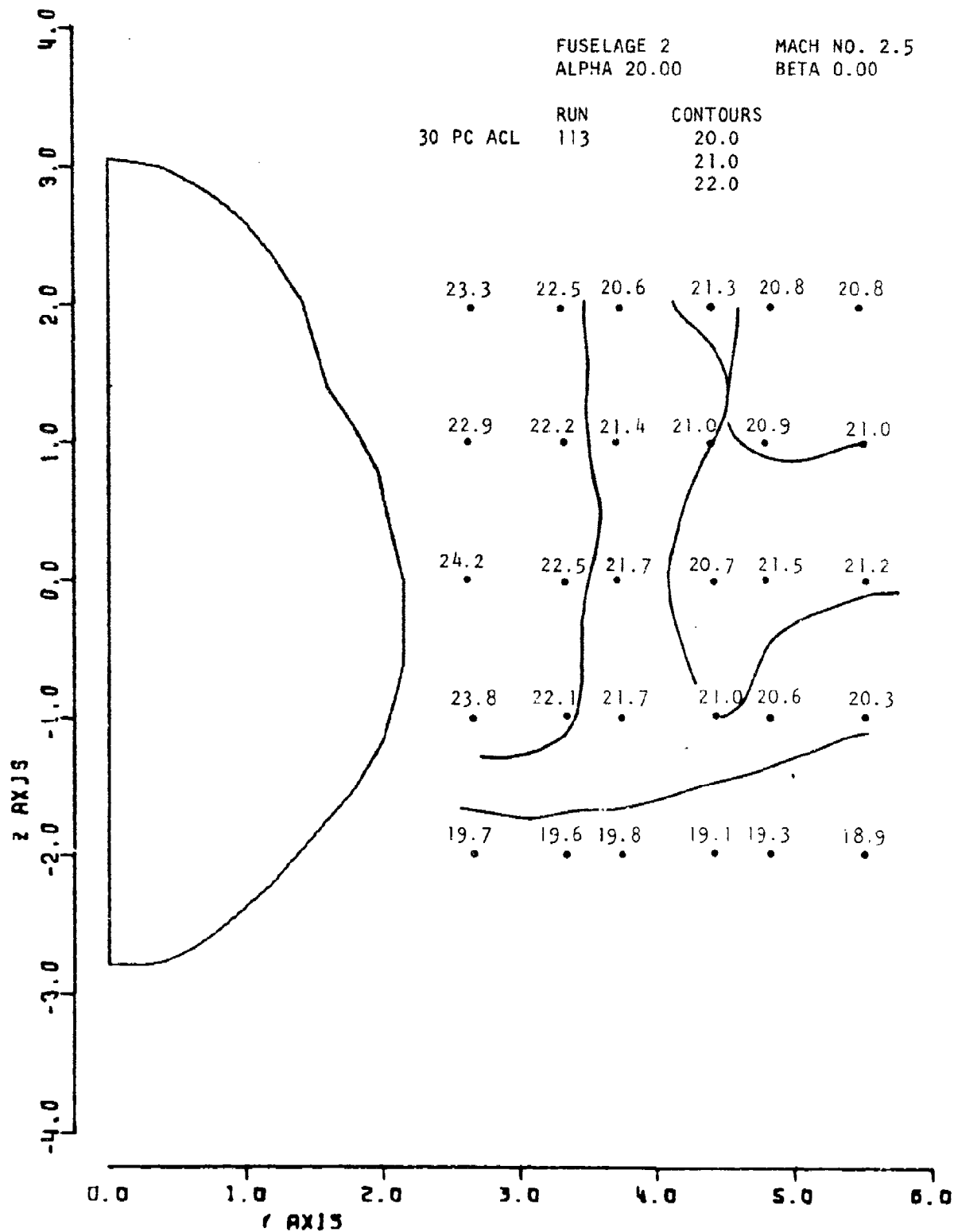


Figure 63. Local Alpha

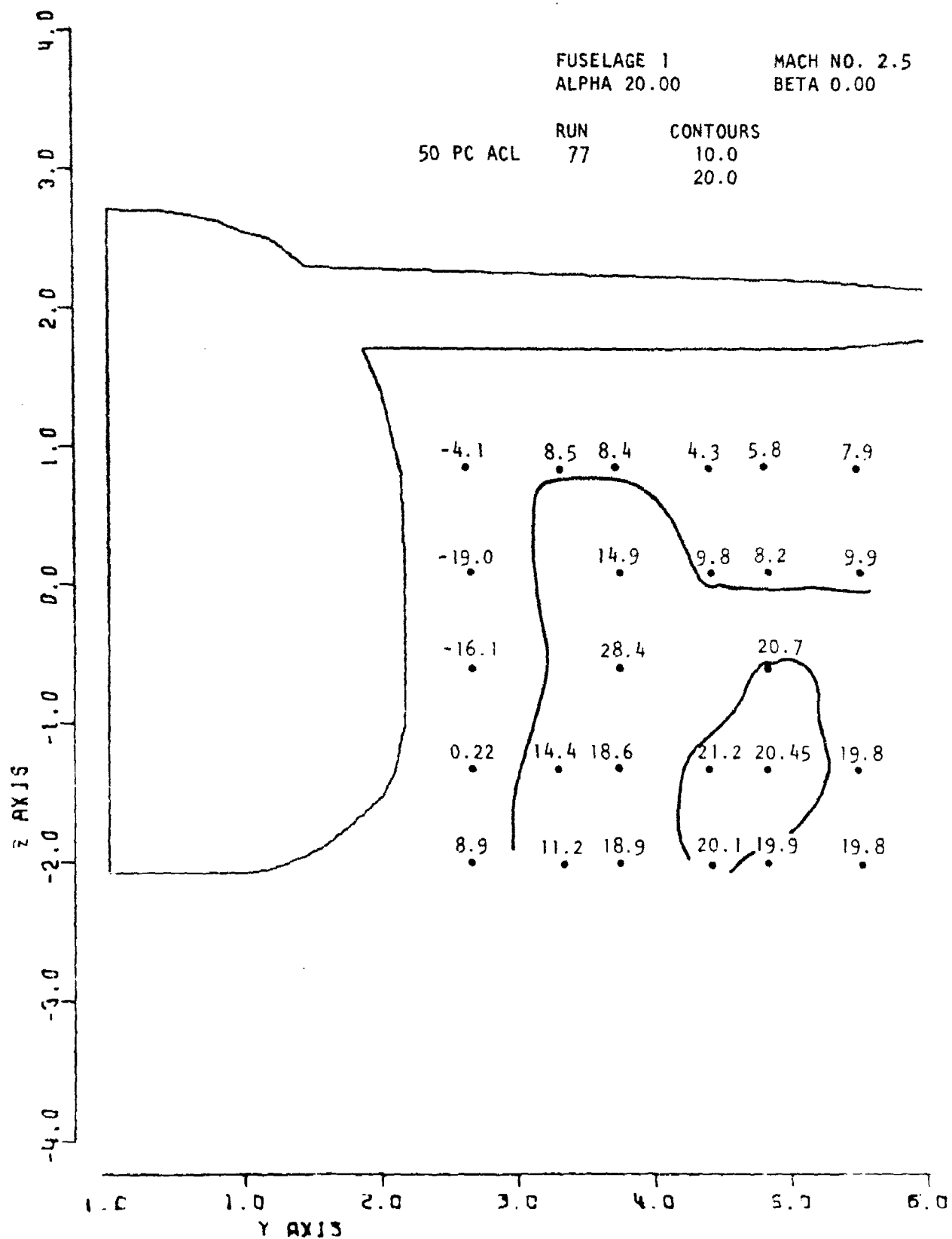


Figure 64. Local Alpha

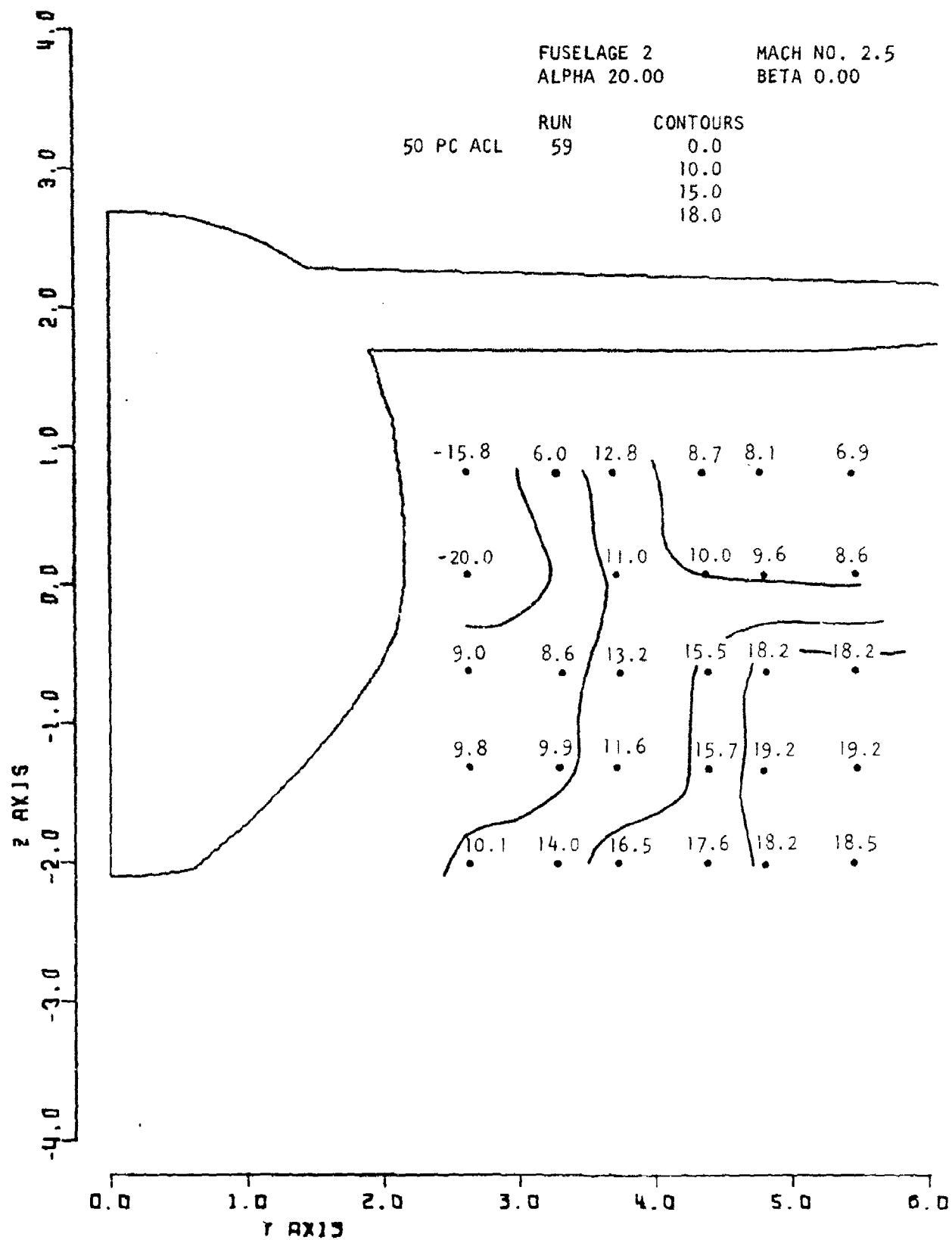


Figure 65. Local Alpha

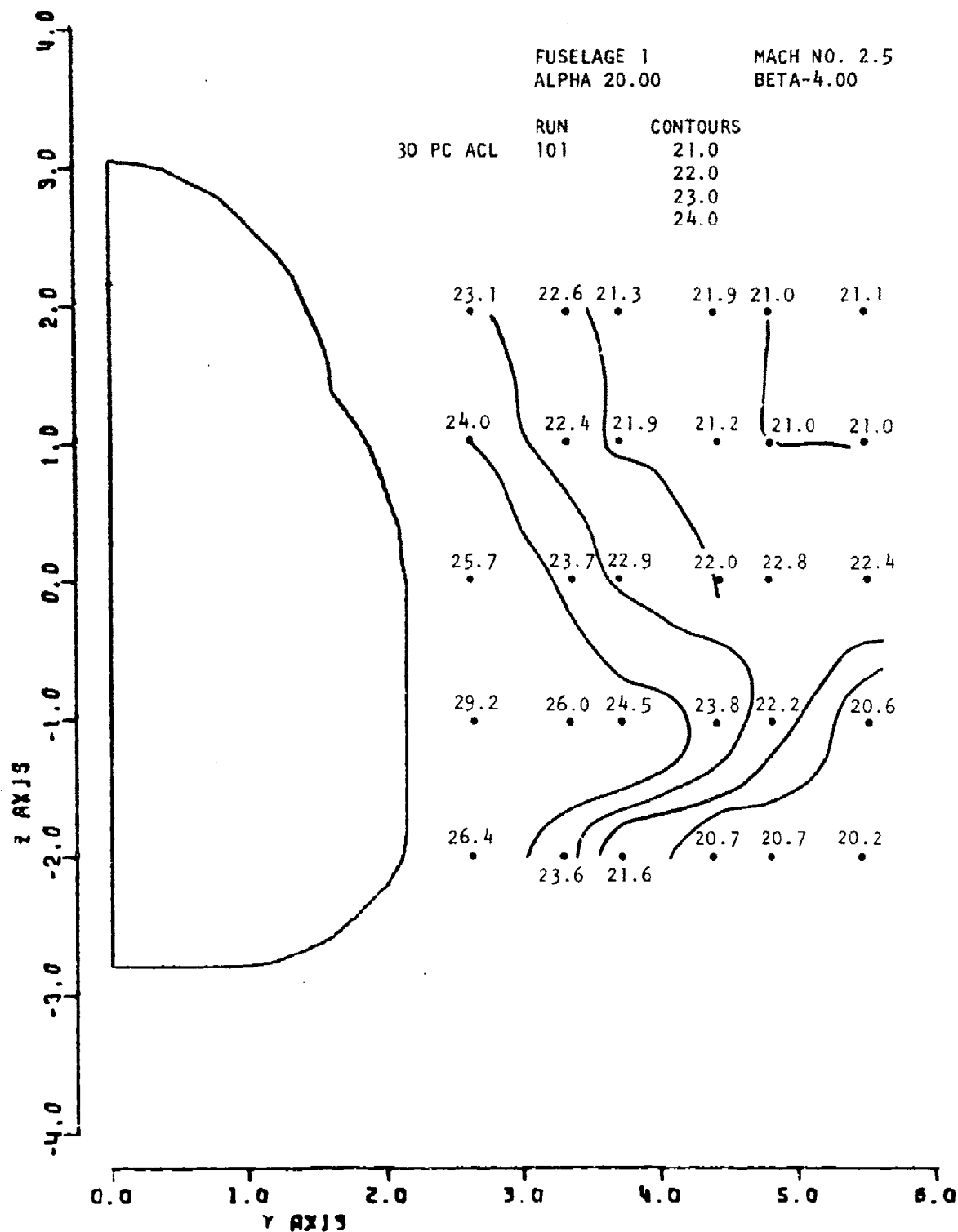


Figure 66. Local Alpha

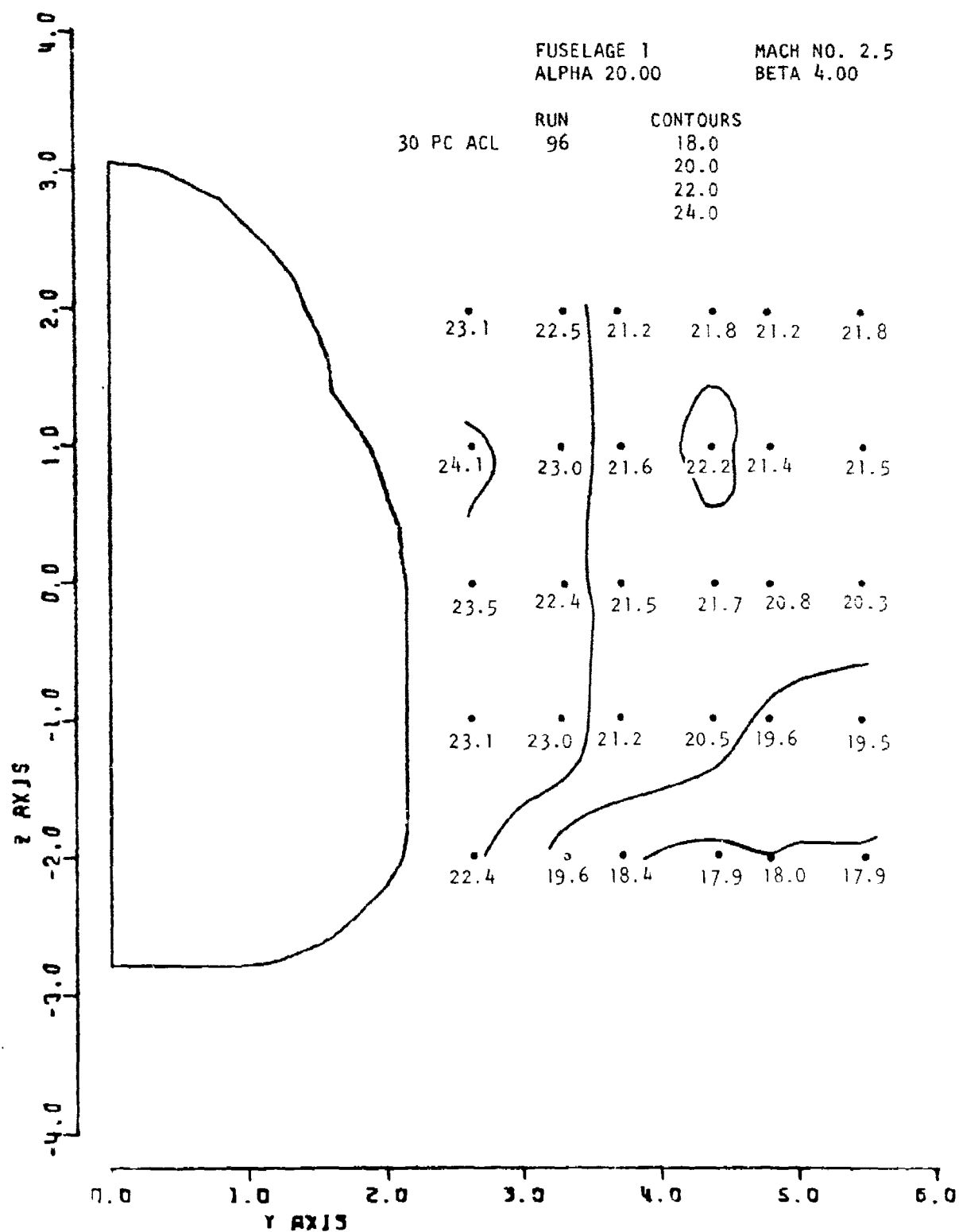
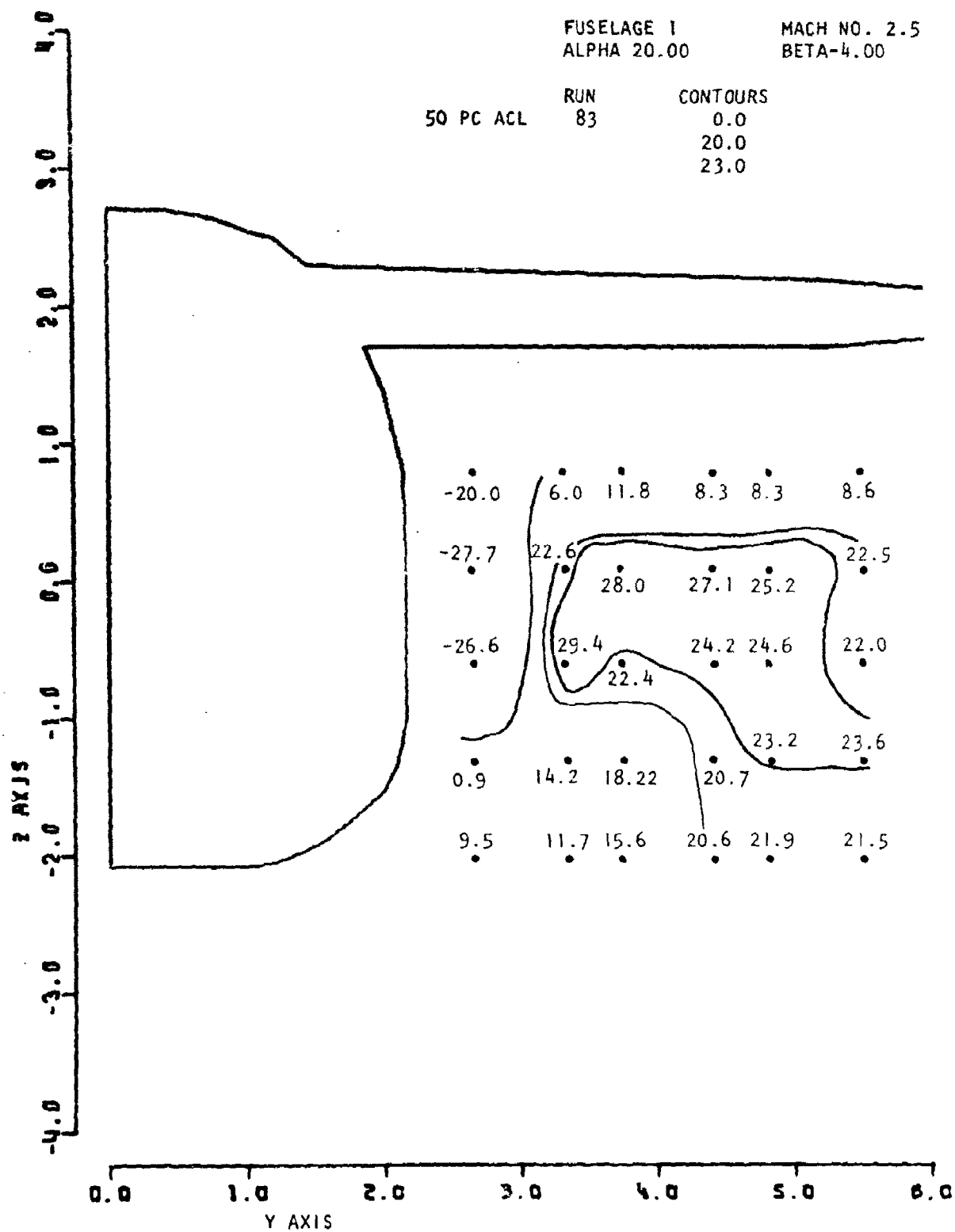


Figure 67. Local Alpha



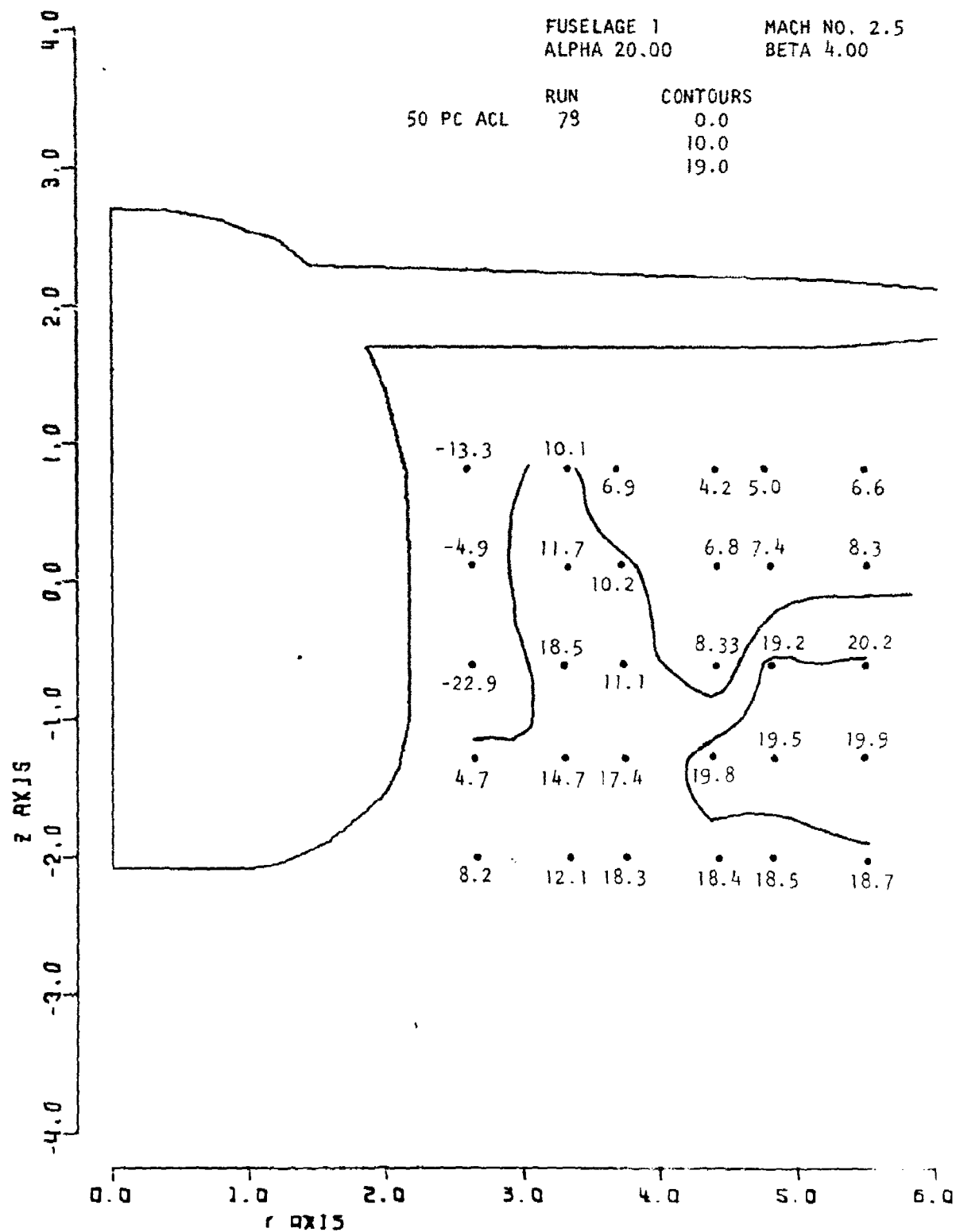


Figure 69. Local Alpha

3.1.3.4 Local Sigma

3.1.3.4.1 Effect of Vehicle Geometry

The same general effects which became evident at the intermediate angle of attack were manifested and more pronounced at this high angle of attack condition. Thus, the local sidewash angles were all negative (outward directed) except for the upper corner of the inboard region where there was a pocket of positive sidewash. As mentioned earlier in connection with the intermediate angle of attack case, positive angles in this region are probably due to the wing-body juncture interference flow effects at the aft station and, due to the lateral flow displacement effect of the canopy at the forward station. Again, the effect of differences in fuselage cross section geometry was negligible. These effects are illustrated for fuselage 1 in Figures 70 and 71.

3.1.3.4.2 Effect of Yaw

At both fore and aft stations the chief effect of 4° yaw was to induce a small increment in sidewash that was positive on the windward side, and negative on the leeward side, as may be seen from Figures 72 to 74 which present data taken at the aft survey station for fuselage 2.

3.2 Mach Number 3.5

3.2.1 Low Angle of Attack

3.2.1.1 Local Mach Number

3.2.1.1.1 Effect of Vehicle Geometry

Local Mach number distributions at the forward 30% ACL station are shown in Figures 75 and 77 for fuselages 1 and 2 respectively. The change in Mach number from 2.5 to 3.5 results in a thinner fuselage nose and canopy shock layer. The flow re-expansion fan associated with the higher Mach number is also shallower and a larger Mach number gradient exists, from body to shock, than is the case at Mach 2.5. The local Mach numbers differed from the free stream Mach number by a greater amount than was observed for the Mach 2.5 case, in keeping with the increased shock wave strength accompanying the higher free stream Mach number.

At the 50% ACL station, for both fuselages, the local Mach numbers in the upper half of the flow field were generally lower than those at the upstream station, while those in the lower half underwent a mild increase from their upstream values. This effect can be seen by comparing Figure 75 with 76, and 77 with 78. This behavior is attributed to the shallower shock and Mach wave angles connected with this higher free

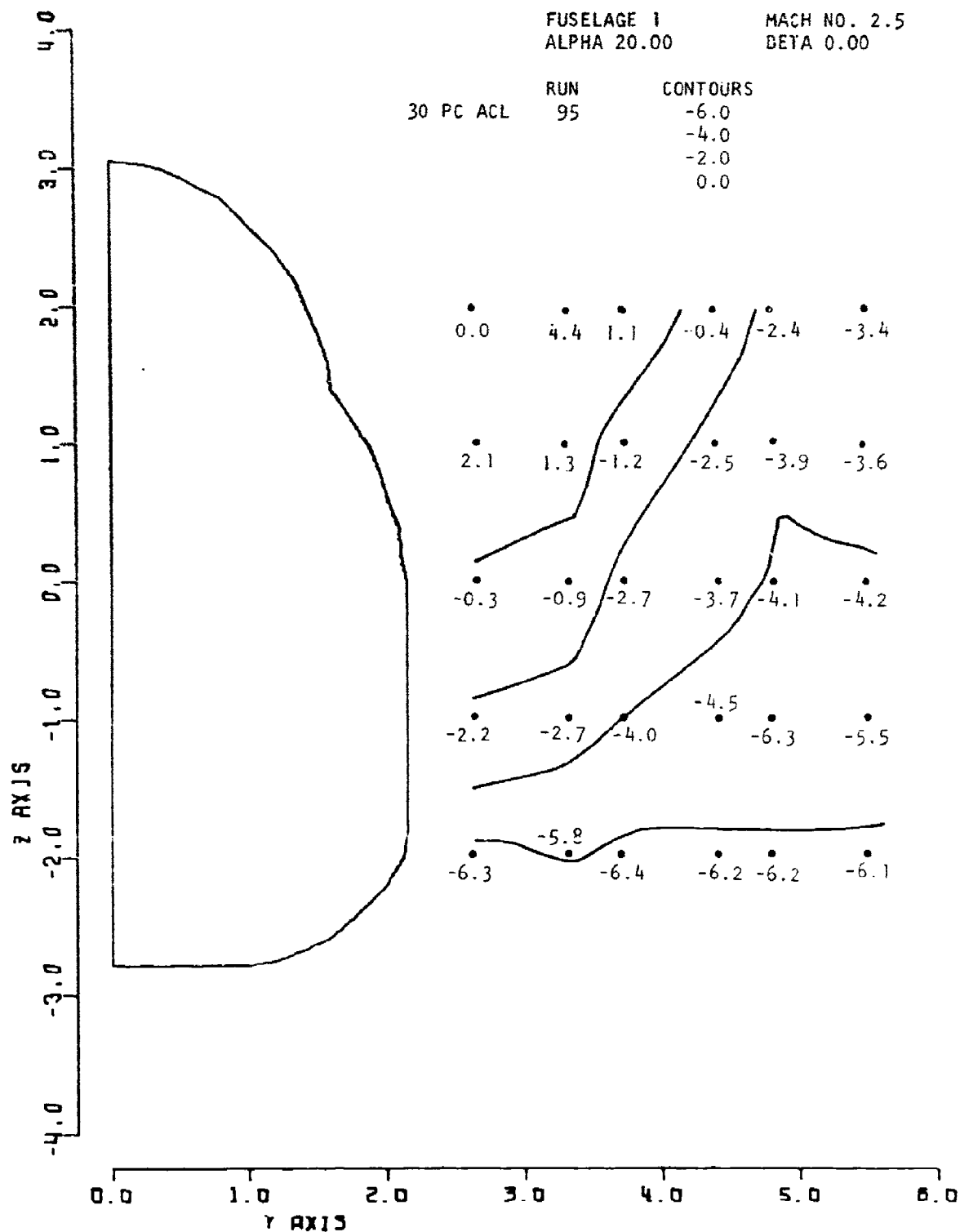


Figure 70. Local Sigma

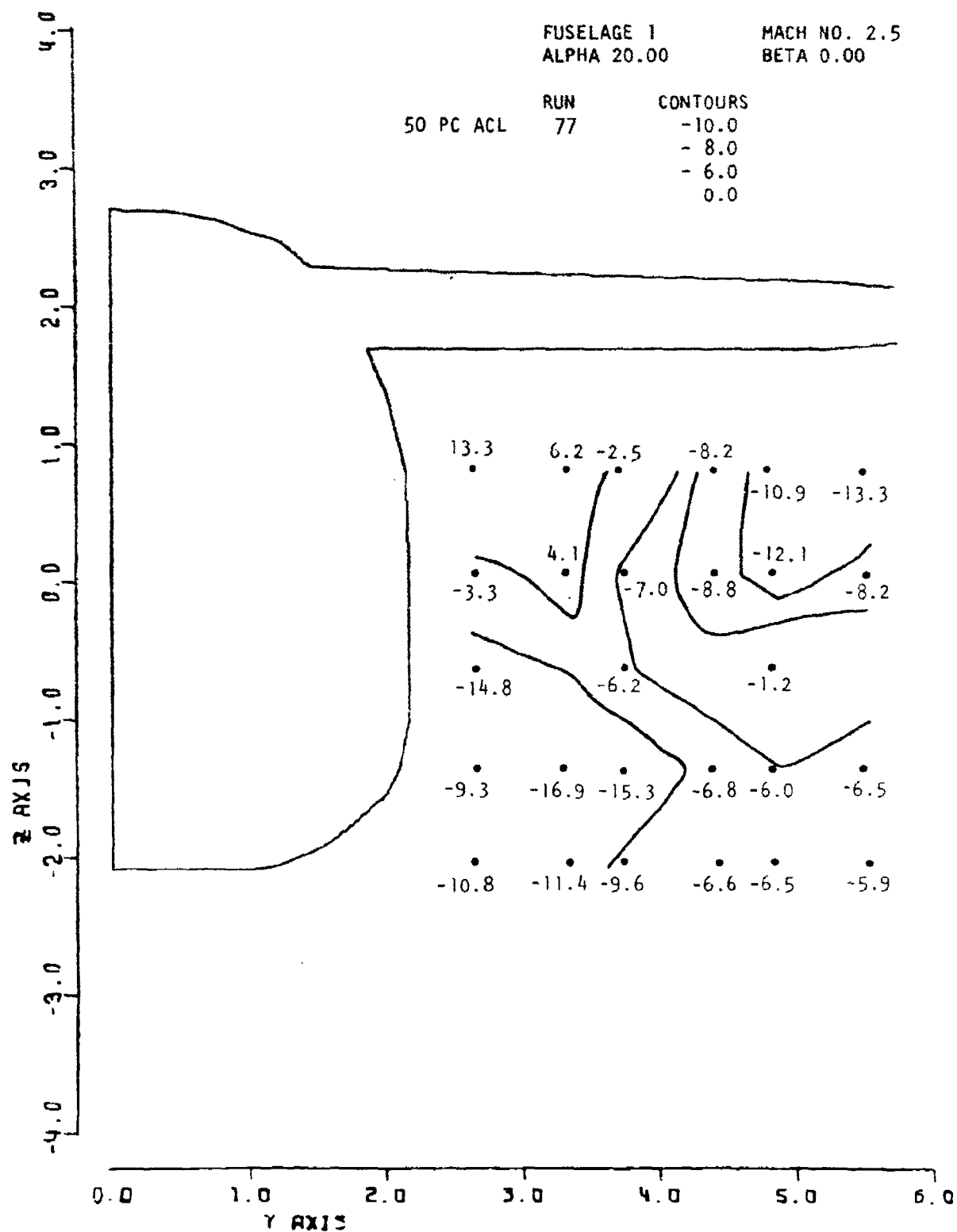


Figure 71. Local Sigma

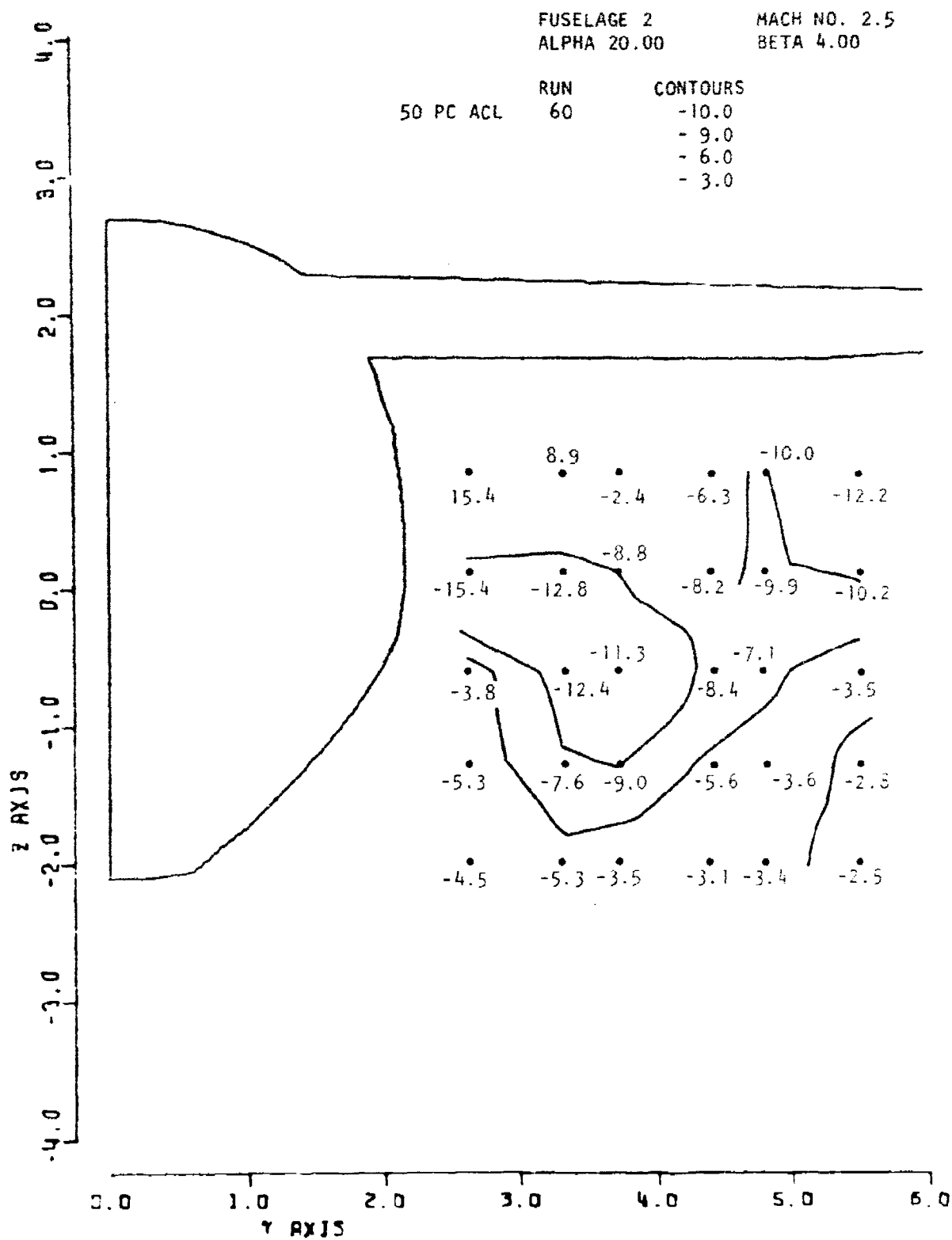


Figure 72. Local Sigma

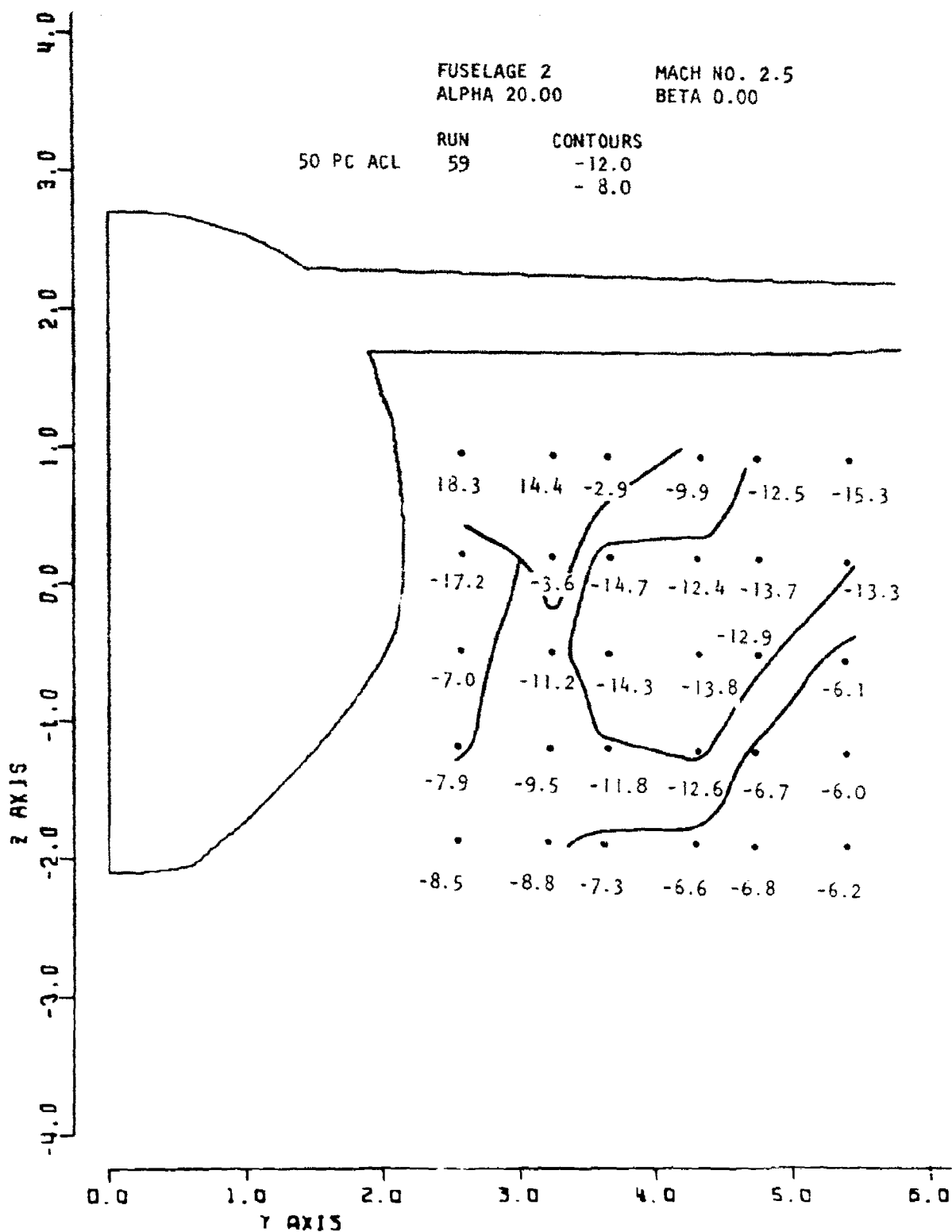


Figure 73. Local Sigma

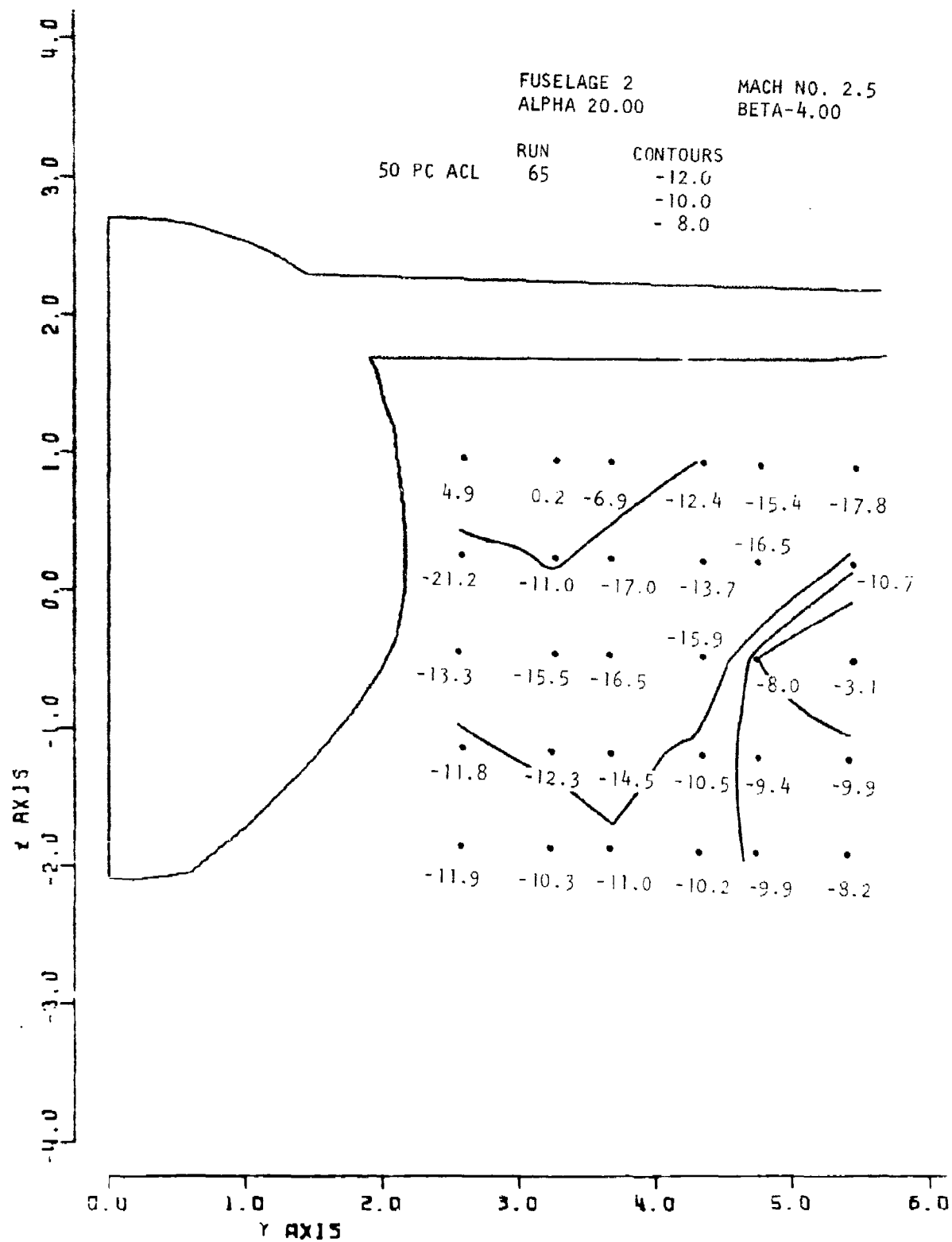


Figure 74. Local Sigma

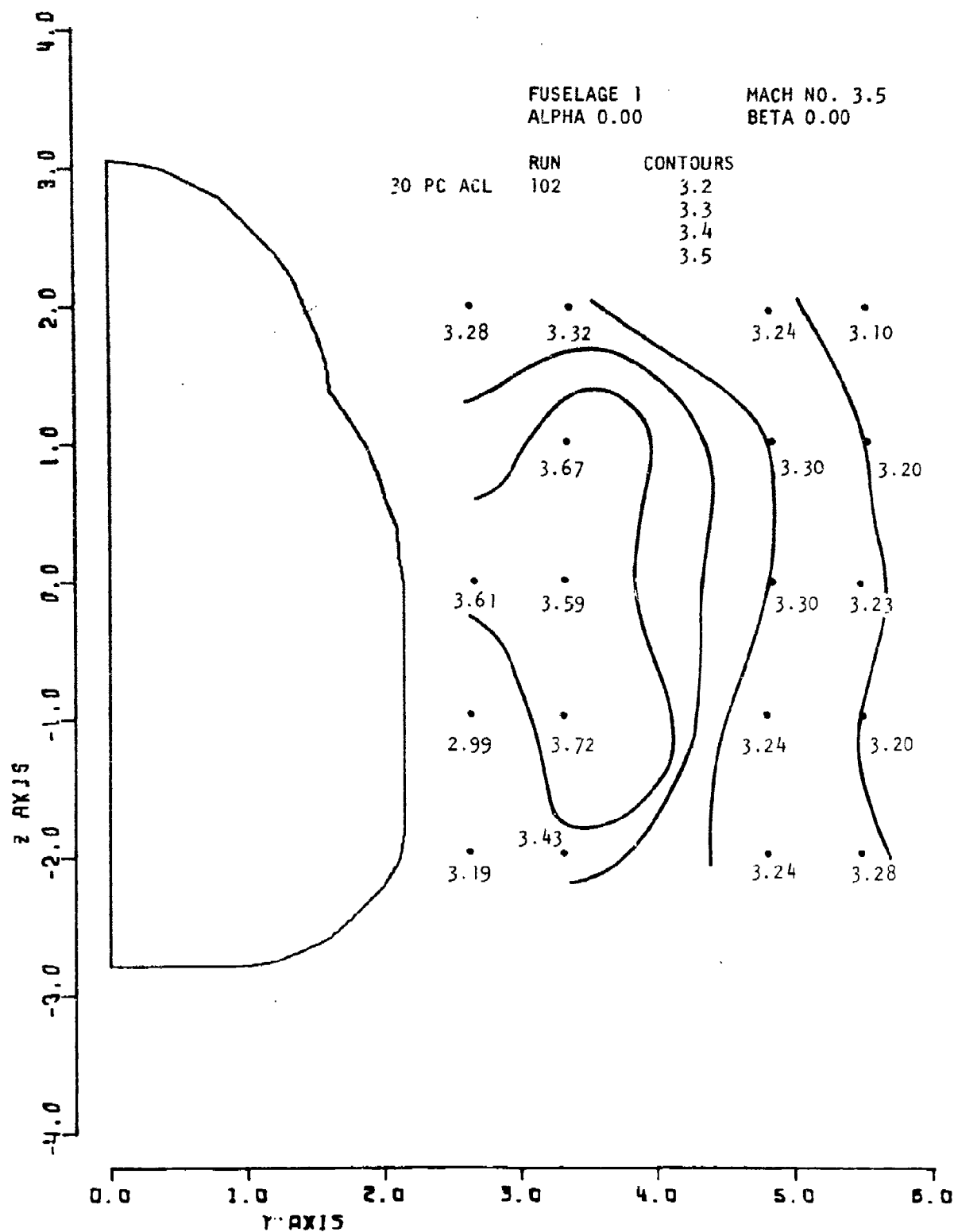


Figure 75. Local Mach No.

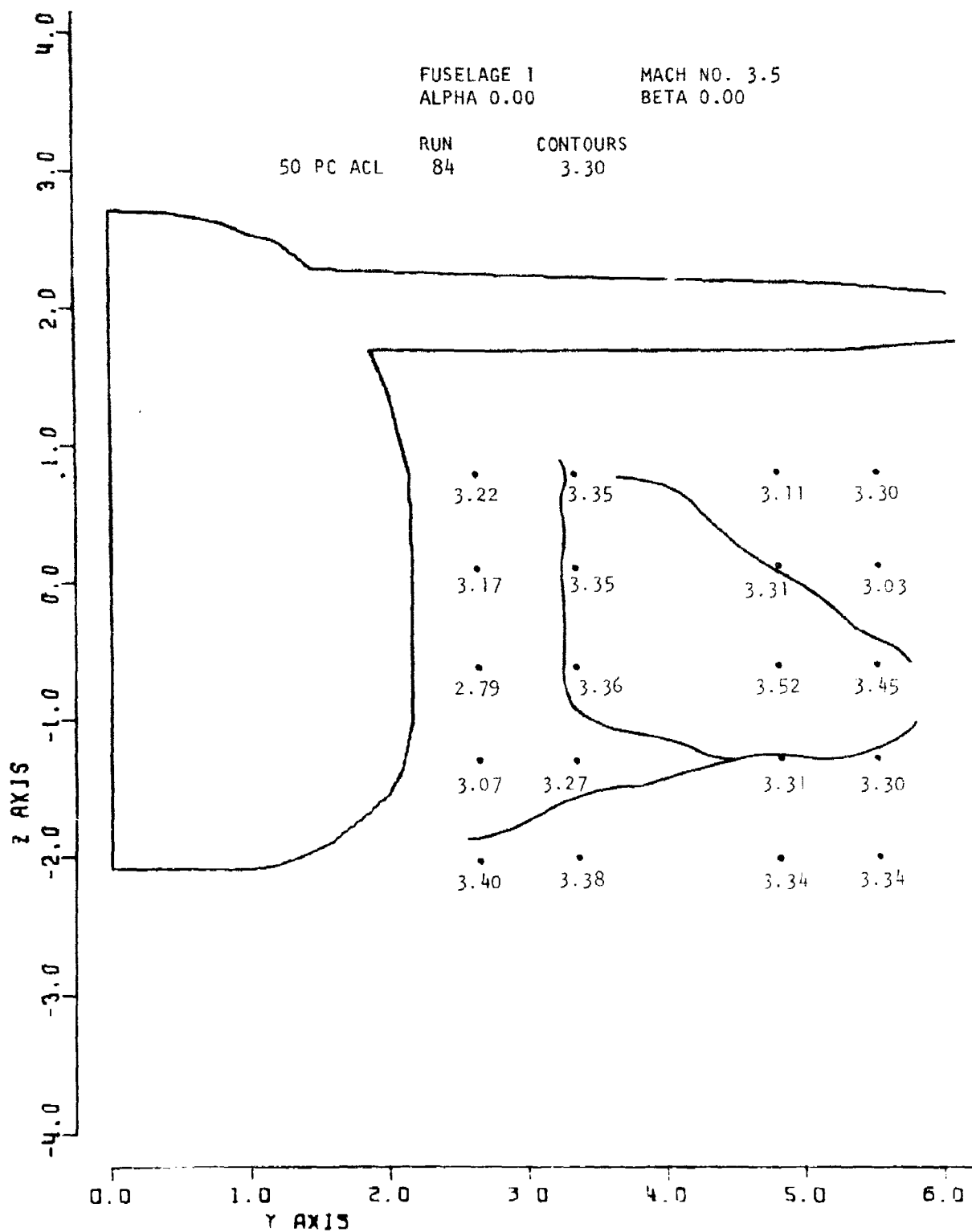


Figure 76. Local Mach No.

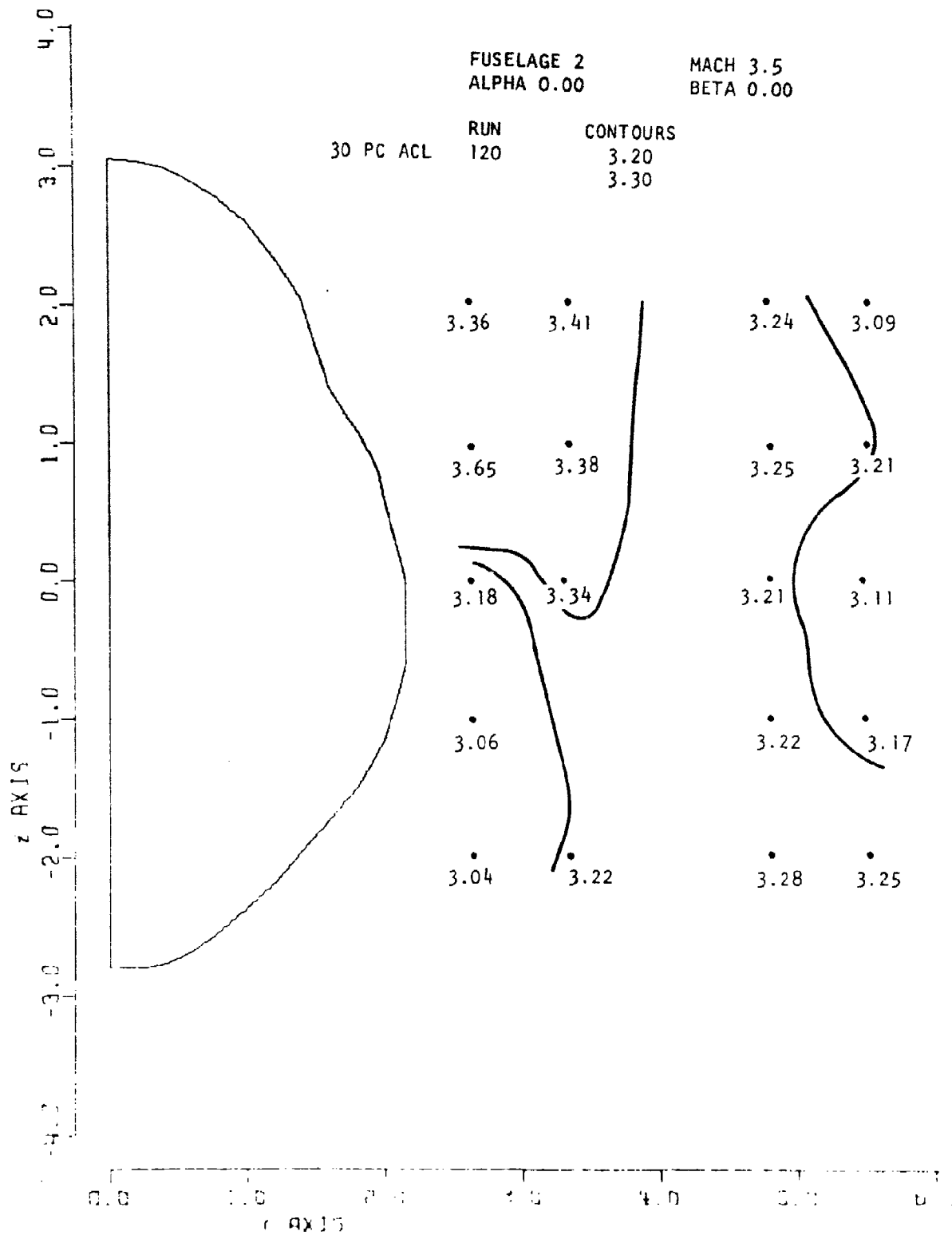


Figure 77. Local Mach No.

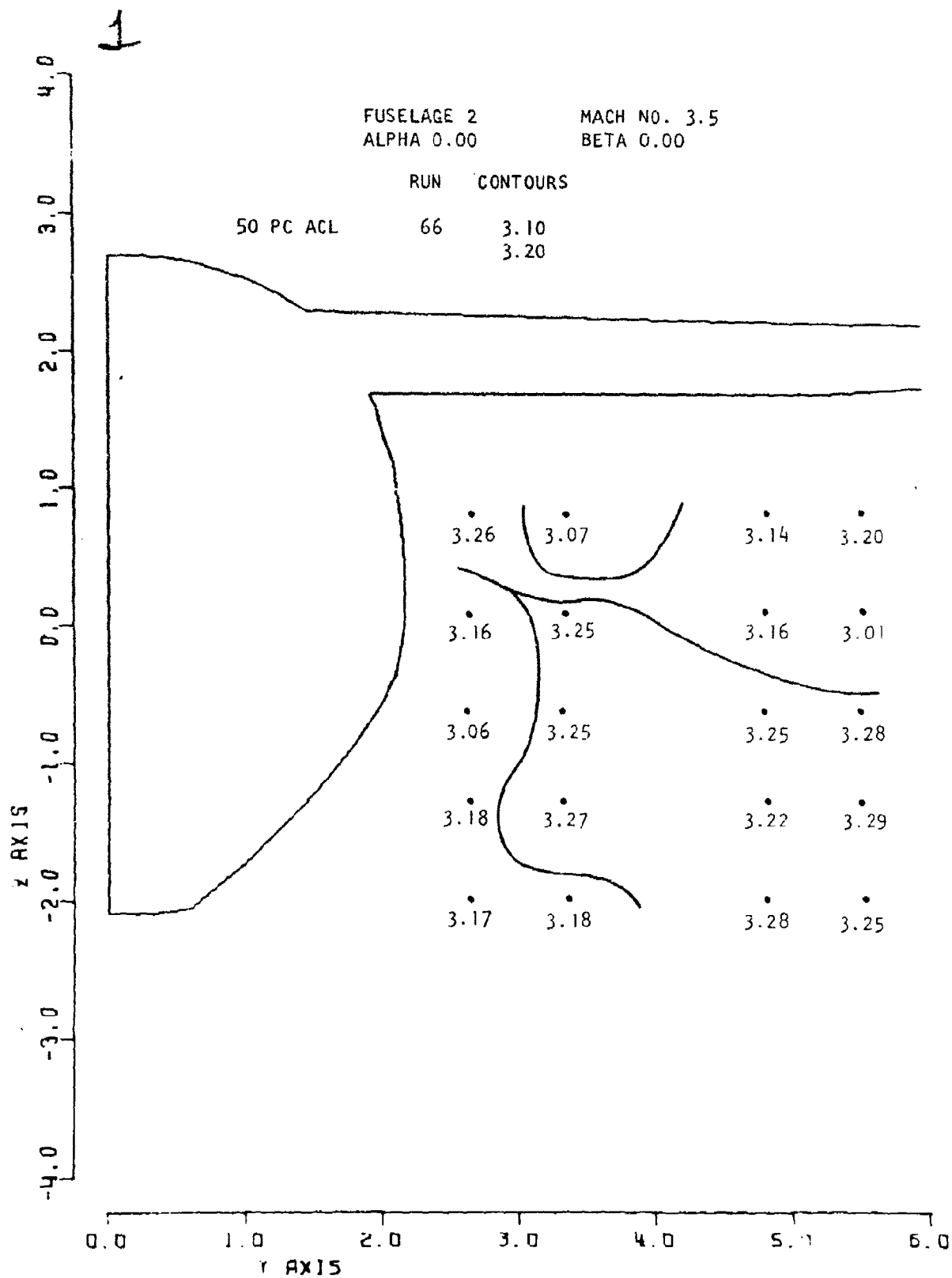


Figure 78. Local Mach No.

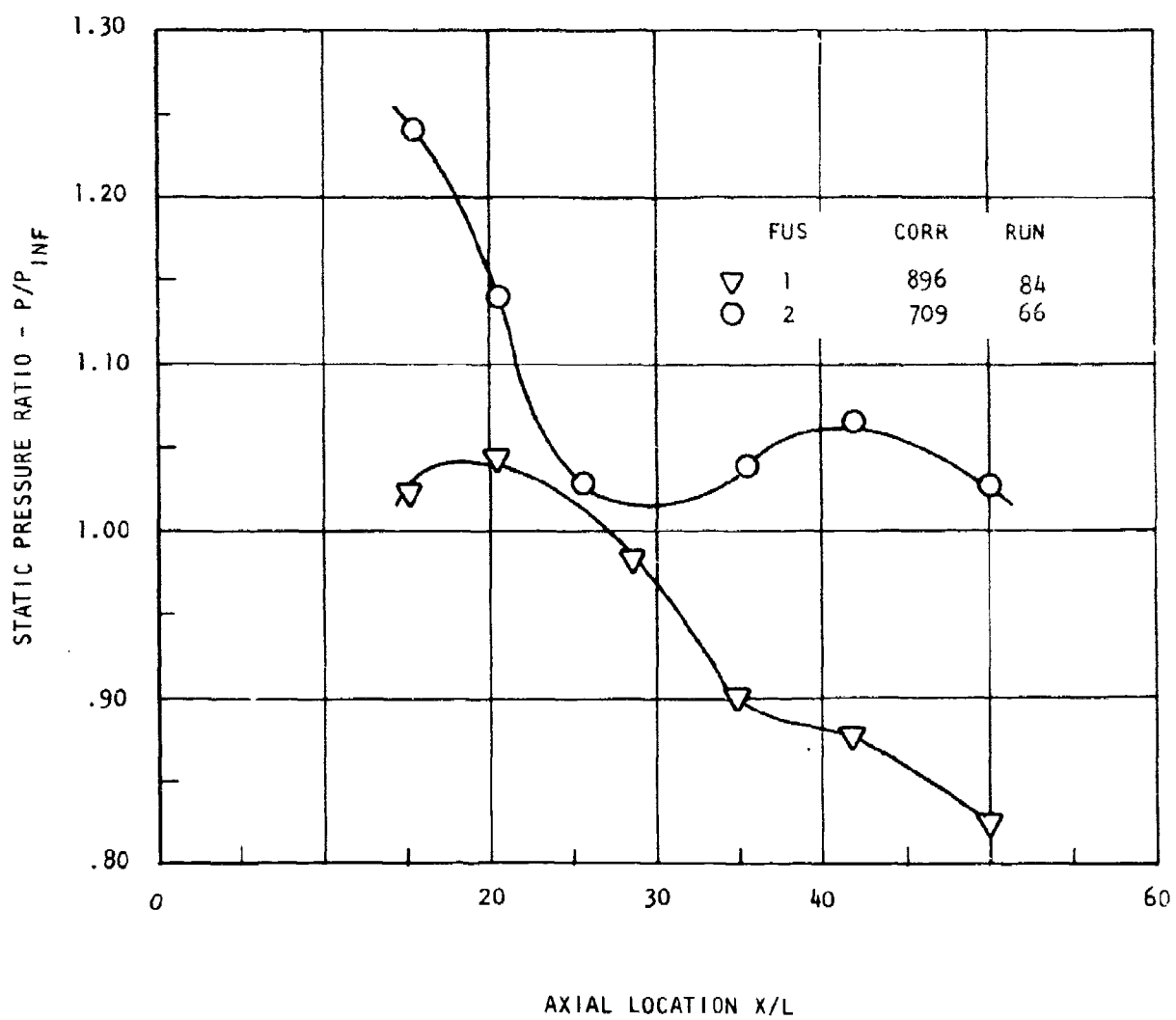


Figure 79. Fuselage Static Pressure Distribution, $\phi = 0^\circ$, $M^\infty = 3.5$, $\alpha = \beta = 0^\circ$

stream Mach number which reduces the lateral extent of the downstream zone of influence of flow disturbances. Accordingly, the reduction in local Mach number in the upper half of the surveyed region can be attributed to the wing-induced compression field which, at this station, extends down to only about half the depth of the survey region. The increase in local Mach numbers in the lower part of the flow field was probably the manifestation of the expansion taking place along the top and sides of the canopy, downstream of the canopy maximum width, and along the lower fuselage contour at this low angle of attack.

At both survey stations the local Mach numbers in the lowest row of the region were highest for fuselage 1, indicating that its flat bottom together with its smaller shoulder radius were better able to isolate the flow expansion field induced by the lower fuselage contour for this combination of low angle of attack and nose droop. This conclusion is borne out by the surface static pressure distributions measured along the lower meridional contour of both fuselages shown in Figure 79. Clearly, as observed earlier in connection with the Mach 2.5 data the larger shoulder radius of fuselage 2 serves to introduce the lower fuselage field into the side flow field, and vice versa, reducing thereby gradients or differences in flow properties in its vicinity.

3.2.1.1.2 Effect of Yaw

The effect of yaw at this Mach number and low angle of attack was to generally increase slightly the local Mach number on the leeward side and decrease those on the windward, relative to the unyawed case, as may be seen from Figures 80 and 81. The same small effects due to differences in fuselage geometry observed for the unyawed case were also present.

3.2.1.2 Total Pressure Recovery

3.2.1.2.1 Effect of Vehicle Geometry

Figures 82 and 83 show average local pressure recovery values of about .90 for both fuselages 1 and 2, which are naturally lower than those of the Mach 2.5 case. The figures show relatively high local values generally with the exception of the lower in-board regions for both fuselage side flow fields. Figures 84 and 85 show downstream station average total pressure recoveries of .78 and .72 for fuselages 1 and 2 respectively. These lower values reflect the additional wing and canopy losses which manifest themselves at this station. It was difficult to discern any significant effects of fuselage geometry at both survey stations.

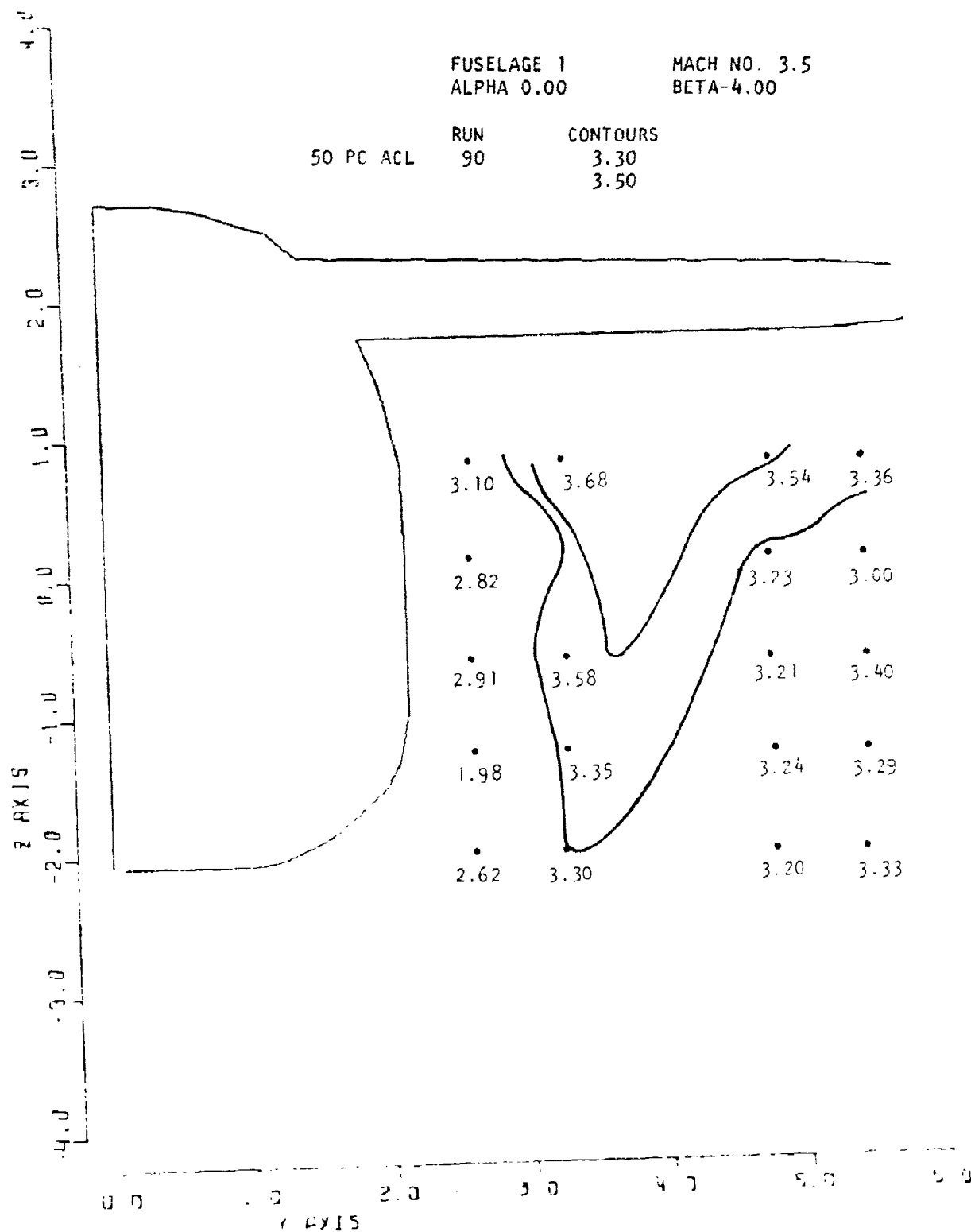


Figure 80. Local Mach No.

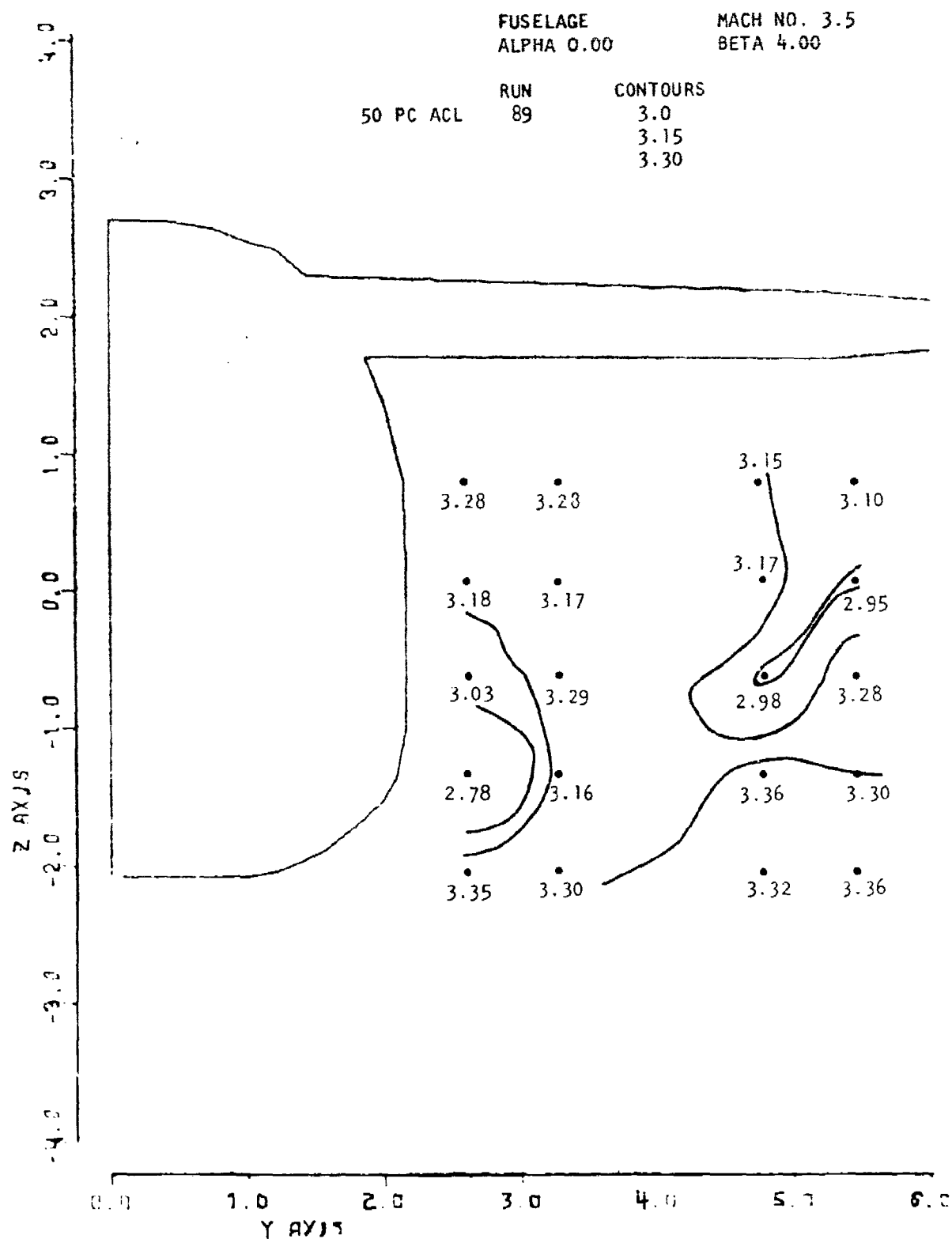


Figure 81. Local Mach No.

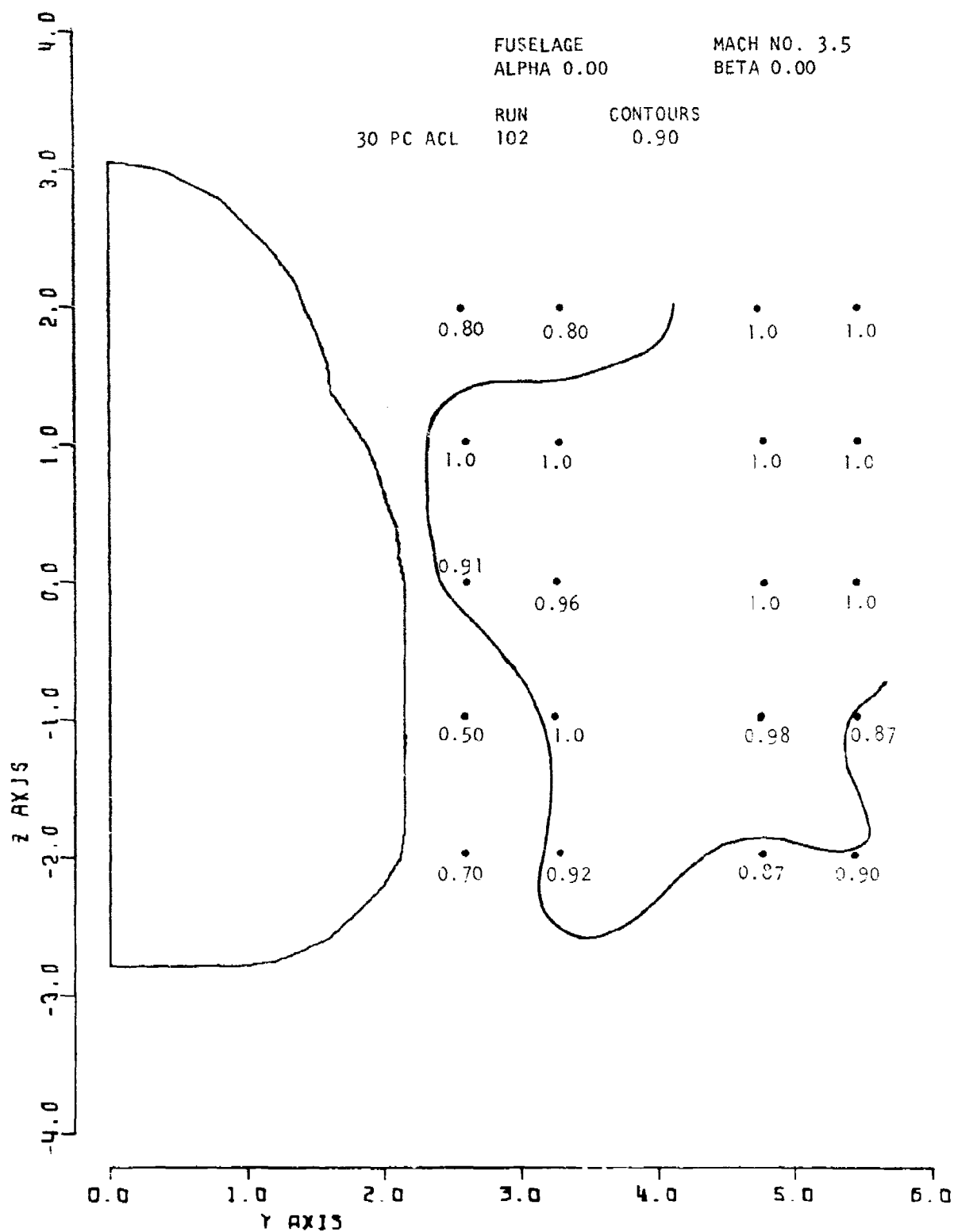


Figure 82. Local PT/PT

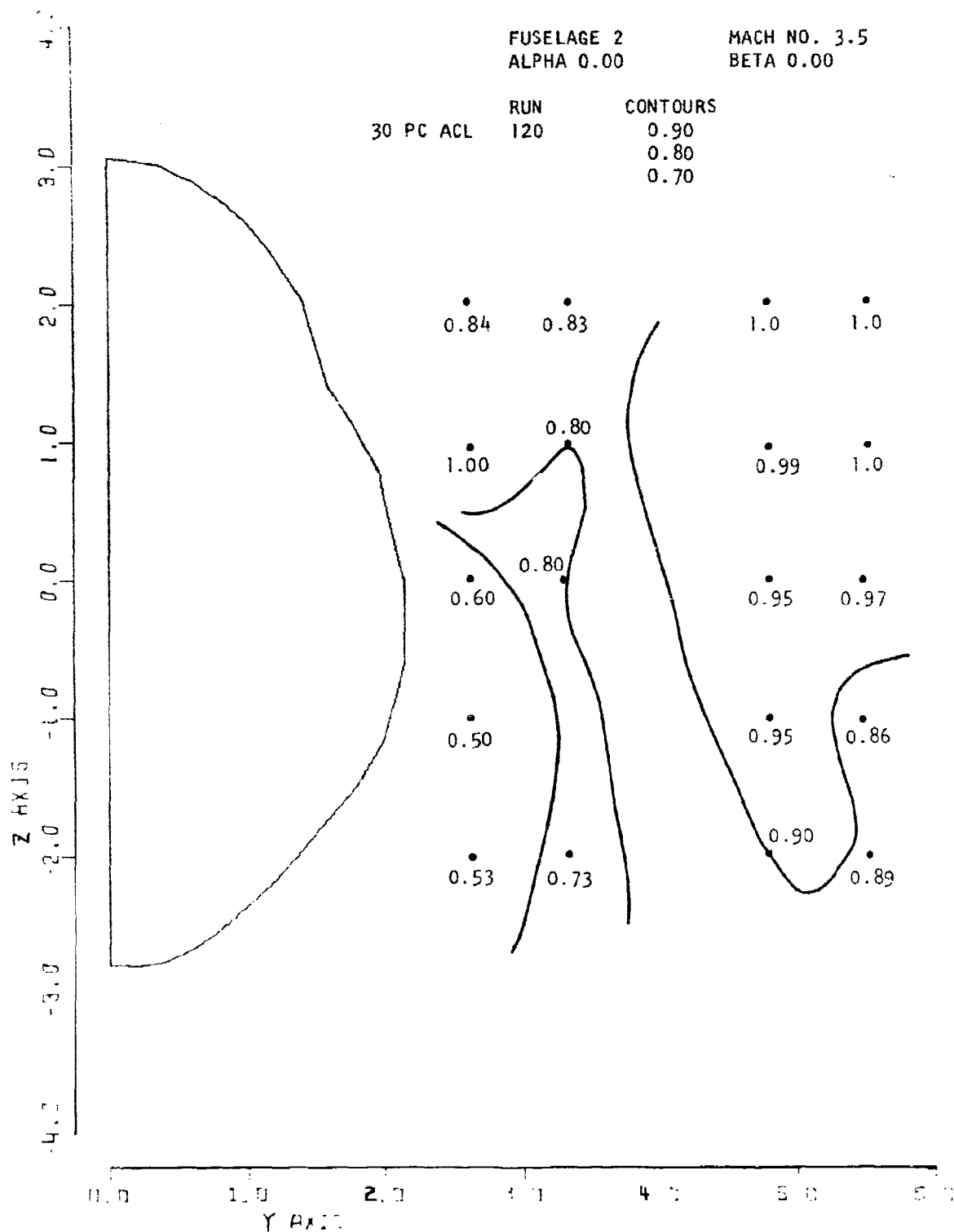


Figure 83. Local PT/PT

3.2.1.2.2 Effect of Yaw

The effect of yaw at this low angle of attack on local total pressure recovery was found to be small for both the leeward and windward sides of both fuselages. As was found to be the case at Mach 2.5, there was little modulation of losses with yaw at this higher Mach number. Figures 86 and 87 illustrate the effects of yaw for the leeward and windward sides, respectively, of fuselage 1 at the aft survey station.

3.2.1.3 Local Alpha

3.2.1.3.1 Effect of Vehicle Geometry

Relative to the Mach 2.5 low angle of attack case, the distribution of downwash at the forward 30% ACL station was similar at Mach 3.5 with somewhat larger values of downwash, however, as shown in Figures 88 and 89, respectively. Thus, the downwash increased in the downward direction along the fuselage side indicating the influence of the stronger canopy pressure field relative to that of the fuselage bottom. At the downstream station the downwash was more uniform due to the wing pressure field coming into play here. This can be seen from Figures 90 and 91 wherein data for both fuselages is presented. Effects of differences in fuselage geometry appeared to be confined to the innermost part of the region with fuselage 2 producing somewhat larger local downwash angles there at the upstream station.

3.2.1.3.2 Effect of Yaw

The effects of yaw were generally the same as those observed at Mach 2.5. Thus, at the forward station the effect of yaw on the leeward side was to reduce the downwash in the lower inboard region and increase it in the upper inboard part. On the windward side the effect of yaw was opposite to that of the leeward side.

At the downstream station on the windward side, the effect of yaw was to increase the level of downwash in the whole region. This is due again to the shielding or restraining effect of the wing on both the basic flow and the superposed simple cross flow due to yaw. On the leeward side, the downwash was reduced over most of the region, due to the cross flow associated with the yawed attitude. These effects were common to both fuselages and are illustrated by the data presented in Figures 92 to 95.

3.2.1.4 Local Sigma

3.2.1.4.1 Effect of Vehicle Geometry

At the forward survey station the effects of fuselage geometry differences were

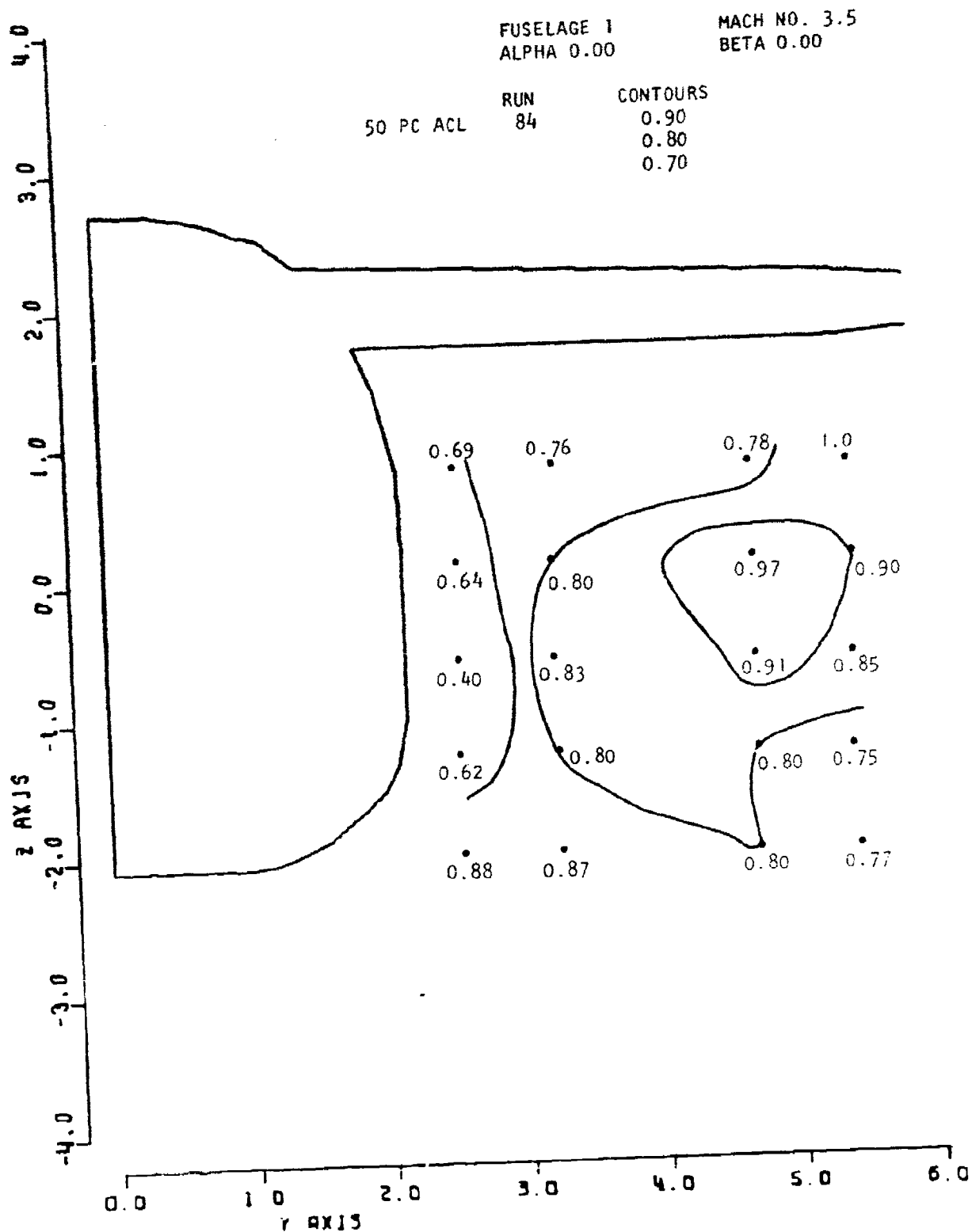


Figure 84. Local PT/PT

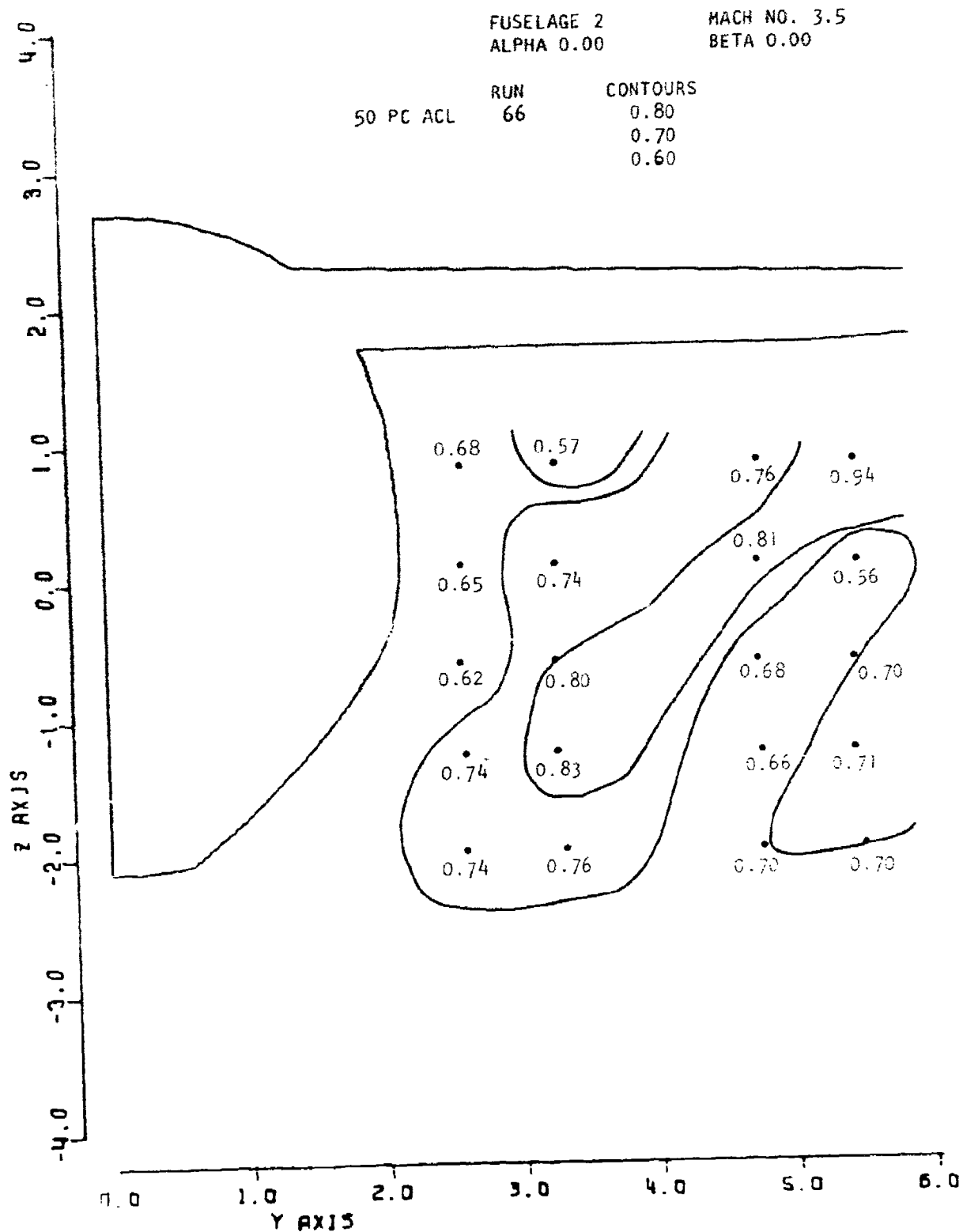


Figure 85. Local PT 'PT

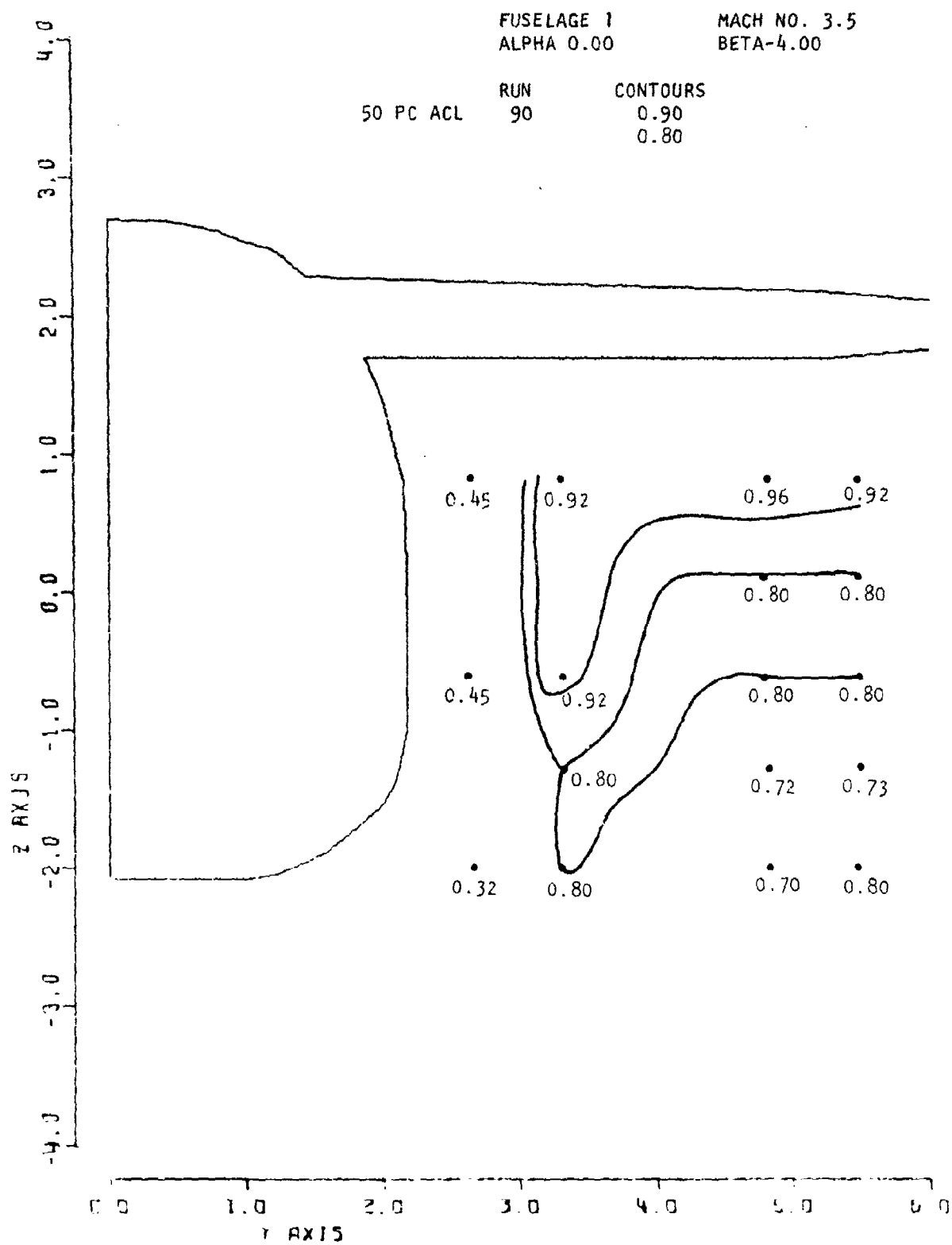


Figure 86. Local PT/PT

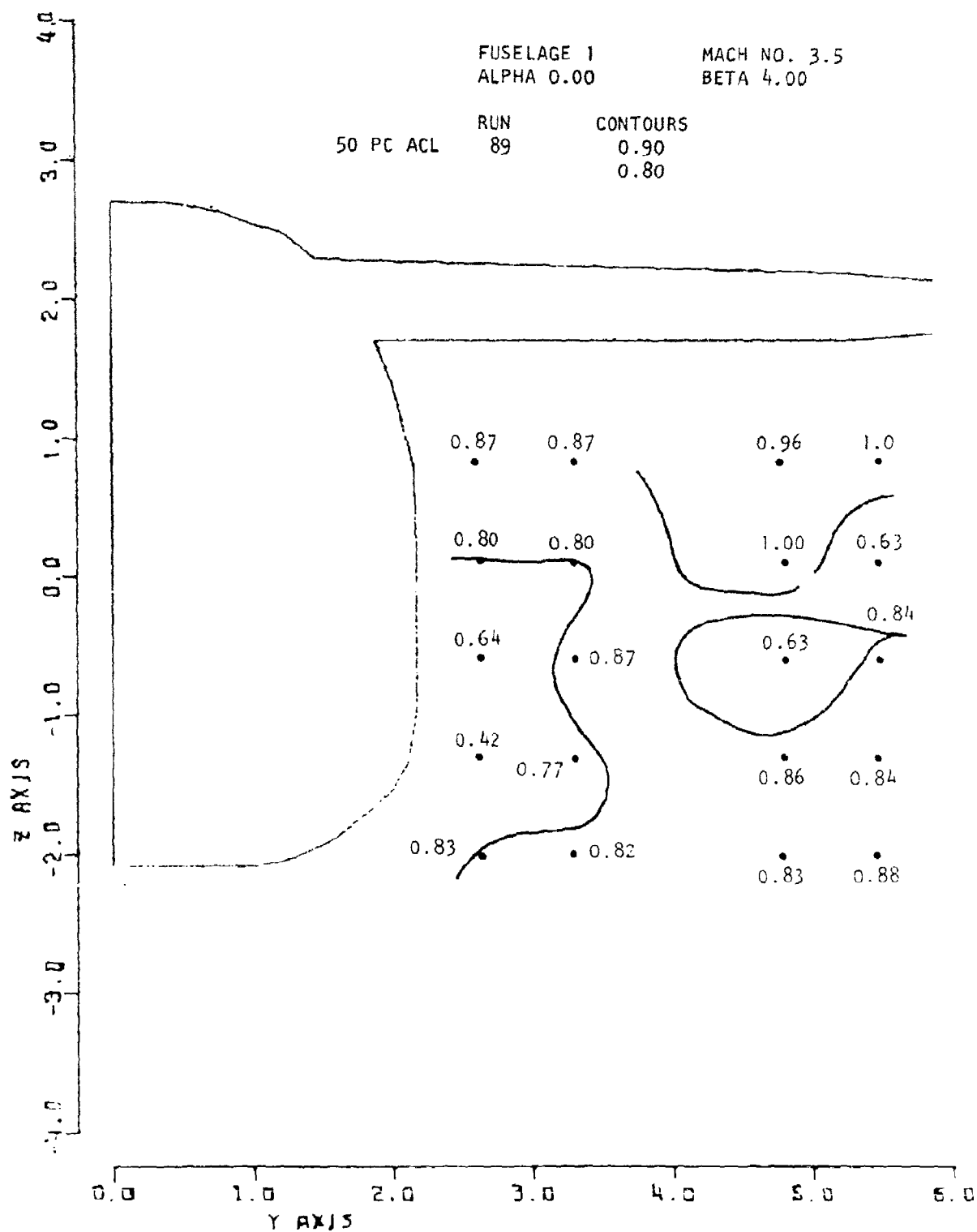


Figure 87. Local PT/PT

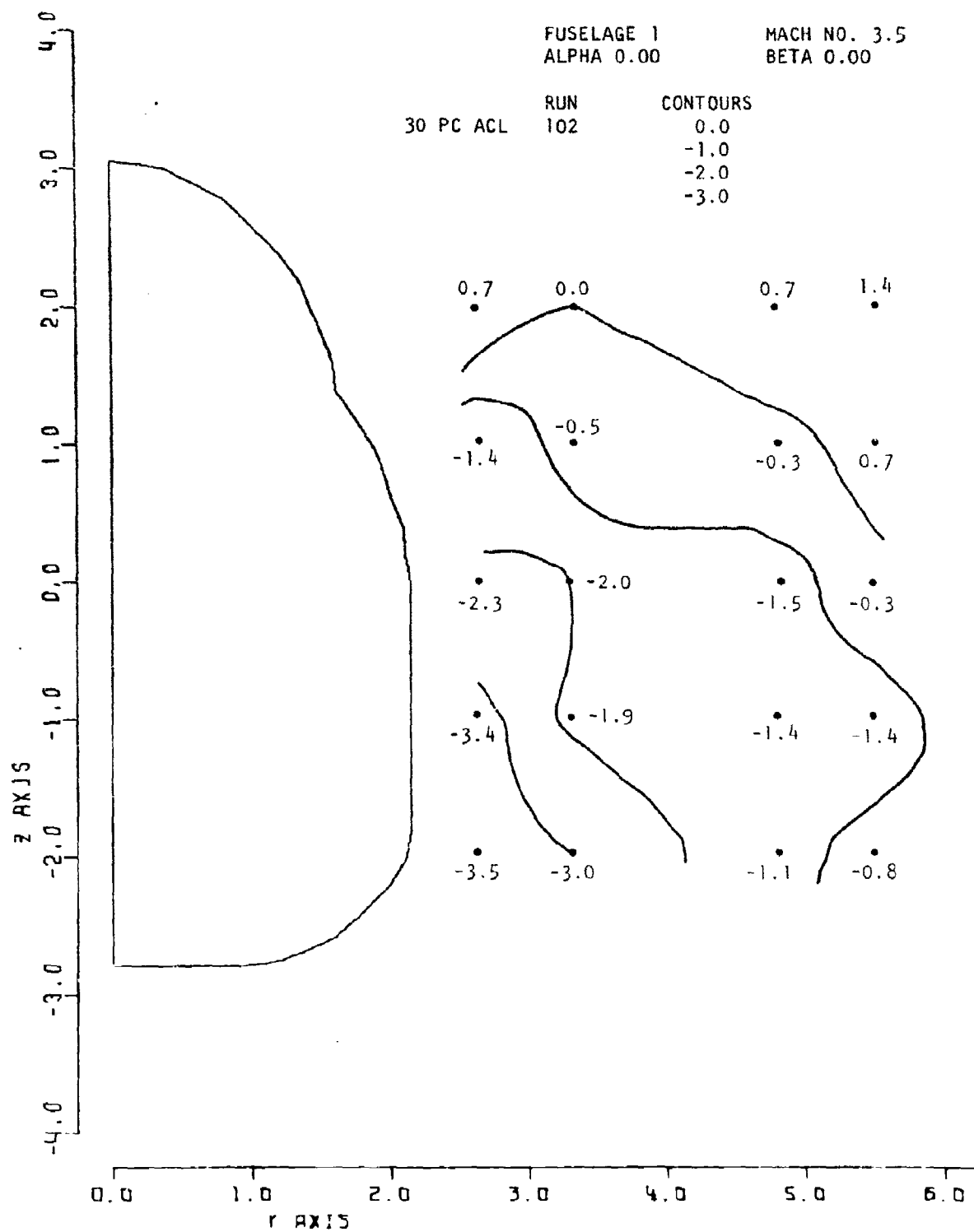


Figure 88. Local Alpha

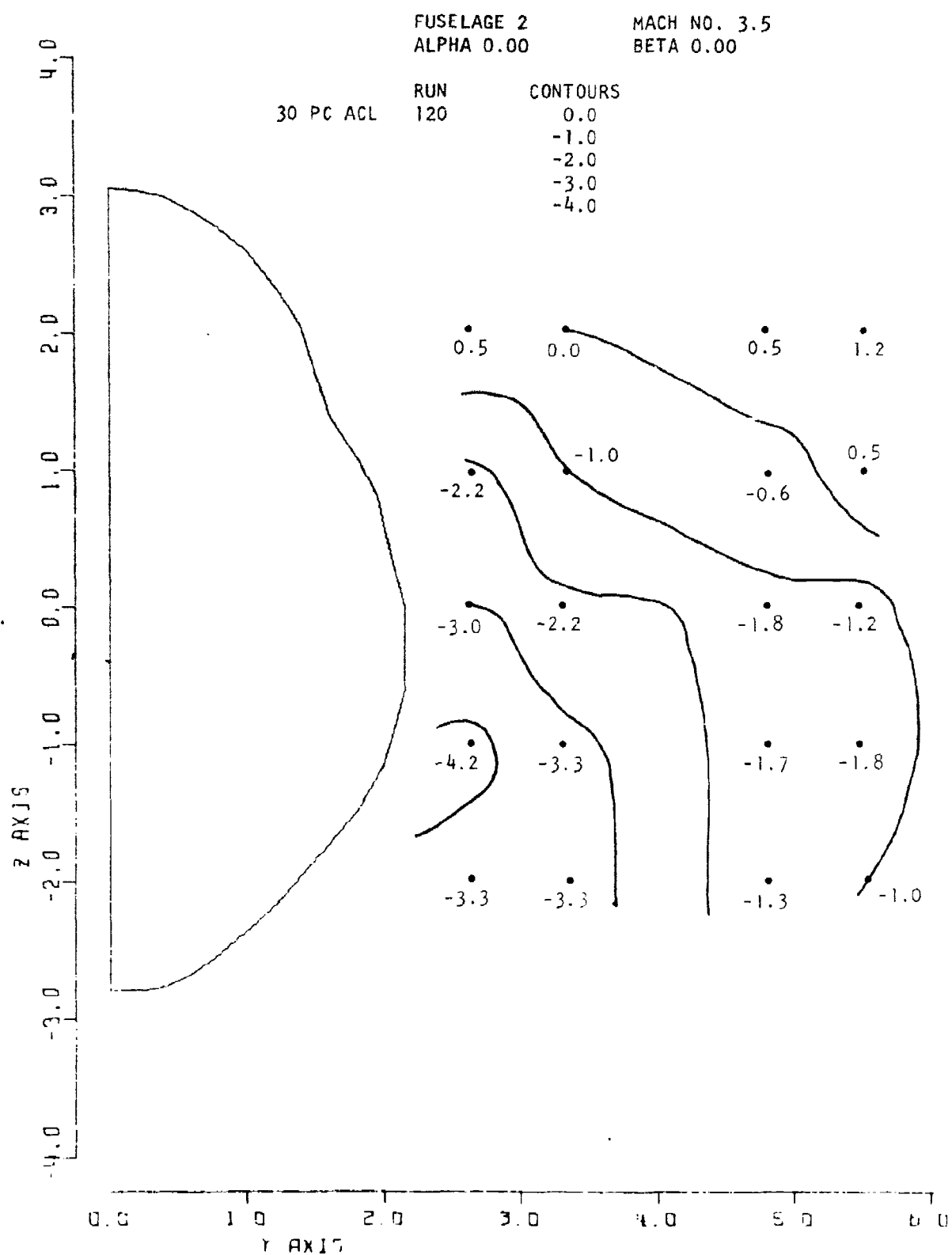


Figure 89. Local Alpha

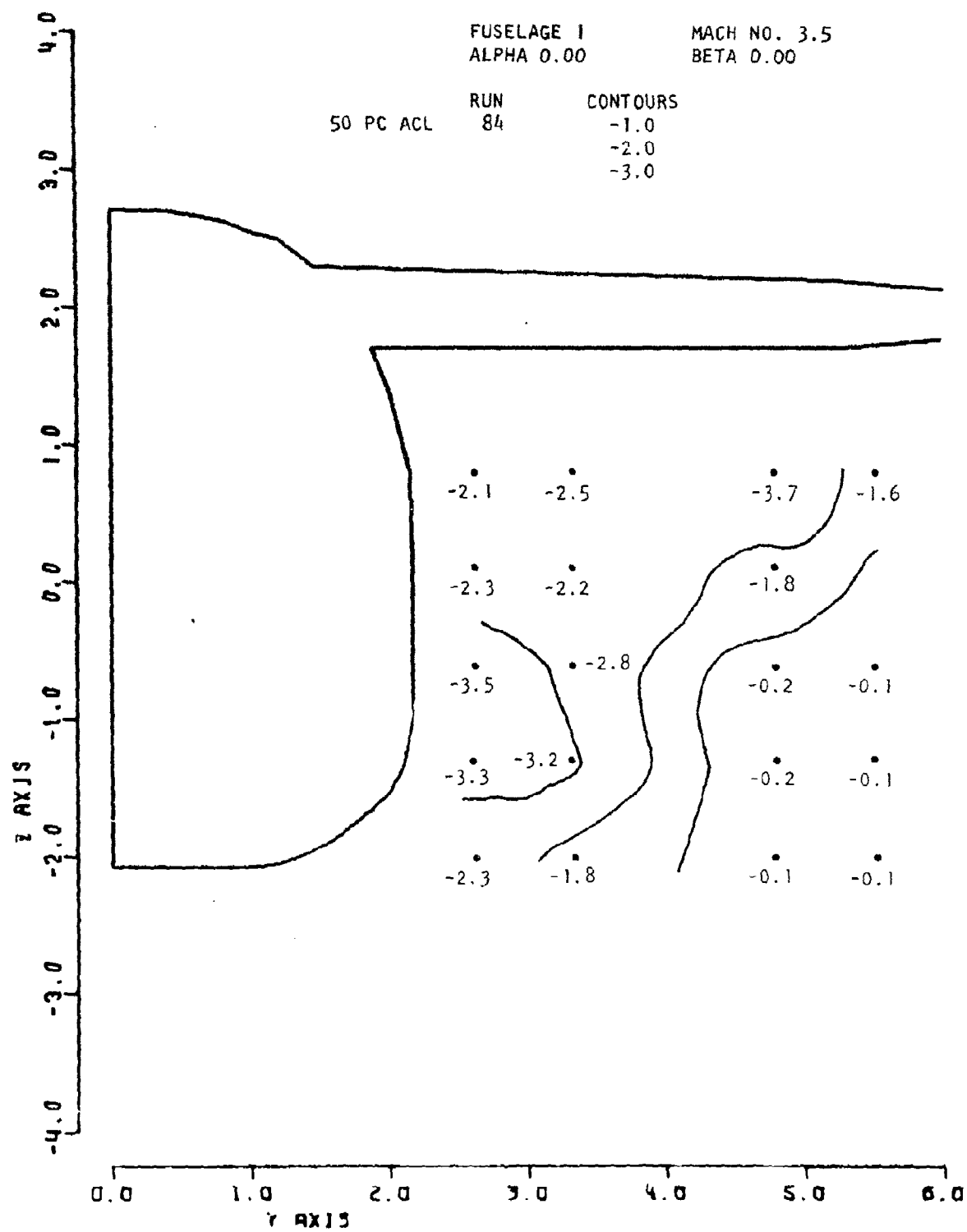


Figure 90. Local Alpha

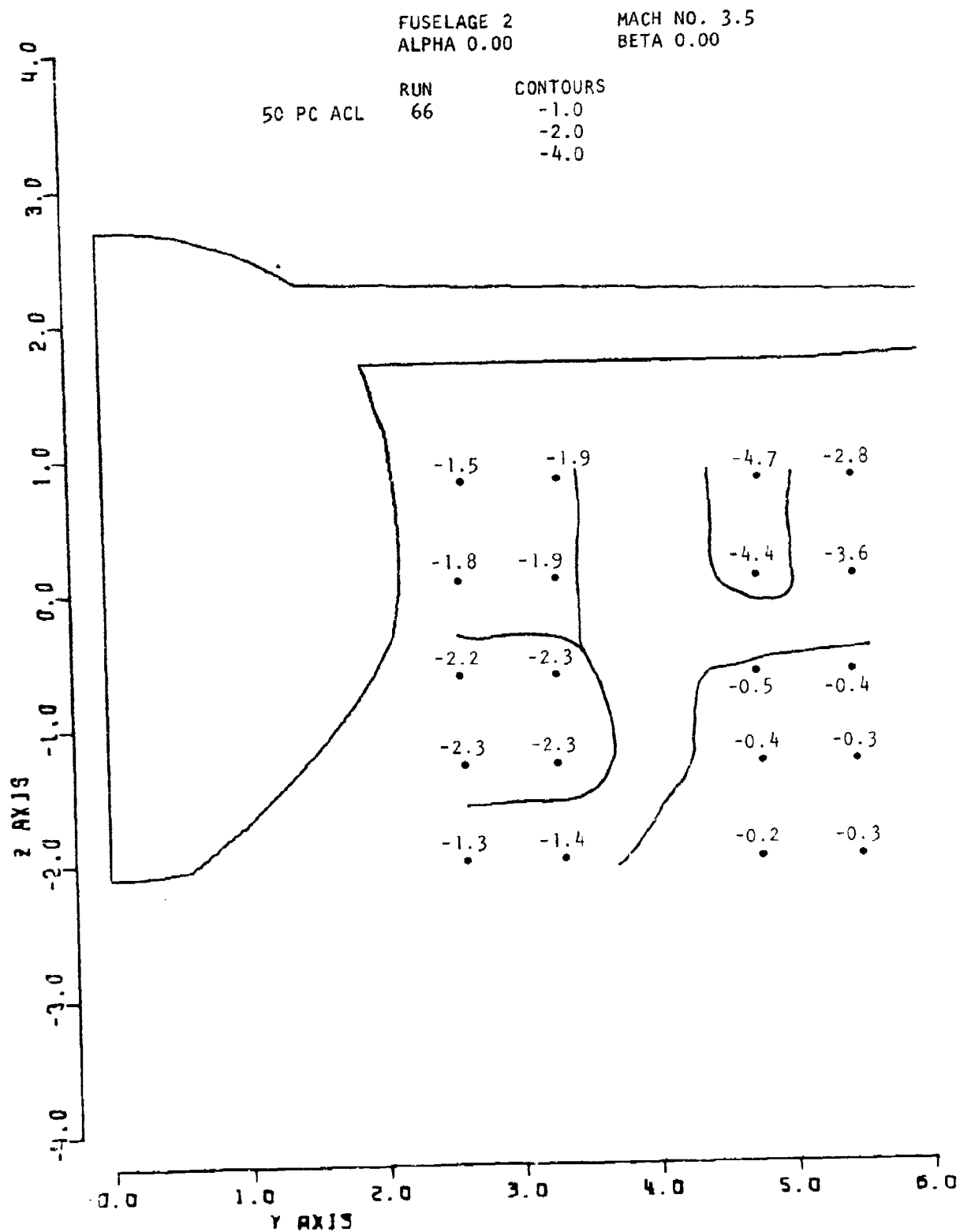


Figure 91. Local Alpha

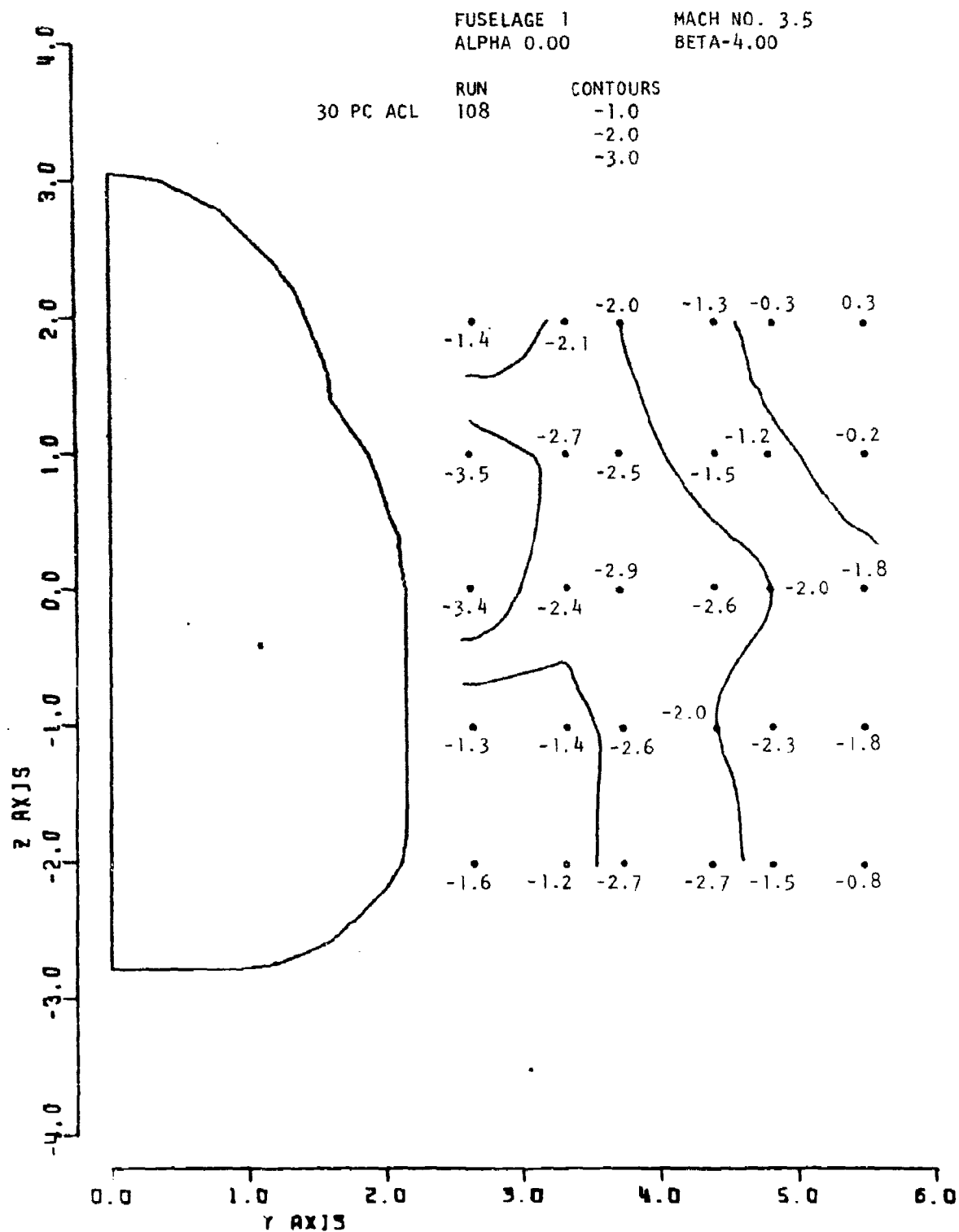


Figure 92. Local Alpha

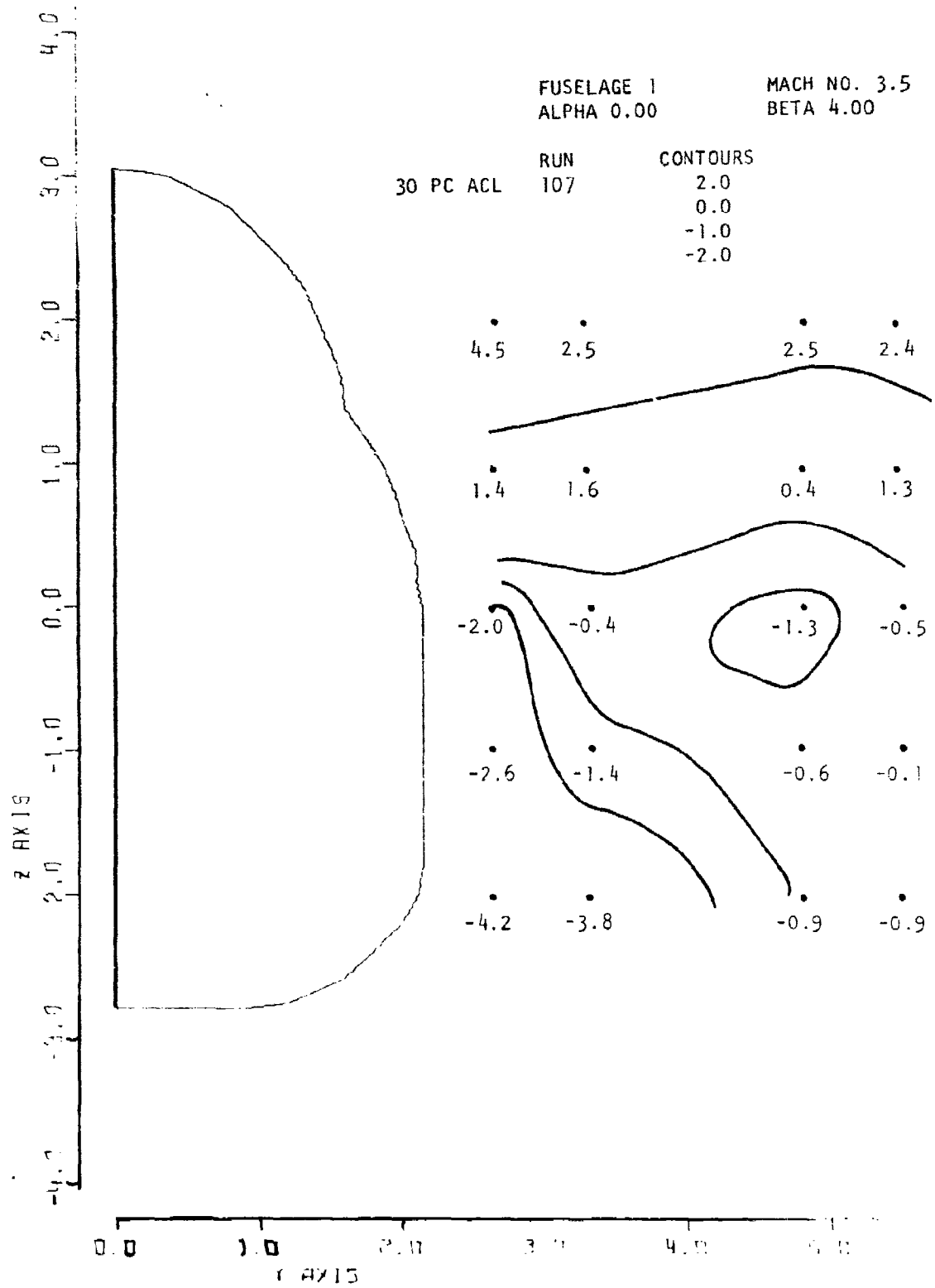


Figure 93. Local Alpha

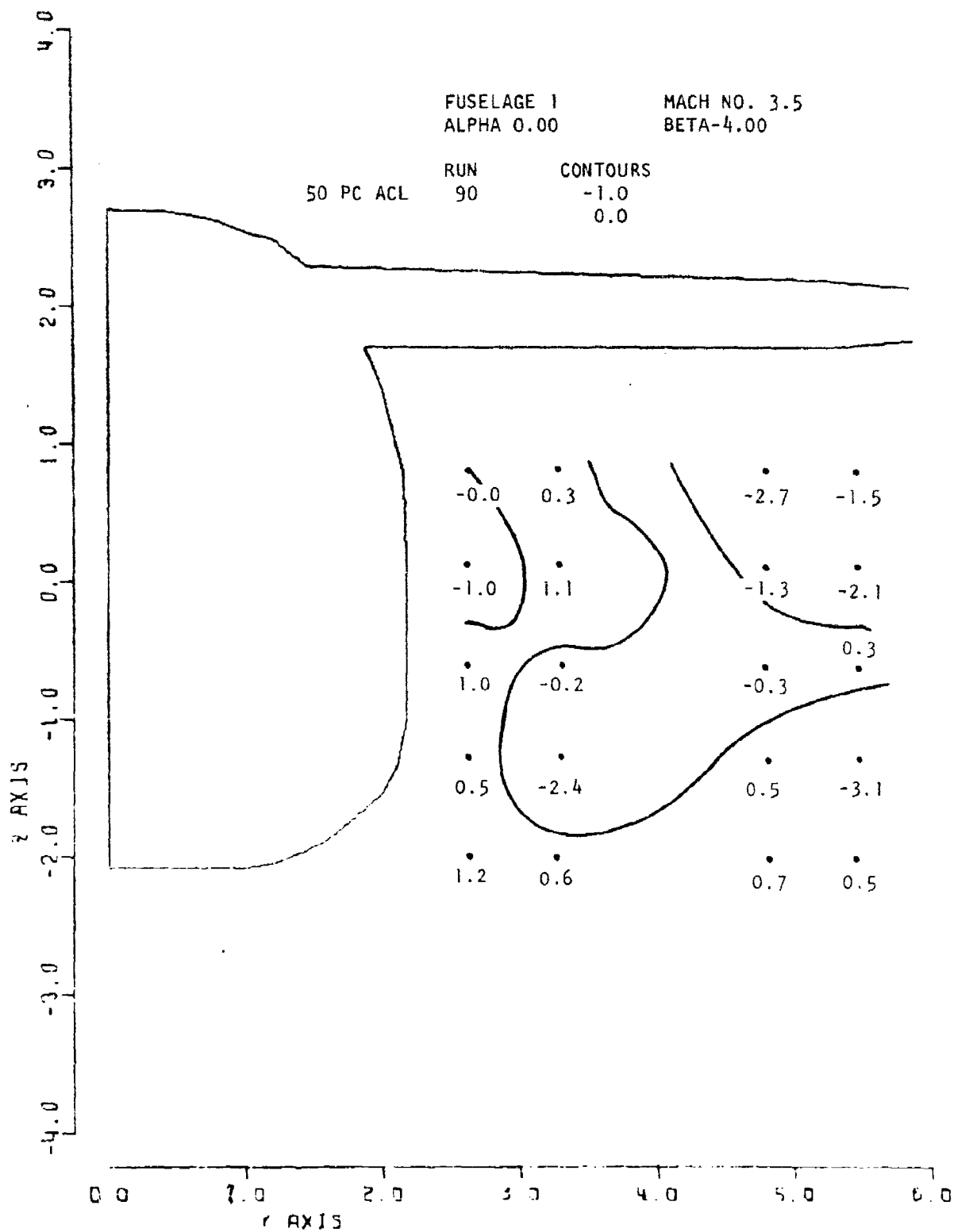


Figure 94. Local Alpha

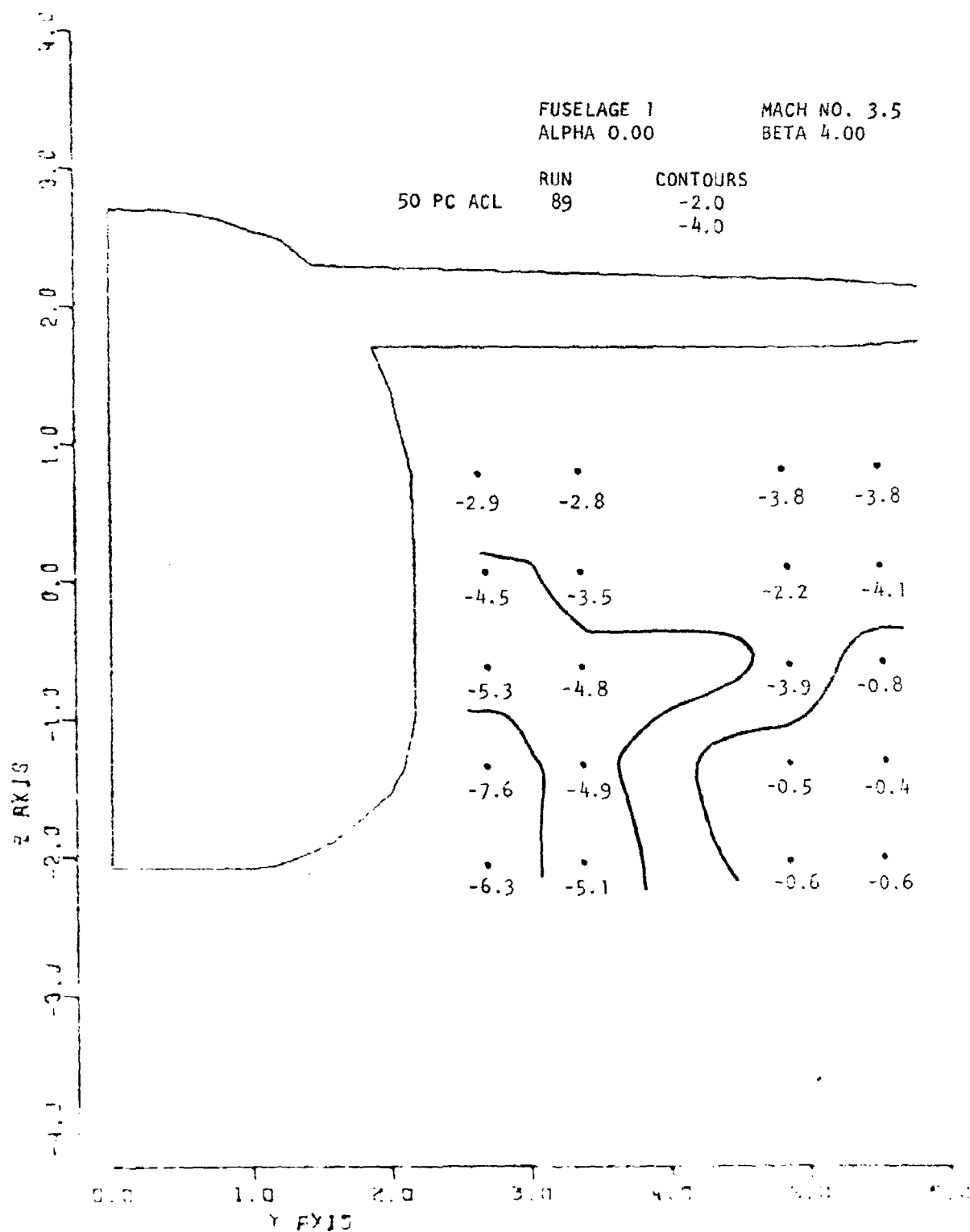


Figure 95. Local Alpha

confined to the inboard region adjacent to the corners and sides of the fuselage as may be seen in Figures 96 and 97. At this Mach number all the local sidewash angles were negative (outwardly directed), unlike the Mach 2.5 case where the sidewash in the lower part of the survey region was positive. This Mach number dependent effect stems from an initially larger pressure rise across the nose and canopy shock waves at Mach 3.5, followed by a delayed re-expansion in the shock layer, due to a shallower expansion fan. Consequently, the relatively higher static pressures residing in the inboard portion of the flow field induce an outward directed sidewash vector rather than the inward directed vector previously seen at Mach 2.5.

At the 50% ACL station the sidewash angles were significantly less negative than the upstream values, reflecting again the presence of the same sidewash influencing factors found at Mach 2.5, namely a more complete re-expansion of the flow and an isolation of the canopy influence due to the presence of the wing. The local sidewash distribution is shown in Figures 98 and 99 for fuselages 1 and 2 respectively.

3.2.1.4.2 Effect of Yaw

On the windward side, local sidewash angles were generally less negative than for the unyawed case. Fuselage 2 by virtue of its larger corner radius, introduced the cross flow into the lower region resulting in more positive sidewash angles there at both stations, as can be seen by comparing Figure 100 to 101, and 102 to 103.

On the leeward side the effect of yaw was to make the local sidewash more negative (directed outwardly) with little effect of fuselage geometry differences at both survey stations. Figure 104 exemplifies the leeward side situation at the rear survey station of fuselage 1. Qualitatively, this is the same behavior evidenced at Mach 2.5.

3.2.2 Intermediate Angle of Attack

3.2.2.1 Local Mach Number

3.2.2.1.1 Effect of Vehicle Geometry

At the forward survey plane increasing the angle of attack to 10° strengthened the pressure field of the lower fuselage to that of the upper, resulting in generally lower local Mach numbers in the lower part of the survey region relative to the upper for both fuselages. At the downstream station the wing surface pressure field reversed this variation of local Mach number producing generally lower local Mach numbers in the upper region relative to the lower region. These effects are evident in Figures 105 and 106.

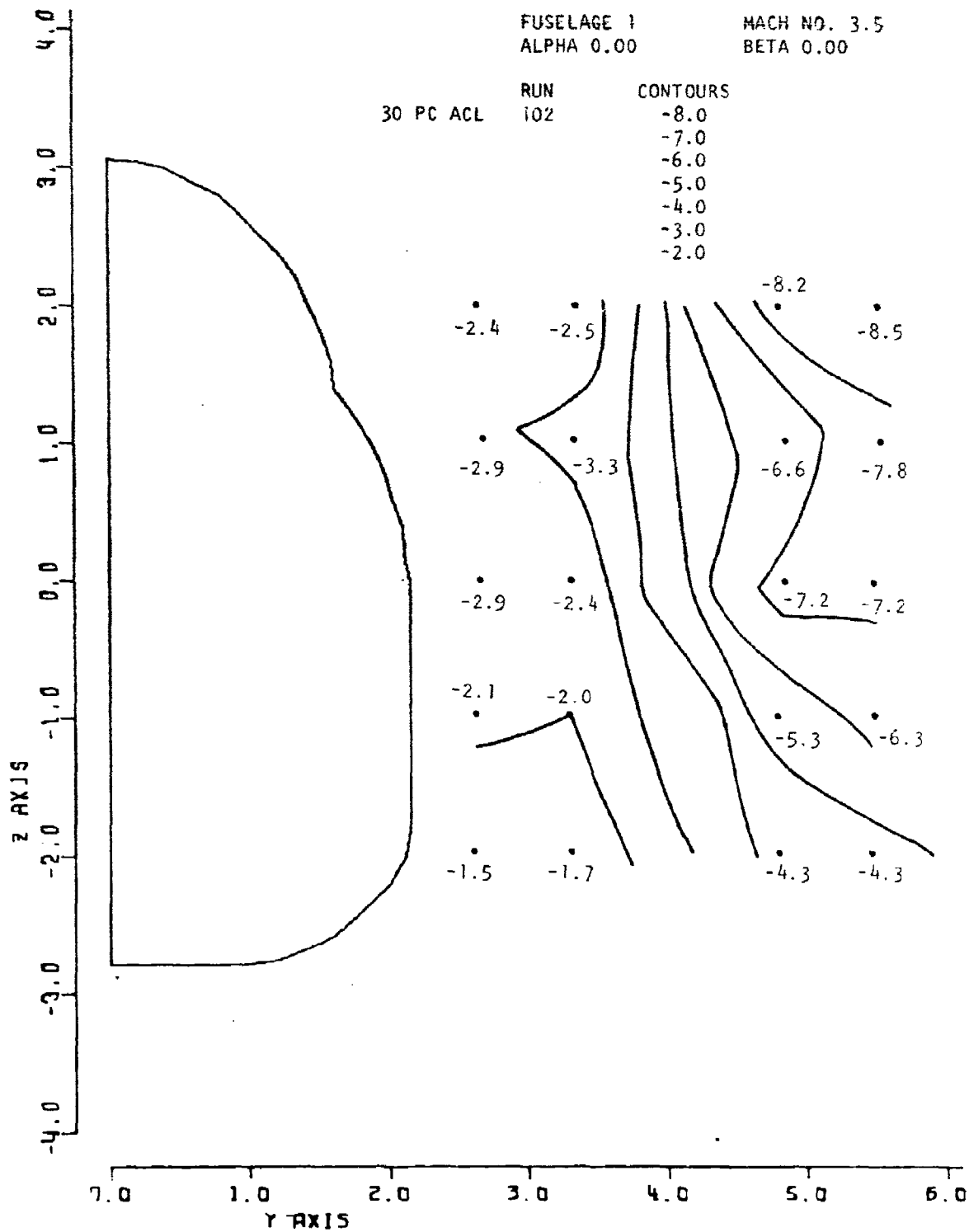
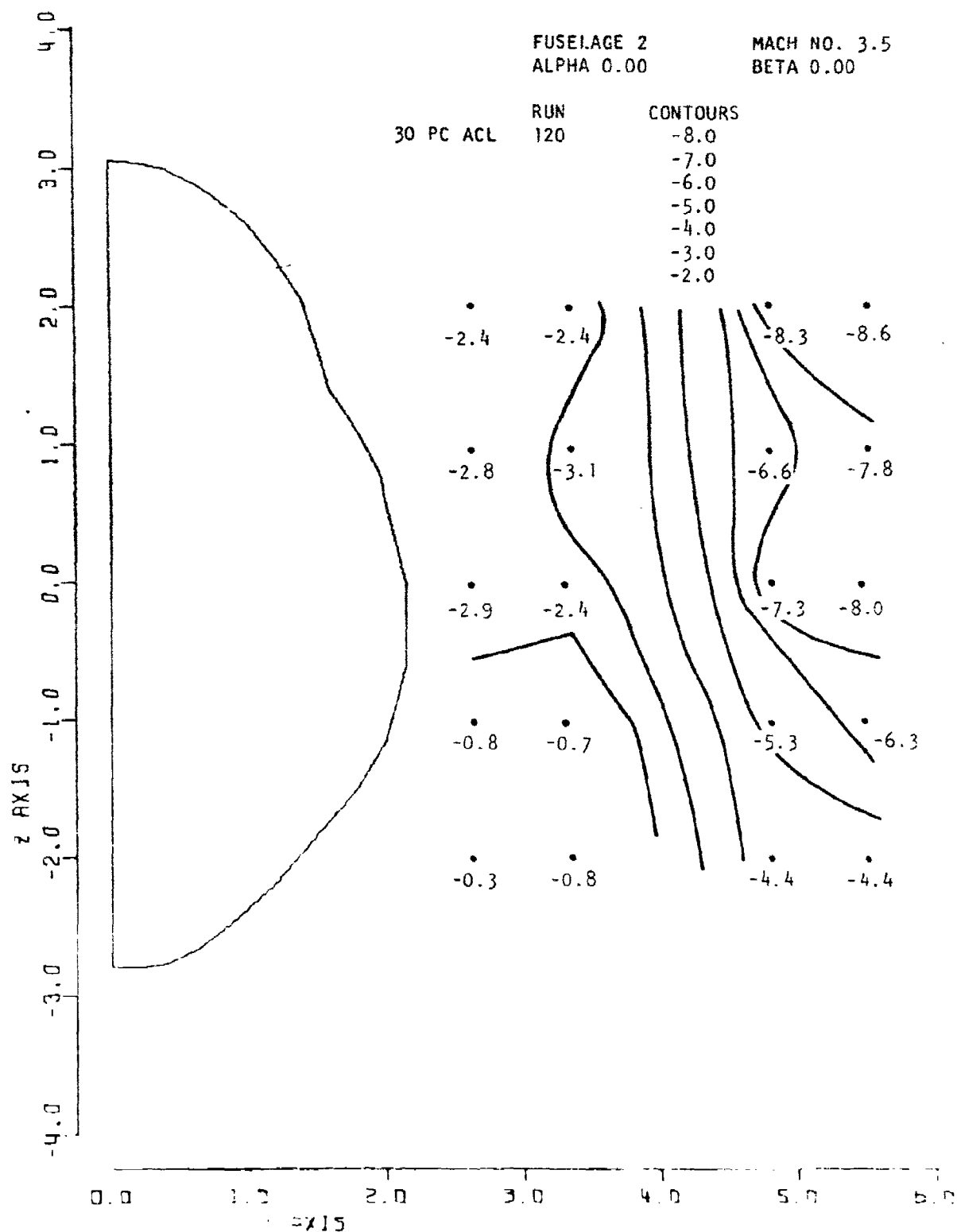


Figure 96. Local Sigma



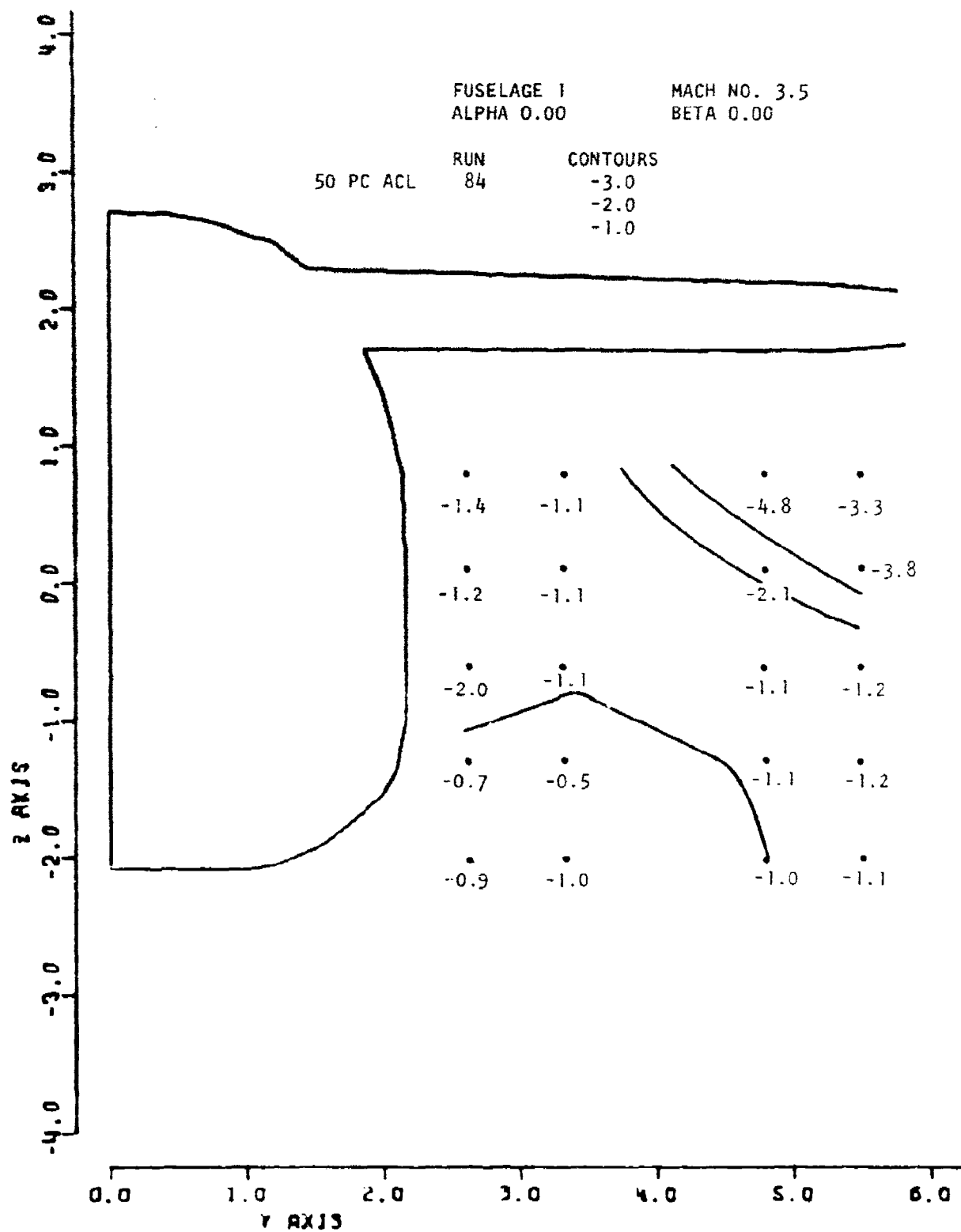


Figure 98. Local Sigma

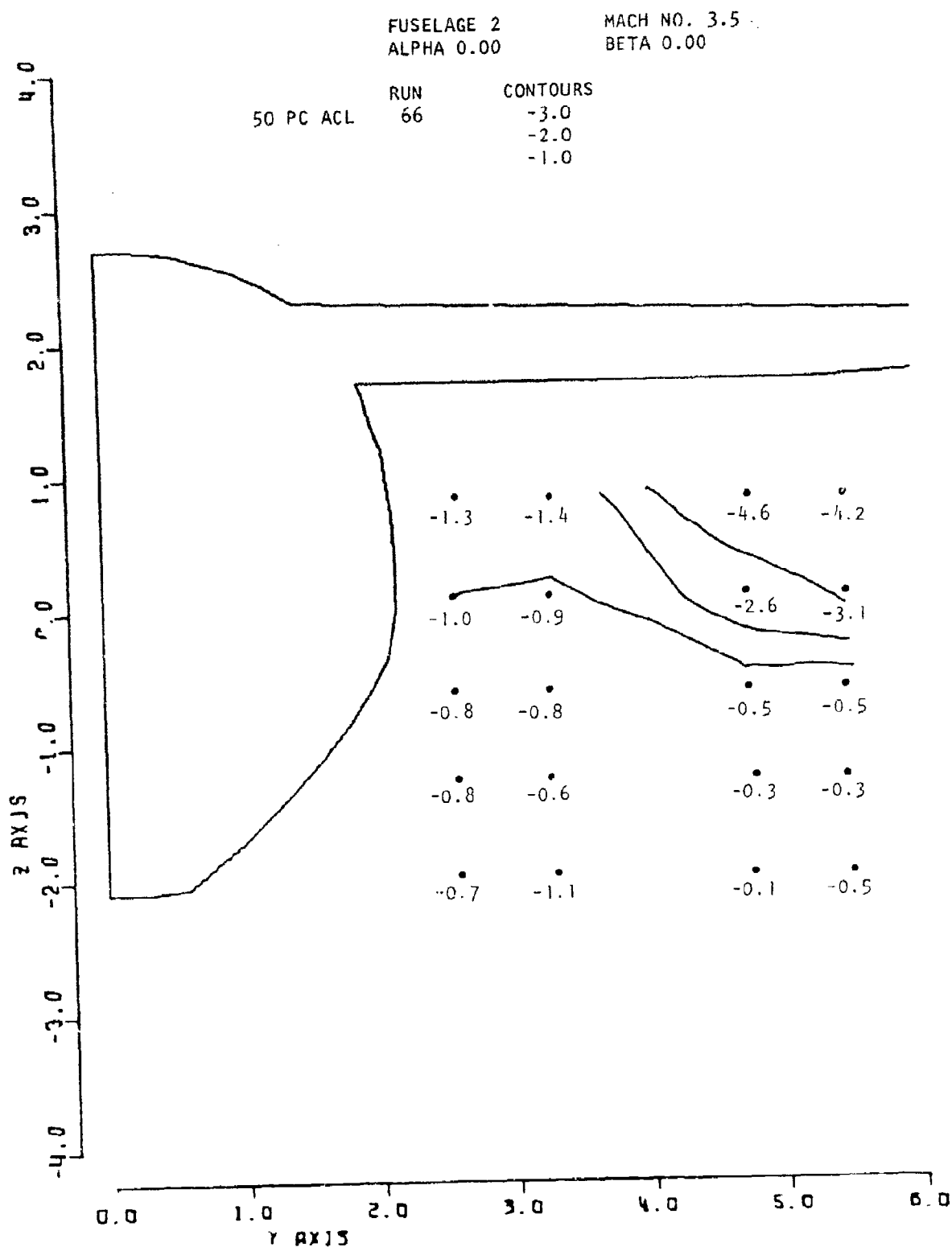


Figure 99. Local Sigma

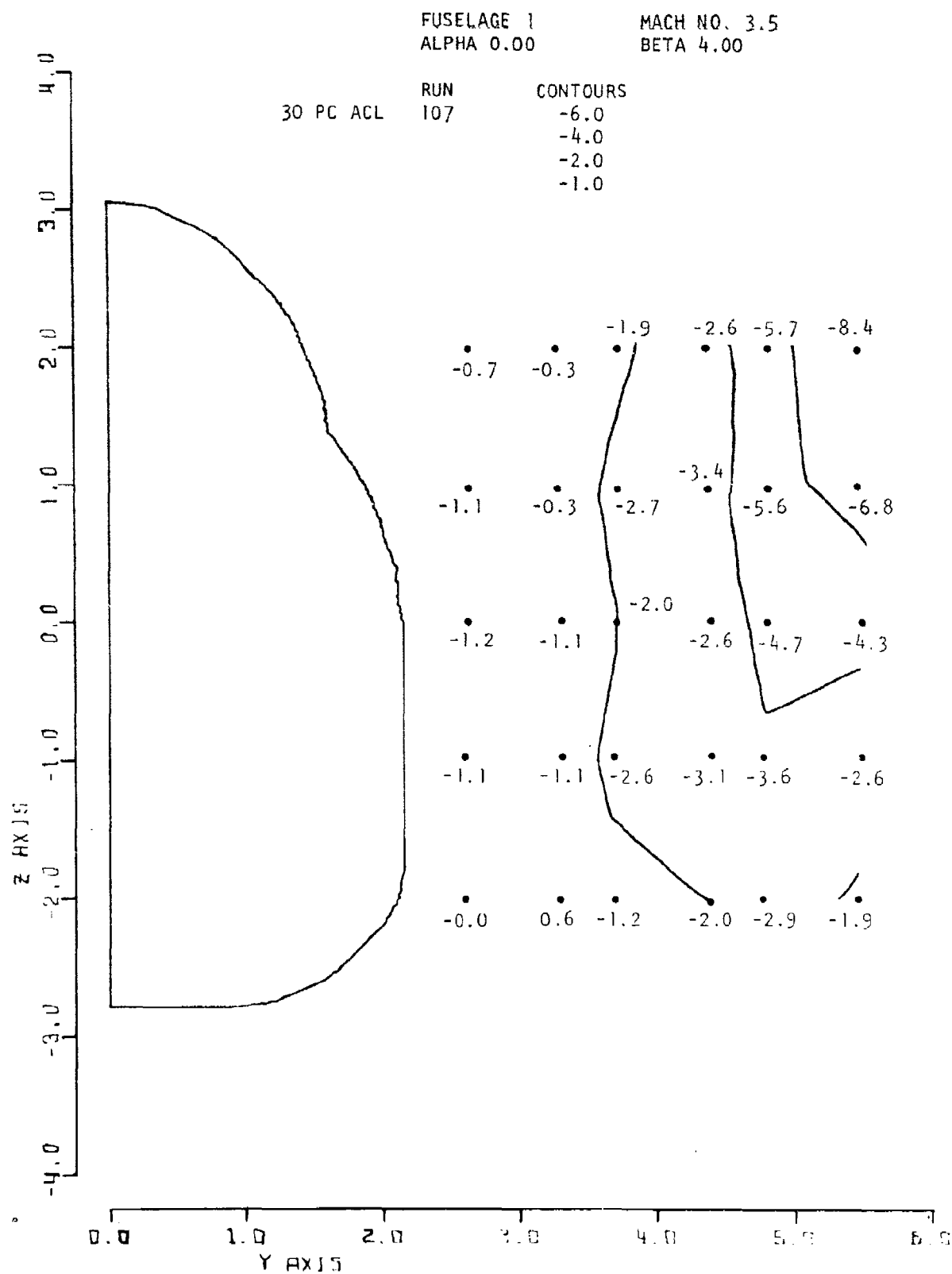


Figure 100. Local Sigma

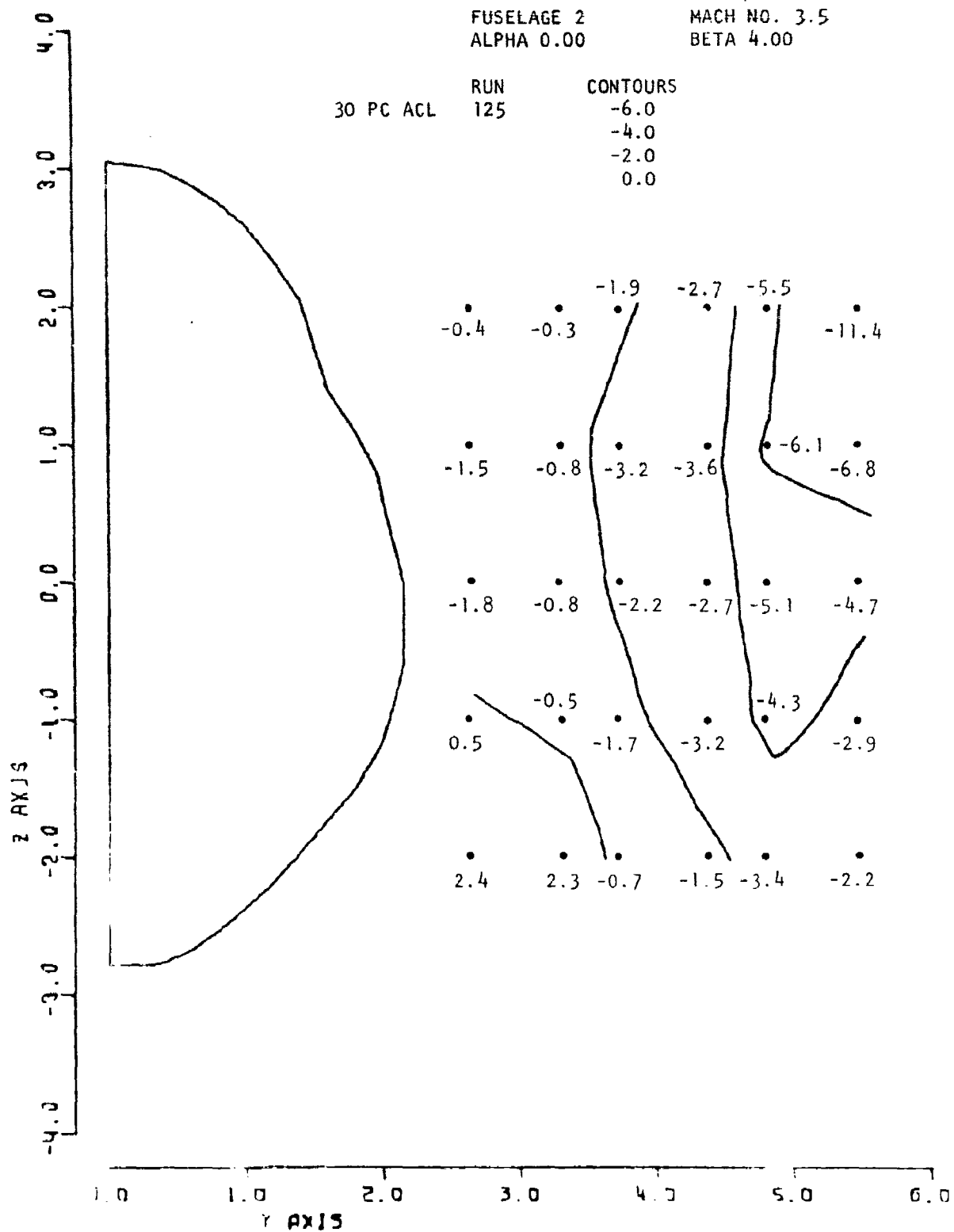


Figure 101. Local Sigma

FUSELAGE 1
ALPHA 0.00

MACH NO. 3.5
BETA 4.00

50 PC ACL RUN CONTOURS
 89 -2.0
 0.0
 1.0

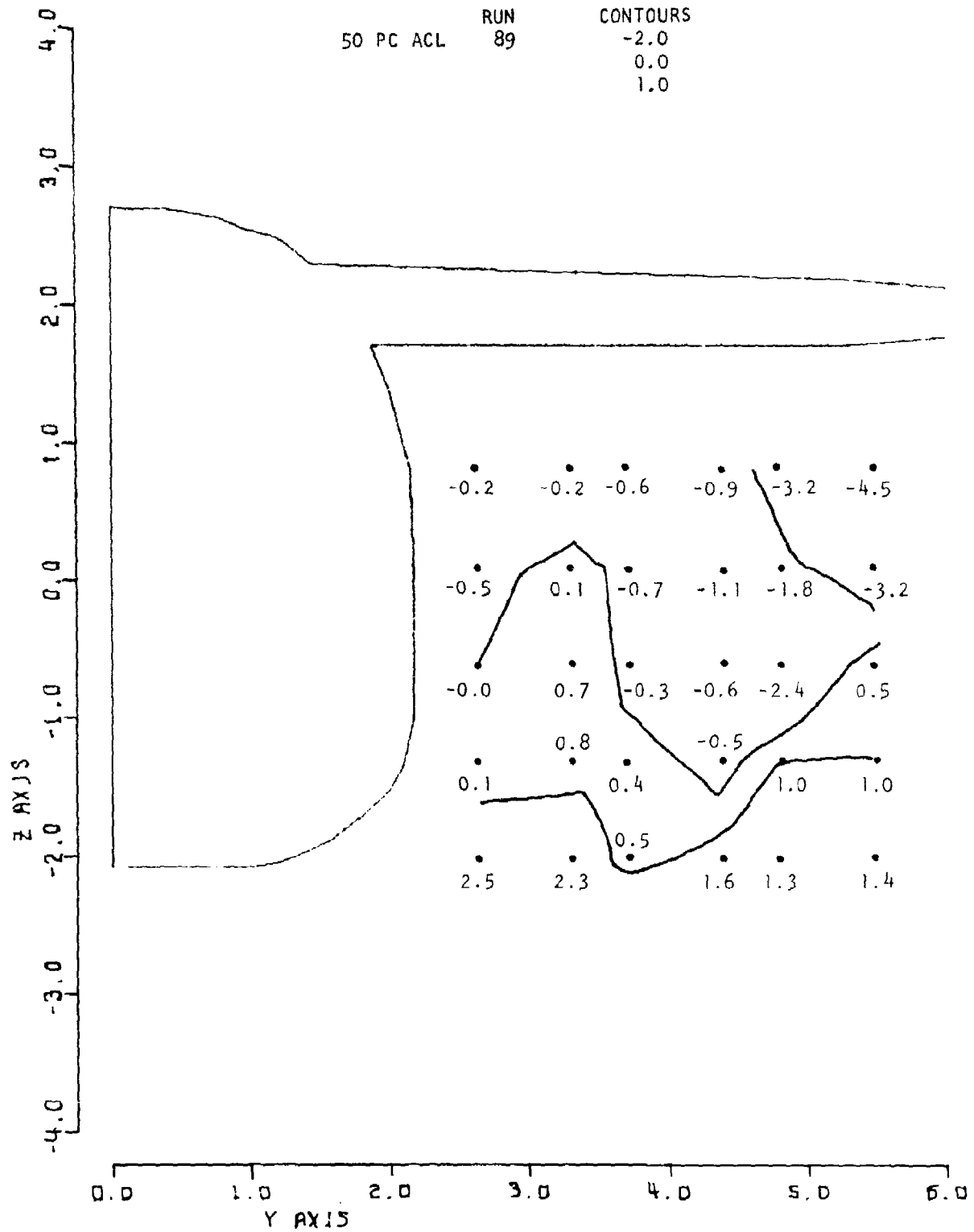


Figure 102. Local Sigma

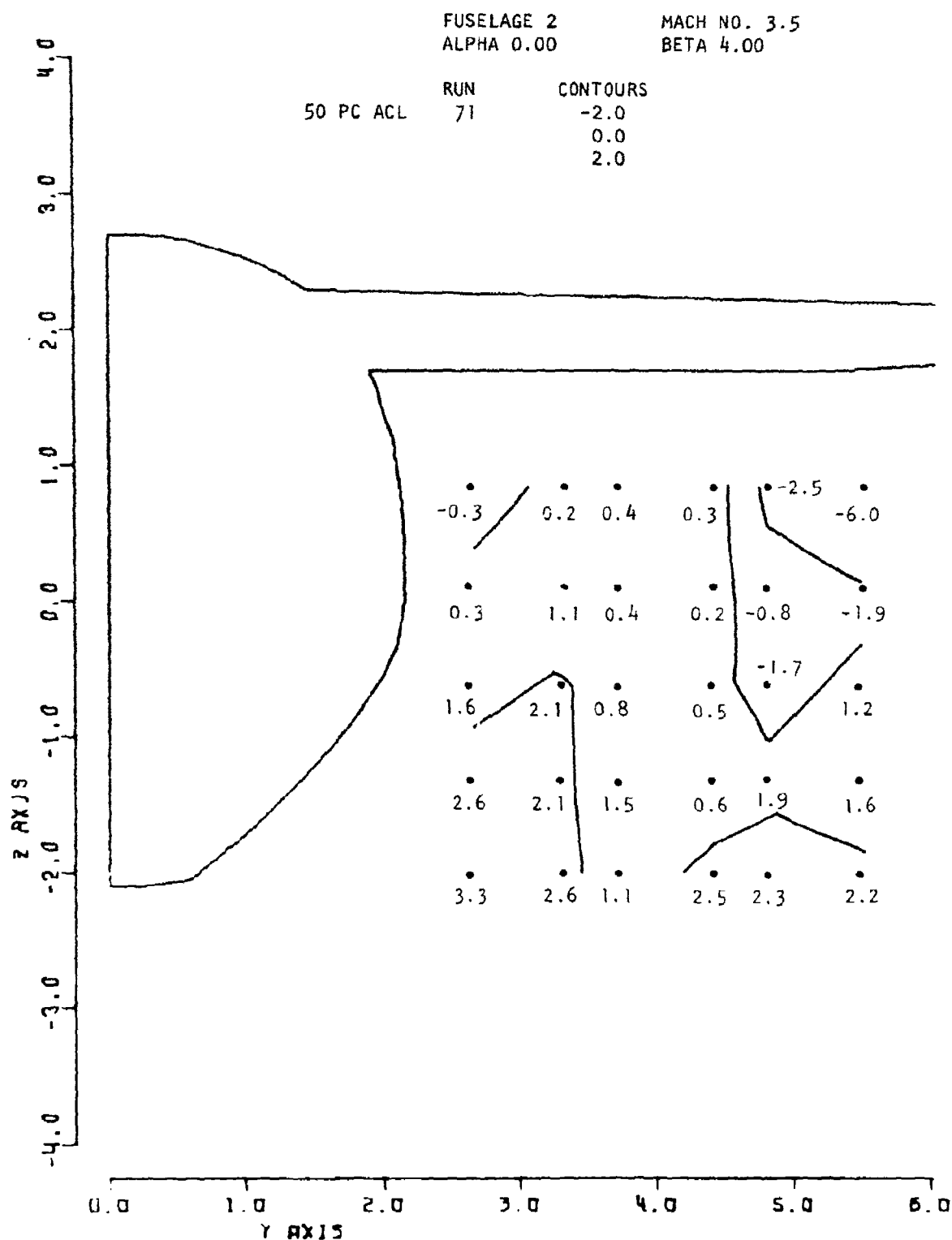


Figure 103. Local Sigma

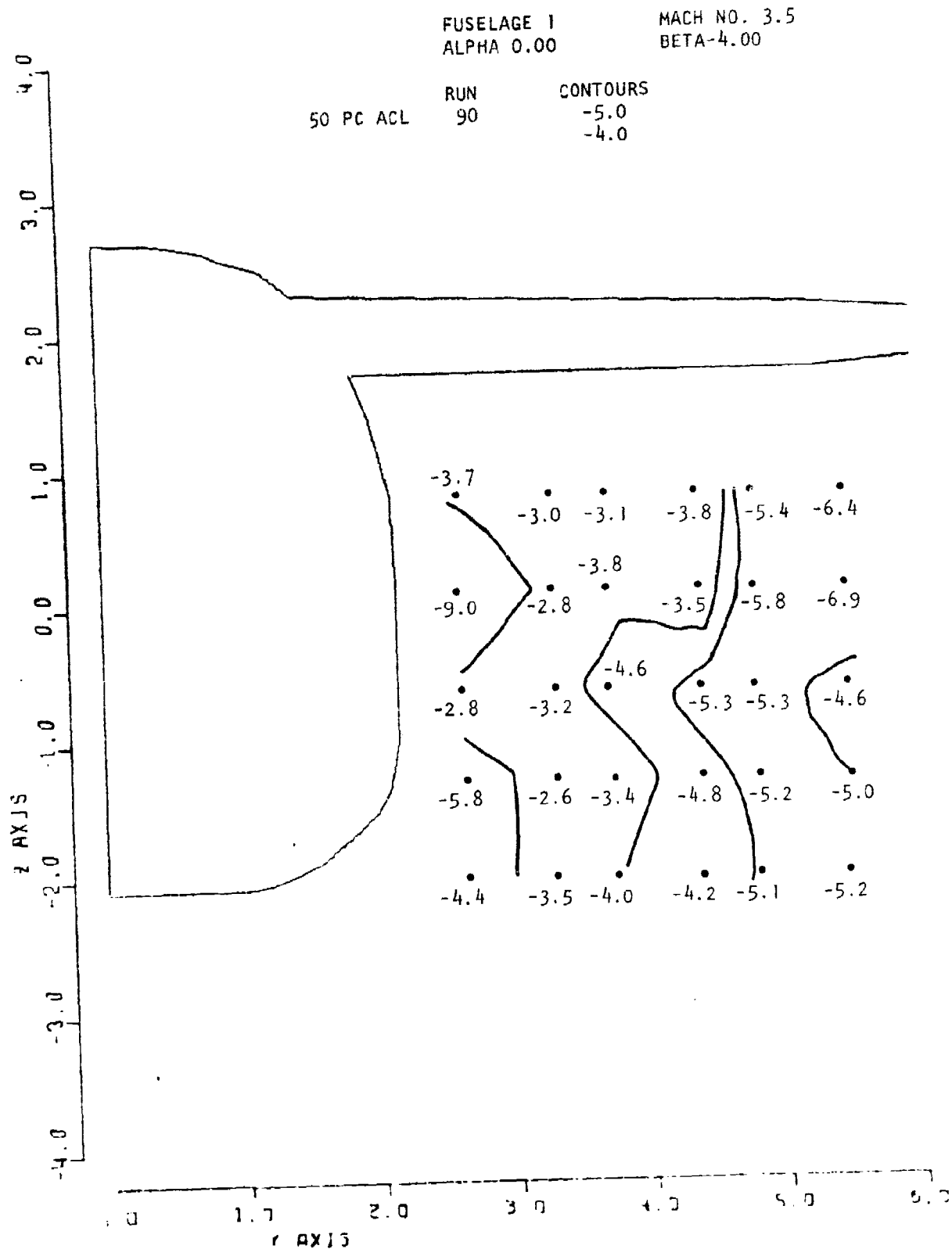


Figure 104. Local Sigma

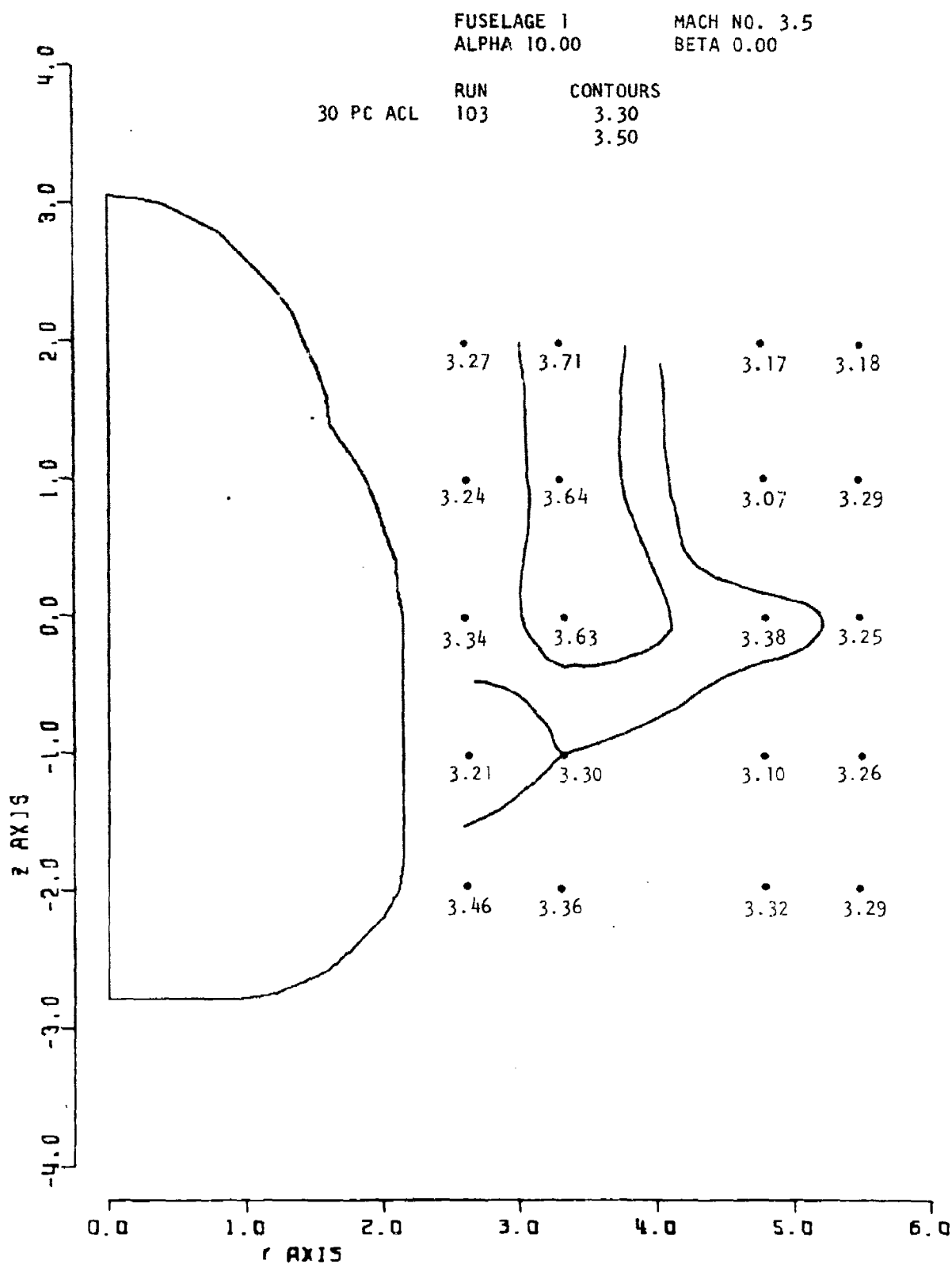


Figure 105. Local Mach No.

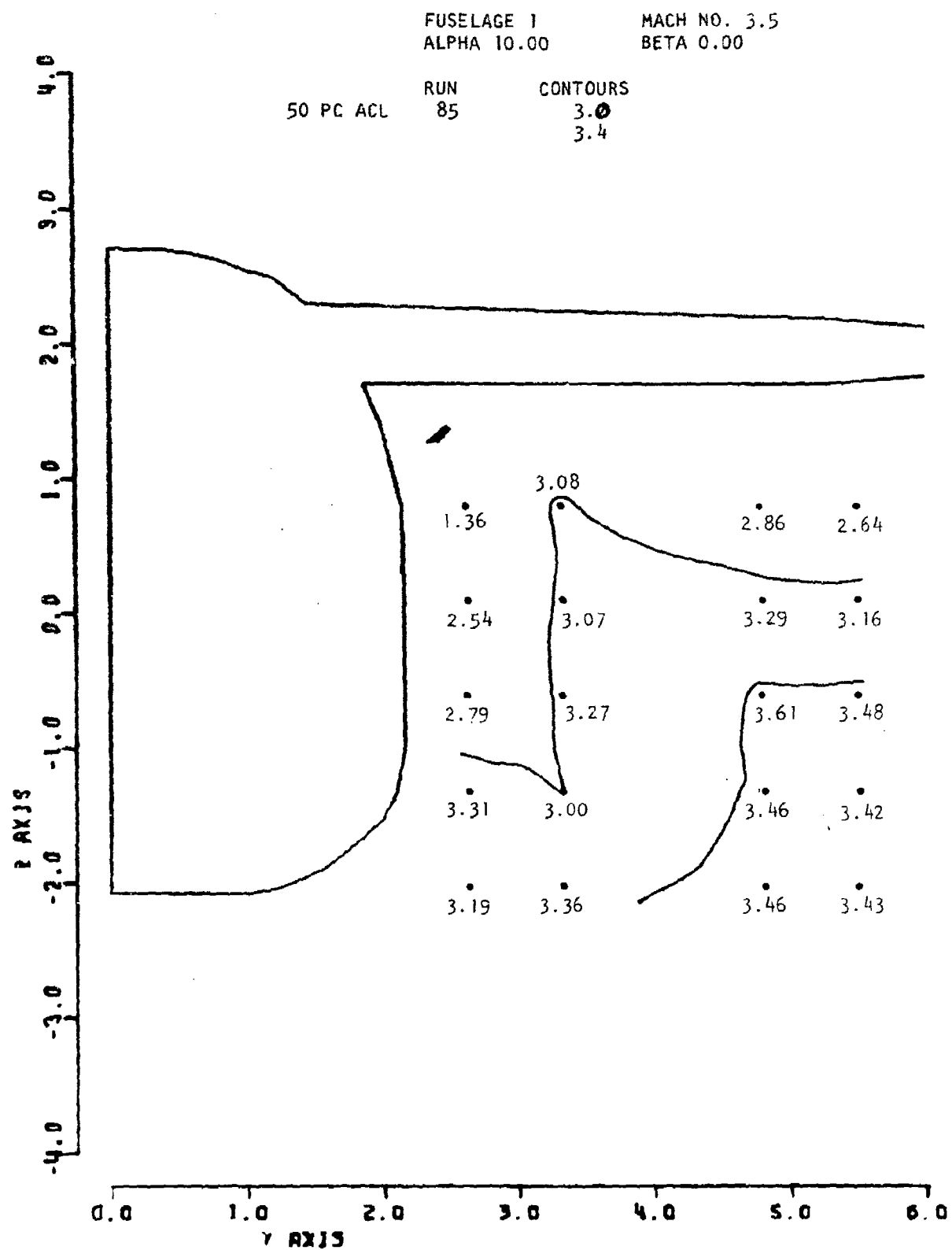


Figure 106. Local Mach No.

Effects of differences in fuselage geometry were rather localized as they were at Mach 2.5, with fuselage 2, by virtue of its larger radius shoulder, introducing the lower surface pressure field into the lower inner part of the survey region with attendant lower local Mach numbers there. This effect is exemplified by comparing Figures 107 and 106.

3.2.2.1.2 Effect of Yaw

The effect of yaw was to increase and lower the local Mach numbers on the leeward and windward sides, respectively, relative to the unyawed case, for both fuselages, as may be seen by comparing Figures 108 and 109 to 106.

3.2.2.2 Total Pressure Recovery

3.2.2.2.1 Effect of Vehicle Geometry

Increasing the angle of attack to 10° resulted in a general lowering of local pressure recoveries for both fuselages with no discernible effect of fuselage geometry. At the aft station recoveries were lower, especially in the inboard upper region, than those upstream, reflecting the presence of some local cross flow separation upstream and/or effect of the strengthened wing shock wave at this angle of attack. The data for fuselage 2 shown in Figures 110 and 111 demonstrate these effects which were typical of both fuselages.

3.2.2.2.2 Effect of Yaw

Yaw had little discernible effect on local recoveries, as was the case for low angle of attack and at Mach 2.5. There was a slight decrease in recovery on the windward side with an accompanying small general improvement on the leeward side.

3.2.2.3 Local Alpha

3.2.2.3.1 Effect of Vehicle Geometry

Increasing the angle of attack to 10° at this Mach number strengthened the lower fuselage pressure field relative to that of the upper fuselage and canopy with the result that all the local angles of attack at the forward survey station were positive, as shown in Figures 112 and 113. Effects of geometry differences between fuselages 1 and 2 appeared to be negligible. The distribution of local angles of attack was comparatively uniform in magnitude.

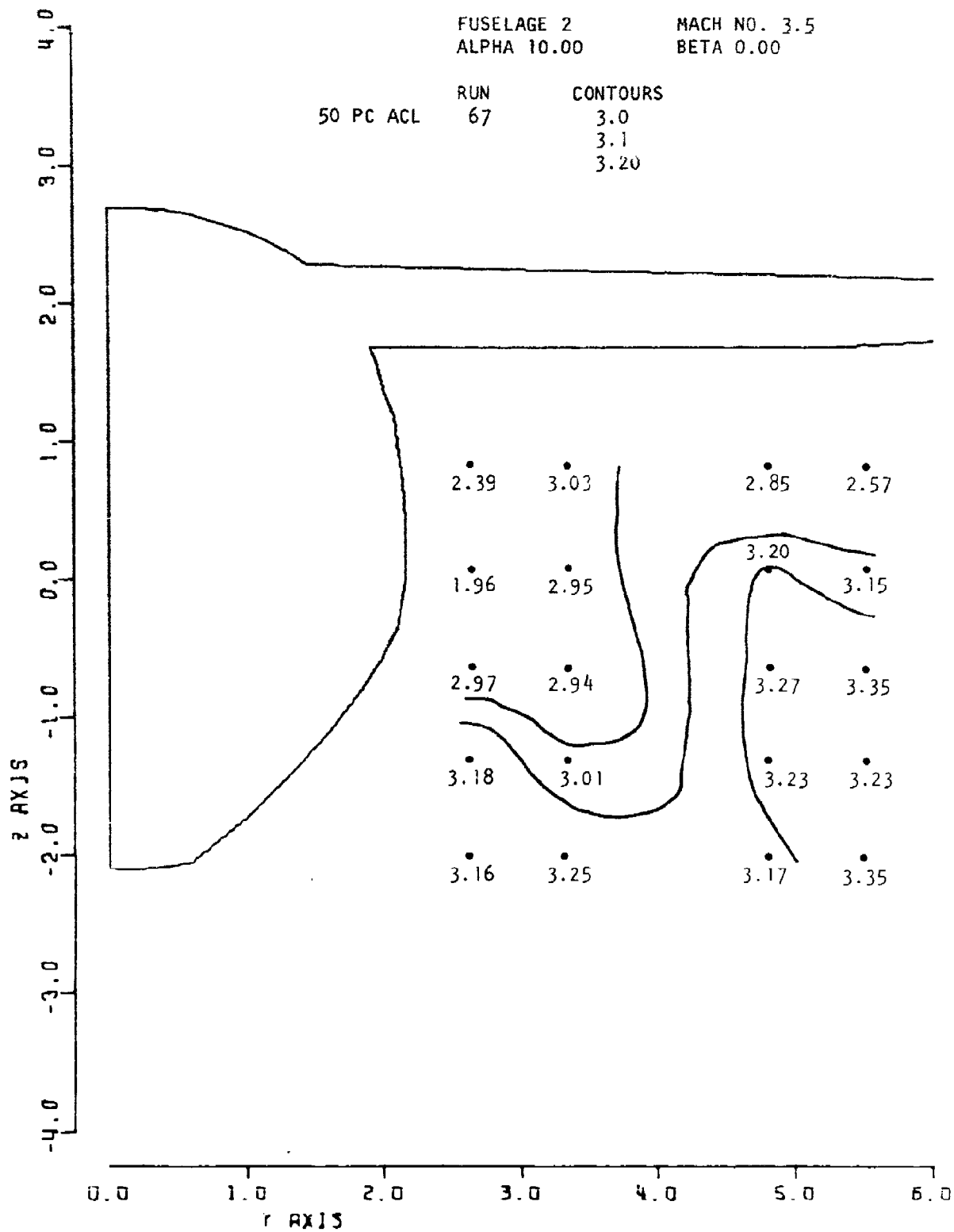


Figure 107. Local Mach No.

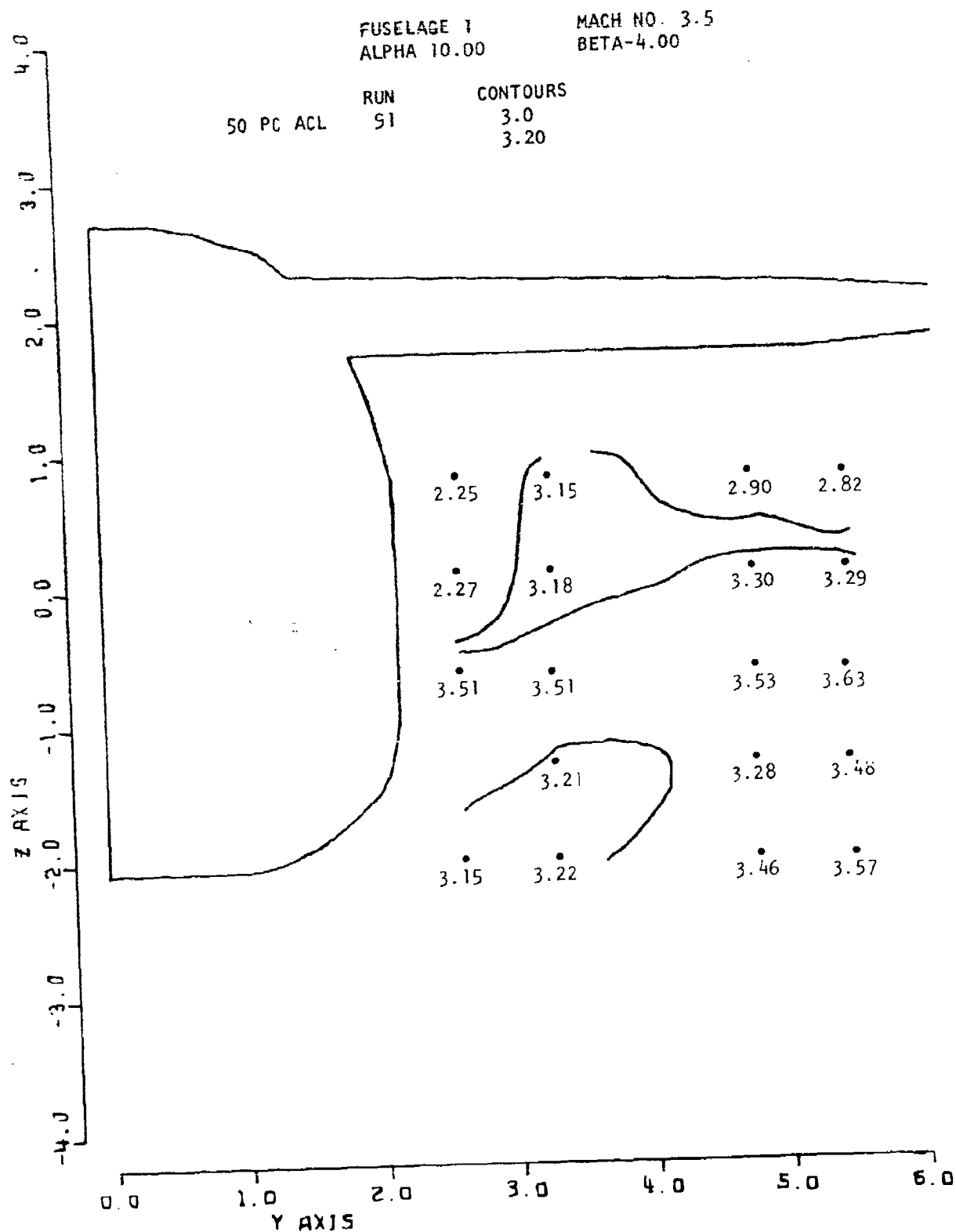


Figure 108. Local Mach No.

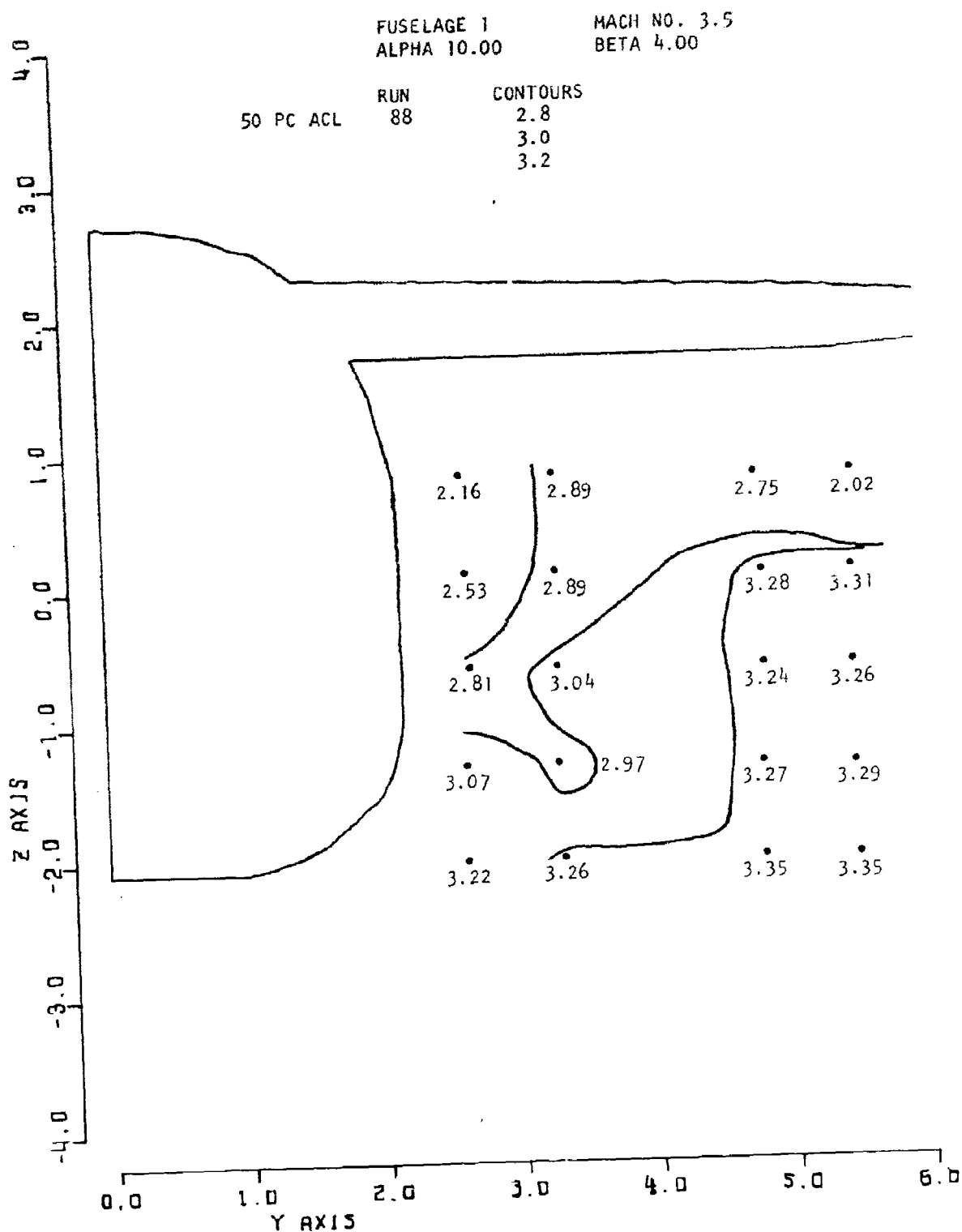


Figure 109. Local Mach No.

FUSELAGE 2
ALPHA 10.00

MACH NO. 3.5
BETA 0.00

30 PC ACL RUN CONTOURS
121 0.80
0.90

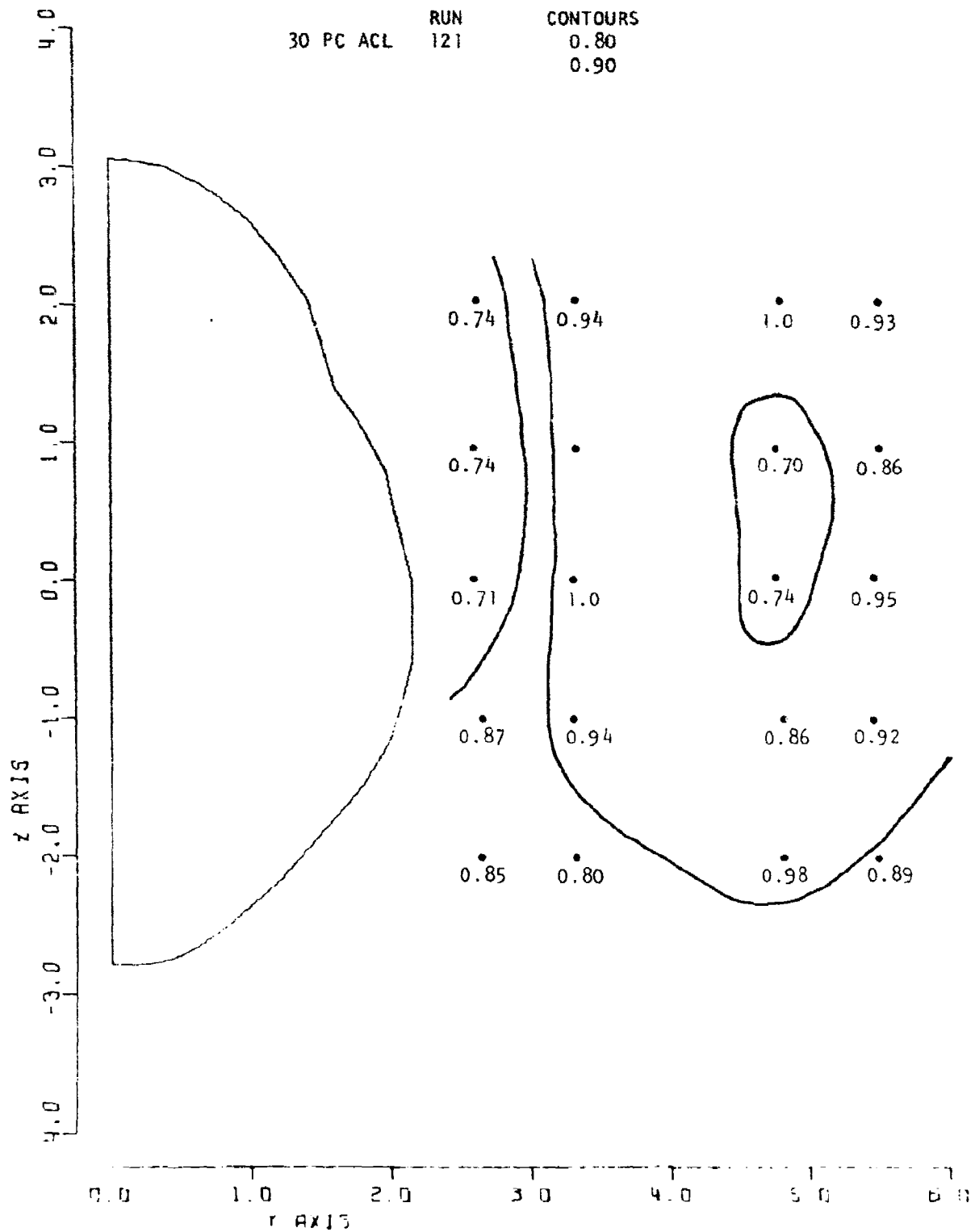


Figure 110. Local PT/PT High

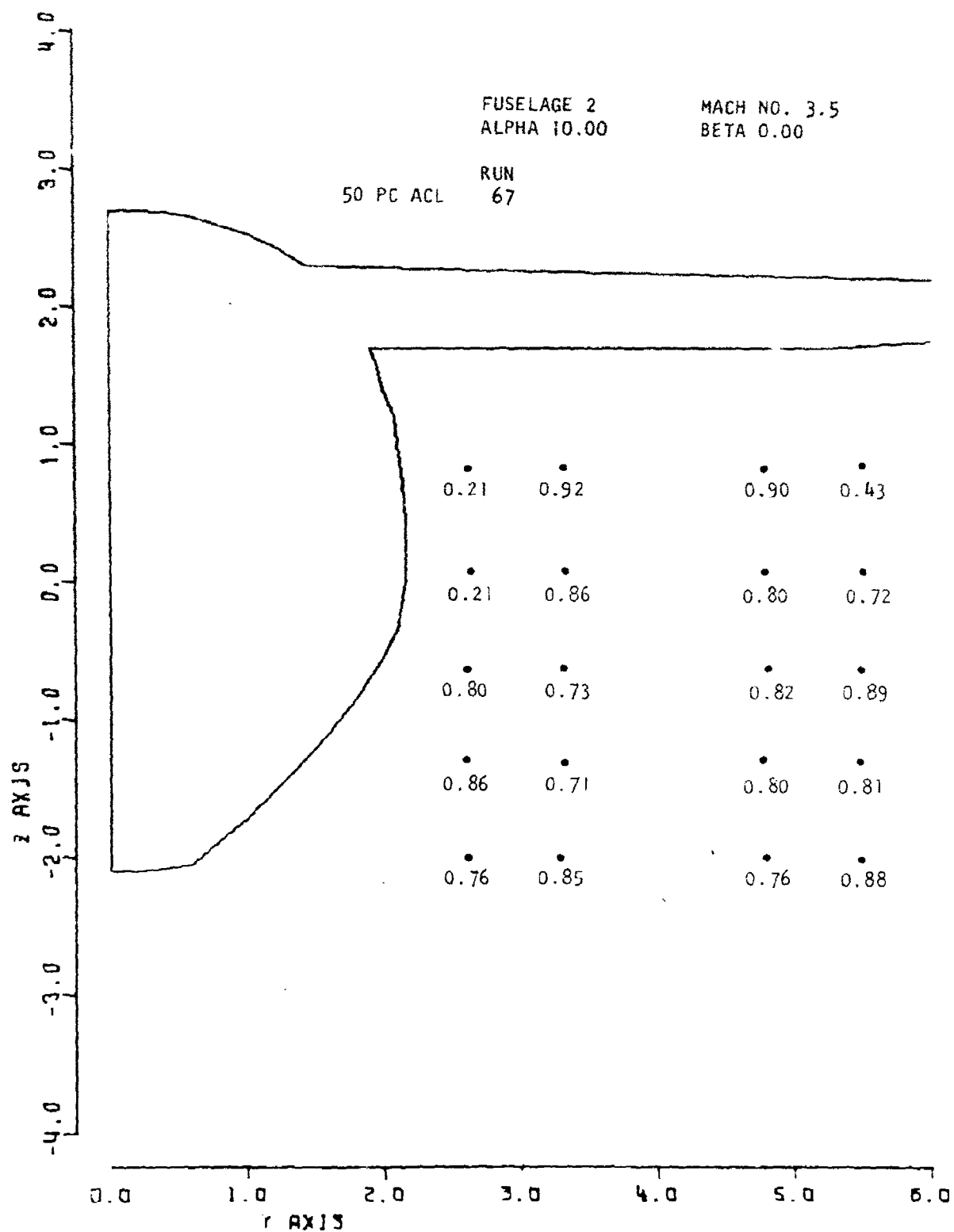


Figure 111. Local PT/PT High

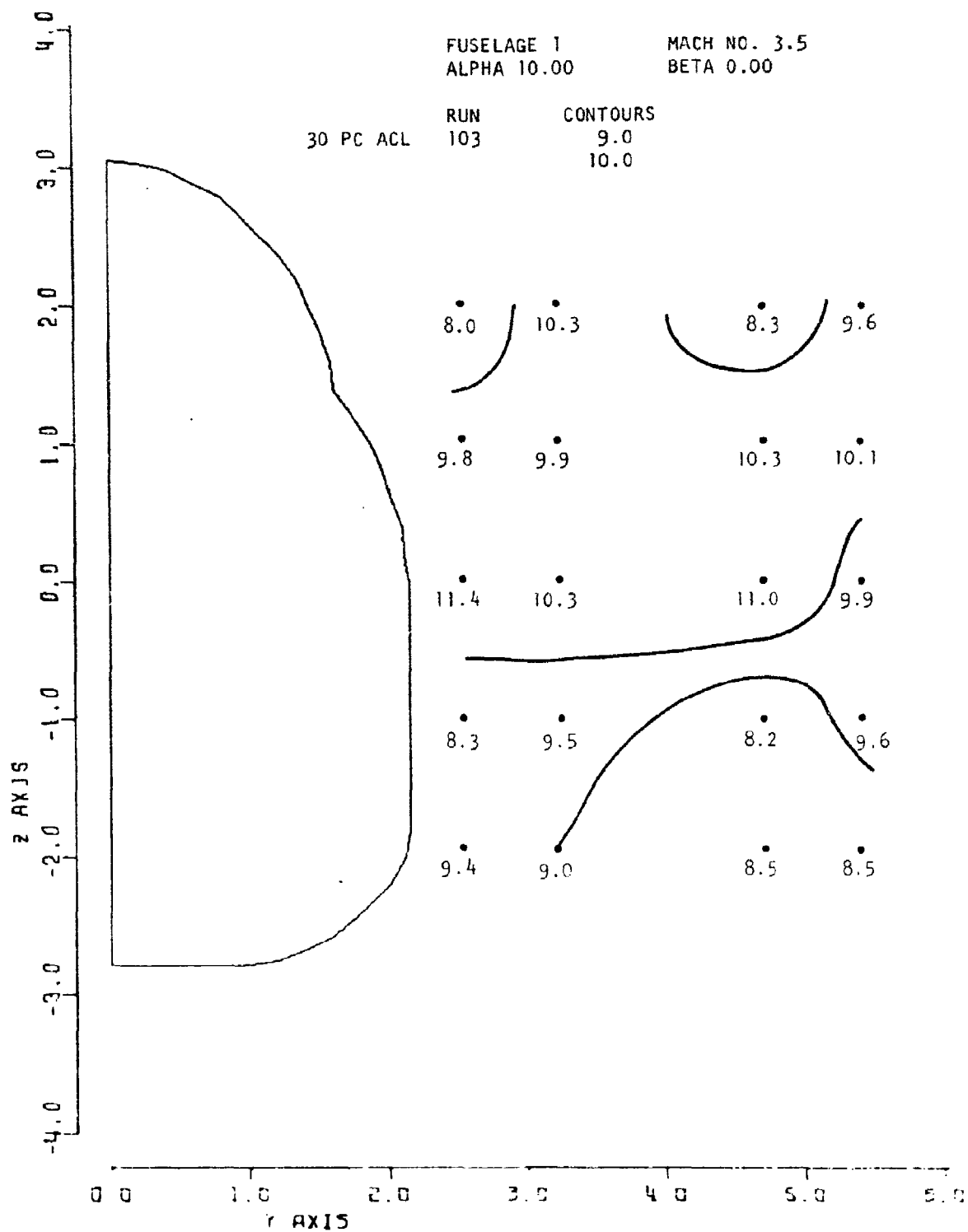


Figure 112. Local Alpha

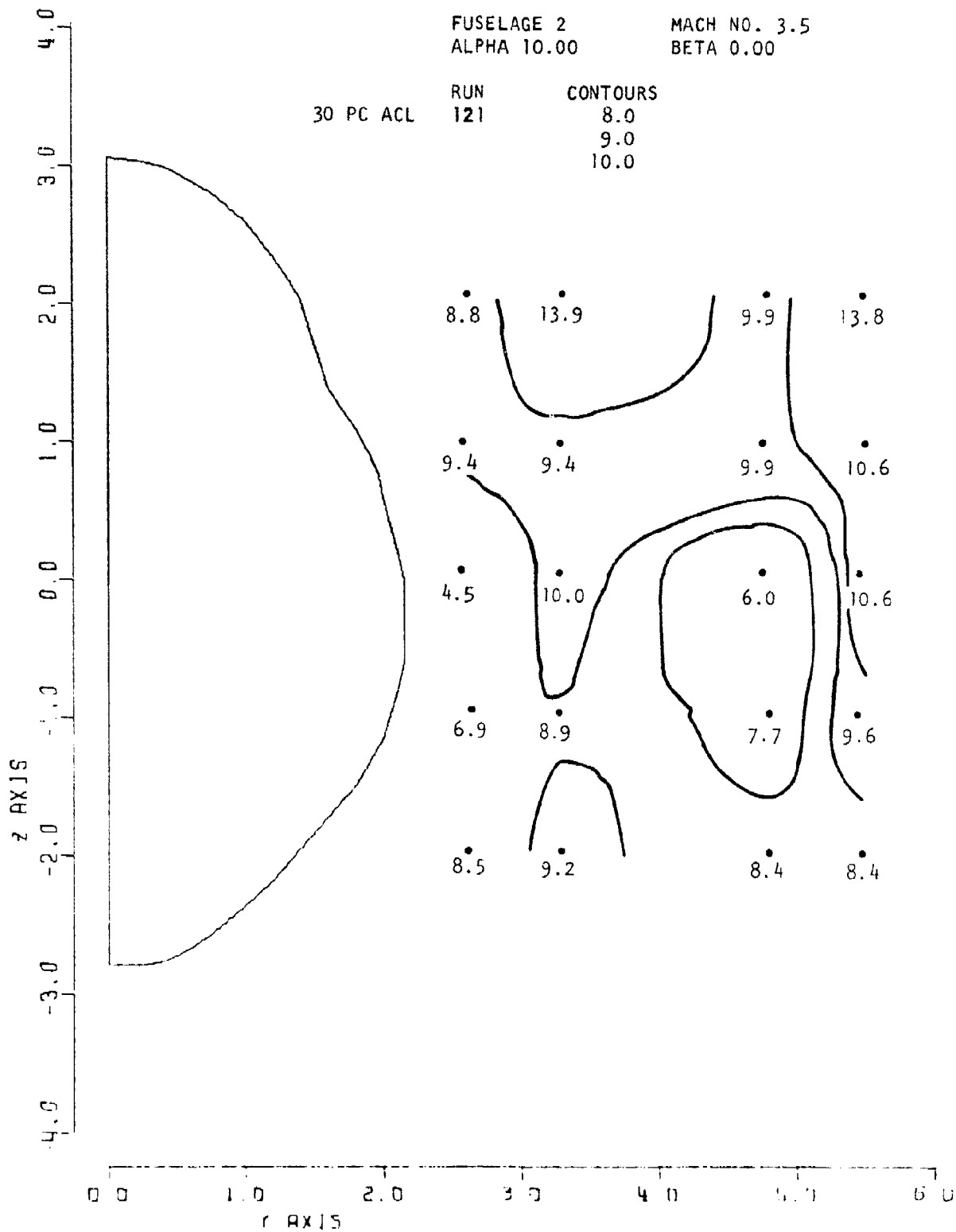


Figure 113. Local Alpha

At the downstream station the local angles of attack decreased especially in the vicinity below the wing where its pressure field was greatest. This was also observed at Mach 2.5. The sharper, less rounded corner of fuselage 1 resulted in slightly larger upwash angles in the region of its corner as compared with fuselage 2, as may be seen from Figures 114 and 115.

3.2.2.3.2 Effect of Yaw

The main effect of yaw on local upwash relative to the unyawed case, was to decrease that in the lower inboard region of the windward side and increase that on the leeward side, at both survey stations independent of fuselage geometry. This can be seen in the data presented for fuselage 1 in Figures 116 and 117.

3.2.2.4 Local Sigma

3.2.2.4.1 Effect of Vehicle Geometry

Fuselage geometry effects were nil at this angle of attack as compared to the zero degree case. The general sidewash at both fore and aft survey regions was negative, with that at the rear station more negative in its inboard region than at the upstream location as may be seen in Figures 118 and 119. This effect of angle of attack is essentially the same as that observed in the Mach 2.5 case.

3.2.2.4.2 Effect of Yaw

As expected, the effect of yaw relative to the unyawed case was to make the sidewash more negative on the leeward and less negative on the windward sides for both fuselages at both survey stations, as may be seen from the data of Figures 120 and 121 for fuselage 1, and Figures 122 and 123 for fuselage 2. The local sidewash was found to be less negative in the region of the lower fuselage corner for fuselage 2, which, with its well rounded lower shoulder, does not tend to isolate the lower fuselage induced pressure field as much as did fuselage 1, a characteristic which has been noted earlier in this report.

3.2.3 High Angle of Attack

3.2.3.1 Local Mach Number

3.2.3.1.1 Effect of Vehicle Geometry

At this high angle of attack increasing the angle of attack from 10° to 20° produced a general lowering of the local Mach numbers at both survey stations. The local Mach

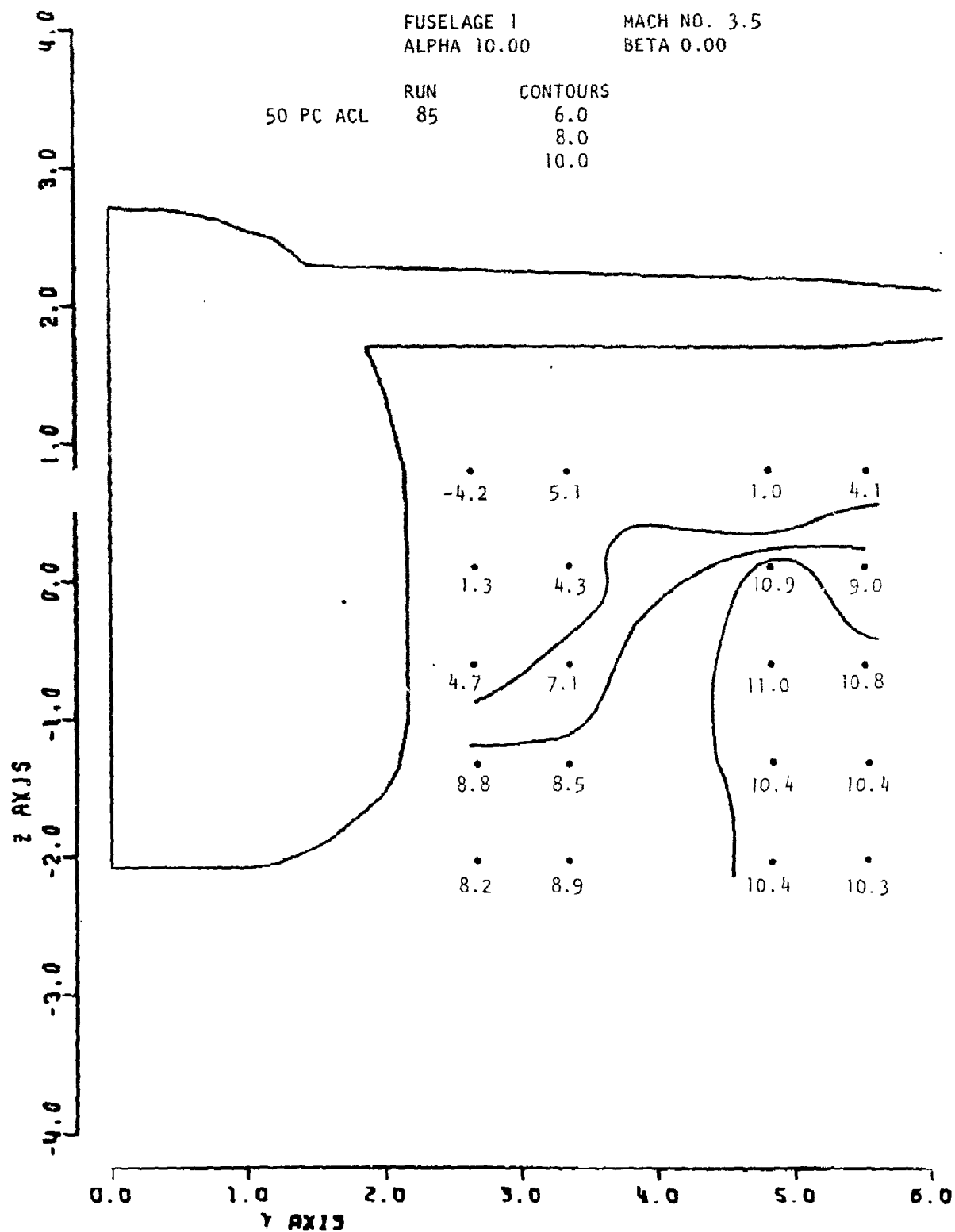


Figure 114. Local Alpha

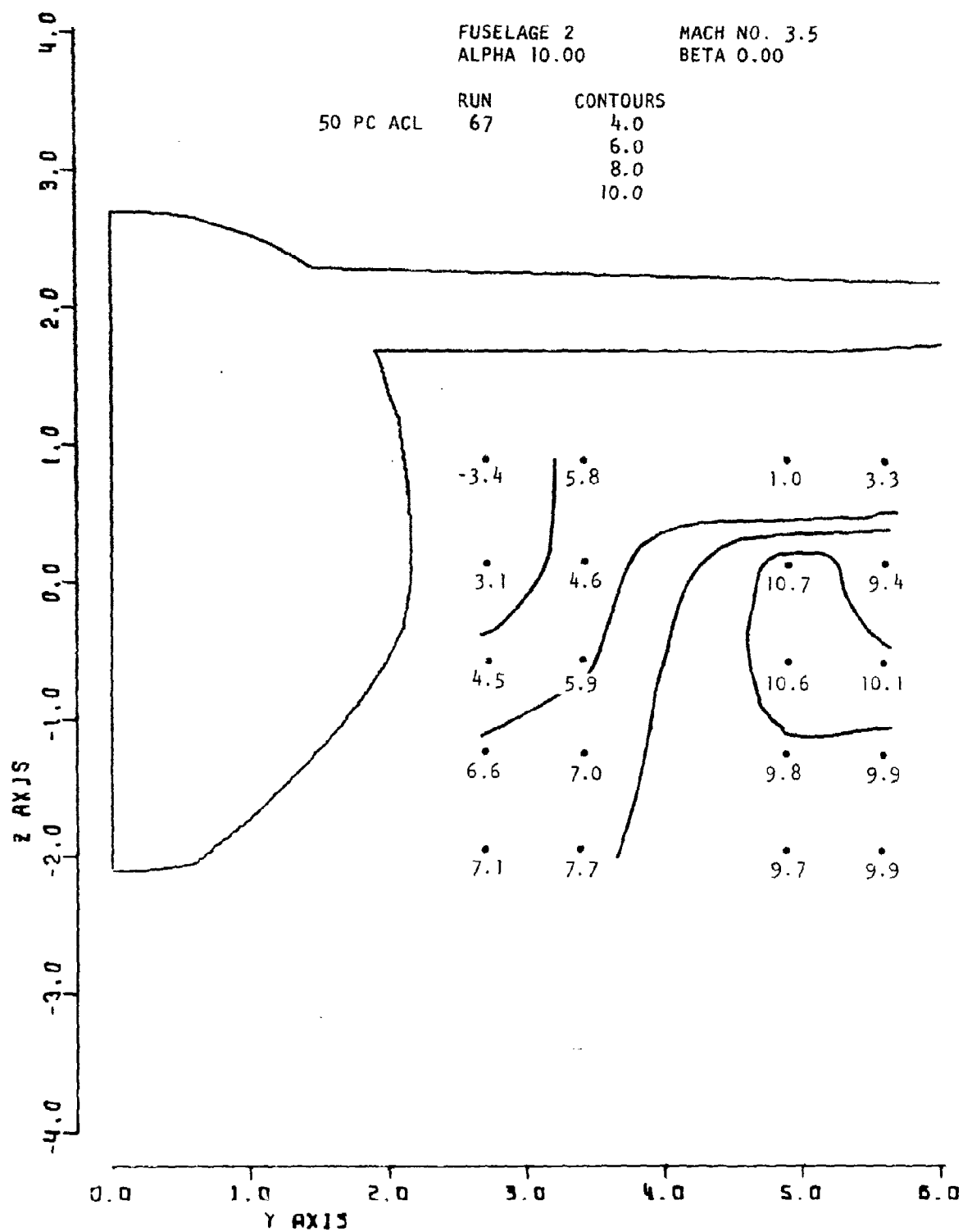


Figure 115. Local Alpha

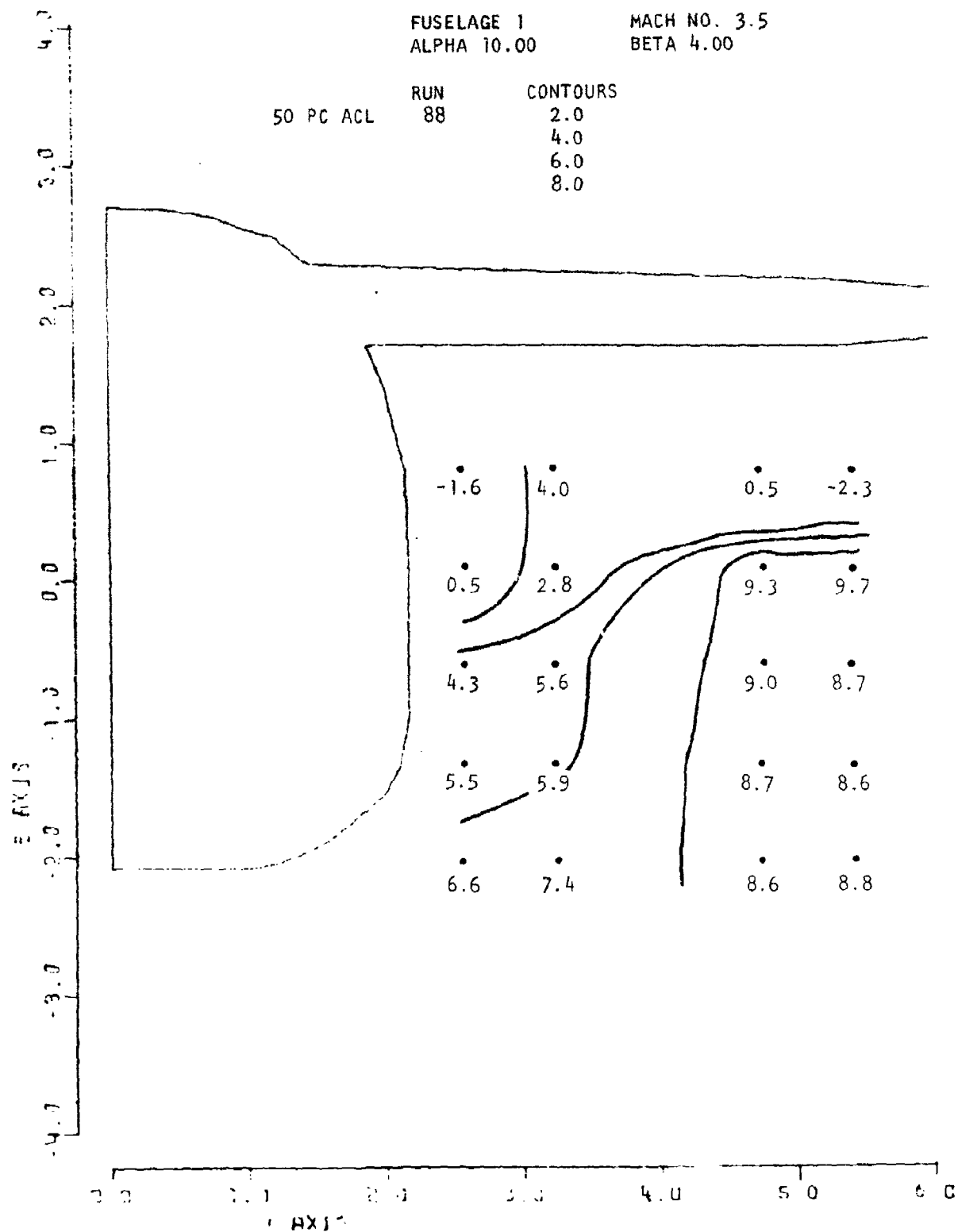


Figure 116. Local Alpha

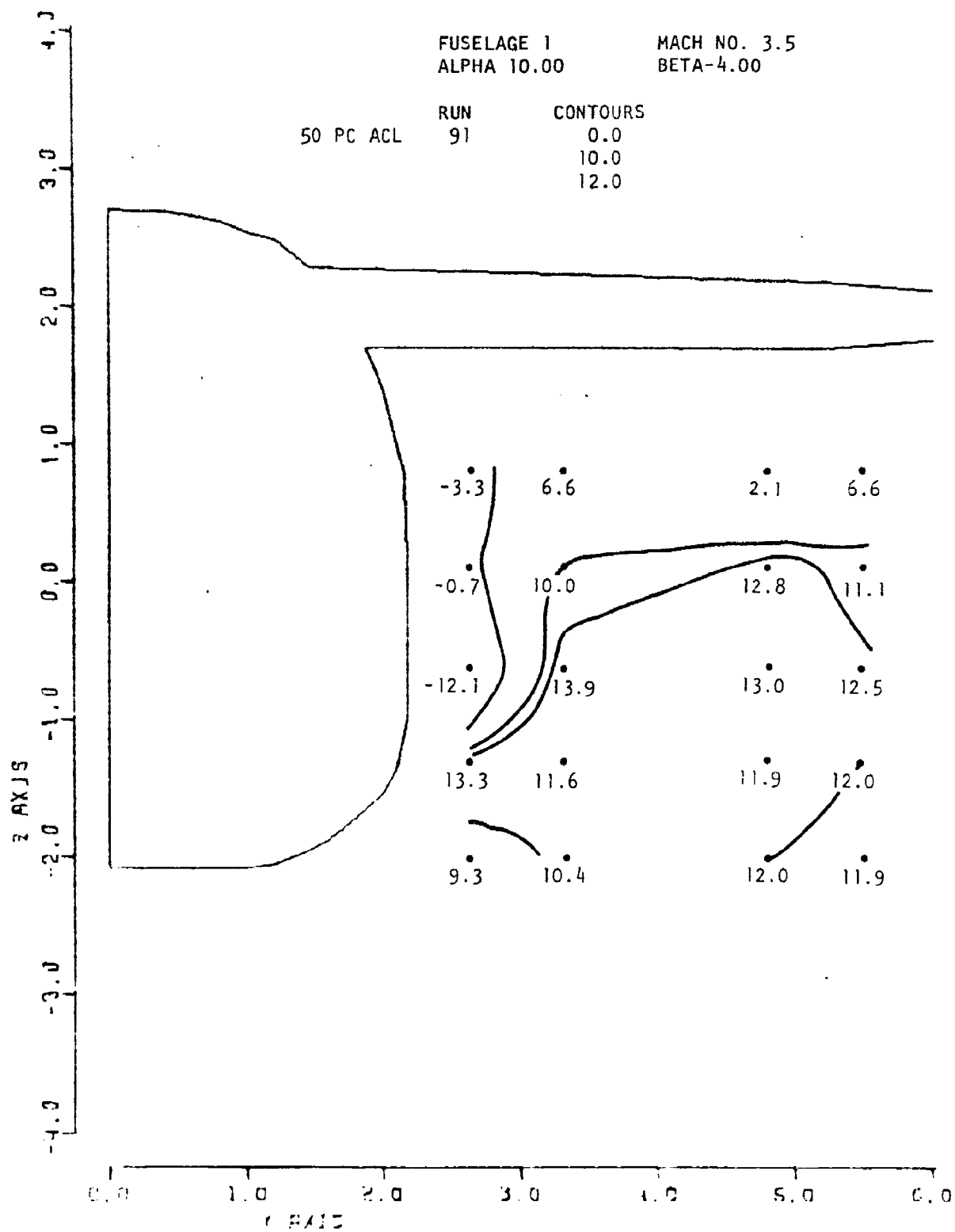


Figure 117. Local Alpha

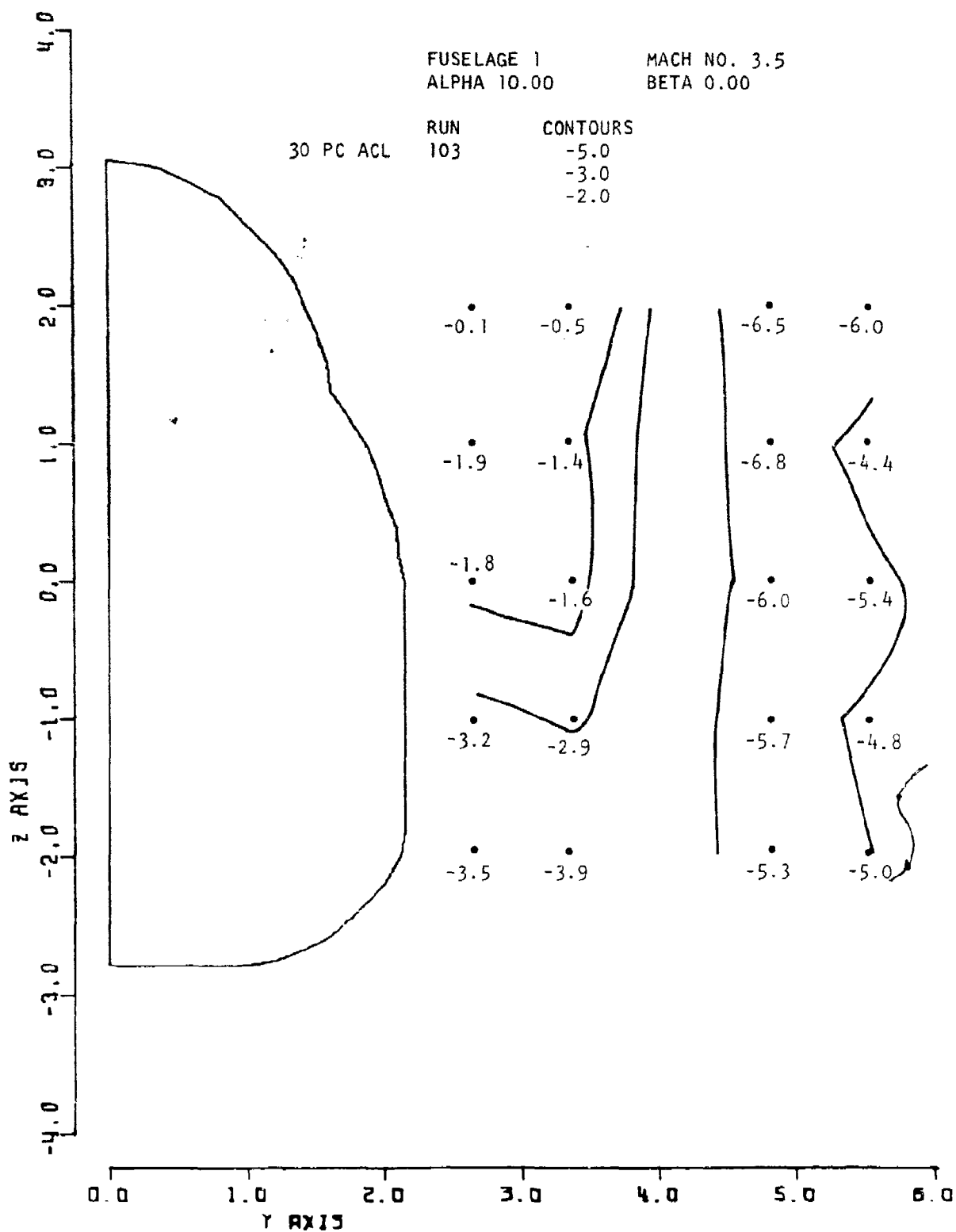


Figure 118. Local Sigma

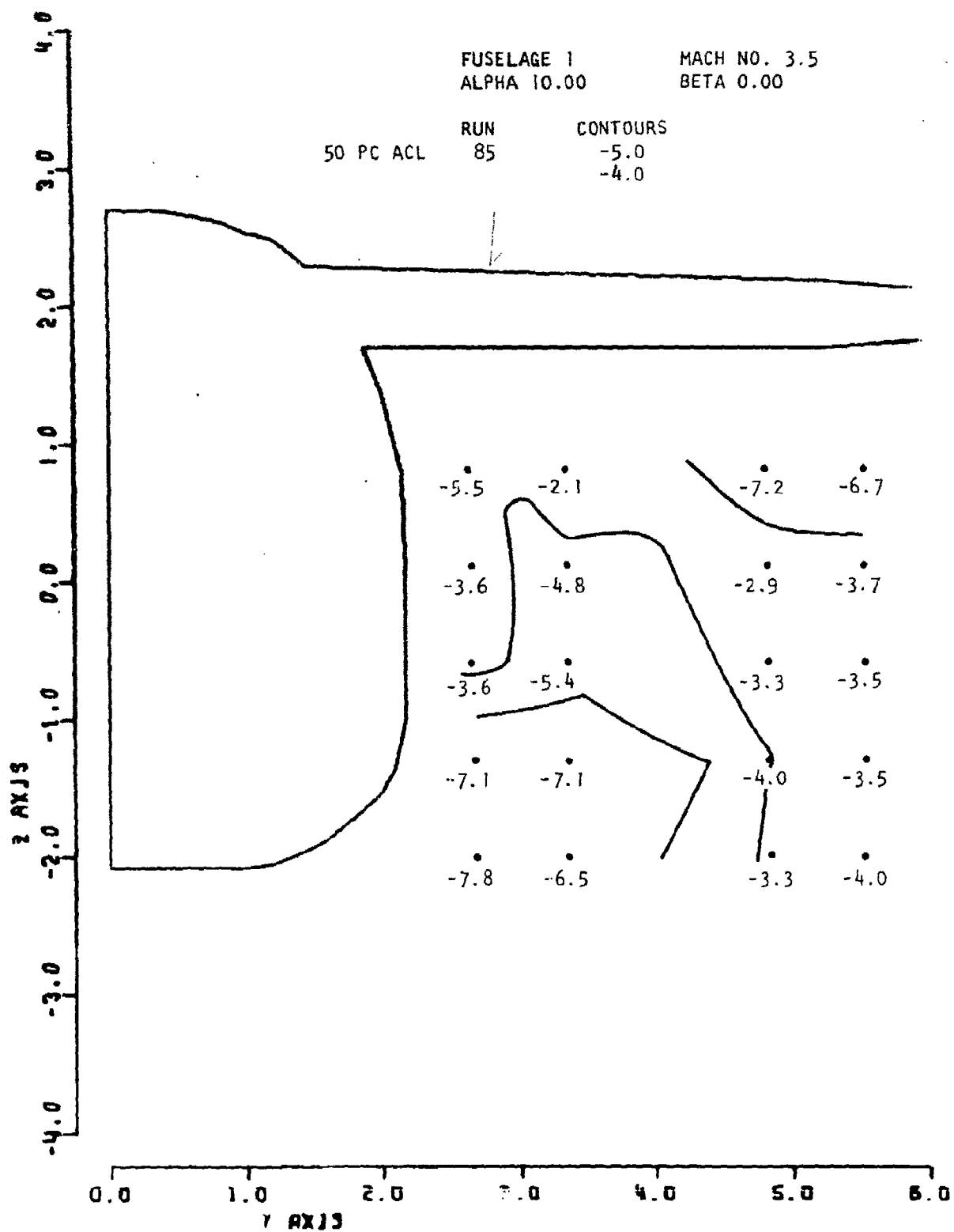


Figure 119. Local Sigma

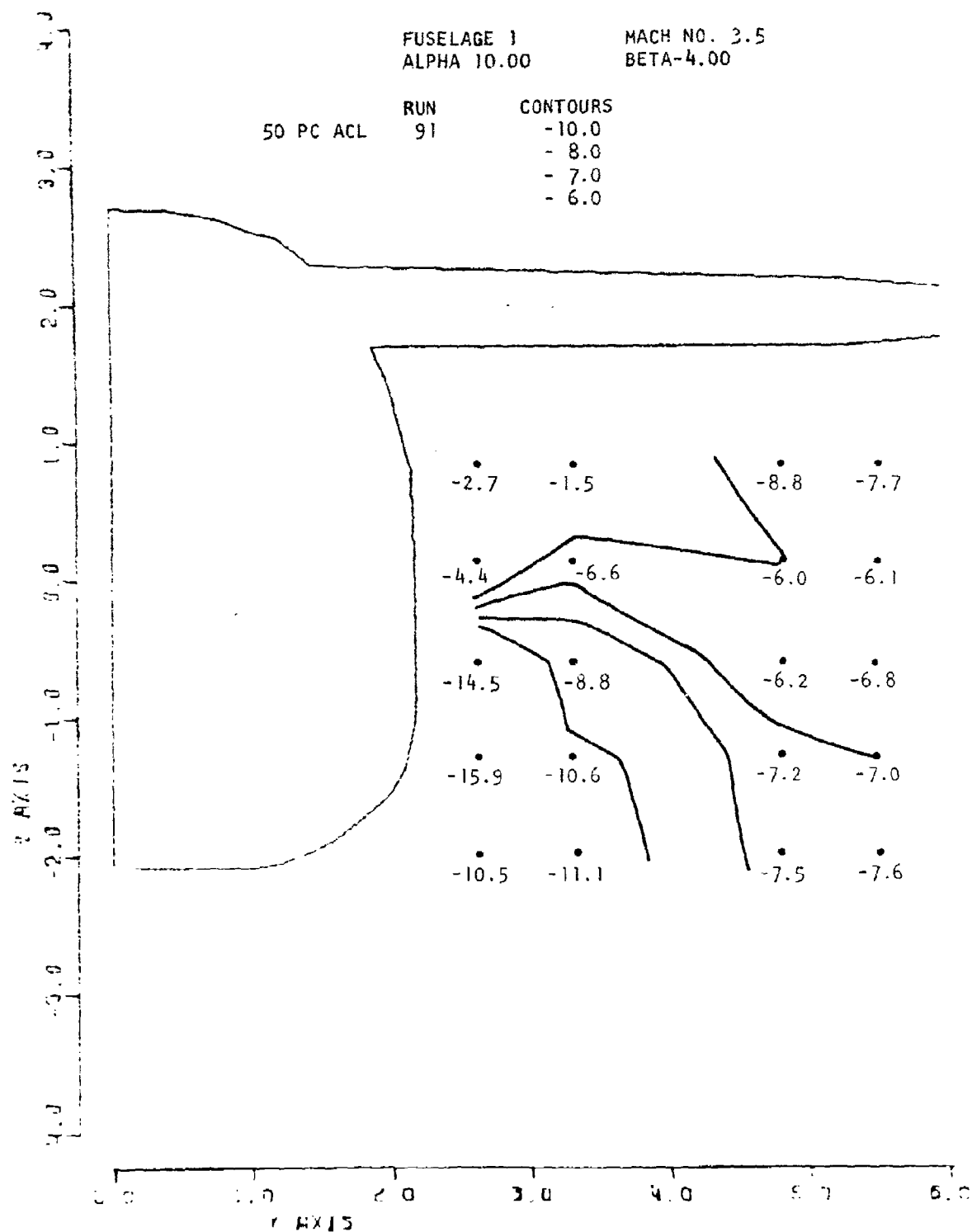


Figure 120. Local Sigma

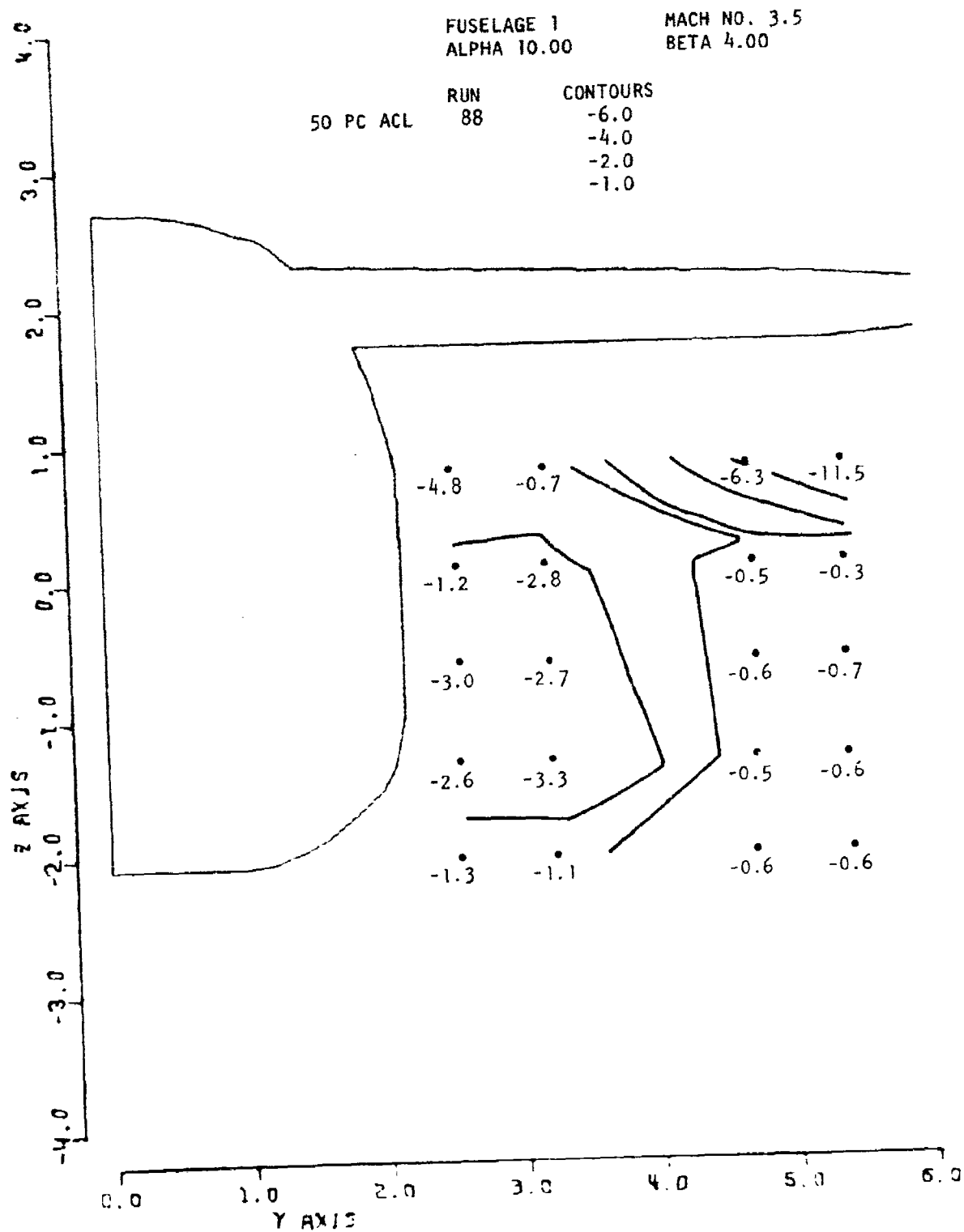


Figure 121. Local Sigma

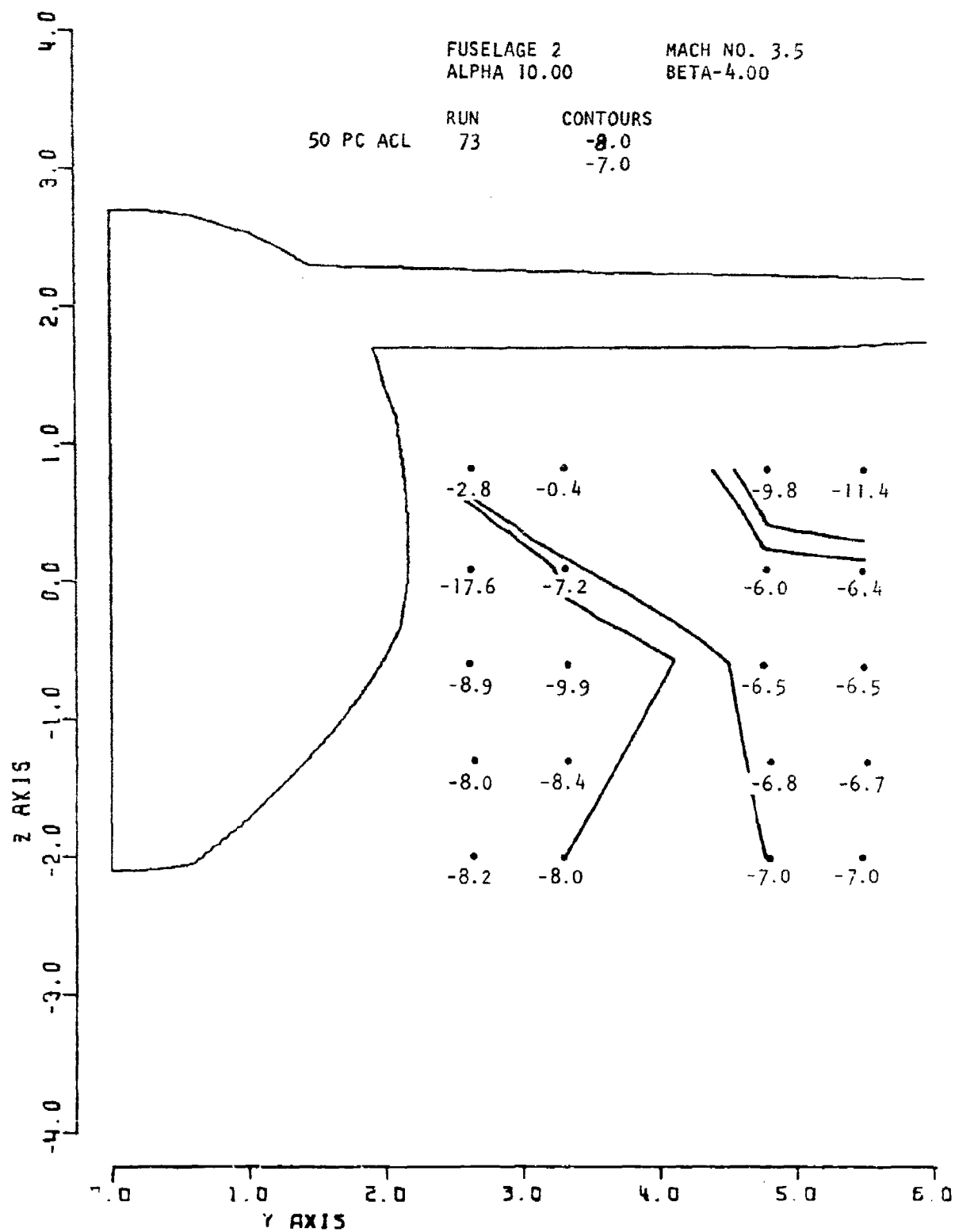


Figure 122. Local Sigma

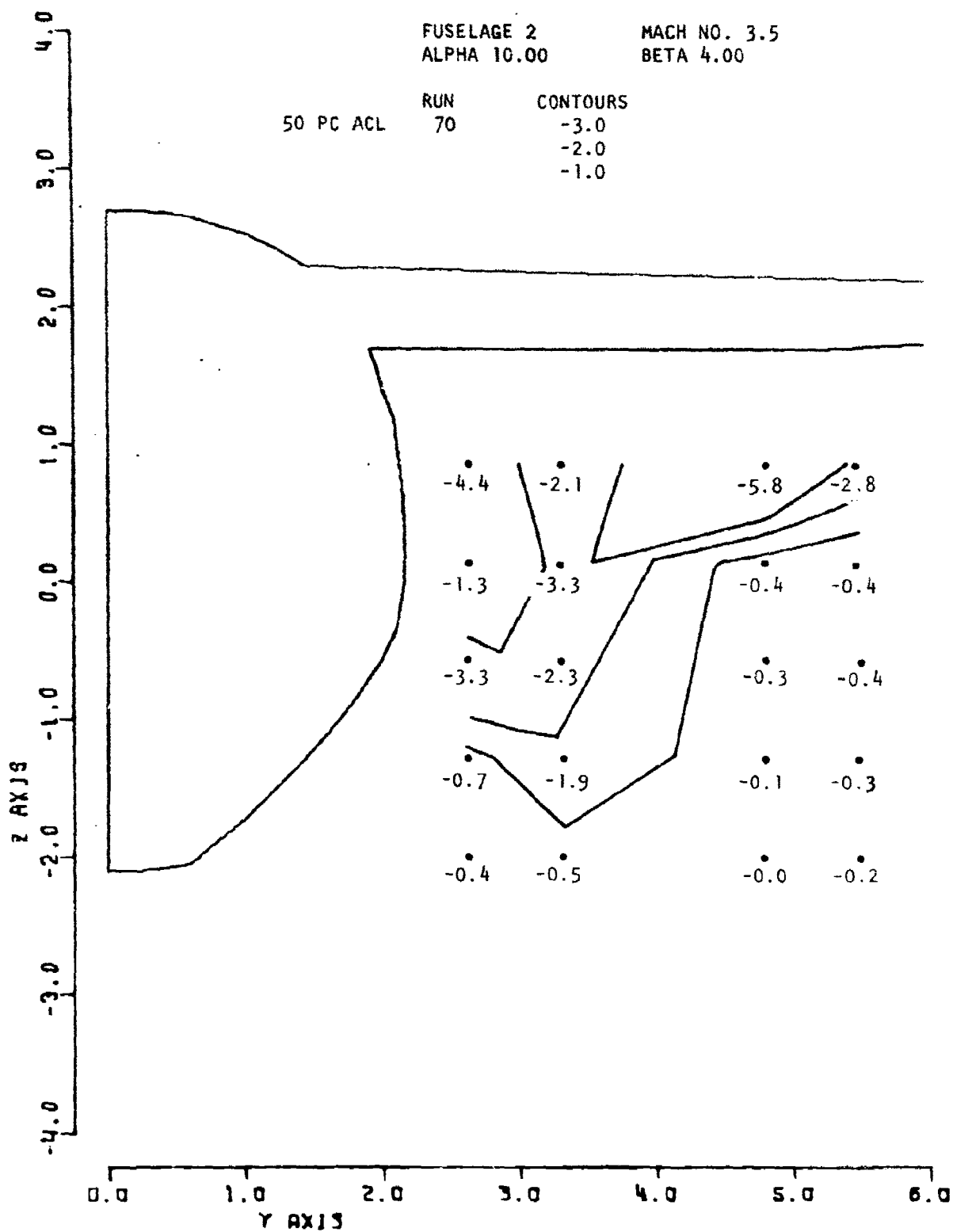


Figure 123. Local Sigma

numbers in the lower inboard region were lower for fuselage 2 than for fuselage 1 at both survey stations.

At the downstream station, the wing compression field manifests itself by the general reduction in local Mach numbers as compared to the upstream values. Figures 124 to 126 illustrate these effects.

3.2.3.1.2 Effect of Yaw

At the aft station the effect of yaw was confined mainly to the inboard part of the survey plane and consisted chiefly of a slight increase of local Mach number on the leeward side, and a comparable small reduction on the windward side, as may be seen in Figures 127 and 128.

3.2.3.2 Total Pressure Recovery

3.2.3.2.1 Effect of Vehicle Geometry

Increasing the angle of attack to 20° did not have any significant impact on the general level of total pressure recovery relative to the intermediate angle of attack case. Figures 129 and 130 show local recoveries in the region adjacent to the side of fuselage 1 that are lower than those for fuselage 2, pointing to the likelihood of a stronger cross flow, and attendant separation losses, for the former as compared to the latter fuselage shape.

3.2.3.2.2 Effect of Yaw

For 4° of yaw there was little effect on recovery. Those on the windward side reduced slightly relative to the leeward side by virtue of the slight change in the shock wave losses accompanying the yawed attitude.

3.2.3.3 Local Alpha

3.2.3.3.1 Effect of Vehicle Geometry

At the forward survey station the effects of geometry differences were localized to the lower part of the surveyed region with fuselage 1 again evidencing slightly higher local angles of attack than fuselage 2 as it did at Mach 2.5. In the upper parts of the flow field region the distribution was comparatively uniform, as may be seen from Figures 131 and 132.

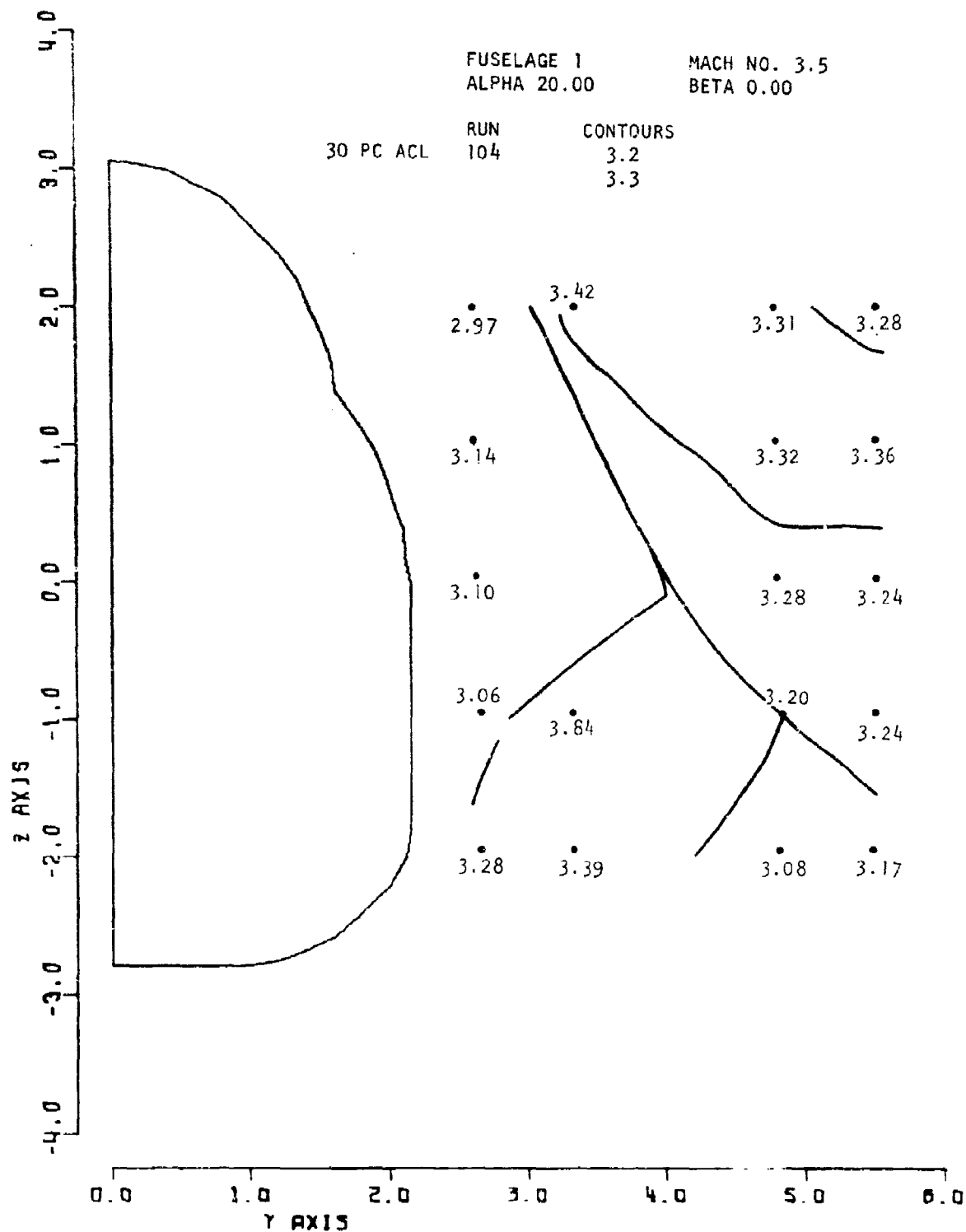


Figure 124. Local Mach No.

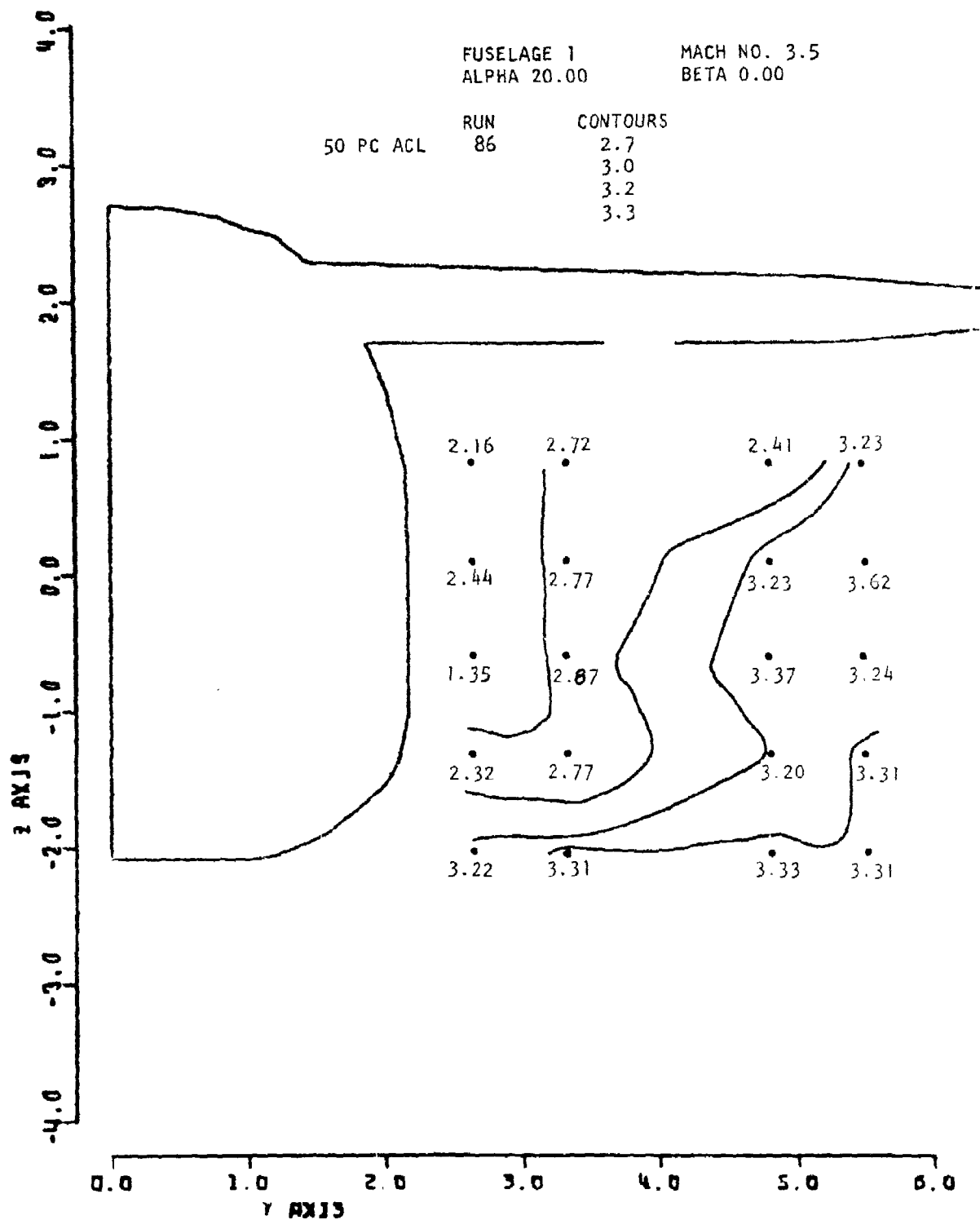


Figure 125. Local Mach No.
14"

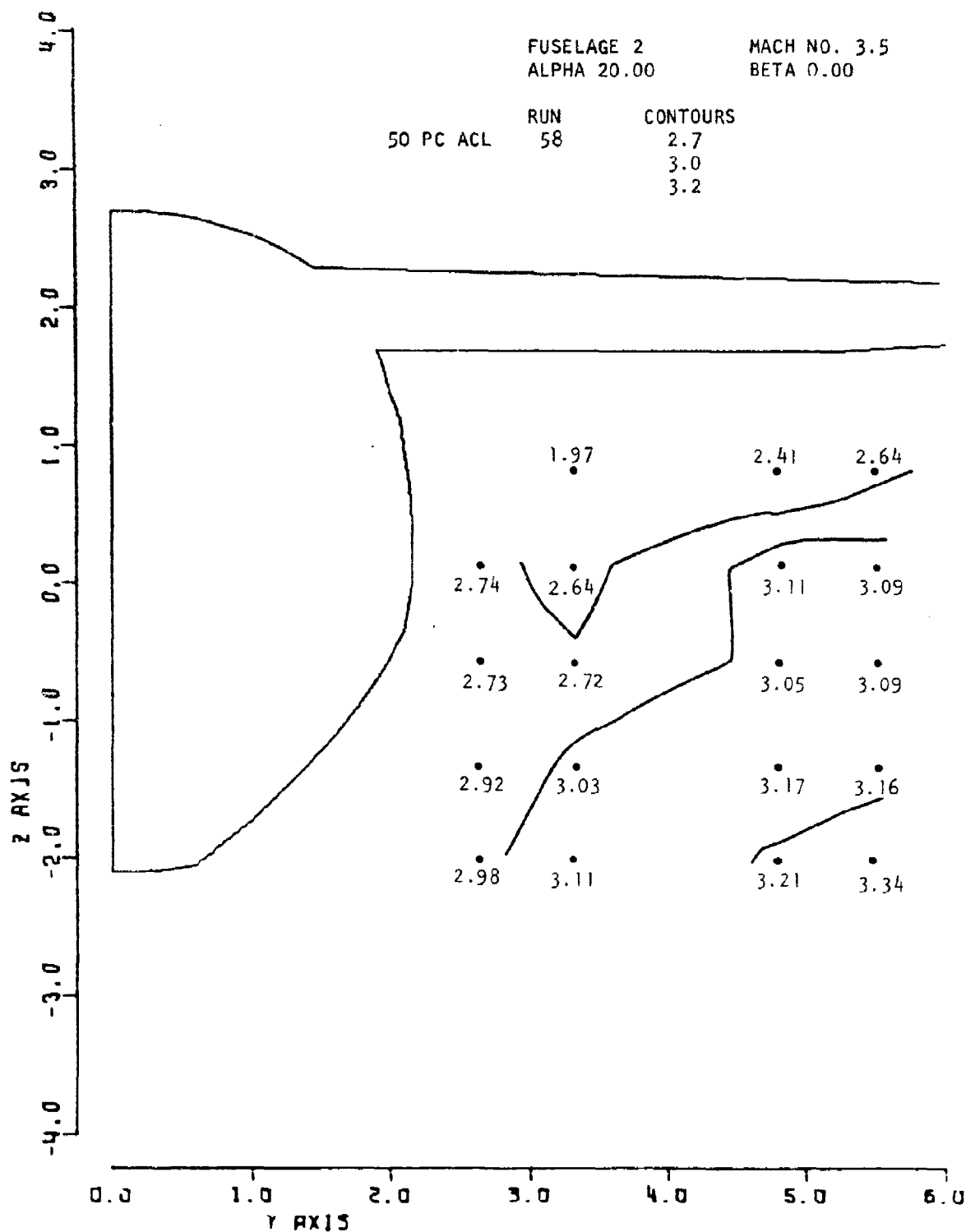


Figure 126. Local Mach No.

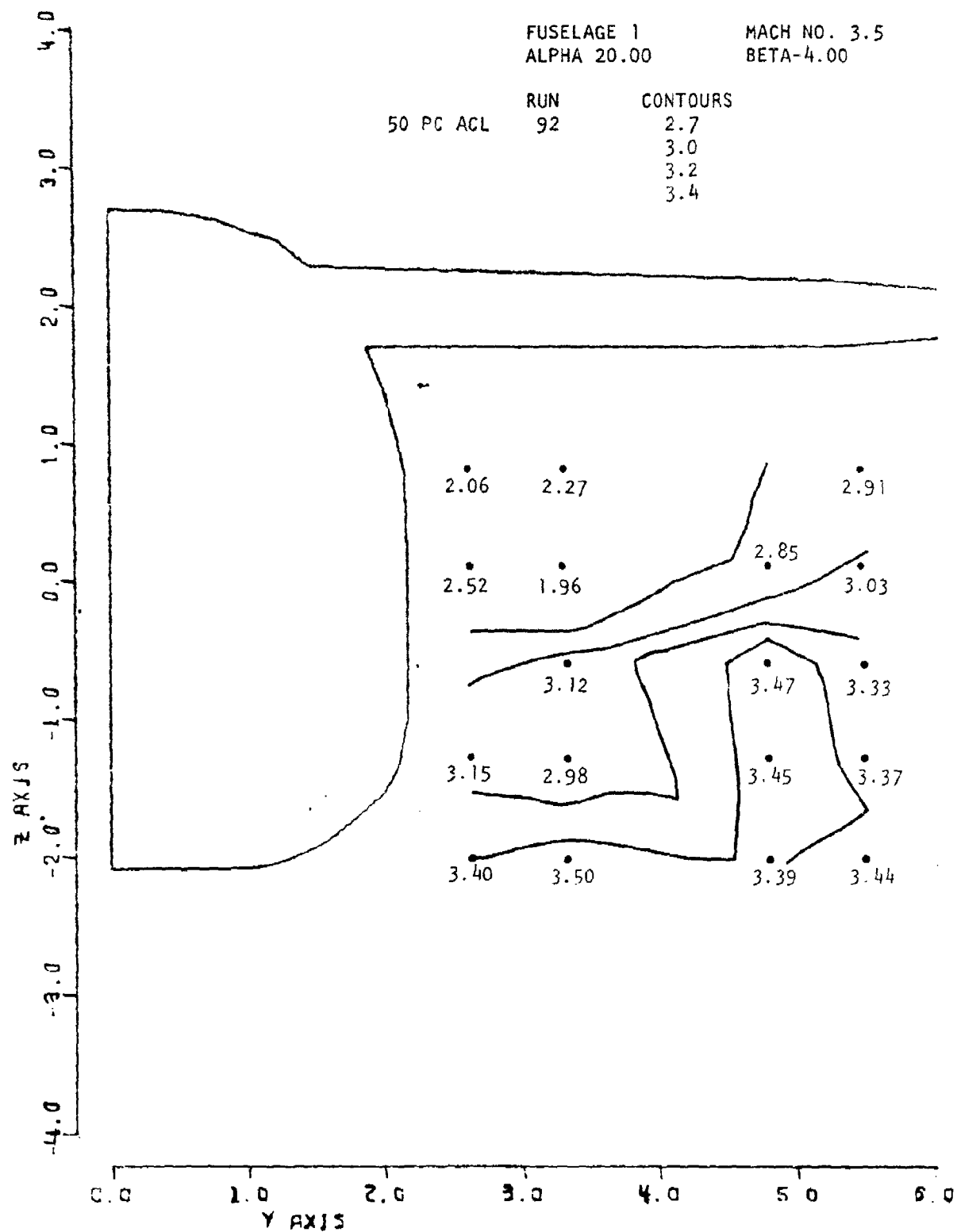


Figure 127. Local Mach No.

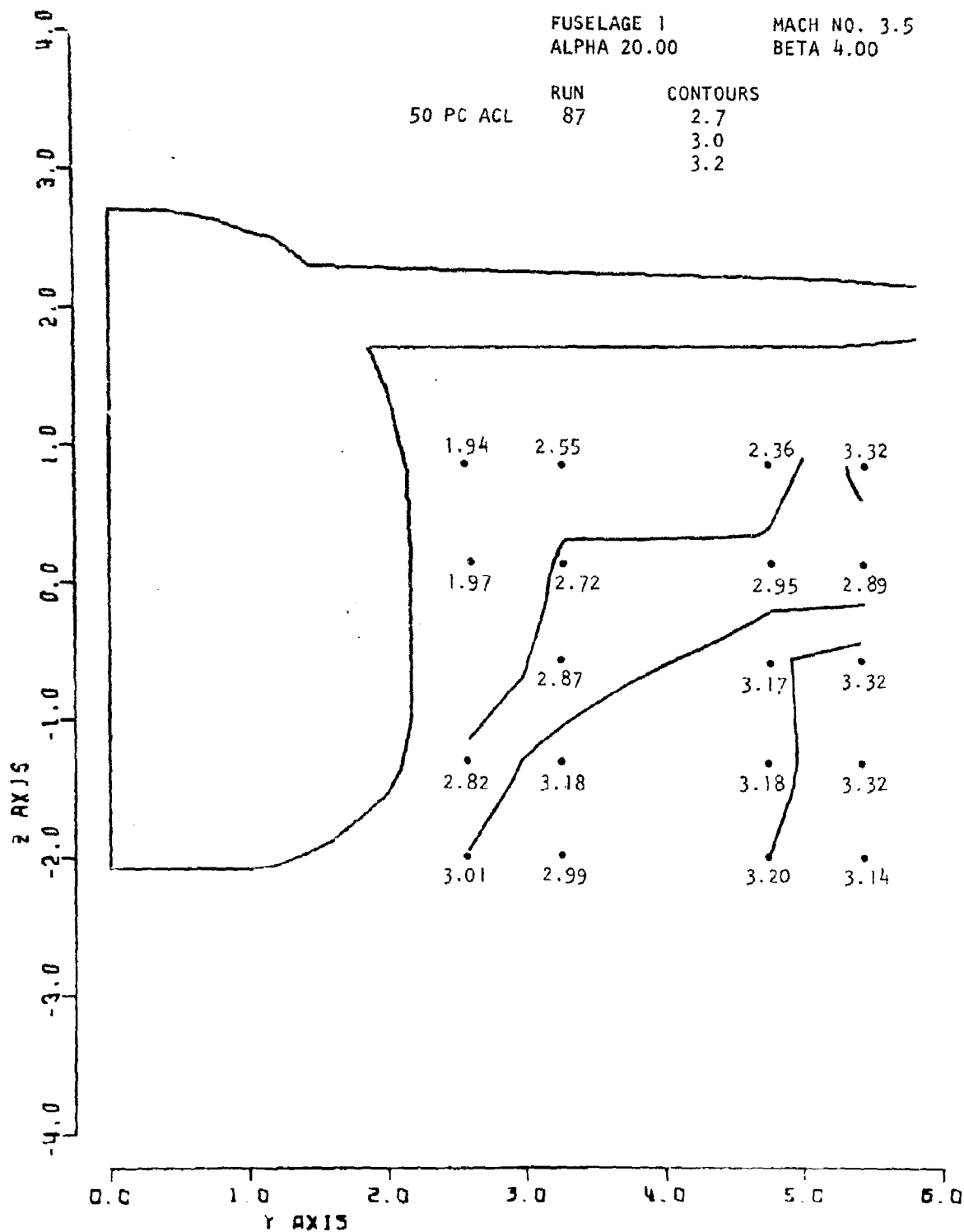


Figure 128. Local Mach No.

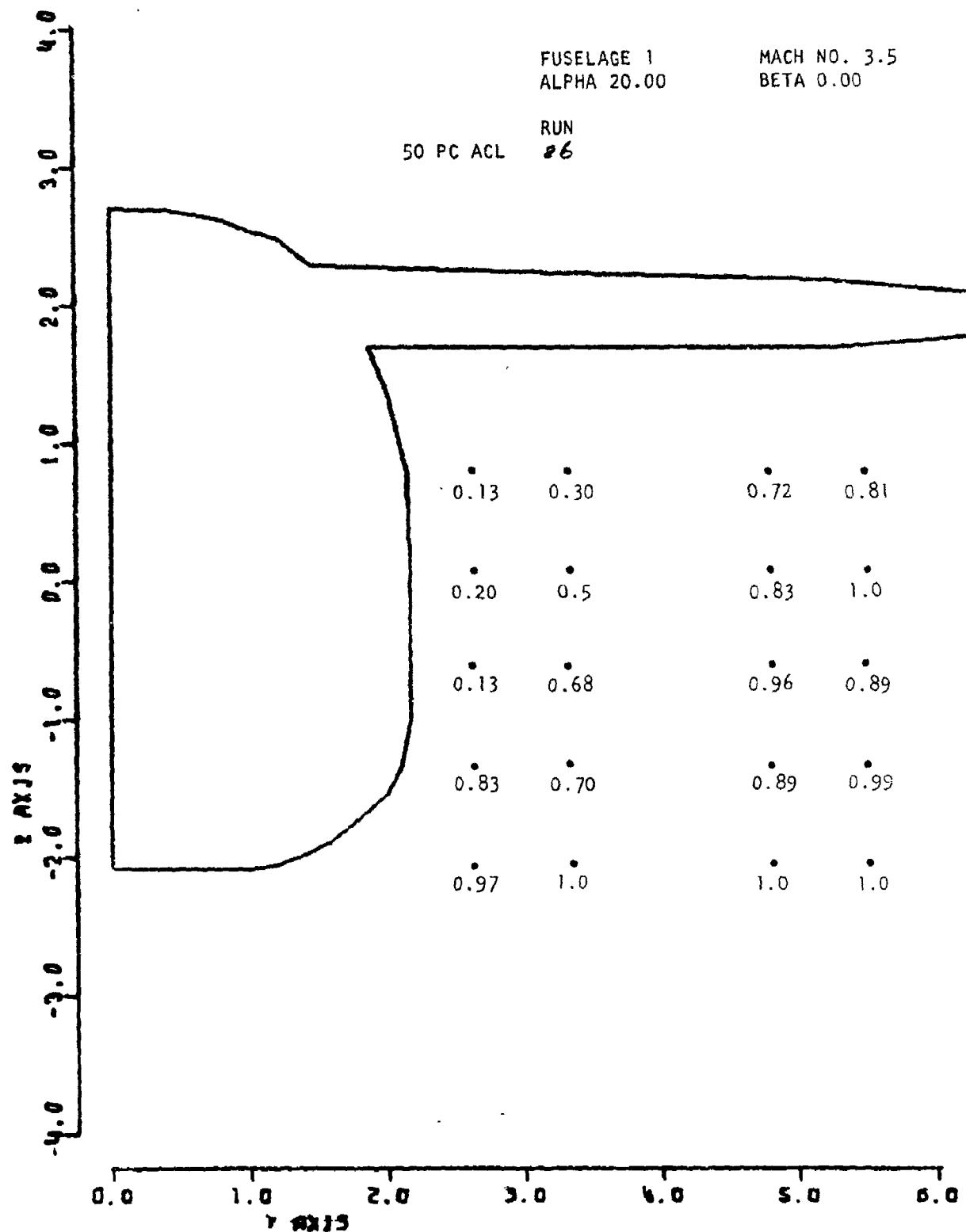


Figure 129. Local PT/PT High

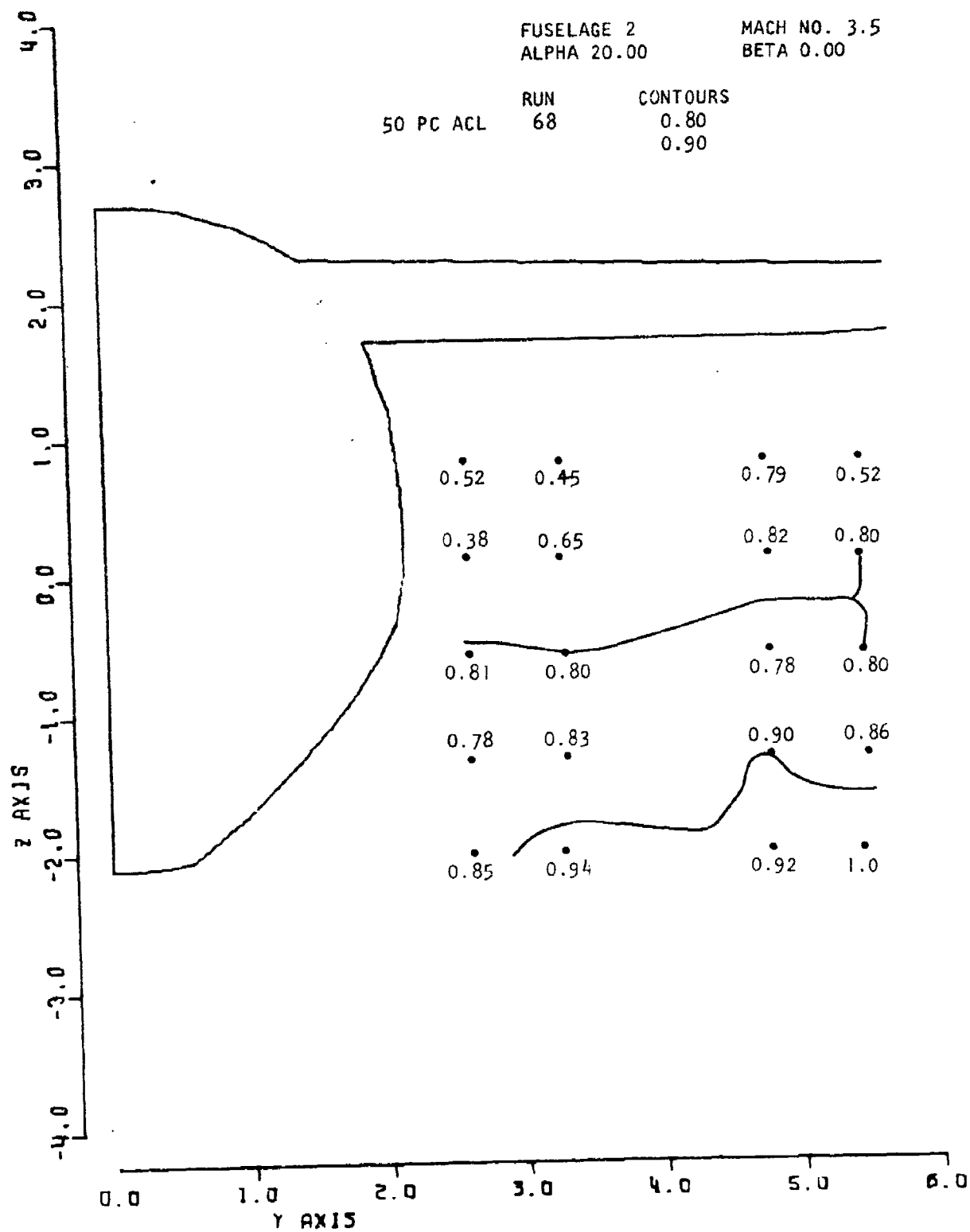


Figure 130. Local PT/PT High

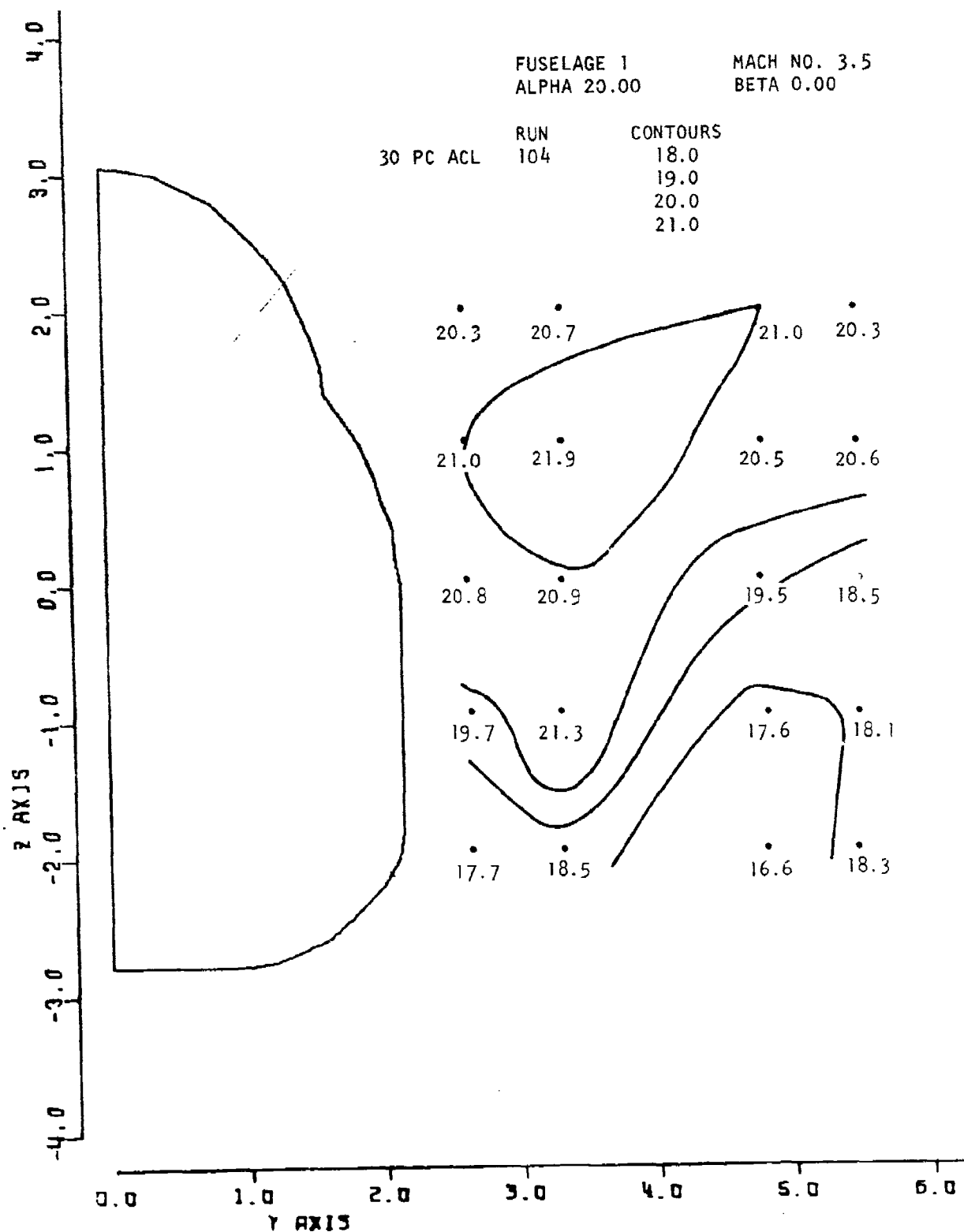


Figure 131. Local Alpha

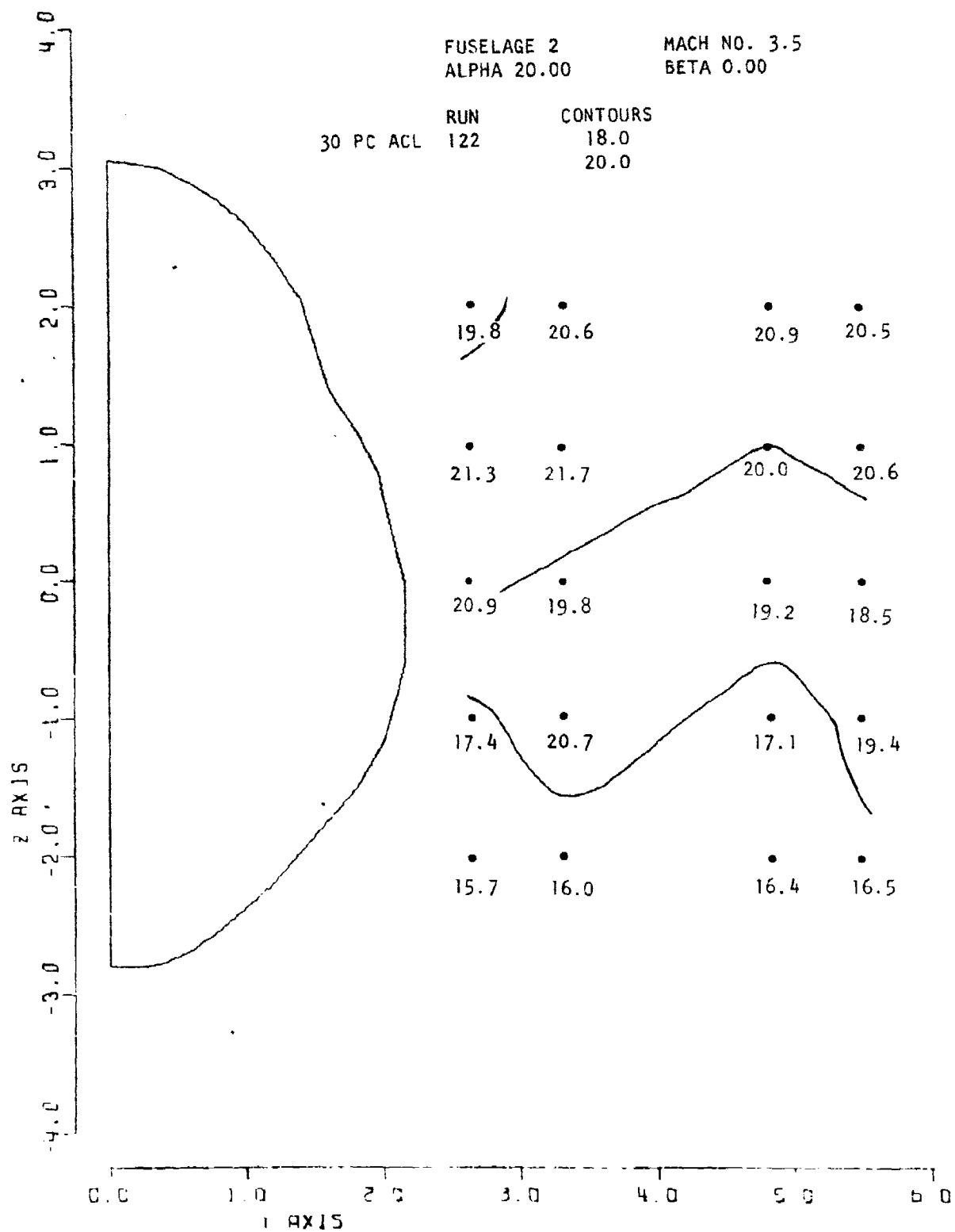


Figure 132. Local Alpha

At the 50% ACL station, there was a decrease in the level of upwash relative to the upstream station with the largest incremental changes occurring in the upper part of the survey region for both fuselages as shown in Figures 133 and 134. This wing induced effect was observed at the intermediate angle of attack case, and at Mach 2.5 as well.

3.2.3.3.2 Effect of Yaw

The effect of yaw at the forward survey station was to increase the upwash slightly in the lower inboard region of the leeward side and to reduce it on the windward side, independent of fuselage geometry differences. The same effect was noted at the aft station, with a somewhat larger area of the survey region affected, however. These effects of yaw, which were also observed at the Mach 2.5 high angle of attack case, may be seen in the data presented for fuselage 1 in Figures 135 to 138.

3.2.3.4 Local Sigma

3.2.3.4.1 Effect of Vehicle Geometry

Relative to the 10° angle of attack case increasing the angle of attack to 20° made the general level of sidewash angles more negative (outwardly directed) at both survey stations for both fuselage shapes. Compared to the high angle of attack data at Mach 2.5, there was no significant effect due to Mach number alone at the aft survey station, whereas at the forward station the level of sidewash became generally more negative by about one or two degrees. The sidewash at the aft station was more negative than at the upstream station, especially in the vicinity of the fuselage side. Fuselage geometry differences produced little effect on the local sidewash angles. These effects are illustrated for fuselage 1 in Figure 139 and 140.

3.2.3.4.2 Effect of Yaw

Yaw resulted in the expected positive increment in sidewash on the windward side and a negative one on the leeward side. The influence of fuselage geometry difference was very small and confined to the vicinity of the lower fuselage corner. Figures 141 and 142 present data for the leeward and windward sides, respectively, of fuselage 1 at the 50% ACL station.

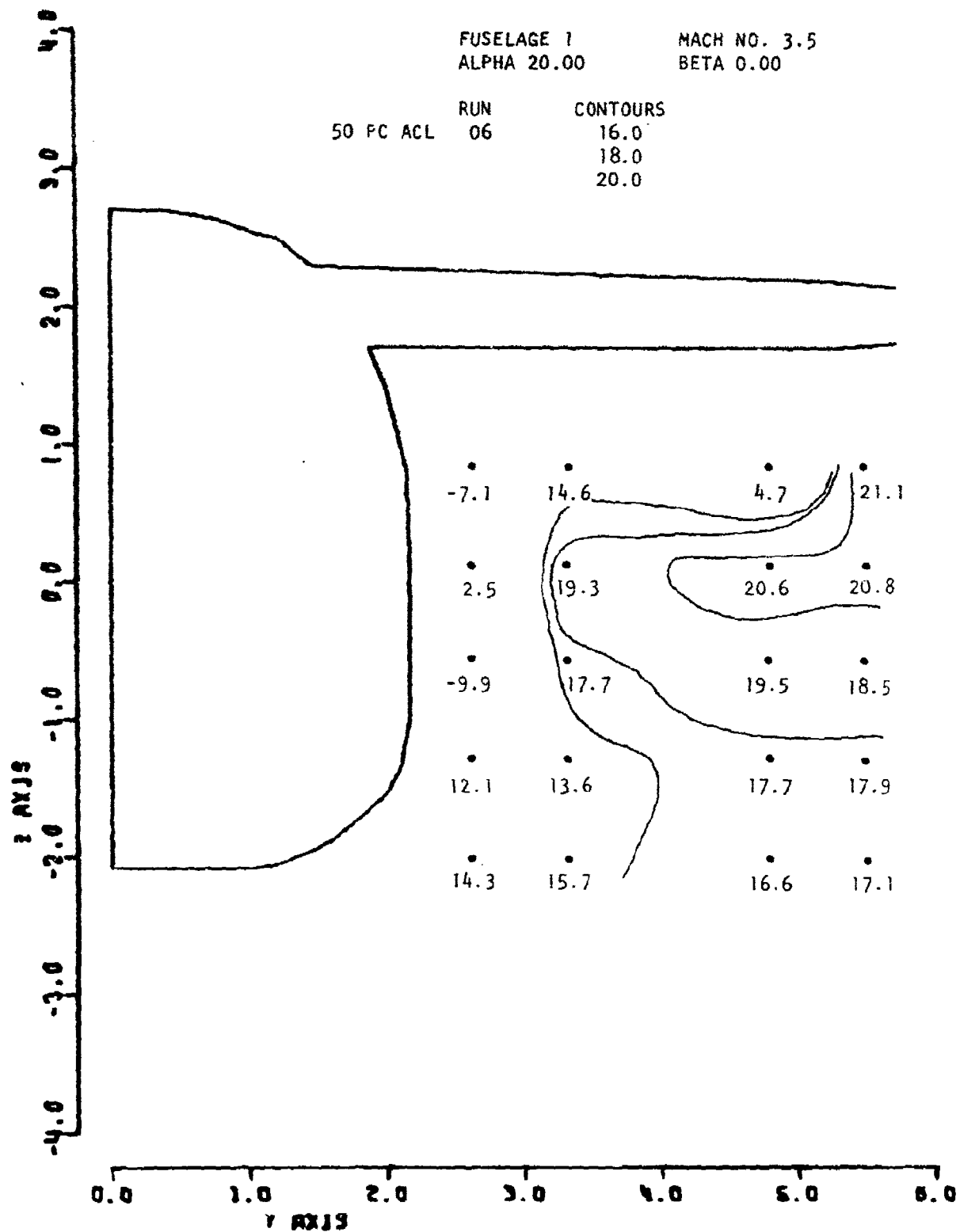


Figure 133. Local Alpha

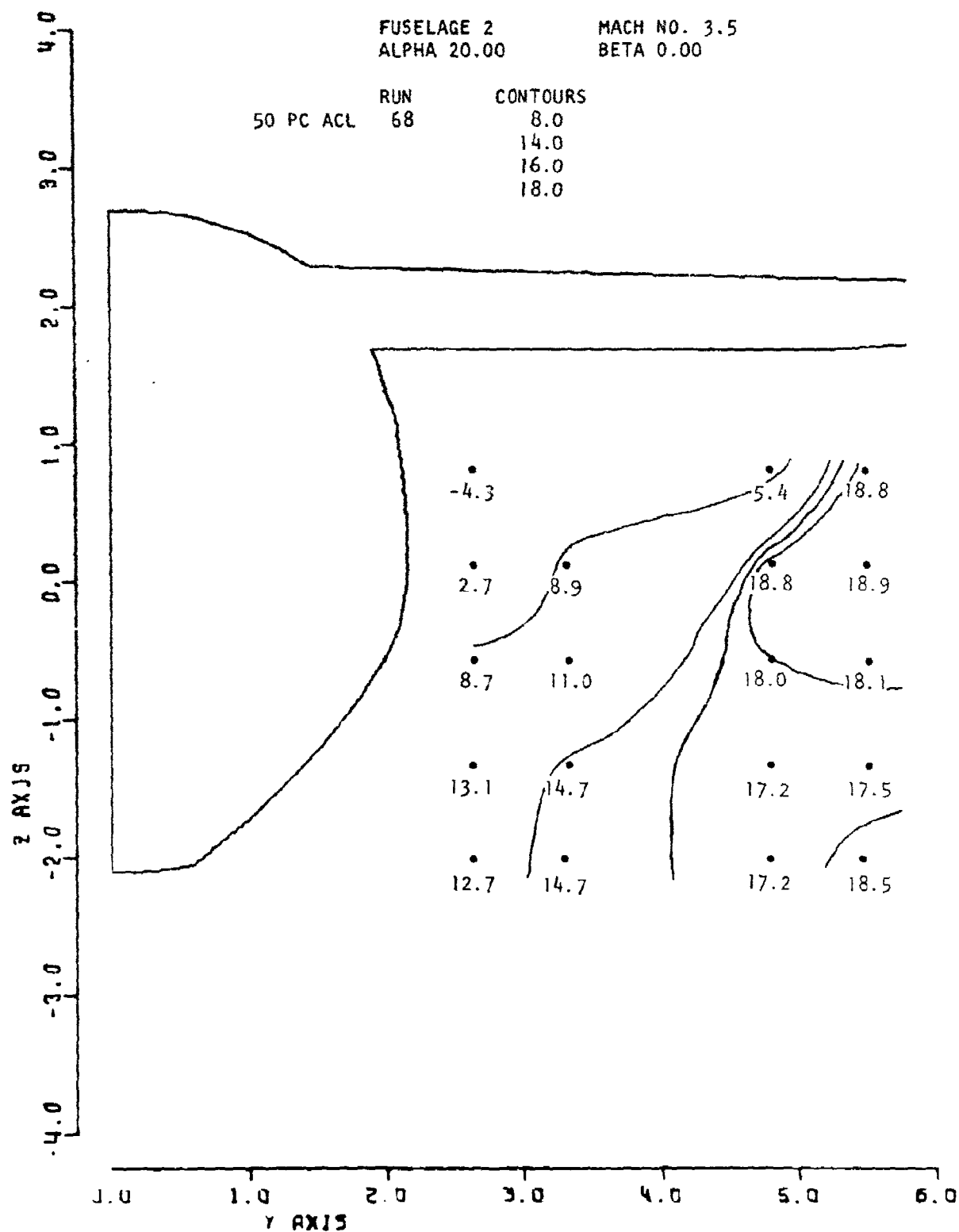


Figure 134. Local Alpha

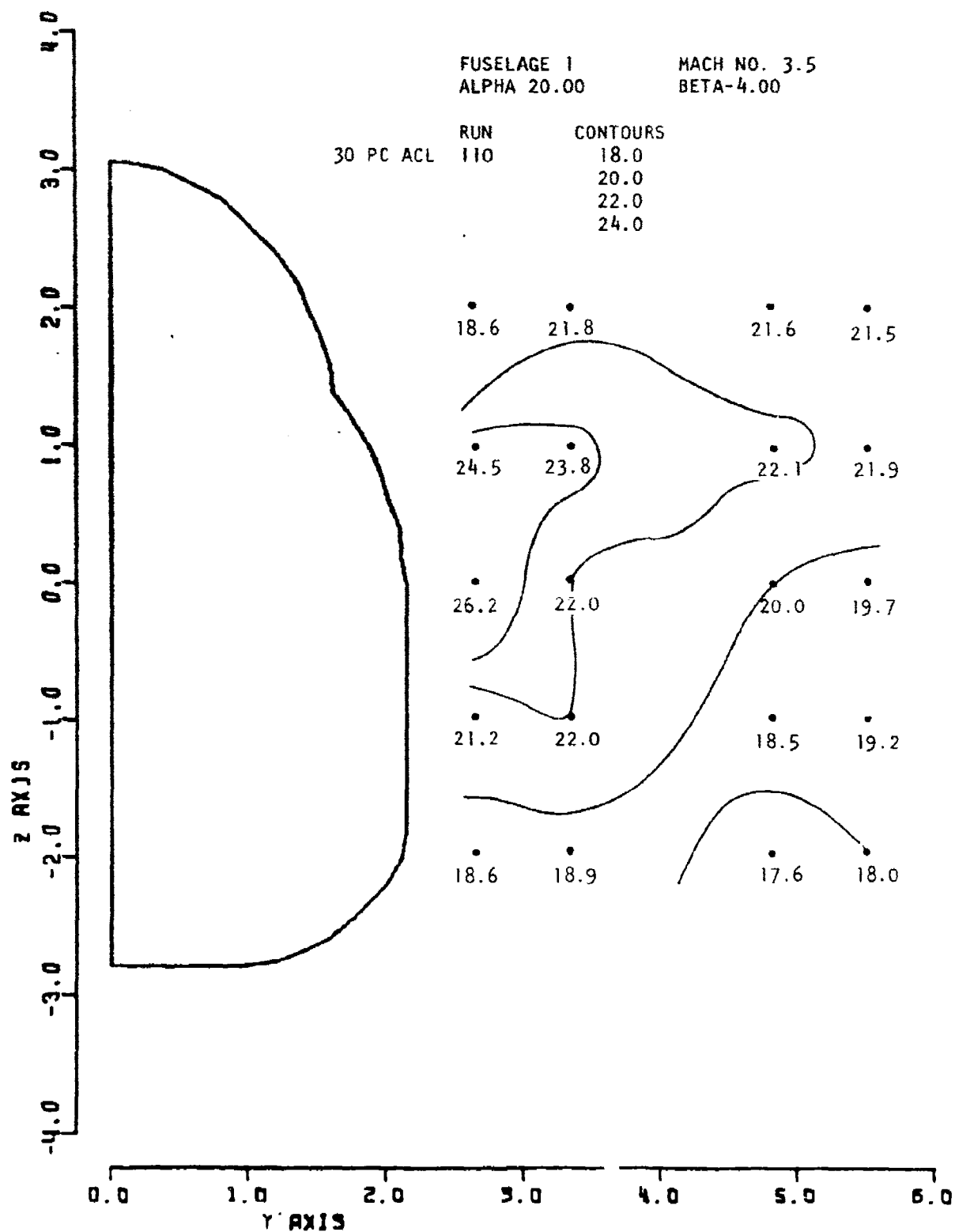


Figure 135. Local Alpha

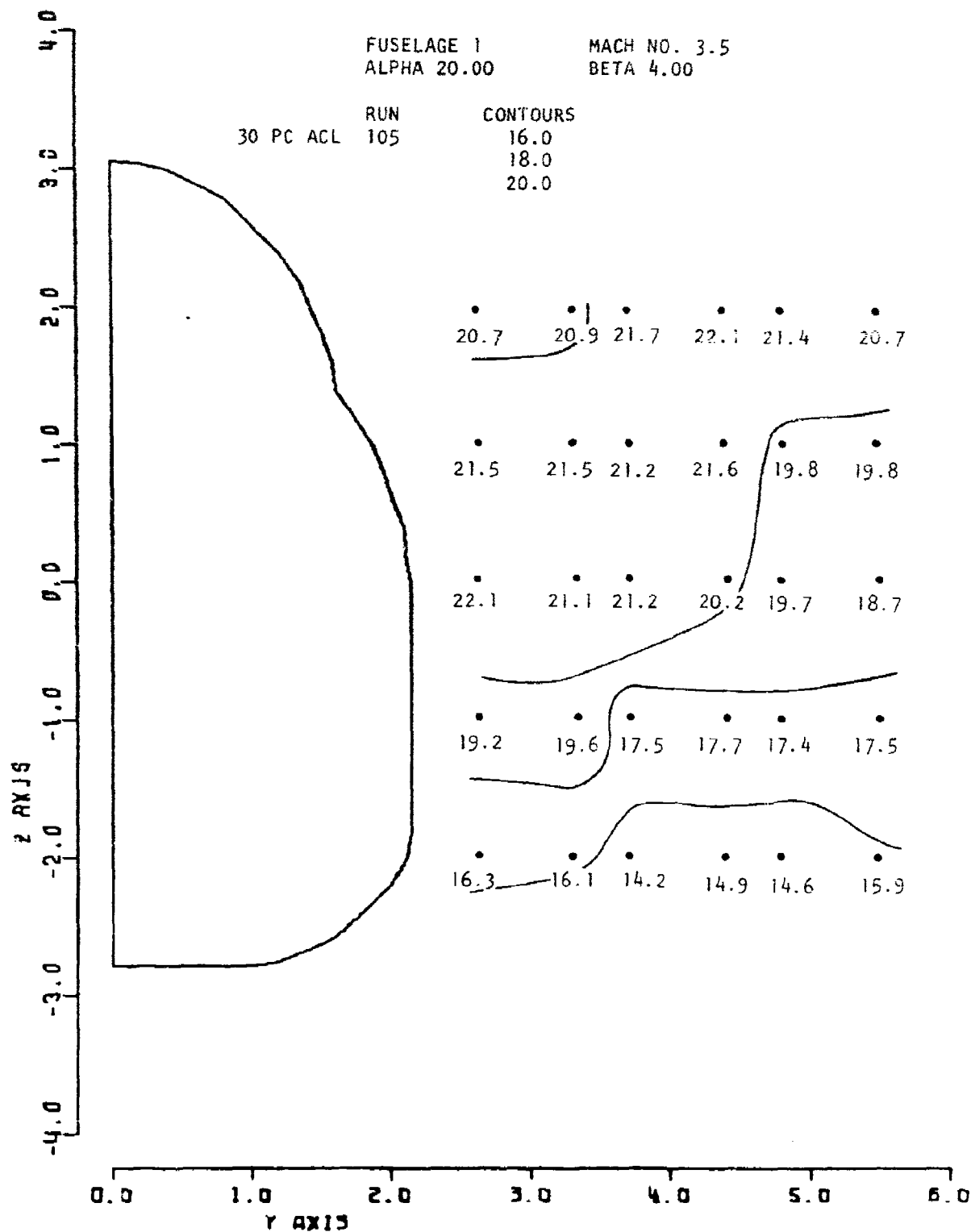


Figure 136. Local Alpha

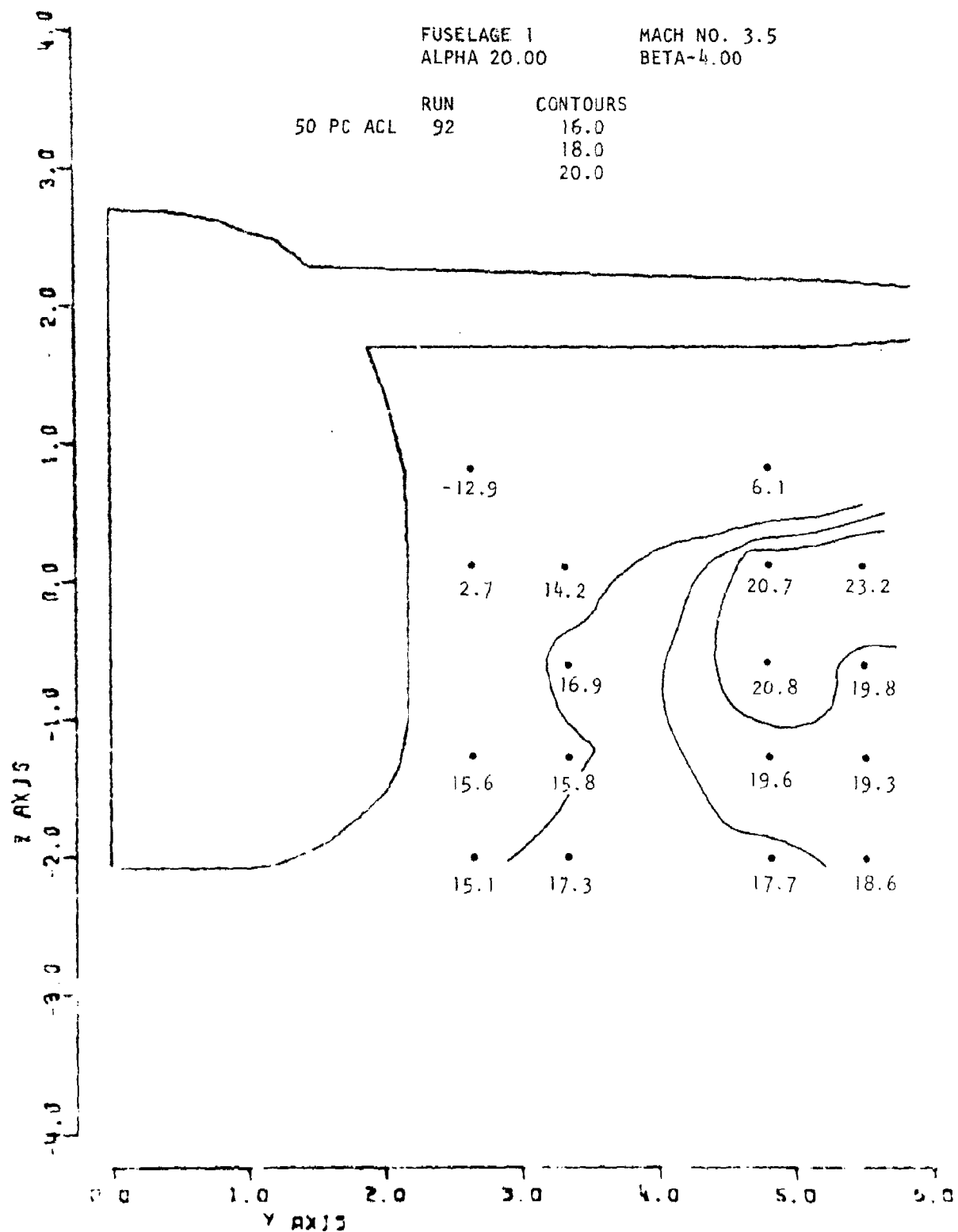


Figure 137. Local Alpha

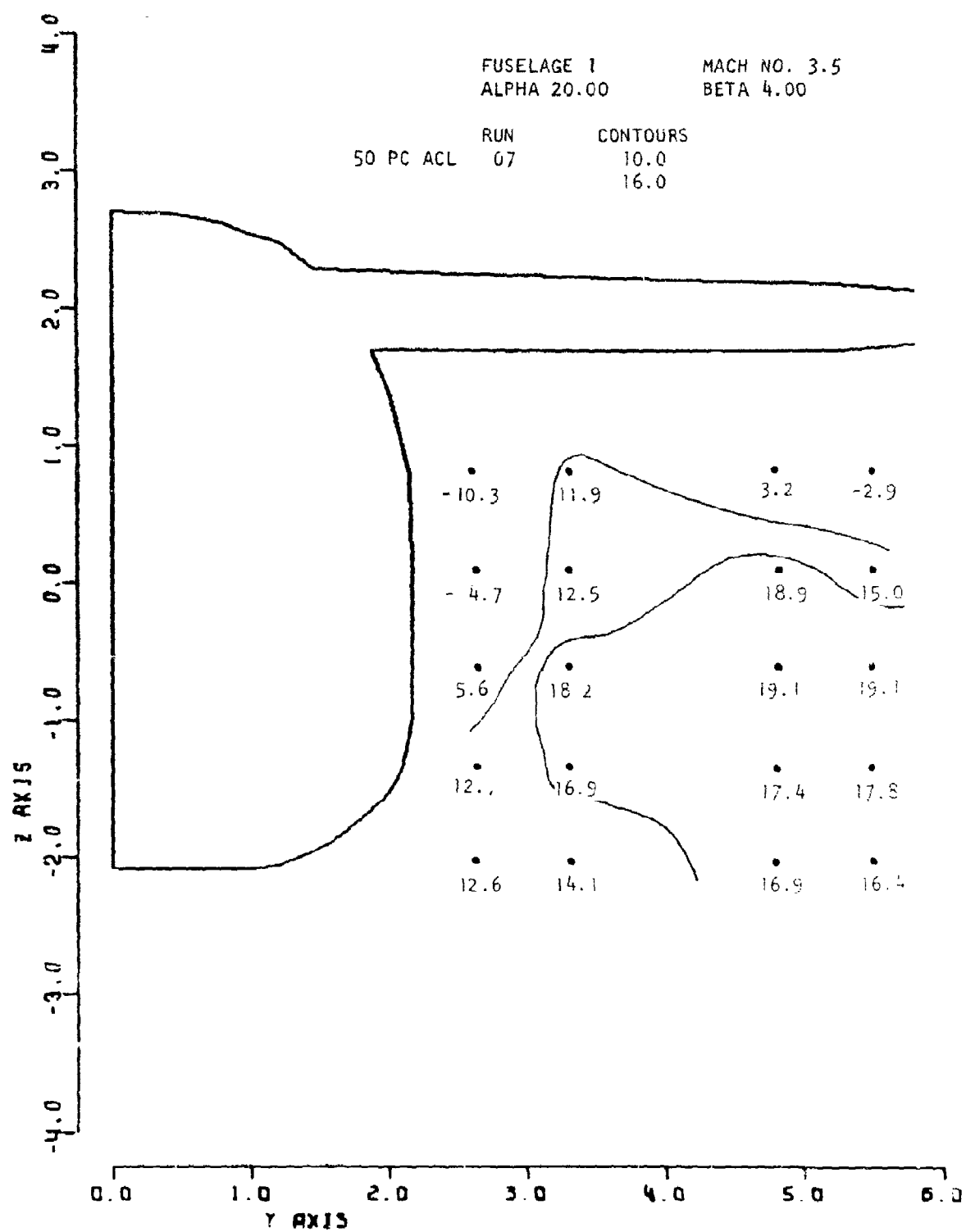


Figure 138. Local Alpha

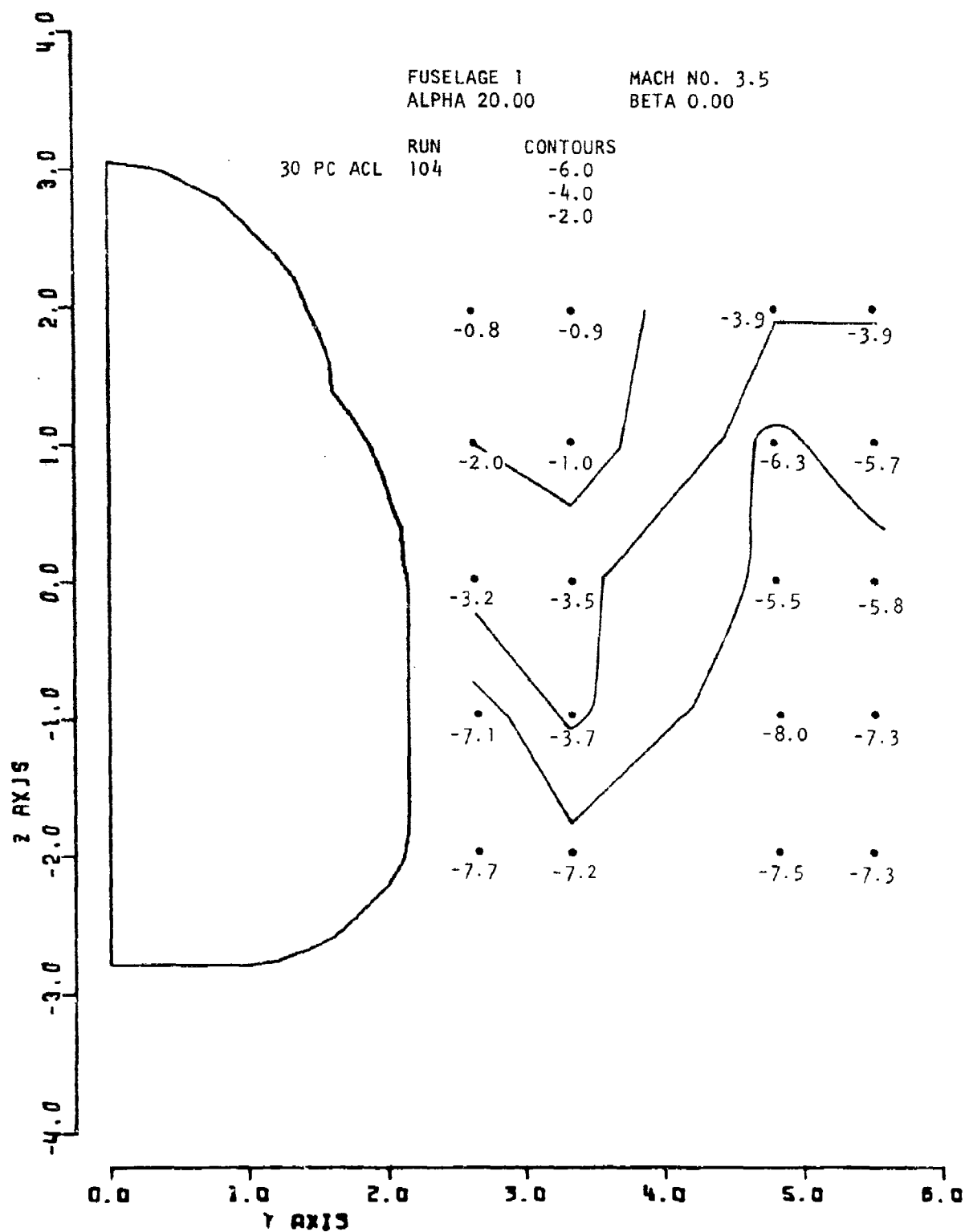


Figure 139. Local Sigma

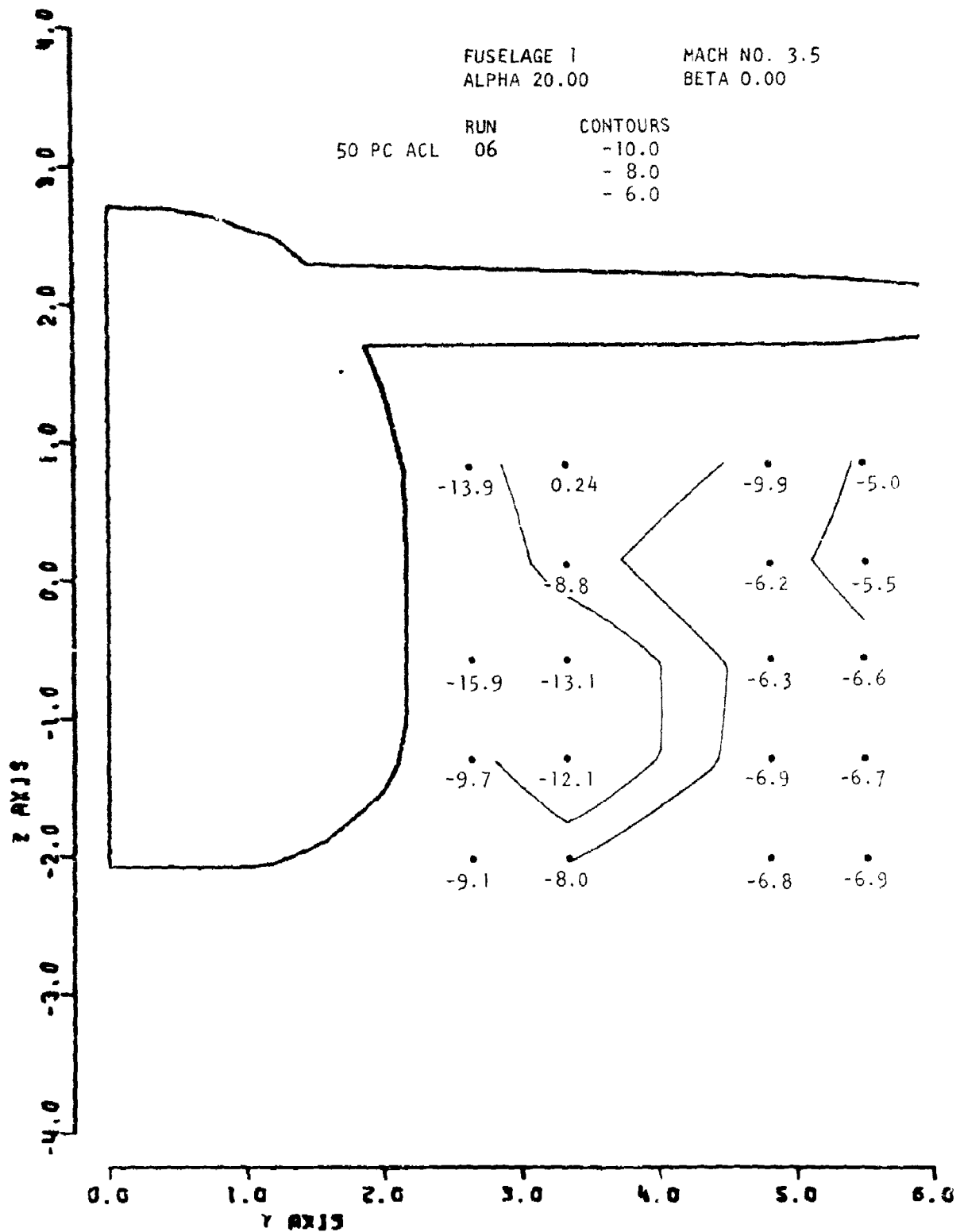


Figure 140. Local Sigma

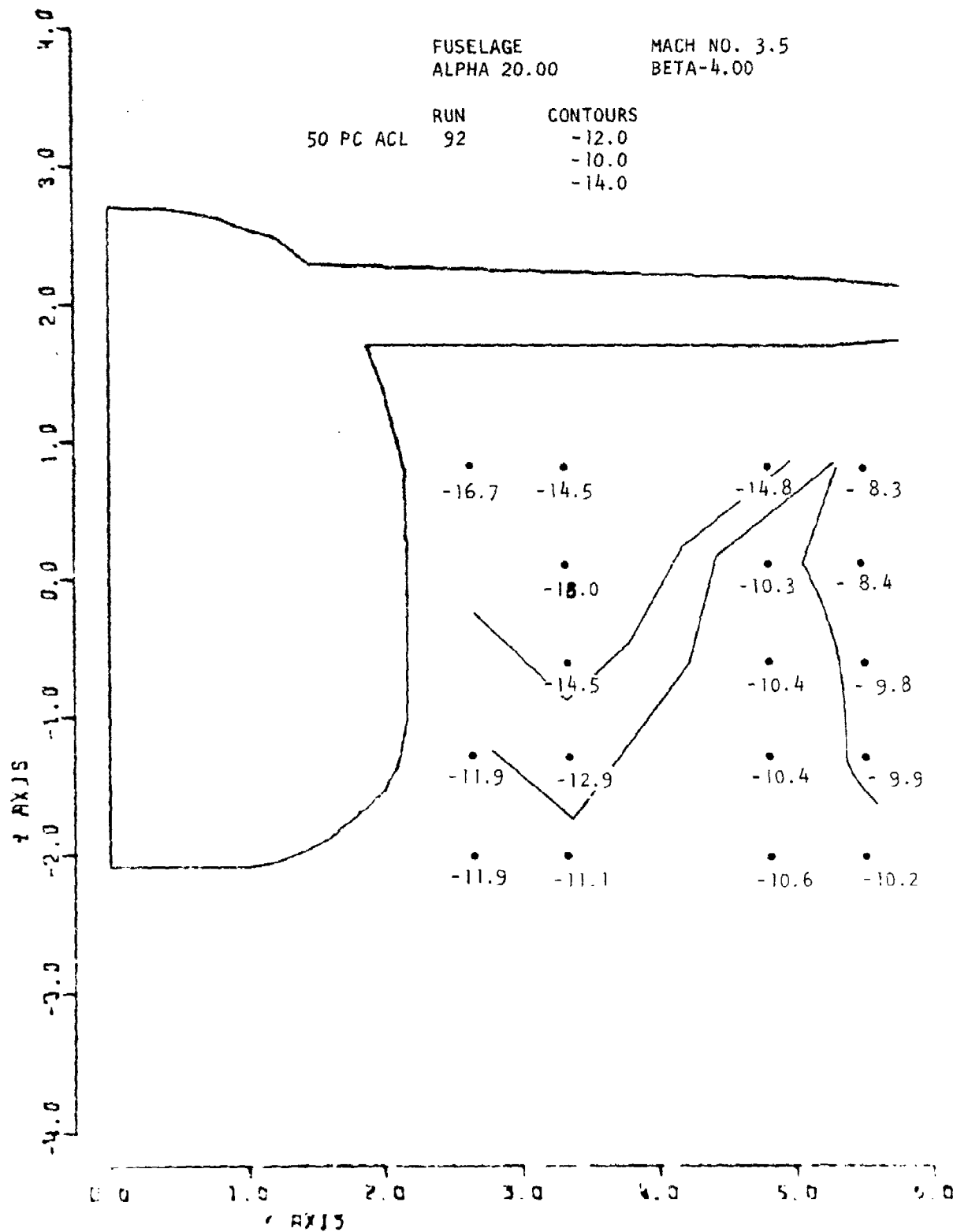


Figure 141. Local Sigma

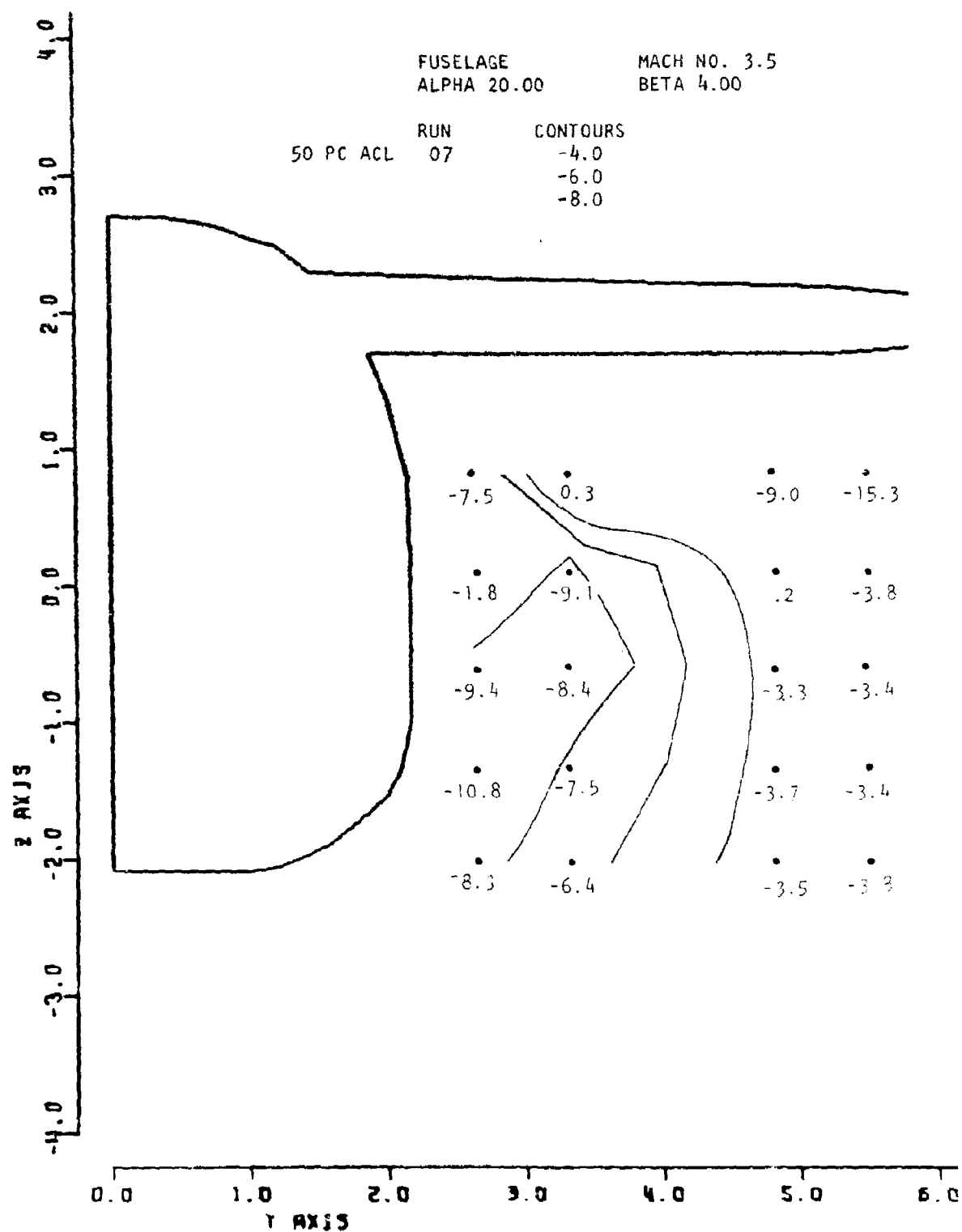


Figure 142. Local Sigma

SECTION IV

CONCLUSIONS

A general summary of the major conclusions which can be drawn from the data obtained in the Mach 2.5 and 3.5 tests with the high design Mach number fuselage configuration is presented in this section. The summary is arranged into four groups corresponding to the following basic flow field parameters: local Mach number, total pressure recovery, angle of attack (α), and sidewash angle (σ). The dependency of these parameters upon angle of attack and yaw, free stream Mach number, and fuselage geometry is briefly assessed. The local Mach number and total pressure recovery data readily permit quantitative performance evaluations of rather generalized vehicle/inlet systems to be made. On the other hand, without rather well defined specific inlet designs, only qualitative assessments such as development risk can be made of the impact of local flow angularity and sidewash.

Local Mach Number

The flow field Mach number level and composition was dictated primarily by free stream Mach number and vehicle angle of attack. The axisymmetric flow fields generated by the fuselage nose and canopy established a radial Mach number profile that became more distinct with increasing free stream Mach number. An excursion to positive vehicle angle of attack superimposed a peripheral Mach number gradient in the inboard region of the forward flow field resulting from increased lower fuselage compression and upper fuselage/canopy expansion. The increase in wing compression with angle of attack produced a general reduction in local Mach number throughout the aft flow field.

As compared to the effects of free stream Mach number and angle of attack, the effects of the fuselage geometry differences proved for the most part to be rather small and were confined to the region of the lower fuselage corner. Excursions in angle of yaw produced secondary changes in the average levels of local Mach number. With increase of free stream Mach number there was a relative decrease in the average level of local Mach number in both the fore and aft survey regions of the flow field. Consideration of this parameter is required primarily for inlet sizing at the design Mach number and for evaluating performance at off design point conditions.

Local Total Pressure Recovery

At low angle of attack local total pressure recovery was sensitive to free stream Mach number but independent of vehicle geometry and yaw angle. The increase in shock losses with increasing Mach number resulted in generally lower recovery at Mach 3.5.

At intermediate angle of attack the forward survey region experienced a reduction in recovery level due to the strengthened lower fuselage shock and canopy shock. Recovery at the aft survey station was reduced further by the stronger wing leading edge shock. In general the recovery remained independent of fuselage corner geometry and vehicle yaw angle.

The predominant parameter at high angle of attack was lower fuselage corner radius. While the cross flow around the large corner radius remained attached that around the small corner radius tended to separate resulting in reduced recovery levels, particularly in the inboard region of the flow field.

The intermediate and high angles of attack, at both Mach numbers, produced sufficiently low recoveries at the aft station in the region close to the sides of both fuselages, and close to the wing lower surfaces, to require that inlets situated at that longitudinal location be separated, or split away, from those surfaces. At the forward station the usual splitter plate arrangement would probably suffice for a side mounted inlet installation.

Local Alpha

Local alpha proved to be most sensitive to vehicle angle of attack, at the forward survey station, and wing compression, at the aft survey station. Fuselage corner geometry introduced second order effects, while free stream Mach number exerted essentially no influence over the composition of the flow field.

At the forward station the larger fuselage corner radius tended to promote downwash at low vehicle angles of attack while inhibiting upwash at intermediate and high vehicle angles of attack. At the aft station the wing dictated flow field angularity. The wing also dampened non uniformities introduced by yaw on both the leeward and windward sides.

Consequently, for maneuvering flight at these Mach numbers the utilization of wing shielding is an important consideration in the selection of inlet placement.

Local Sigma

Local sigma proved most sensitive to vehicle angle of attack and fuselage corner radius, and vehicle cross-sectional area progression. At low angle of attack the axisymmetric fuselage nose and canopy generated flow fields established a basically negative sidewash condition at the forward survey station except near the lower fuselage corner where the fuselage of larger corner radius induced a locally positive sidewash. At the aft station this negative composition essentially disappeared as the diminishing fuselage cross-section produced a nearly complete re-expansion of the flow. At intermediate angle of attack the increase in both fuselage cross flow and wing compression established a more negative level of sidewash. This trend continued into the high angle of attack range. Therefore, although fuselage corner radius and free stream Mach number had some influence on local sidewash characteristics their effects were small compared to those of angle of attack, yaw and wing compression at the Mach numbers tested. Consequently, local sidewash angles merit careful attention when designing for maneuvering flight capability.

Performance Evaluation

The flow field data presented here can be applied directly to specific induction system designs by considering the candidate inlet to be submerged within the flow field. Use of the data in this manner will permit both quantitative and qualitative assessments of the impact of the local approach flow upon the inlet design.

For the pre-preliminary design phase screening of inlet locations and aircraft general arrangement a broader overlook is more appropriate. To this end, therefore, the parameters of total pressure recovery, angularity, and sidewash have been statistically averaged, as was done for the test results presented in Volume I, for each of the two fuselages for $M_\infty = 2.5$ and 3.5 and angles of attack and yaw applicable to cruise/acceleration and maneuvering flight conditions. Plots of these parameters are presented in Figures 143 through 150. They can be used individually to evaluate a particular flight condition or cross plotted to evaluate a postulated flight trajectory.

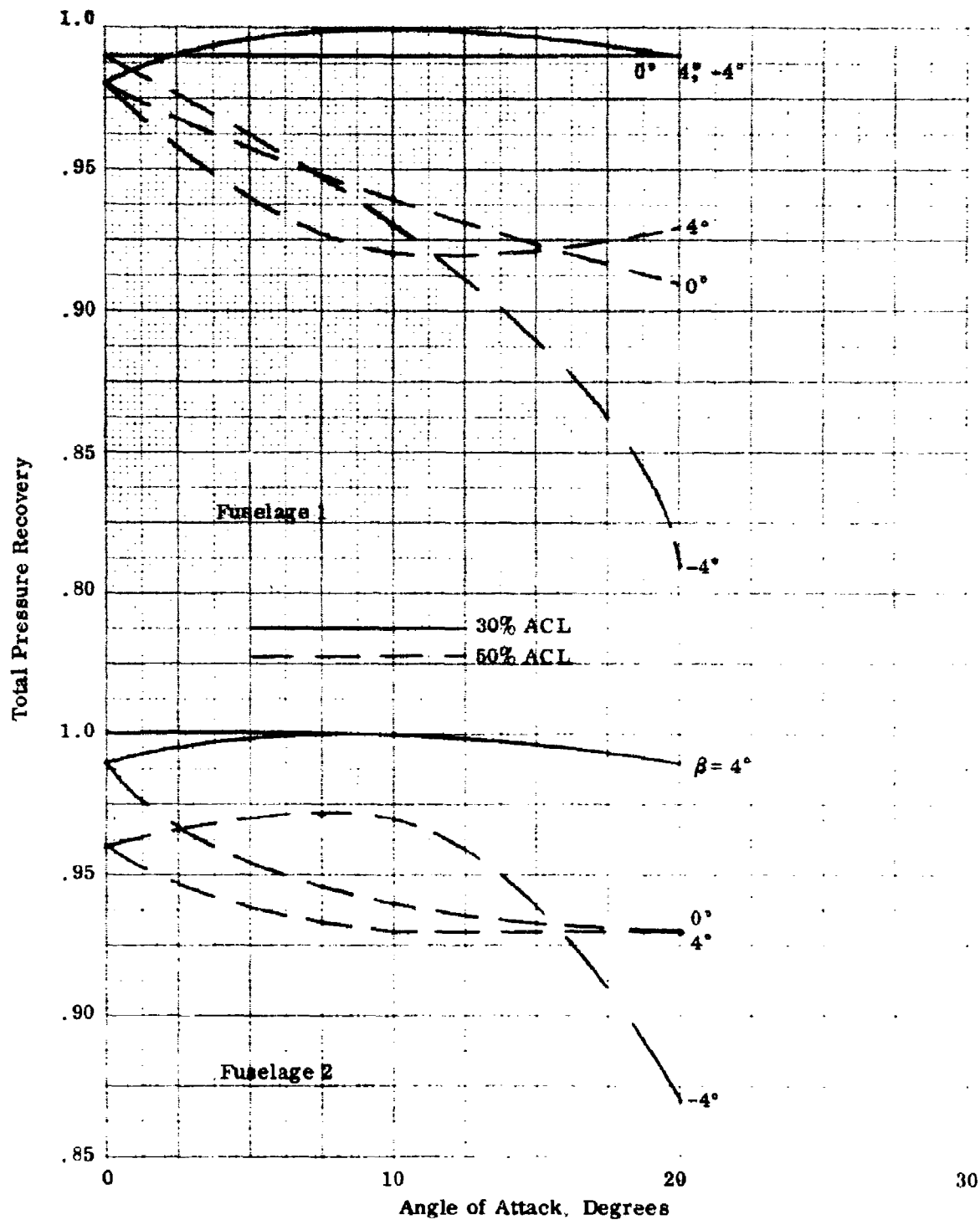


Figure 143. Average Total Pressure Recovery, $M_\infty = 2.5$



Total Pressure Recovery

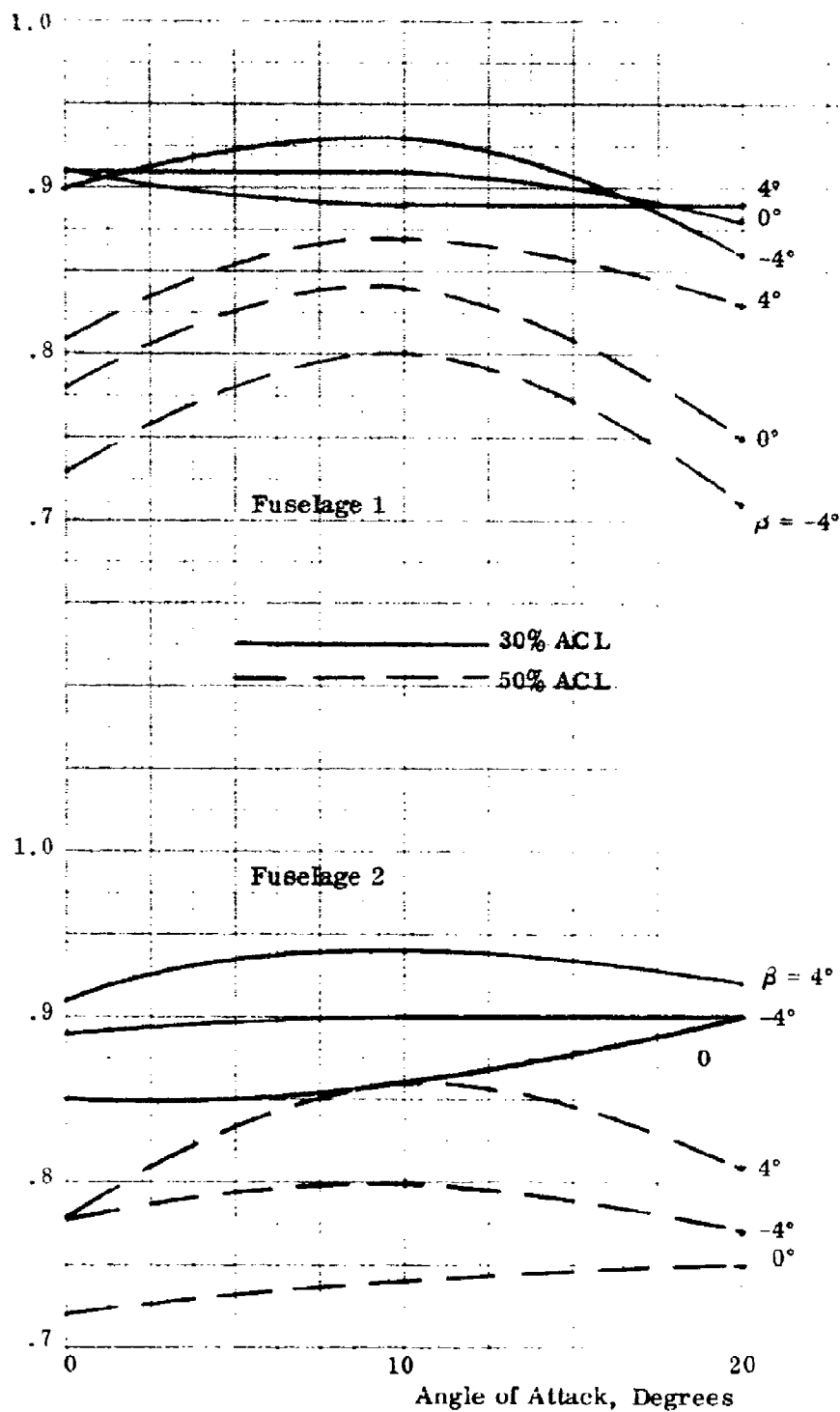


Figure 144. Average Total Pressure Recovery, $M_\infty = 3.5$

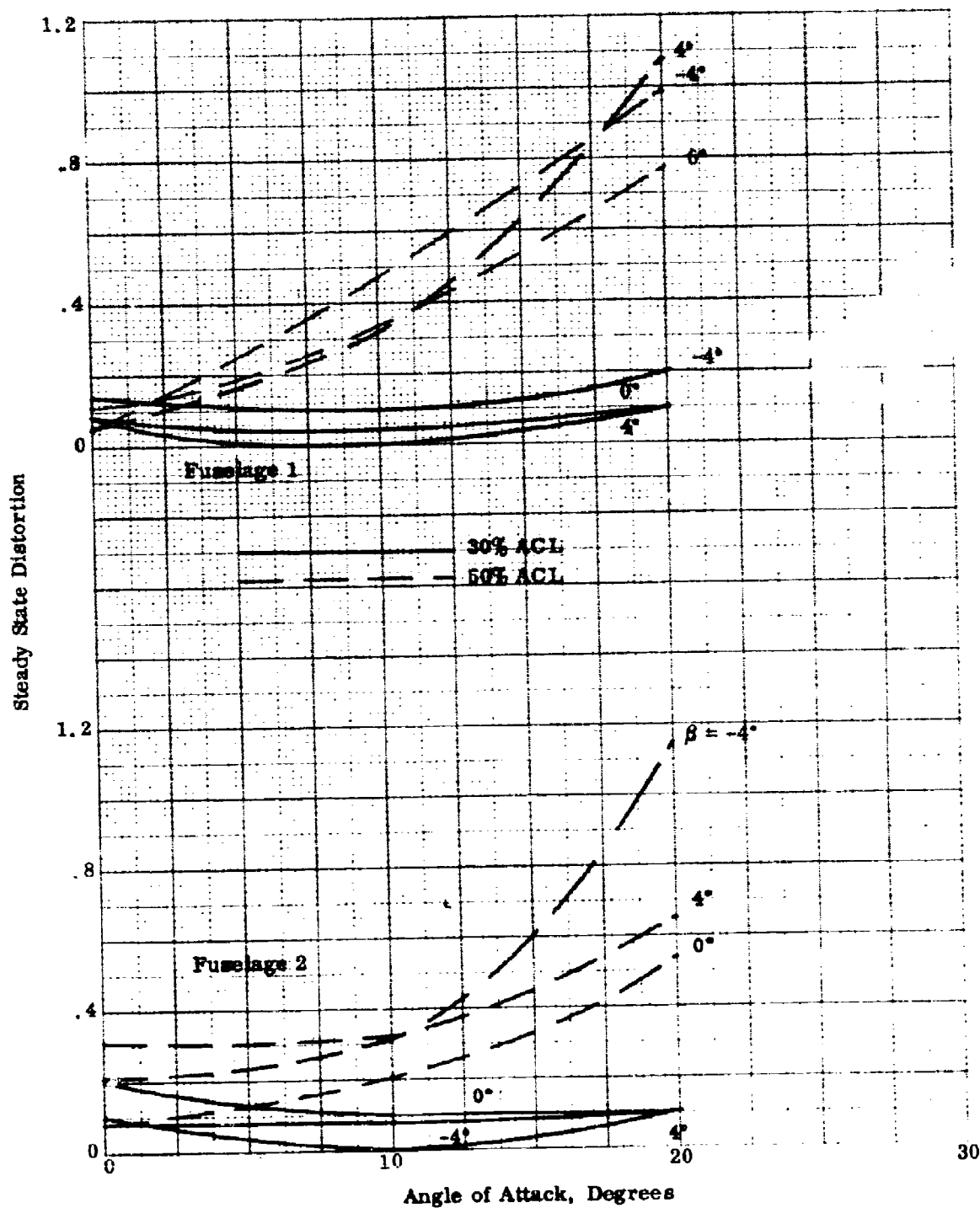


Figure 145. Average Steady State Distortion, $M_\infty = 2.5$

17-5874-1001

Steady State Distortion

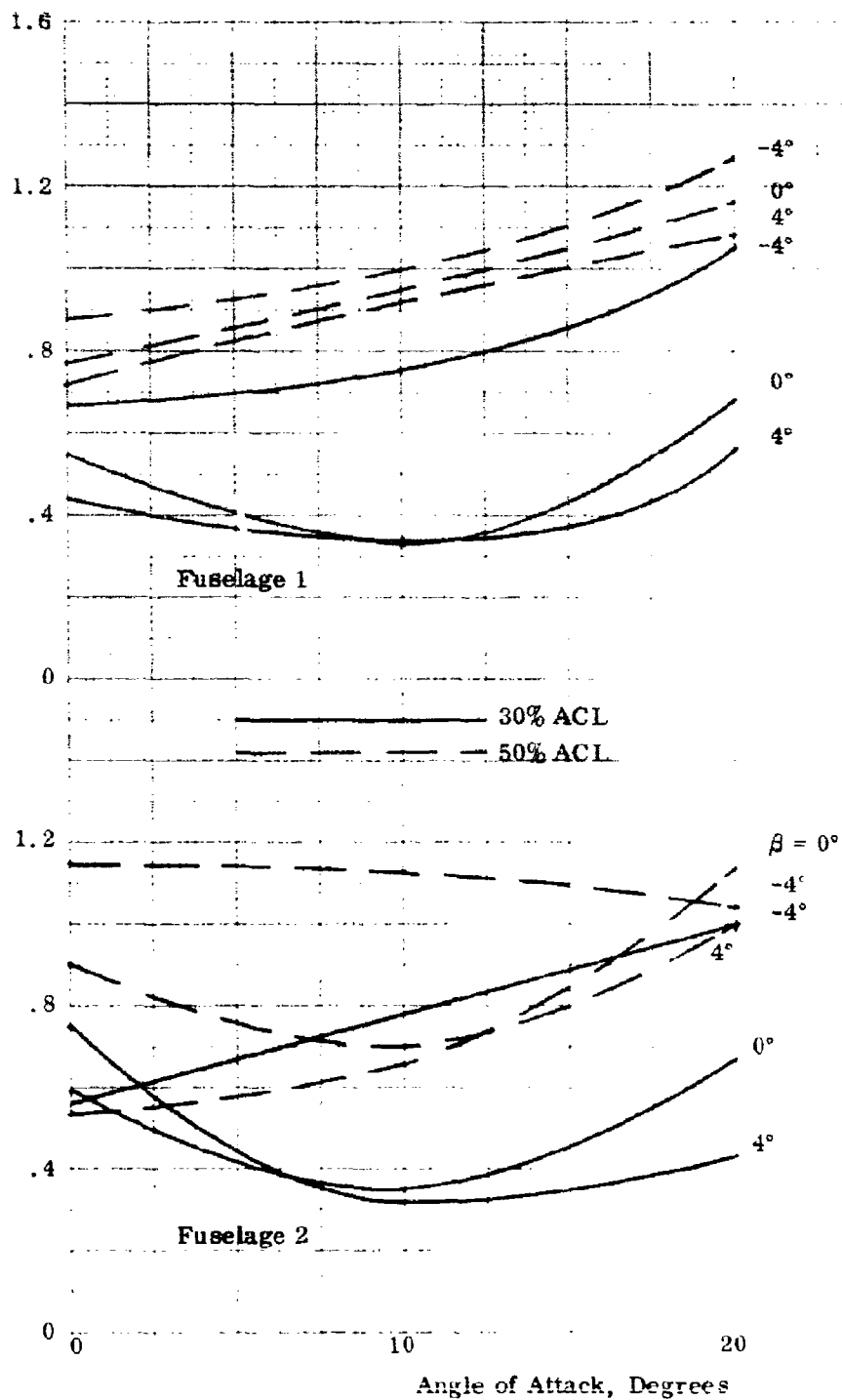


Figure 146. Average Steady State Distortion, $M_\infty = 3.5$

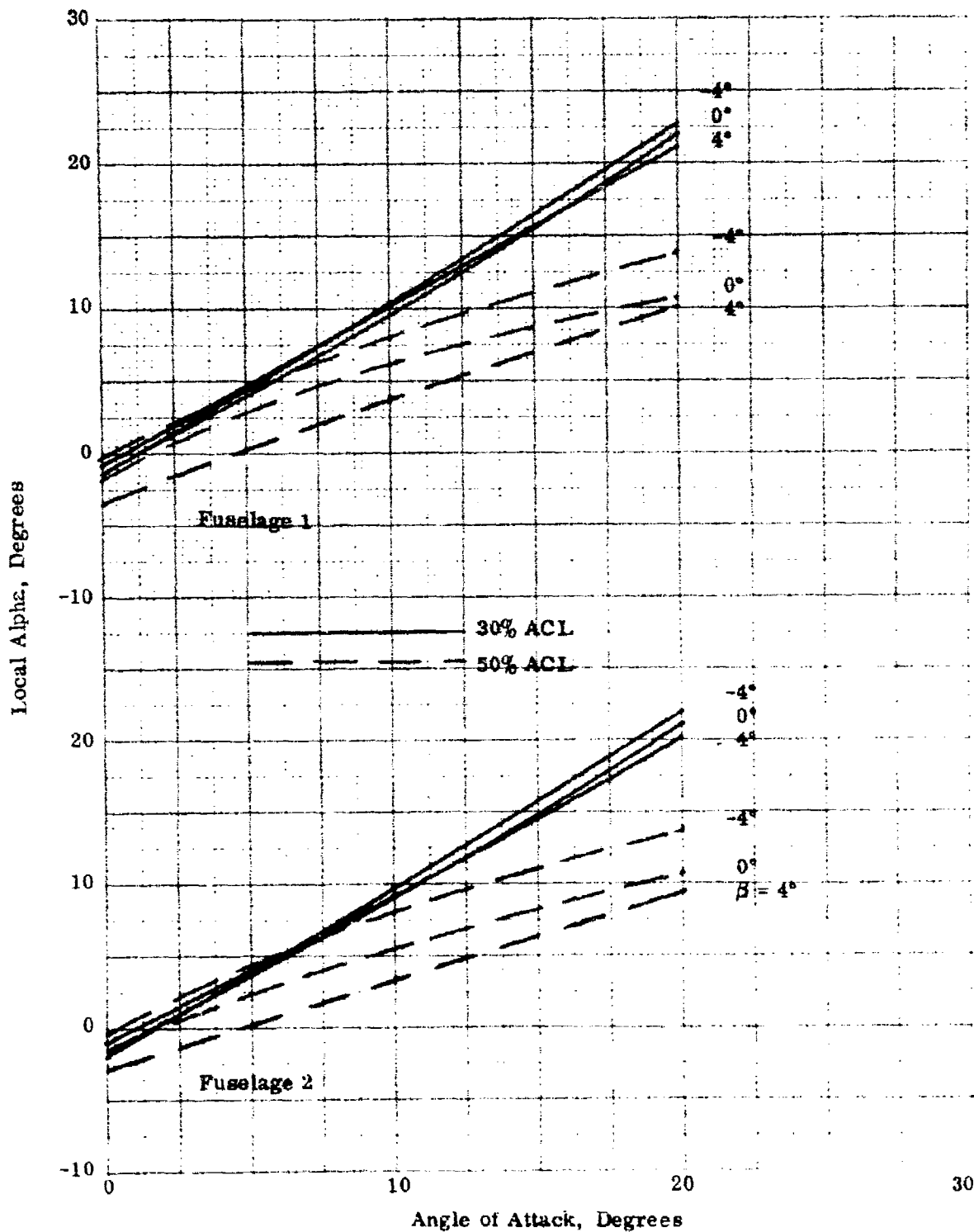


Figure 147. Average Local Angle of Attack, $M_\infty = 2.5$

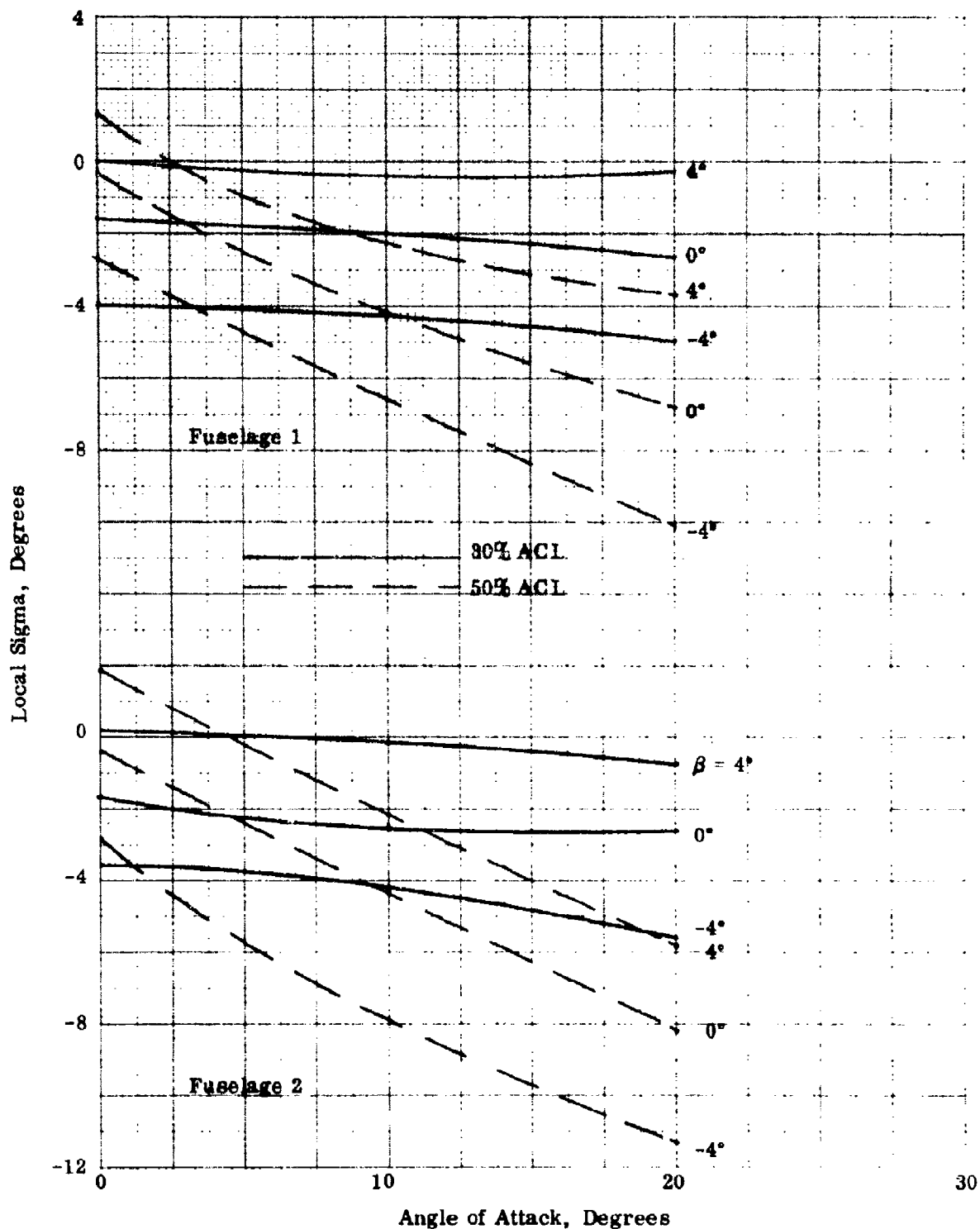


Figure 149. Average Local Sidewash, $M_\infty = 2.5$

TECHNICAL CHART

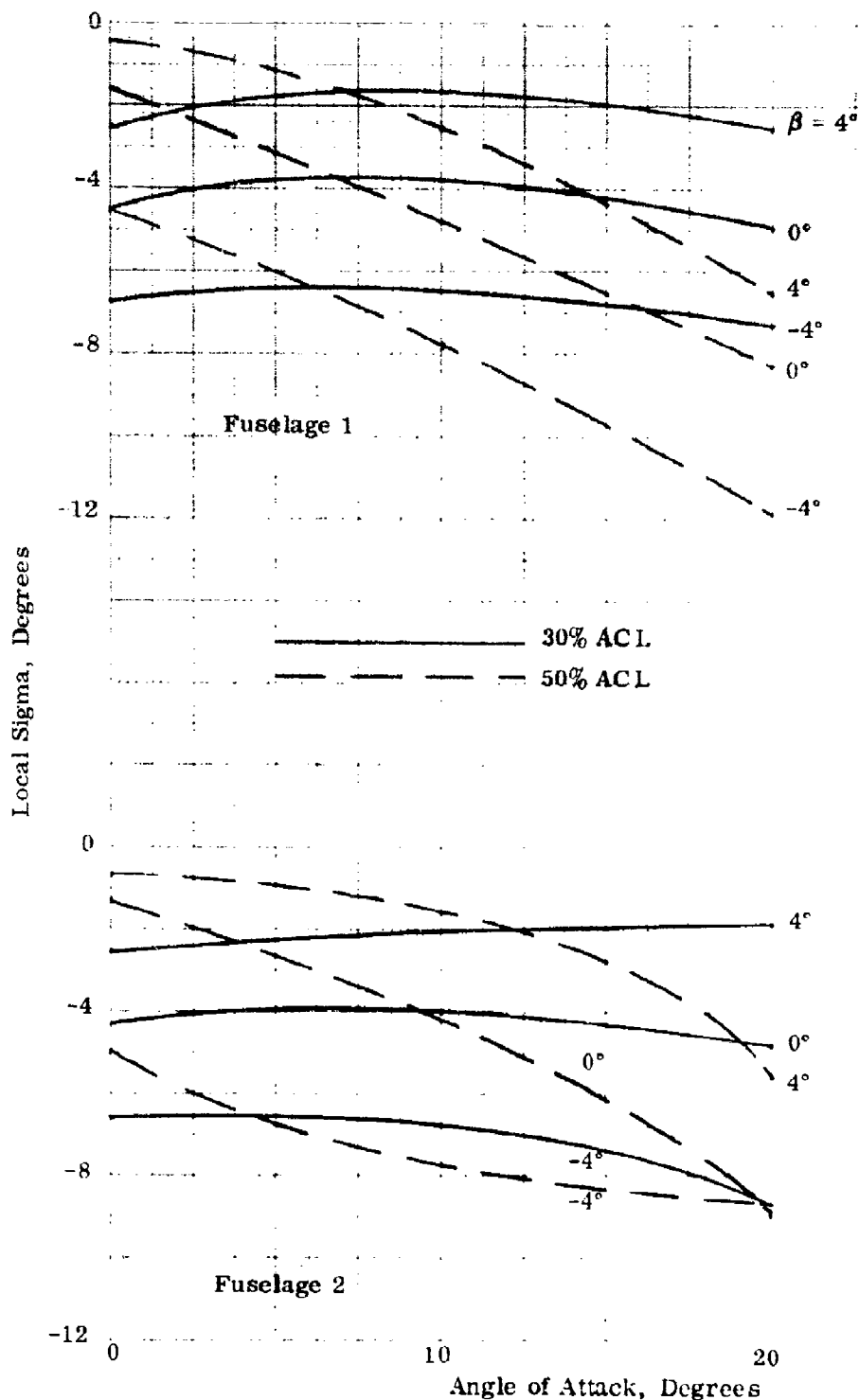


Figure 150. Average Local Sidewash, $M_\infty = 3.5$

UNCLASSIFIED

Security Classification

DOCUMENT CONTROL DATA - R & D

(Security classification of title, body of abstract and indexing annotation must be entered when the overall report is classified)

1. ORIGINATING ACTIVITY (Corporate author) Fairchild Industries Inc. Fairchild Republic Company Farmingdale, New York 11735		2a. REPORT SECURITY CLASSIFICATION Unclassified
		2b. GROUP
3. REPORT TITLE INVESTIGATION OF THE EFFECTS OF AIRFRAME DESIGN ON INLET FLOW FIELDS		
4. DESCRIPTIVE NOTES (Type of report and inclusive dates) Final Report, 1 March 1971 to 28 May 1973		
5. AUTHOR(S) (First name, middle initial, last name) Constant Prokop, Fairchild Industries, Fairchild Republic Company		
6. REPORT DATE May 1973	7a. TOTAL NO. OF PAGES 191	7b. NO. OF REFS
8a. CONTRACT OR GRANT NO. F33615-71-C-1451	9a. ORIGINATOR'S REPORT NUMBER(S) AFFDL-TR-72-11, Volume II	
b. PROJECT NO. 1476		
c. 147603	9b. OTHER REPORT NUMBER (Any other numbers that may be assigned this report) N/A	
d.		
10. DISTRIBUTION STATEMENT Distribution limited to U. S. Government agencies only; test and evaluation; February 1972. Other requests for this document must be referred to AF Flight Dynamics Laboratory (FXM), Wright-Patterson AFB, Ohio 45433.		
11. SUPPLEMENTARY NOTES		12. SPONSORING/MONITORING ACTIVITY Air Force Flight Dynamics Laboratory Air Force Systems Command Wright-Patterson AFB, Ohio 45433
13. ABSTRACT The modern tactical class of aircraft weapon systems is required to perform effectively over a wide range of flight Mach number and altitude, providing large thrust margin and high maneuvering capability throughout the normal operating envelope. To achieve this combination of performance and maneuverability, a sophisticated propulsion system closely integrated with the airframe is required. Operational experience indicates that the vehicle induced flow environment can influence the performance of these closely integrated propulsion systems with the effects ranging from minor performance degradation to engine flame-out. Recent exploratory and development research programs have served to improve the basic understanding of the effects of airframe-inlet interaction. These programs accomplished their major goals in that a large bank of relevant experimental data was generated and a basic understanding of the flow phenomena was obtained. The objective of the program reported herein was to expand this data bank by (1) providing a more extensive spacial documentation of the vehicle flow fields, (2) an increase in the Mach number regime included, and (3) investigations of additional geometric variables potentially impacting upon the propulsion system design process. All major program goals were attained.		

DD FORM 1473

Unclassified

Security Classification

UNCLASSIFIED

Security Classification

14 KEY WORDS	LINK A		LINK B		LINK C	
	ROLE	WT	ROLE	WT	ROLE	WT
Protuberances						
Canard Surfaces						
Strakes						
Missiles						
Fuselage Nose Geometry						
Cambered Fuselage						
Canopy Geometry						
Flow Field Survey						
Boundary Layer						
Fuselage Static Pressure						
Flow Field						
Local Mach Number						
Effect of Vehicle Geometry						
Effect of Protuberances						
Effect of Yaw						
Total Pressure Recovery						
Local Alpha						
Local Sigma						

UNCLASSIFIED

Security Classification